The automated fiber placement (AFP) process of thermoplastic tape with in-situ consolidation is a promising technology to enable a resource-efficient production of load-optimized, near-net shape lightweight parts. However, it is prone to difficult processing due to its complexities and interacting parameters. This results in time-consuming experiments generating a lot of resource-consuming waste. To prevent this from happening and to make the production process more resource-efficient and simpler, a realistic process modeling within a digital twin can be a solution. For this reason, this thesis develops a methodology for a digital twin for the AFP process of thermoplastic, tailored composites blanks.

In the last decades, a vast process knowledge has been gained in research offering a bouquet of validated modeling solutions for the AFP process. Within this thesis, a detailed study leads to the selection of adequate models for the transfer into a digital twin. The temperature evolution within the laminate during processing is a crucial characteristic. It strongly influences the quality of the final part. Quality indicators, such as the consolidation degree and crystallization ratio, are based on well-established analytical models. A first feasibility study of applying these models to gain a more part-oriented, realistic model shows the potentials for the digital twin. Based on its findings, a digital twin is proposed by specifying the required information, the suitable models as well as additional part-oriented characteristics, such as the path-dependent cooling time.

An experimental validation of the proposed digital twin is conducted on the AFP production system, PrePro2D®. Due to is fully integrated hardware, the system allows to smoothly assess, synchronize, and store all relevant data without the need of further data preparation. Although various material characteristics are taken from literature, the validation shows good agreement with the digital twin prediction. However, it also gives insight into the gaps of the model. The aggregation of information to capture a holistic process view still incorporates many underlying assumptions. This thesis summarizes with an overview of solutions improving the prediction quality of the digital twin. In conclusion, this dissertation elaborates a new solution space for complex manufacturing problems of the FRP industry with the help of digitization.

ISBN 978-3-98555-195-8

PROZESSTECHNOLOGIE

PROZESSTECHNOLOGIE

Digital Twin Methodology for the Automated Fiber Placement with In-situ Consolidation of Thermoplastic Tape

Malena Schulz

ERGEBNISSE AUS DER PRODUKTIONSTECHNIK

Malena Schulz

Digital Twin Methodology for the Automated Fiber Placement with In-situ Consolidation of Thermoplastic Tape

Edition Wissenschaft Apprimus

Digital Twin Methodology for the Automated Fiber Placement with In-situ Consolidation of Thermoplastic Tape

Methodik zur Erstellung eines digitalen Zwillings für den Thermoplast-Tapelegeprozess mit in-situ Konsolidierung

Von der Fakultät für Maschinenwesen
der Rheinisch-Westfälischen Technischen Hochschule Aachen
zur Erlangung des akademischen Grades einer
Doktorin der Ingenieurwissenschaften
genehmigte Dissertation

vorgelegt von

Malena Barbara Schulz

Berichter/in:

Univ.-Prof. Dr.-Ing. Christian Brecher
Univ.-Prof. Dr.-Ing. Jürgen Fleischer

Tag der mündlichen Prüfung: 13. November 2023

ERGEBNISSE AUS DER PRODUKTIONSTECHNIK

Malena Schulz

Digital Twin Methodology for the Automated Fiber Placement with In-situ Consolidation of Thermoplastic Tape

Herausgeber:
Prof. Dr.-Ing. T. Bergs
Prof. Dr.-Ing. Dipl.-Wirt. Ing. G. Schuh
Prof. Dr.-Ing. C. Brecher
Prof. Dr.-Ing. R. H. Schmitt

Band 1/2024

Bibliografische Information der Deutschen Nationalbibliothek
Die Deutsche Nationalbibliothek verzeichnet diese Publikation in der Deutschen Nationalbibliografie; detaillierte bibliografische Daten sind im Internet über https://portal.dnb.de abrufbar.

Malena Schulz:

Digital Twin Methodology for the Automated Fiber Placement with In-situ Consolidation of Thermoplastic Tape

1. Auflage, 2024

Gedruckt auf holz- und säurefreiem Papier, 100% chlorfrei gebleicht.

Wissenschaftsverlag des Instituts für Industriekommunikation und Fachmedien
an der RWTH Aachen
Steinbachstr. 25, 52074 Aachen
Internet: www.apprimus-verlag.de, E-Mail: info@apprimus-verlag.de

Printed in Germany

ISBN 978-3-98555-195-8

D 82 (Diss. RWTH Aachen University, 2023)

Vorwort

Die vorliegende Dissertation entstand neben meiner Tätigkeit als wissenschaftliche Mitarbeiterin und Gruppenleiterin am Fraunhofer-Institut für Produktionstechnologie IPT in Aachen. Ich glaube, es gibt kaum einen anderen Ort, an dem ich so viele professionelle, aber auch emotionale Erfahrungen in so kurzer Zeit sammeln konnte.

Ich danke meinem Doktorvater Prof. Dr.-Ing. Christian Brecher für das entgegengebrachte Vertrauen und die eingeräumte inhaltliche Freiheit bei der Erstellung dieser Arbeit. Mein weiterer Dank gilt Prof. Dr.-Ing. Jürgen Fleischer als zweiten Berichter, sowie Prof. Dr.-Ing. Christian Hopmann für den Vorsitz der Prüfungskommission. Auch bedanke ich mich bei Dr.-Ing. Henning Janssen für die umfangreichen Freiräume bei der Leitung und Durchführung vielfältiger Industrie- und Forschungsprojekte.

Ein großes Dankeschön gilt meinem damaligen Team der Faserverbundtechnik. Eure Neugier und euer Ehrgeiz haben mich stets begeistert und motiviert. Es war mir eine große Freude, diese Jahre mit euch gestalten zu dürfen. Hervorheben möchte ich meinen Dank an Ralf Weber, Tim Nagel, Martin Schwane und Leyre Rus Gelo. Ohne eure tatkräftige Unterstützung bei der Entwicklung und Umsetzung diverser Produktionsanlagen wären viele Projekte nicht möglich gewesen. Ich danke auch allen meinen Abschlussarbeitern und -arbeiterinnen sowie studentischen Hilfskräften, die ich am Institut kennenlernen und betreuen durfte. Weiterhin möchte ich mich bei allen weiteren Kolleginnen und Kollegen am Fraunhofer IPT bedanken, die durch ihren Spaß an der Arbeit, ihr Engagement und ihren Intellekt jeden Tag zu einem besonderen Tag gemacht haben. Es hat mir sehr viel Freude bereitet, mit euch diverse Ideen und Vorhaben umzusetzen. Es gab keinen Tag, an dem ich nicht gerne zum Institut ging.

Dass der notwendige Entfaltungsfreiraum bis hin zu meiner Promotion geschaffen wurde, verdanke ich meinen Eltern Barbara Schulz-Herbertz und Joachim Schulz. Hierbei geht mein größter Dank an meine Mutter. Du hast meine Ideen und Wege immer befürwortet und mich auch dazu ermutigt in Aachen zu promovieren. Ohne das stabile und optimale Umfeld, das du als alleinerziehende Mutter dreier Kinder geschaffen hast, hätte ich diesen Weg nicht gehen können. Ein weiterer Dank gilt meinen verstorbenen Großeltern, Rudolf und Margarete, und meinen beiden Geschwistern, Matthias und Mirjam. Diese Familie zu erleben ist immer wieder eine Bereicherung und Motivation.

Ein besonderer Dank gilt meinem Ehemann Thomas, für die Ausdauer, Geduld und Zuwendung bei der Erstellung meiner Dissertation. Ich freue mich jeden Tag über unsere gegenseitige Förderung in unseren privaten und beruflichen Herausforderungen sowie über deine grenzenlose Liebe für unsere Familie. Hiermit steht uns nichts im Wege gemeinsam mit unserer Tochter Paula die Zukunft zu gestalten.

Malena Schulz Wolfertschwenden, im Dezember 2023

Summary

The automated fiber placement (AFP) process of thermoplastic tape with in-situ consolidation is a promising technology to enable a resource-efficient production of load-optimized, near-net shape lightweight parts. However, it is prone to difficult processing due to its complexities and interacting parameters. This results in time-consuming experiments generating a lot of resource-consuming waste. To prevent this from happening and to make the production process more resource-efficient and simpler, a realistic process modeling within a digital twin can be a solution. For this reason, this thesis develops a methodology for a digital twin for the AFP process of thermoplastic, tailored composites blanks.

In the last decades, a vast process knowledge has been gained in research offering a bouquet of validated modeling solutions for the AFP process. Within this thesis, a detailed study leads to the selection of adequate models for the transfer into a digital twin. The temperature evolution within the laminate during processing is a crucial characteristic. It strongly influences the quality of the final part. Quality indicators, such as the consolidation degree and crystallization ratio, are based on well-established analytical models. A first feasibility study of applying these models to gain a more part-oriented, realistic model shows the potentials for the digital twin. Based on its findings, a digital twin is proposed by specifying the required information, the suitable models as well as additional part-oriented characteristics, such as the path-dependent cooling time.

An experimental validation of the proposed digital twin is conducted on the AFP production system, PrePro2D®. Due to is fully integrated hardware, the system allows to smoothly assess, synchronize, and store all relevant data without the need of further data preparation. Although various material characteristics are taken from literature, the validation shows good agreement with the digital twin prediction. However, it also gives insight into the gaps of the model. The aggregation of information to capture a holistic process view still incorporates many underlying assumptions. This thesis summarizes with an overview of solutions improving the prediction quality of the digital twin. In conclusion, this dissertation elaborates a new solution space for complex manufacturing problems of the FRP industry with the help of digitization.

Kurzfassung

Das Tapelegeverfahren mit in-situ Konsolidierung ist eine vielversprechende Technologie, die eine ressourceneffiziente Produktion von lastoptimierten, endkonturnahen Leichtbauteilen aus thermoplastischen Faserverbundkunstoffen (FVK) ermöglicht. Das Verfahren ist jedoch aufgrund der vielen interagierenden Parameter komplex. Dies führt zu zeitaufwändigen und ressourcenintensiven Experimenten. Um dies zu vermeiden und den Produktionsprozess ressourceneffizient und einfacher zu gestalten, hilft eine realistische Prozessmodellierung innerhalb eines digitalen Zwillings. Die vorliegende Dissertation erarbeitet schrittweise einen solchen digitalen Zwilling für den Tapelegeprozess.

In den letzten Jahrzehnten wurde in der Literatur ein umfangreiches Prozesswissen erworben, das einen Strauß validierter Modellierungslösungen für den Tapelegeprozess bietet. Die detaillierte Untersuchung dieser zur Verfügung stehenden Modellierungslösungen führt zur Auswahl geeigneter Modelle für den digitalen Zwilling. Die Temperaturentwicklung innerhalb des Laminats während der Verarbeitung ist ein entscheidendes Merkmal, da sie die Qualität des Endprodukts stark beeinflusst. Qualitätsindikatoren wie der Konsolidierungs- und der Kristallisationsgrad basieren auf gut etablierten analytischen Modellen. Eine erste Machbarkeitsstudie zur Nutzung dieser Modelle für ein bauteilorientiertes, realistisches Modell zeigt die Potenziale des digitalen Zwillings. Basierend auf diesen Erkenntnissen wird ein digitaler Zwilling erarbeitet, indem die benötigten Informationen, die geeigneten Modelle sowie zusätzliche bauteilorientierte Merkmale, wie z.B. die pfadabhängige Abkühlzeit, spezifiziert werden.

Eine experimentelle Validierung des digitalen Zwillings wird auf dem Tapelegesystem PrePro2D® durchgeführt. Dank seiner voll integrierten Hardware ermöglicht das System die reibungslose Auswertung, Synchronisierung und Speicherung aller relevanten Daten, ohne dass eine weitere Datenaufbereitung erforderlich ist. Obwohl verschiedene Materialeigenschaften aus der Literatur abgeleitet werden, zeigt die Validierung eine gute Übereinstimmung mit der Vorhersage des digitalen Zwillings. Sie gibt aber auch Aufschluss über die Lücken des Modells. Die Aggregation von Informationen zur Erfassung einer ganzheitlichen Prozessbetrachtung beinhaltet immer noch viele zugrunde liegende Annahmen. Diese Dissertation schließt mit einer Zusammenfassung über Lösungen zur Verbesserung der Vorhersagequalität des digitalen Zwillings ab. So erarbeitet diese Dissertation einen neuen Lösungsraum für komplexe Fertigungsprobleme der FVK-Industrie mithilfe der Digitalisierung.

Content

Inhaltsverzeichnis

Abbreviations

Abkürzungsverzeichnis

AFP	Automated fiber placement
ANN	Artificial neural networks
ATL	Automated tape laying
B2B	Business to business
BLISK	Blade integrated disk
BMBF	Bundesministerium für Bildung und Forschung (English: Federal Ministry of Education and Research in Germany)
CAD	Computer aided design
CAM	Computer aided manufacturing
CF	Carbon fiber
CFD	Computational fluid dynamics
CLT	Classical laminate theory
CMC	Ceramic matrix composites
CPPS	Cyber-physical production systems
DED	Directed energy deposition
DIN	Deutsches Institut für Normung (English: German Institute for Standardisation Registered Association)
DoB	Degree of Bonding
DoC	Degree of Crystallinity
DoE	Design of experiments
DSC	Differential scanning calorimetry
E&E	Electrical and electronics
EMC	Electromagnetic compatibility
ERP	Enterprise resource planning
EU	European Union
FDM	Finite difference method
FE	Functional entity
FEA	Finite element analysis
FEM	Finite element method

FFF	Fused filament fabrication
FRP	Fiber-reinforced plastics (German: Faserverbundkunststoffe (FVK))
FTCS	Forward time centered space
GUI	Graphical user interface
GPR	Gaussian process regression
HDPE	High-density polyethylene
I4.0	Industry 4.0
ILSS	Interlaminar shear strength
IoP	Internet of production
IoT	Internet of things
IIoT	Industrial internet of things
ISO	International Organization for Standardization
LATW	Laser-assisted tape winding
LFT-D	Long fiber thermoplastic directmolding
LMBH	LightMatBatteryHousing
LMPAEK	Low melt polyaryletherketone
L-PBF	Laser powder bed fusion
MAE	Mean absolute error
MES	Manufacturing execution system
ML	Machine learning
MMC	Metal matrix composites
MSE	Mean squared error
MVS	Multivariate sensor
NC	Numerical control
OEE	Overall equipment efficiency
OME	Observable manufacturing domain
PA	Polyamide
PDE	Partial differential equation
PE	Polyethylene
PEI	Polyetherimide
PEEK	Polyetheretherketone
PEKK	Polyetherketoneketone

PET	Polyethylene terephthalate
PGD	Proper generalized decomposition
PLC	Programmable logic controller
PMC	Polymer matrix composites
PP	Polypropylene
PPS	Polyphenylen sulfide
PVDF	Polyvinylidene fluoride
R&D	Research and development
RBDO	Reliability-based design optimization
RTM	Resin transfer molding
SCADA	Supervisory control and data acquisition
SLM	Selective laser melting
TGA	Thermogravimetric analysis
TTCB	Thermoplastic tailored composite blanks
UD	Unidirectional
VAT	Variable angle tows

Formula Symbols

Formelzeichen

Latin symbols, capital letters

A	m^2	Area
A_L	m^2	Surface heat area
Bi	-	Biot number
E	Pa	Young´s modulus
D_B	$[0 \dots 1]$	Degree of bonding
D_{IC}	$[0 \dots 1]$	Degree of intimate contact
D_{AH}	$[0 \dots 1]$	Degree of autohesion
F	N	Force
F_{cons}	N	Consolidation force
Fo	$-$	Fourier number
G	Pa	Shear modulus
ΔH_m	J/g	Melting enthalpy
ΔH_m^0	J/g	Melting enthalpy of the 100 % crystalline form of the thermoplastic matrix
I	m^4	Area moment of inertia
$K(T)$	$1/min$	Crystallization rate constant at temperature T
K_{max}	$1/min$	Max. crystallization rate constant
M	g/mol	Molecular weight
M_c	g/mol	Critical molecular weight
N	$-$	Number of layers
P_{cons}	Pa	Consolidation pressure
P_L	W	Laser power
Q	J	Heat (energy)
$\dot{Q}$	W	Heat flow
$\dot{Q}_{cond}$	W	Heat flow by conduction
$\dot{Q}_{conv}$	W	Heat flow by convection
$\dot{Q}_{laser}$	W	Laser heat flow

$\dot{Q}_{rad}$	W	Heat flow by radiation
$\dot{Q}_{sub}$	W	Heat flow to the substrate
R	$J/(mol \cdot K)$	Universal gas constant: $8.314\,J/(mol \cdot K)$
R^*	-	Proportional coefficient for the influence of the surface roughness
T	K	Temperature
T_{env}	K	Environmental temperature
T_{fc}	K	Final crystallization temperature
T_g	K	Glass transition temperature
T_i	K	Initial temperature
T_{ic}	K	Initial crystallization temperature
T_m	K	Melting temperature
T_{np}	K	Surface temperature in the nip-point / process zone
$T_{p,c}$	K	Peak crystallization temperature
T_{stress}	K	Stress-free temperature
T_{tool}	K	Tool temperature
T_∞	K	Far field temperature
V	m^3	Volume

Latin symbol, lower-case letters

a	m/s^2	Acceleration
a^{max}	m/s^2	Max. acceleration
a_0, b_0, w_0	m	Surface parameter of the to the model of LEE AND SPRINGER [LEE87, p. 1032]
c_p	$J/(kg \cdot K)$	Specific heat coefficient
d	m	Thickness of the body
$d_{substrate}$	m	Thickness of the substrate
f	Hz	Frequency
h	m	Height
h_{air}	$W/(m^2 \cdot K)$	Convective heat transfer coefficient to the air
h_{conv}	$W/(m^2 \cdot K)$	Convective heat transfer coefficient

h_{tape}	m	Tape height
h_{tool}	$W/(m^2 \cdot K)$	Tool convective heat transfer coefficient
j	m/s^3	Jerk
j^{max}	m/s^3	Max. jerk
$k(T)$	$1/min$	Isothermal crystallization rate constant at temperature T
k_n	$W/(m \cdot K)$	Thermal conductivity in n-direction
l_x	m	Length in x-direction
l_y	m	Length in y-direction
n	$-$	Avrami constant
n_{sys}^t	$-$	Number of multiple tows
n^θ	$-$	Number of tows with fiber angle θ per layer
$\dot{q}_0''$	W/m^2	Surface heat flux
$\dot{q}_n''$	W/m^2	Heat flux in n-direction
$\dot{q}_0''(t)$	W/m^2	Incident surface heat flux at time t
$\dot{q}'''$	W/m^3	Volumetric energy source
t	s	Time
t_a	s	Acceleration time
t_{AH}	s	Time for autohesion
t_c	s	Cooling time
t_f	s	Final time
t_{IC}	s	Time for intimate contact
t_j	s	Jerk time
t_L	s	Irradiation time
t_{aux}	s	Auxiliary time
t_{main}	s	Main process time
t^{part}	s	Part production time
t_{aux}^{part}	s	Part-dependent auxiliary times
t_{aux}^{sys}	s	System-dependent auxiliary times
t_{main}^{part}	s	Part-dependent main times
$t_{main}^{process}$	s	Process-dependent main times

t_P	s	Total considered time
t_{return}	s	Return time
t_R	s	Reptation time
t_w	s	Reptation / Welding time
t_χ	s	Time for crystallization
v	m/s	Velocity
v^{max}	m/s	Max. velocity
v_f	$-$	Fiber volume content
v_m	$-$	Matrix volume content
v_P	m/s	Process velocity
w	m	Width
w_0	m	Initial width
w_{tape}	m	Tape width
x_L	m	Irradiation length

Greek symbols

α	m^2/s	Thermal diffusivity
α_T	$1/K$	Thermal expansion coefficient
δ_{melt}	mm	Melt pool depth
ε	$-$	Emissivity
ϵ_i	$-$	Strain in direction i
θ	°	Fiber orientation
κ	$1/m$	Warpage
$\mu_0(T)$	$Pa \cdot s$	Temperature-dependent viscosity
ν	$-$	Poisson ratio
ρ	kg/m^3	Density
σ_i	Pa	Stresses in direction i
σ_{ILSS}	Pa	Interlaminar shear strength
σ	$W/(m^2 \cdot K^4)$	Stefan-Boltzmann constant: $5.67 \cdot 10^{-8}\ W/(m^2 \cdot K^4)$
τ	s	Nucleation time
φ_f	$-$	Fiber mass content

φ_m	–	Matrix mass content
$\chi(t)$	–	Relative degree of crystallization at time t
$\chi_{1/2}$	–	Isothermal crystallization half-time
$\chi_v(t)$	–	Crystallization volume at time t
$\chi_{v\infty}$	–	Crystallization volume at equilibrium conditions

1 Introduction

Einleitung

Climate crises, material and energy shortages increase the pressure to solve the problem of wasting material and energy. Lightweight design is emerging as a significant component of the solution due to its material efficiency. Load-optimized part designs or the application of materials with high specific characteristics, normalized to the material´s density, allow to decrease part weight. This is especially relevant for the mobility sector. Higher specific powers, but also higher ranges or lower energy consumptions are a result.

In recent years, a paradigm shift has taken place in lightweight design. Lightweight materials, especially composite plastics, have great potential not only to address energy consumption during usage, but also at an earlier stage of value creation, the production process. The automated fiber placement (AFP) with in-situ consolidation of thermoplastic composites is a potential technology addressing both. First, it allows to manufacture load-optimized, lightweight parts. Second, it reduces energy consumption by minimizing scrap and by its efficient, energy saving process design.

The benefits of using thermoplastic composites are, amongst others, increased automation potential, short cycle times, improved recycling as well as beneficial material characteristics, such as chemical resistance or high elongation at break [NEIT14, p. 392]. These beneficial characteristics have increased the use of thermoplastic composites, especially in the transportation, electrical and electronics (E&E) and consumer goods sector. A recently published market survey shows that injected molded composites parts were used up to $69\ \%$ in the transportation sector in 2020 having a market share of $23\ \%$ (global composite market in 2021: 12.1 million tons in volume / $\$37$ billion in value) [PERR22, p. 24]. In 2021, thermoplastic raw material manufacturers accounted for $40 - 50\%$ of the worldwide resin suppliers [PERR22, p. 14]. These numbers primarily account for thermoplastic composites with short and long fibers which are processed by injection molding or similar production technologies. In future, it is expected that more parts will be combined with continuous, unidirectional (UD) fiber-reinforced inlays to even increase its lightweight potential.

In recent years, placing unidirectional thermoplastic tape with in-situ consolidation has gained increased attention in industry. First, it enables the creation of load and waste optimized composites which for example can be used as inlays during injection molding. Second, it allows to neglect further subsequent consolidation steps and therefore results in reduced production time. The consolidation between the layers happens by locally applying pressure and thermal energy to melt the thermoplastic matrix of the incoming tape and the substrate. Thereby a local consolidation process between both layers takes place. Since the 1990s the Fraunhofer Institute for Production Technology IPT investigates the AFP process with in-situ consolidation and has designed several system technologies to produce composite parts. Although methodologies for finding process parameters have been developed, the experience shows that processes are

closely linked to the individual system and that part quality is not only a function of normalized process parameters. There exists a complex interaction of diverse influences. Especially, upscaling the flexible production of tailored composite blanks demonstrates how process robustness is dependent on geometry, production time as well as layup strategies. All these factors influence the heat evolution within the part during processing. [JANS20; YASS18]

With the ongoing fourth industrial revolution *Industry 4.0* (I 4.0), the concepts of *Internet of Things* (IoT), *Cyber-Physical Production Systems* (CPPS) and the digital twinning of products and systems are regarded as solutions to cope with manufacturing complexities [ACAT13, p. 5]. The increased assessment of production data and their analysis by data-driven methods have already shown promising results for complex manufacturing processes. For this reason, this study proposes to create a digital twin enabling a transfer from idealized, analytical process models towards a more realistic, part-oriented process prediction. The data-driven digital twin shall allow to incorporate a vast amount of data, select relevant data for fast-computing simulations and derive manufacturing strategies for a large-volume production of thermoplastic composite blanks.

Within the scope of this thesis, a digital twin for the AFP process with in-situ consolidation to produce tailored composites blanks out of unidirectional, thermoplastic tape is derived and experimentally analyzed. Based on previous findings in the field of composites as well as other manufacturing technologies, current modeling techniques are examined and selected for implementation and experimental validation. Focus is especially the interaction between part geometry, process and system technology. This results in a digital twin framework allowing to assess process and productivity metrics only by using a thermal image camera as process sensor. Its benefits and challenges regarding the implementation of the digital twin are analyzed and recommendations are given to simplify its usage. It is the first tool enabling a part-oriented process analysis and prediction of quality indicators. Finally, the digital twin is utilized as a tool for deriving manufacturing strategies for an upscaled production. The thesis concludes by presenting a methodology for implementing and improving the digital twin for the AFP process and relates it into the ISO 23274 standard for digital twins for manufacturing.

Einleitung

Klimakrise, Lieferengpässe und die Energiekrise erhöhen den Druck auf Gesellschaft, Politik und Industrie, Lösungen für die konsequente Reduzierung von Ressourcen- und Energiebedarf zu finden. Aufgrund des optimierten Materialeinsatzes zeichnet sich der Leichtbau als ein wesentlicher Bestandteil des Lösungsweges ab. Belastungsoptimiertes Bauteildesign oder die Verwendung von Werkstoffen mit hohen spezifischen Materialeigenschaften, die auf die Dichte normiert sind, ermöglichen eine Reduzierung des Bauteilgewichts. Das ist insbesondere für den Mobilitätssektor relevant, um höhere spezifische Leistungen, aber auch höhere Reichweiten und niedrigere Energieverbräuche zu erzielen.

In den letzten Jahren hat sich ein Paradigmenwechsel im Leichtbau vollzogen. Leichtbaumaterialien wie Faserverbundkunststoffe (FVK) haben ein großes Potenzial, den Energieverbrauch nicht nur während der Nutzung, sondern bereits während des Produktionsprozesses und damit in früheren Phasen der Wertschöpfung zu senken. Das automatisierte Tapelegen mit in-situ Konsolidierung thermoplastischer FVK ist eine solche Produktionstechnologie, die eine Ressourcenreduktion während Erzeugung und Nutzung ermöglicht. Zunächst erlaubt es die Herstellung belastungsoptimierter Leichtbauteile. Des Weiteren werden Energieverbräuche durch die Minimierung von Verschnitt und einen effizienten Prozess reduziert.

Der Vorteil thermoplastischer FVK sind unter anderem ein hohes Automatisierungspotential, kurze Zykluszeiten, verbesserte Recyclingmöglichkeiten sowie auch die vorteilhaften Materialeigenschaften, wie beispielsweise chemische Beständigkeit und die hohe Bruchdehnung [NEIT14, p. 392]. Diese Eigenschaften führen zu einer gestiegenen Nachfrage, insbesondere im Transport-, Elektronik- und Konsumgütersektor. Eine vor kurzem veröffentliche Marktstudie zeigt, dass im Jahr 2020 kunststoffgespritzte FVK Bauteile zu 69% im Transportsektor eingesetzt werden. Dieser hat einen globalen Marktanteil von 23% (globaler FVK Markt in 2021: 12,1 Mio. Tonnen / $37 Mrd. in Wert) [PERR22, p. 24]. Im Jahr 2021 machten die Hersteller thermoplastischer Rohstoffe 40-50% der weltweiten Lieferanten für Matrixsysteme aus [PERR22, p. 14]. Diese Zahlen beziehen sich hauptsächlich auf thermoplastische FVK mit Kurz- und Langfasern, die durch das Kunststoffspritzgießen oder ähnlichen Technologien verarbeitet werden. Es wird jedoch erwartet, dass immer mehr Bauteile mit Einlegern aus unidirektionalen (UD) Endlosfasern kombiniert werden, um so die mechanischen Eigenschaften sowie auch das Leichtbaupotenzial größtmöglich auszuschöpfen.

In den letzten Jahren gewinnt das Verarbeiten unidirektionaler thermoplastischer Halbzeuge, sogenannte *Tapes*, mit in-situ-Konsolidierung in der Industrie zunehmend an Interesse. Es erlaubt die Herstellung belastungs- und verschnittoptimierter Bauteile, die beispielsweise als Einleger im Spritzgussprozess verwendet werden können. Ein wesentlicher Vorteil ist die Vernachlässigung nachgelagerter Konsolidierungsschritte, wodurch Prozessschritte eingespart werden. Die Konsolidierung der einzelnen Lagen geschieht während der Bauteilherstellung durch das lokale Applizieren von Druck und thermischer Energie. Dies führt zu einem Schmelzen der thermoplastischen Matrix des

Tapes sowie des Substrats und es findet eine lokale Konsolidierung beider Lagen statt. Das Fraunhofer-Institut für Produktionstechnologie IPT untersucht bereits seit den 1990er Jahren das automatisierte Tapelegen mit in-situ Konsolidierung und hat bereits unterschiedliche Produktionssysteme für die Herstellung von FVK-Bauteilen entwickelt. Obwohl Methoden zur Ermittlung von Prozessparametern umgesetzt wurden, zeigt die Erfahrung, dass Prozesse eng mit dem individuellen System verknüpft sind und dass die Bauteilqualität nicht nur eine Funktion der normierten Prozessparameter ist. Es herrscht eine komplexe Interaktion unterschiedlicher Einflussfaktoren. Insbesondere die Hochskalierung der flexiblen Produktion belastungsoptimierter FVK-Bauteile deutet darauf hin, wie sehr Prozessrobustheit mit der Bauteilgeometrie, Produktionszeit und Ablegestrategie zusammenhängt. [JANS20; YASS18]

Mit der laufenden vierten industriellen Revolution *Industrie 4.0* (I4.0) werden die Konzepte *Internet of Things* (IoT), *Cyber-Physical Production Systems* (CPPS) und die digitalen Zwillinge von Produkten und Systemen als Lösungen zur Bewältigung der Komplexität der Produktion angesehen [ACAT13, p. 5]. Die verstärkte Erfassung von Produktionsdaten und deren Analyse durch datengetriebene Methoden haben bereits vielversprechende Ergebnisse für komplexe Fertigungsprozesse gezeigt. Aus diesem Grund wird in dieser Dissertation vorgeschlagen, einen digitalen Zwilling zu erstellen, der einen Übergang von idealisierten, analytischen Prozessmodellen zu einer realistischeren, bauteilorientierten Prozessvorhersage ermöglicht. Der datengesteuerte digitale Zwilling soll es ermöglichen, eine große Menge an Daten zu integrieren, relevante Daten für schnelle Computersimulationen auszuwählen und Fertigungsstrategien für eine hochskalierte Produktion von thermoplastischen Laminaten abzuleiten.

Hierfür wird im Rahmen dieser Arbeit ein digitaler Zwilling für den AFP-Prozess mit in-situ Konsolidierung zur Herstellung von belastungsoptimierten Laminaten aus unidirektionalem, thermoplastischem Tape abgeleitet und analysiert. Basierend auf bisherigen Erkenntnissen im Bereich der FVK sowie anderer Fertigungstechnologien werden aktuelle Modellierungstechniken untersucht und für die Implementierung und Validierung ausgewählt. Der Fokus liegt dabei insbesondere auf dem Zusammenspiel von Bauteilgeometrie, Prozess und Anlagentechnik. Das Ergebnis ist ein digitaler Zwilling, der es ermöglicht, Prozess- und Produktivitätskennzahlen allein durch den Einsatz einer Wärmebildkamera als Sensor zu bewerten. Die Vorteile und Herausforderungen bei der Implementierung des digitalen Zwillings werden analysiert und Empfehlungen zur Vereinfachung seiner Nutzung gegeben. Schließlich wird durch den digitalen Zwilling erstmals eine bauteilorientierte Prozessanalyse und Vorhersage von Qualitätsindikatoren ermöglicht, die als Werkzeug zur Ableitung von Fertigungsstrategien für eine hochskalierte Produktion genutzt werden können. Die Dissertation schließt mit der Vorstellung einer Methodik zur Implementierung und Erprobung des digitalen Zwillings für den AFP-Prozess ab und integriert diesen in das neue Rahmenwerk der aktuellen ISO 23274 Norm für digitale Zwillinge in der Produktion.

2 State of the art in research and industry

Stand der Technik in Forschung und Industrie

The strive for reducing the world's ecological footprint has forced the governments, the industry and the people to act. The increasing costs of energy stands in contrast with the individual consumption increase. For this reason, a solution must be found to stabilize energy consumption without exploiting natural resources and the ecology.

Decreasing the weight of transportation systems is one method to lower energy consumption. The usage of lightweight materials has risen strongly in the last decades and fiber-reinforced plastics (FRPs) have become one of the major hopes in industry. It is the wish to gain high-end mechanical properties with little weight and costs, that motivates the industry to focus on FRP. In particular the aviation and automotive industry integrate more and more FRPs into their products so that fuel usage shrinks and the power-to-weight ratio rises. [HENN17, p. 127; FLEI18, p. 603]

A further method to decrease energy consumption is to foster resource-efficient production technologies aiming to reduce the overall energy needed for the manufacturing of parts. This entails on the one hand energy-efficient machines and on the other hand intelligent and adaptive processes. Through a smart usage of different tools and a holistic perspective it is possible to reduce development as well as production times which goes hand in hand with decreasing overall energy input. The ideas of I4.0 and the *Internet of Production* (IoP) are suitable practices which allow a holistic and adaptive production design within a sustainable circular economy. [PUTZ17, p. 145]

This chapter gives an overview of the state of the art regarding fiber-reinforced plastics with focus on thermoplastic composites being an enabler for automated composite production. The promising manufacturing technology of the automated fiber placement with in-situ consolidation is highlighted with its benefits, but also its challenges. To address these, the beneficial digitalization tools conceptualized by I4.0 / IoP, such as the digital twin, are presented and discussed for manufacturing applications. The combination of both, simple speaking the digitization of the AFP process, is the basis for the research questions at hand in this thesis.

2.1 Fiber-reinforced plastics (FRP)

Faserverbundkunststoffe (FVK)

The reason for the increasing usage of FRPs is their superior material properties. They are characterized by corrosion and fatigue resistance, strong damping capacities and particularly high specific strength and modulus values. These characteristics are achieved by combining at least two different materials: a polymer matrix and fibers as reinforcement. A further advantage is their anisotropy enabling specific designs customized to loading conditions.

A composite itself consists of at least two entities separated by an interphase. A composite material includes two or more materials, a matrix material and a reinforcement

material. Whereas the matrix is used to hold the other constituents and is continuous, the reinforcement can either be continuous or discontinuous. The volume fraction of a composite is a significant parameter to get a first characterization of the composite. For instance, in a two-phase system the volume content of the matrix material is $v_m = 1 - v_f$ with v_f being the fiber volume content. It is important to state that a material which creates second or intermetallic phases by itself is not considered as a composite. [ABOU13, p. 3]

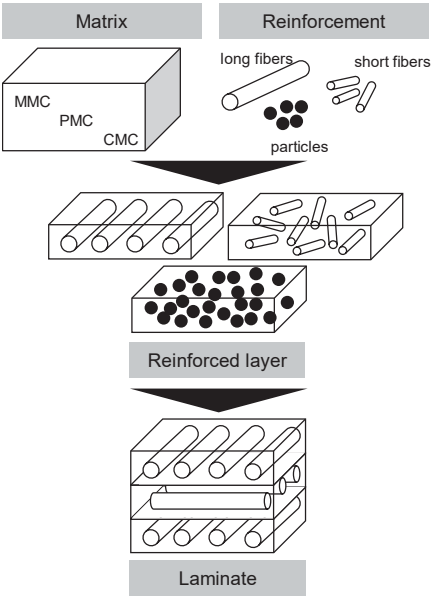

Figure 2.1: General structure of composite materials

Allgemeine Struktur von Verbundwerkstoffen

Generally, composite materials are classified according to the matrix material on the one hand and on the other hand according to the form of the reinforcement, see Figure 2.1. Common matrix material categories are metal matrix composites (MMCs), polymer matrix composites (PMCs) and ceramic matrix composites (CMCs). The function of the matrix is to fix fibers as well as to transfer loads to and between the fibers. Reinforcements can either be discontinuous in form of particles or whiskers, continuous fibers or woven fibers. The material, form and orientation of the reinforcement define if the material is isotropic or anisotropic, its properties and how it behaves according to external loads. [ABOU13, p. 3; WITT14, p. 33; FLEI18, p. 603]

Isotropic material behavior can be expressed by the linear elastic relationship between strains ϵ and stresses σ, see equation (2.1) for a simplified 2-dimensional example, which is characterized by the three elastic constants: Young's modulus E, Poisson's ratio υ and the shear modulus G.

$$\begin{Bmatrix} \epsilon_x \\ \epsilon_y \\ \gamma_{xy} \end{Bmatrix} = \begin{pmatrix} \frac{1}{E} & -\frac{\nu}{E} & 0 \\ -\frac{\nu}{E} & \frac{1}{E} & 0 \\ 0 & 0 & \frac{1}{G} \end{pmatrix} \begin{Bmatrix} \sigma_x \\ \sigma_y \\ \tau_{xy} \end{Bmatrix}. \tag{2.1}$$

Anisotropic material behavior distinguishes between the directional dependencies of the elastic constants. One of the most general forms is the case of a unidirectional-reinforced fiber composite with perpendicular fiber orientation as in Figure 2.2. Since Young's modulus is different in all directions with respect to fiber orientation $E_1 \neq E_2 \neq E_3$ it is said to be *orthotropic*. Often transversal isotropy is assumed implying $E_2 = E_3$ [KRES14, p. 13]. Thus, equation (2.1) turns into

$$\begin{Bmatrix} \epsilon_1 \\ \epsilon_2 \\ \gamma_{12} \end{Bmatrix} = \begin{pmatrix} \frac{1}{E_1} & -\frac{\nu_{21}}{E_2} & 0 \\ -\frac{\nu_{12}}{E_1} & \frac{1}{E_2} & 0 \\ 0 & 0 & \frac{1}{G_{12}} \end{pmatrix} \begin{Bmatrix} \sigma_1 \\ \sigma_2 \\ \tau_{12} \end{Bmatrix}. \tag{2.2}$$

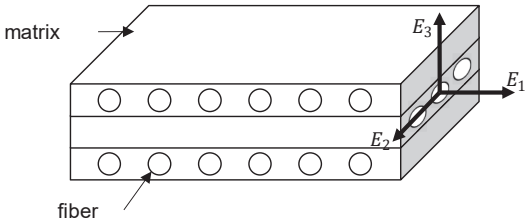

Figure 2.2: Anisotropic material characteristics with unidirectional, reinforced layers

Anisotrope Materialeigenschaften mit unidirektional verstärkten Lagen

By assembling composites further customized material behavior can be obtained by the structure itself. This is usually the case with PMCs by stacking plies with different fiber orientation or reinforcement patterns and creating a laminate as shown in Figure 2.2. All components of a composite material influence the body's structure and material properties, such as thermal resistance, strength or Young's modulus. It can be represented as a homogeneous material with anisotropic properties by the classical laminate theory (CLT) being an extension of the theory on bending of homogeneous plates. For further reading, please refer to [ABOU13; KRES14].

2.2 Automated fiber placement (AFP) of thermoplastic tape

Das automatisierte Tapelegen thermoplastischer Tapes

In recent years, the AFP and automated tape laying (ATL) have become established production technologies for the automated manufacturing of composite parts. Both fiber deposition technologies use *tape* material as raw material. It comprises of endless, unidirectional, evenly distributed fibers pre-impregnated within a thermoset or thermoplastic matrix. Both technologies are distinguished by the width of the processed tape material. A convenient definition is that the ATL processes one tape having a width between $75 - 300\ mm$, usually with thermoset tapes. This allows the laying of large composite structures, such as fuselage parts in aviation or wind rotor blades in the energy sector, with high productivity rates. The AFP processes up to 32 tows or narrow-slitted tape simultaneously allowing the manufacturing of more complex composite parts, e.g. by fiber steering. [LUKA12, p. 997]

The first machines were developed in the 1970s as carbon-fibers became more and more commercially available. At the beginning most of the machines were designed to process prepreg tape material out of carbon-fibers within an epoxy resin. Thermoplastic tape materials gained increased attention in the late 1980s and beginning 1990s. In this time, heating devices were installed on the tape laying applicator to increase the tack of the prepreg material during laying. The advantageous side-effect was that such heat sources could also be used to melt thermoplastic matrices. This was especially beneficial for components, which are too big for the given autoclaves, such as for the aerospace sector [LUKA12, p. 1000f]. For this reason, the AFP process with in-situ consolidation for thermoplastics gained increased attention in the 1990s and first authors, such as GROVE [GROV88] and MANTELL AND SPRINGER [MANT92B], started to investigate the processing more closely (see chapter 4.1).

The benefit of in-situ consolidation, being an *out-of-autoclave* process, has been accompanied by the increased automation potential of thermoplastic composites. Especially since the 2010s cost-driven sectors, such as the automotive sector, have focused more and more on the integration of thermoplastic composites into their series production. To be highlighted is the process of *overmolding* (details in section 2.2.3). This process, a combination of thermoforming and injection molding, enables a cost-effective and automated high-volume production of functionalized, light-weight structures. The European Green Deal, announced in December 2019 by the European Union (EU), has additionally pushed the usage of thermoplastic matrices in industry. Due to their material characteristics, thermoplastics are suitable for sustainable recycling strategies. These do not exist for thermoset matrices being their major drawback.

Parts produced by the AFP process with in-situ consolidation proof to be highly suitable for the above-mentioned requirements: out-of-autoclave process, high degree of automation, functionalization, and sustainable recycling. In addition, the AFP process allows the production of lightweight designs by a near-net-shape production. This enables not only the reduction of waste during manufacturing, but also the flexible creation

of load-optimized parts. According to STEYER [STEY12, p. 6] the AFP process can be classified according to Figure 2.3. Depending on the matrix system, the heating technology as well as the desired part geometry, the AFP system can adjust to the specific production use case.

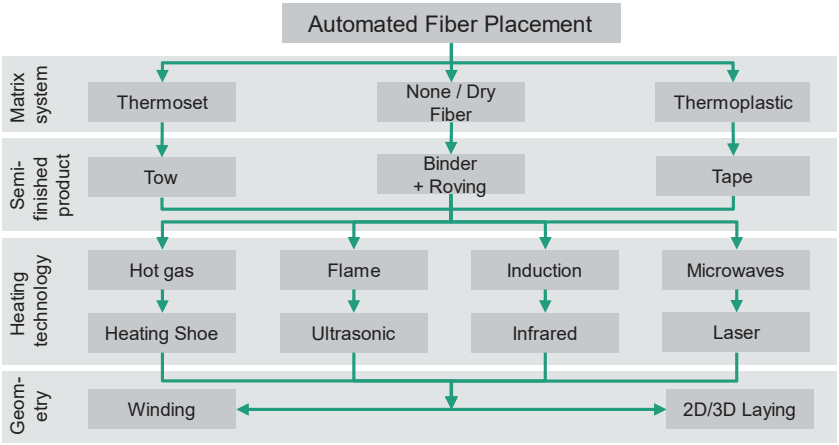

Figure 2.3: Classification of the AFP process with in-situ consolidation, adapted from [STEY12, p. 6]

Klassifizierung des AFP-Verfahrens mit in-situ-Konsolidierung, in Anlehnung an [STEY12, p. 6]

2.2.1 Description of the AFP process with in-situ consolidation

Beschreibung des AFP Prozesses mit in-situ Konsolidierung

The AFP process can be considered as an additive manufacturing process. The tape layers are automatically stacked in an additive manner and are consolidated in-situ by locally applying thermal energy. The specific process area, the so-called *nip-point* zone, is shown in Figure 2.4. First, the tape is fed into the process area and beneath the consolidation roller. In this zone a heat source, e.g. a diode laser, melts the thermoplastic matrix of the incoming tape and the substrate in the nip-point zone. Afterwards, the consolidation roller applies pressure onto the melted tape and substrate. The right combination of time, pressure and heat finally creates a bond between both materials. At the same time, the bonded material begins to cool and solidify until the applicator head returns for the next layer or the manufacturing is completed. By applying the right combination of process parameters a fully consolidated laminate is manufactured in one step.

In most cases, the optimization strategy for high quality parts targets a full consolidation between the incoming tape layers and the substrate. A full consolidation means that both parts are bonded by material interlocking without the existence of any voids

or other defects in the interlaminar area. This means that the matrix of the tape and the substrate become one (with the assumption that both matrix systems are the same). This occurring interaction between material and process is generally characterized by *intimate contact* and *autohesion*. Understanding these mechanisms and relating them to the consolidation degree has been research focus since the beginning of thermoplastic tape laying.

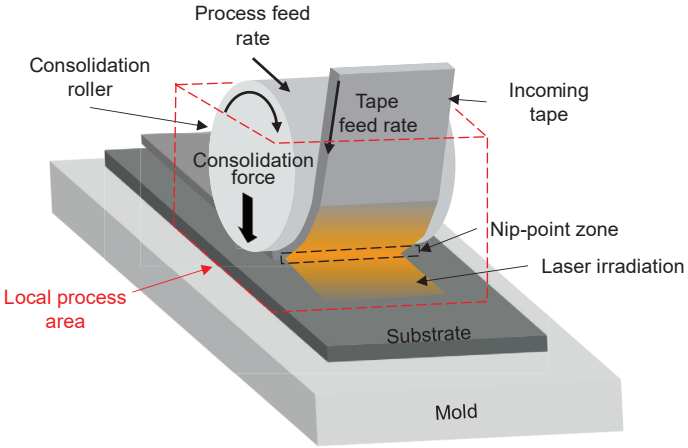

Figure 2.4: Principle of the AFP process with in-situ consolidation

Prinzip des AFP-Verfahrens mit in-situ Konsolidierung

Intimate contact is a necessary condition for consolidation. It describes the contact between the incoming tape and the substrate in the nip-point area. Relevant influences on the degree of intimate contact D_{IC} are the geometrical condition of the tape material, characterized by the surface roughness and waviness in the melted state, its temperature-dependent viscosity as well as the consolidation pressure of the roller [DARA85; MANT92b]. The degree of intimate contact D_{IC} is a value between 0 and 1, the latter implying a full intimate contact. Only in the area of intimate contact *autohesion* can take place, being a further prerequisite for consolidation. In this phase, the polymer matrix of tape and substrate interdiffuse and the materials interlock (see Figure 2.5) in reference to the reptation model by DE GENNES [GENN71]. The corresponding variable D_{AH} $(0 < D_{AH} < 1)$ expresses the degree of autohesion and is influenced by time, temperature and the polymer. Combining both, D_{IC} and D_{AH}, results in the final degree of bonding D_B (DoB) and gives an estimate of the consolidation degree. [PITC97; YANG02; YANG03]

A further focus of research has been the estimation of additional quality indicators, such as the crystallization and residual stress development within the laminate during processing. Whereas the first one influences the final mechanical strength of the part, the latter gives insight into the deformation and shape retention of the laminate. A detailed description of the here-mentioned models is presented in chapter 4.

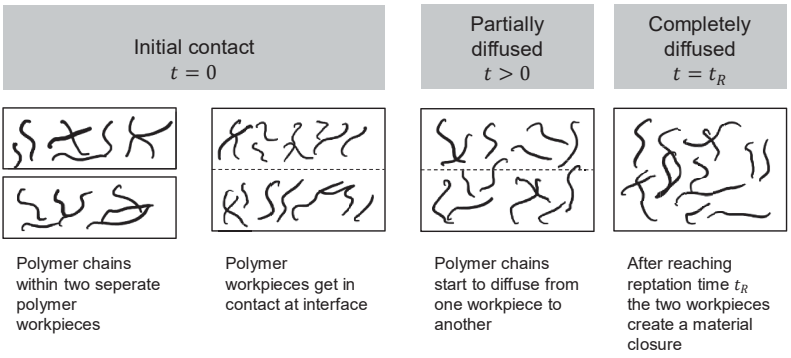

Figure 2.5: Autohesion phenomenon of the AFP process with in-situ consolidation, adapted from [DARA85, p. 7]

Autohäsionsphänomen des AFP-Prozesses mit in-situ Konsolidierung, in Anlehnung an [DARA85, p. 7]

2.2.2 Manufacturing strategies of thermoplastic fiber placement

Fertigungsstrategien des thermoplastischen Tapelegeprozesses

A manufacturing strategy for the AFP process implies two perspectives:

1. The *idealistic* perspective: the right choice of process parameters in the local process area around the nip-point, the process moment, as shown in Figure 2.4,
2. the *realistic* perspective: the right choice of process parameters regarding the whole laminate.

The *idealistic* perspective considers the process in the nip-point zone. It focuses on the area the applicator is currently processing and how the local process parameters, such as the thermal energy, affects the constituents within this area. In contrast, the *realistic* perspective mirrors the effects of the processing on the whole laminate. For example, this implies the transient temperature evolution at each time in space. For both perspectives, there exists an interdependency between the previously mentioned quality indicators, consolidation, crystallization and residual stresses, and the manufacturing strategy which has to be kept in mind during process preparation.

The *idealistic* perspective. With the beginning of thermoplastic fiber placement with in-situ consolidation, literature has been focusing on the instantaneous process moment, as shown in Figure 2.4, to derive the fitting process parameters. The literature can be roughly classified into three categories:

1. The derivation of interactions between quality indicators, process parameters (temperature, time and pressure) and material characteristics (e.g. viscosity) (see section 2.2.1 and 4.1),
2. the development of thermal models enabling the right setting of the temperature and, thus, its thermal source, e.g. the irradiation intensities and distribution, and

3. experimental investigation to derive the right set of process parameters with regard to the targeted quality indicator.

In the 1980s and 1990s, authors such as [DARA85; LEE87; MANT92b; SARR95; PITC97], began to model the process in order to find the correlations between the laminate quality and the processing conditions for thermoplastic composites. As explained in the previous section, the scientific basis for the process modeling and the first models regarding quality, such as the degree of bonding, have been formed at this time. This research has shown that there is a strong relation between the quality indicators and temperature evolution within the incoming tape and substrate material. Temperature is the governing variable in the equation and is dominated by the system and process conditions. Heat transfer models have been adjusted with the boundary conditions of the AFP process and the influences on quality indicators, such as crystallinity, have been evolved. Experimental validations have shown the feasibility of the models for deriving manufacturing strategies. [MANT92b; SARR95; SONM97a]

The development of thermal models is crucial to understand the transient behavior during the AFP processing and its influence on the thermoplastic composite material. At the beginning, the main target of the literature has been to understand the thermochemical effects on crystallinity and residual stresses to forecast the materials mechanical characteristics after manufacturing (details in section 4.1) [MANT92b; SARR95; SONM97a; SONM97b]. Later, these models are further developed to control the thermal energy input. The interdependencies between the quality indicators and the thermal gradients within the materials show the strong influence of the processing. Authors, such as GROUVE [GROU12], BARASINSKI [BARA11], LEVY [LEVY14], SCHÄFER ET AL. [SCHA17] and WEILER [WEIL18], implement the heat transfer equation for the AFP process to derive process parameters, such as the required laser power of a diode laser. GROUVE develops a combined optical and thermal model to accelerate process optimization. The created numerical process design tool allows to simulate the influence of radiation on the temperature gradients in the nip-point area [GROU12, p. 27-48]. BARASINSKI ET AL. as well as LEVY ET AL. illustrate how a degree of bonding $D_B < 1$ affects the thermal resistance between tape and substrate, thus, the temperature development around the nip-point area and, finally, the required thermal energy [BARA11, p. 188-189; LEVY14, p. 494-496]. WEILER conducts a theoretical in-depth thermal analysis targeting increased process speeds of $\gg 500\ mm/s$. By estimating the temperature gradients within the incoming tape and substrate, the author can analytically derive the required thermal energy and use it as a basis for controlling the heating device. All authors show that with the help of a profound thermal modeling and by combination with quality indicators, manufacturing strategies for the AFP process with in-situ consolidation can be derived. This allows to accelerate process optimization and finding the right choice of process parameters. A detailed description of a thermal model for AFP is presented in section 4.1.1.

Next to the experimental validations, which have been conducted in the above-mentioned studies, plain experimental studies have been conducted to assess the process window of the AFP process with in-situ consolidation. Amongst others, the authors

KHAN ET AL. [KHAN13] conduct an extensive parametric study to experimentally assess the interdependency of process parameters and quality indicators. They also included system characteristics, such as the roller diameter and the heating length, to give suggestions for an optimized manufacturing strategy. Similar experimental studies have been conducted by DREHER ET AL. [DREH], SCHULZ ET AL. [SCHU19a; SCHU18], BAUMANN ET AL. [BAUM21] for different tape materials and qualities to find suitable process conditions with respect to quality indicators. Often used experimental methods to test for quality indicators are, for example, the interlaminar shear strength (DIN EN ISO 14130) for evaluating the consolidation, and three-point bending (DIN EN ISO 14125) tests for quantifying the mechanical characteristics.

In summary, even modeling the idealistic case, which focuses only on the process moment / nip-point zone, is defined by a complex interaction of process parameters, material characteristics and system specifications.

The *realistic* perspective. A realistic view on manufacturing system implies the softening of modeling assumptions to forecast quality indicators or process parameters for the manufacturing of a *real* part. In this context, a real part is a laminate which contains the requirements of the targeted application. This means that its thickness, size, geometry, and fiber orientation may vary from the *idealistic* perspective. Desired properties are not dependent on standardized material tests on coupon level but rather tested on the final component. Little work has been done to create models bridging the gap from coupon level to the final *real* part.

An established method to get closer to the final part is the finite element analysis (FEA). FEA is based on a numerical discretization method which subdivides a system in a finite number of single elements and nodes to calculate the effects of a specific input. The idea is to approximate exact problems, whose continuity can only be represented by mathematical statements implying infinitesimal calculus and infinite number of elements. Within the context of engineering, the idea of finite elements came up by partitioning a continuum and representing each part by elastic bars in the beginning of the 20th century. Because of the increasing computational capacities, the methodology of this standard discrete problem evolved over the years becoming common practice in research and industry. For this reason, FEA is profoundly investigated and a preferred method of estimating a state of a system. System boundaries and underlying assumptions can be adapted to the specific problem. This allows a realistic modeling of complex system and processes. However, the primary drawback is the extensive numerical calculations requiring computational capacities and time: The more realistic the model becomes, the more computational expensive it gets. [ZIEN05]

The main usage of FEA in composites is the structural analysis of a part. It is used to estimate the mechanical/thermal/chemical properties of the part in a quasi-static or in a dynamic load case. The processing of composites, which is focused in this thesis, has gained increased attention in recent years. Conventional FEA software can handle more and more complexity and offers simplified modeling by user-friendly graphical user interfaces (GUI). Various processes, for example autoclave curing [BARA17, p.

383-387], resin transfer molding (RTM) [BARA17, p. 387] as well as the AFP of thermoplastic tape [STOK15], have been studied by using FEA. It is a powerful, but also numerically costly tool to derive manufacturing strategies with a more realistic picture of the manufacturing process of composites.

In recent years, more and more research has been done in applying classical numerical techniques to solve complex problems. The finite difference method (FDM) is an established straightforward numerical tool whose integration is regaining popularity. Similar to FEA, FDM discretizes a problem into spatial and time steps, a so-called mesh. Derivatives are derived by the difference between the small intervals [SMIT85, p. 3]. This enables a linearization of differential equations and approximates the solution. For transient problems with a simple geometry, FDM can be a suitable method since it is less computational expensive compared to FEA. A short computing time is especially relevant in the context of Industry 4.0 to enable online adaptation during a series production (see section 2.3).

In the last years, FDM is broadly used to model additive manufacturing processes, such as selective laser melting (SLM) or directed energy deposition (DED) for metals, as well as fused filament fabrication (FFF) for polymers. A FDM based method for these manufacturing technologies has been developed, for example, by STOCKMANN ET AL. [STOC19]. The main aim of the authors is to create a computing tool designed for an industrial environment with little computing power to predict outputs in real-time. The targeted model is the heat transfer during processing. The authors show that their simplified approach has small deviations from the experimental validation. A further FDM based approach is developed by ZAAMI ET AL. [ZAAM21a] for the AFP process of thermoplastics, more precisely, the laser-assisted tape winding (LATW). The authors develop a local and global optical-thermal model for the winding of thermoplastic composite type-IV pressure vessels to predict the thermal history during processing. Whereas the local model forecasts the temperature of tape and substrate in the nip-point, the global model estimates the temperature evolution, such as cooling, in the non-irradiated areas of the vessel [ZAAM21a, p. 1076].

To conclude, the brief introduction of FEA and FDM shows that both methods are suitable numerical tools to characterize complex manufacturing process for composites. FEA is suitable to model parts with high geometrical complexities and various boundary conditions with the drawback of becoming computational expensive. For simplified geometries and layups, FDM seems to be a suitable approach for forecasting a process with less computing time allowing an implementation within the context of I4.0.

2.2.3 Thermoplastic UD-tapes and their applications in industry

Thermoplastische UD-Tapes und die Anwendungen in der Industrie

From the perspective of the semi-finished product, pre-impregnated, unidirectional tape has three main advantages. First, the structural strength of the fibers is best exploited when they are arranged in an endless, unidirectional manner. Second, the pre-impregnation moves an important process step to the beginning of the process chain

allowing the creation of composites with high fiber-volume content and accuracy. Third, the manufacturing process being based on a straightforward, continuous pultrusion process is cost-efficient. [JANS20, p. 17; SALA97, p. 637]

From the perspective of manufacturing the final part, additional advantages for tape occur. As explained in section 2.2.1, automated, additive manufacturing processes exist enabling the manufacturing of near-net-shape composite parts with load-optimized layups. This allows a significant reduction of scrap compared to conventional composite manufacturing technologies, such as RTM or the use of conventional thermoplastic composite blank, so called organosheets, with scrap rates of $25\text{-}30\%$ [KROP17, p. 96].

Table 2.1: Overview of common thermoplastic, UD-tape manufacturers

Übersicht der gängigen Hersteller von thermoplastischen UD-Tapes

Company	Country	Products
Barrday	Canada	PEKK, PEEK, PEI, PVDF, PPS, PA
Celanese	USA	PP, PA6, PA66
DSM	Netherlands	PA410, PA6
Evonik	Germany	PA12, PEEK
Sabic	Netherlands	PP, PE
SGL	Germany	PP, PA
Solvay	Belgium	PPA, PPS, PVDF, PEEK, PEKK
Suprem	Switzerland	PA12, PEEK
Toray	Japan	HDPE, PP, PA6, PET, PPS, PEKK, PEEK, LMPAEK

Due to the mentioned advantages, the usage of tape material has increased significantly in recent years. Especially, the rising portfolio of commercially available UD-tape with a thermoplastic matrix, as listed in Table 2.1, indicates that industry believes that thermoplastic composites are a solution for large-scale series production of lightweight components. In the following, promising *out-of-autoclave* manufacturing technologies suitable for series production, as well as demonstration cases for the use of thermoplastic UD-tapes in final products are shortly introduced. The focus here are production technologies which imply a (discontinuous) stacking of the composite material with different fiber orientations. For this reason, other (continuous) technologies, such as pultrusion or winding, are neglected here.

Thermoforming. Thermoforming is the shaping of an organosheet by using heat and pressure. In general, an infrared heating field heats the blank to a softening state. Afterwards, it is placed into a press and formed, e.g. by a stamp forming process. This procedure has gained attractiveness since thermoplastic composite blanks, also known as organosheets, became available on the market. They consist of fibers impregnated with a thermoplastic matrix. They are shaped as a blank and are generally manufactured continuously by using a double-belt press. In most cases, organosheets

have continuous, woven fabrics with an orthotropic layup, hereinafter named as *conventional organosheet*. Another procedure to manufacture organosheets is the use of UD-tape by AFP without or with in-situ consolidation, as introduced in section 2.2.1. More information of the process can be found in [NEIT14, p. 396; JANS20, p. 32].

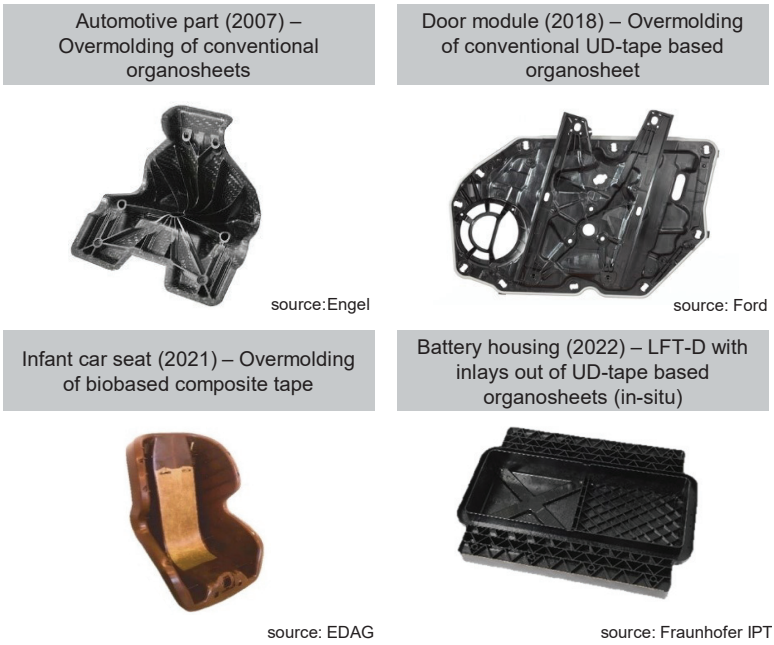

Figure 2.6: Examples of applications produced by the overmolding and LFT-D process with organosheets or tapes as inlays

Beispiele für Anwendungen, die im Overmolding- und LFT-D-Verfahren mit Organoblechen oder Tapes als Inlays hergestellt werden

Overmolding. A preferred process with a high degree of automation is the overmolding of organosheets or of single tape strips. They are commonly thermoformed into a shape and overmolded by injection molding with the same matrix creating a material interlocking. This hybrid structure can be produced in a two-shot or one-shot process. The latter, also known as inmould-forming, has been investigated in a German public-funded project by the University of Erlangen [MÜLL07]. The benefit is the high degree of automation as well as the possibility to functionalize the component by metallic inserts or joining elements. Nowadays, this process can be found in various industrial applications, especially in the automotive sector. Figure 2.6 gives an overview of selected application cases of the past as well as future applications, e.g. by the use of bio-based materials. A detailed explanation of the process can be found in [EICK13, p. 25; JANS20, p. 35; KROP17, p. 98-99].

Long Fiber Thermoplastic Directmolding (LFT-D). An additional process suitable for series production, which allows the integration of composites with endless fibers, is the LFT process. LFT-D is a one-step process which introduces fiber rovings into the molten state of the thermoplastic polymer in the extrusion unit. Within the extruder, the fibers are cut into lengths of up to $80\ mm$ [KRAU03, p. 290]. Afterwards, the compound is fed into a press in which the final part is formed. The process is especially advantageous as it integrates several steps in the process chain in one. Inlays, such as composite blanks or metallic inserts, can be joined simultaneously.

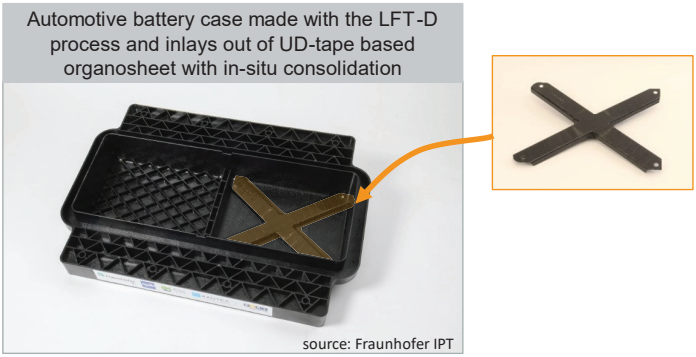

Figure 2.7: Example of hybrid LFT-D parts combined with UD-tape: Components of the battery module in LMBH [BAUM19]

Beispiel für hybride LFT-D-Teile in Kombination mit UD-Band: Komponenten des Batteriemoduls in LMBH [BAUM19]

A prominent example of a multi-functional hybrid automotive part has been developed in the project *SMiLE* [MAIN18]. The project partners have manufactured a composite rear floor module for electric cars which combines a UD-tape based tailored composite blank with LFT-D and aluminum profiles. A similar hybrid battery module molded with LFT-D is developed in the public funded project *LightMatBatteryHousing* (LMBH). The module additionally combines functionalized tapes, e.g. for electromagnetic compatibility (EMC), as well as in-situ consolidated tailored UD-tape based blanks during the LFT-D compression molding process.

Until now, conventional organosheets are mostly used in industrial applications as they offer fully impregnated and stacked laminates which can be procured off-the-shelf. UD-tapes are mostly integrated as a single layer in overmolded parts. As presented here, research shows the potentials of using UD-tape based blanks instead of conventional organosheets. The major drawbacks of the latter are the high amounts of scrap (up to 30%), the limited flexibility to optimize the layup according to the required load path as well as the inability to have laminates with different thicknesses, such as tapered laminates or local reinforcements. [EICK13, p. 24; NEIT14, p. 168-184; KROP17, p. 96]

The manufacturing of thermoplastic tailored composite blanks (TTCB) out of UD-tape is a suitable solution for enabling near-net shape laminates with load optimized layups

(see Figure 2.8). An automated production method is the AFP process. It can either imply in-situ consolidation, as described in section 2.2.1, or a stacking of tapes which are locally tacked by spot welding. The latter requires a subsequent consolidation step. This can be done by using a double-belt press (e.g. FORCE process chain by Neue Materialien Bayreuth GmbH [KROP17, p. 97]) or infrared heating (e.g. Fiberforge & Fibercon process chain by Dieffenbacher GmbH [LINK18]). An overview of AFP systems with and without in-situ consolidation can be found in [JANS20, p. 25-29].

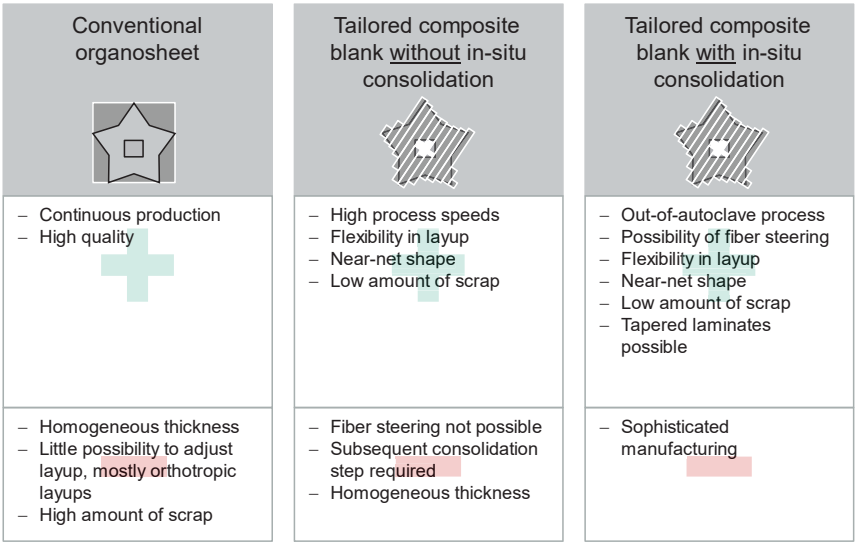

Figure 2.8: Comparison of conventional organosheets, tailored composite blanks without and with in-situ consolidation

Vergleich von konventionellen Organoblechen und Tailored Composite Blanks ohne und mit in-situ Konsolidierung

The use of thermoplastic composite materials is especially highlighted due to its automation potential as well as the reduction of steps in the process chain. Manual stacking of composite sheets or the laborious preparation for the autoclave curing by vacuum bagging is making the use of thermoset composites uneconomical for series production. A more detailed description of composite manufacturing processes as well as its advantages and disadvantages can be found in [NEIT14; FLEI18].

2.2.4 Interim conclusion

Zwischenfazit

The AFP of thermoplastic composites with in-situ consolidation is a promising manufacturing process for large series production of composite parts. Due to its out-of-autoclave process character, not only load-optimized structures can be produced in near-net shape, but also overall efforts can be reduced. However, its industrialization is still hampered by complex manufacturing conditions.

To find process windows for the in-situ tape laying process, several studies have been conducted in recent years. Amongst others, STEYER [STEY12], KERMER-MEYER [KERM15] or GROUVE [GROU12] profoundly investigate the tape laying process by listing and validating process models. These comprise, for example, of intimate contact development, autohesion, bonding, void consolidation, deconsolidation, thermal degradation, generation of residual stresses, crystallization, and melting kinetics [YASS18, p. 1686]. YASSIN AND HAJJATI [YASS18, p. 1685-1711] give an overview on the various research conducted in the field of automated tape laying with in-situ consolidation. This comparative overview also shows how many process studies have been conducted in order to find process parameters and to characterize the process. They confirm that the process window for the in-situ AFP process is narrow due to the high temperature and material dependency for gaining full consolidation.

To bridge the gap between idealistic process models and modeling techniques for realistic composite parts, novel methods need to be found. Motivated by the concept of I4.0 and the increasing availability of computing capacities, more and more data-driven modeling strategies have been implemented in the field of production engineering. They demonstrate the possibility to handle complex interactions by intelligently linking manufacturing data through the digital twin. To evaluate the application for the AFP with in-situ consolidation, the next section introduces this topic and examines applications in diverse manufacturing processes.

2.3 Industry 4.0 and the Internet of Production

Industrie 4.0 und das Internet of Production

The term *Industry 4.0* is contextualized with the initiative of the German Federal Ministry of Education and Research (Bundesministerium für Forschung und Bildung BMBF) empowering the German industry to face challenges by digitizing the value chain. This fourth industrial revolution aims to increase productivity by intelligent monitoring and decision making throughout the production process. Therefore, a comprehensive digitization of the product creation process needs to be implemented [BUND21]. The final report of the I4.0 working group which was supported by the German government states: “In the manufacturing environment, vertical networking, end-to-end engineering and horizontal integration across the entire value network of increasingly smart products and systems is set to usher in the fourth stage of industrialization – *Industrie 4.0*.” [ACAT13, p. 21]

To gain the interoperability, each production step is equipped with its own CPPS allowing to react on changes and to optimize independently. The resulting connectivity of entities enables a resilient and transformable production environment within and across each step of the value chain and of each hierarchy level. This is especially relevant during the production of the product itself. By matching each production process on its previous one or by learning from the overall product outcome, production processes can become more efficient and resources can be saved. [BREC11, p. 67; BAUE16; PENN19; STAR17, p. 169]

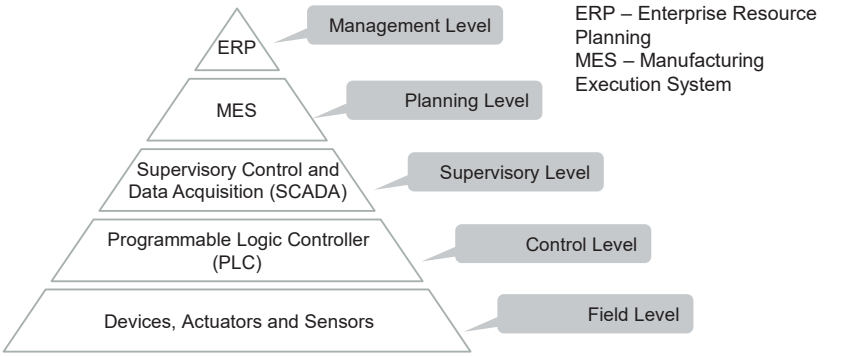

Figure 2.9: Automation pyramid, adapted from [DIN14]

Automatisierungspyramide in Anlehnung an [DIN14]

A production system is built upon a heterogeneous hardware architecture, which consists of different components of various manufacturers. The assessed data of these components are already gathered and displayed on the PLC and SCADA level. This can be seen as the major outcome of the third industrial revolution or Industry 3.0 and is represented by the well-known automation pyramid illustrated in Figure 2.9. It is the steppingstone of I4.0. Related to the IoT for the consumer market, the *Industrial Internet of Things* (IIoT) and the *Internet of Production* (IoP) summarize the importance of CPPS and the seamless integration of data and their semantics for process prediction. The acquisition of process data allows to fusion the physical and the virtual world. Systems can autonomously self-optimize and react on external forces by continuously increasing process knowledge and by exchanging methods and knowledge across domains. Figure 2.10 illustrates the various possibilities and domains of IoP within a production environment as described by the interdisciplinary research cluster *Internet of Production (IoP)* at RWTH Aachen University (cf. iop.rwth-aachen.de). The overall goal is not only to understand complex processes but also to decrease process development times.

In the context of production, autonomous systems are machines which can decide autonomously without being explicitly programmed or trained. Their sensomotoric skills allow to react on changing conditions so that they can be integrated into a flexible production environment [ROSE15, p. 569]. In contrast to automated systems, they do not rely on programmed sequences of action but can modify their own actions based on the given task or changes in the environment. Autonomous systems are key enabler for a matrix production. It is characterized as a production system being able to dynamically react on internal and external influences and to have an independent production pace [ECHS20, p. 2]. A prerequisite is that the production system has a holistic knowledge of its environment. This does imply sensor data and information from other sources, such as the geometry of the produced part, the required tools, the system configuration and more. The information collected during the product life cycle, including the development and production phase, with respect to that specific produced part

is gathered within its digital twin (see section 2.3.1). The implementation of autonomous systems can happen on various levels: from a complete autonomous production site to the autonomy of the manufacturing system and its specific process.

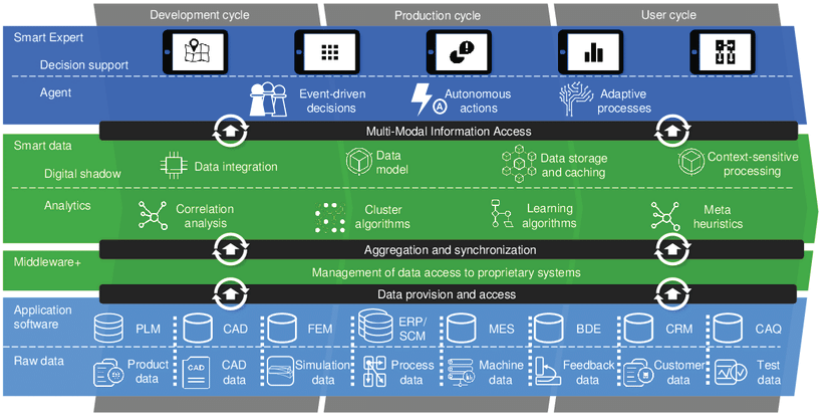

Figure 2.10: Internet of Production (IoP) [SCHU17, p. 121]

Internet of Production (IoP) [SCHU17, p. 121]

Besides the possibilities of the IoP for process prediction, there exist major challenges hampering the implementation in industry. From an information technology (IT) perspective, PENNEKAMP ET AL. [PENN19] derive three objectives for an infrastructure enabling IoP: seamless low-latency analysis of data, scalable data processing and storage, and secure industrial collaboration. These are challenges which emerge as soon as one decentralizes the data flow coming from diverse manufacturing systems, shop floors or even different companies. When coming to the manufacturing system and process level, such IT infrastructures become important if one relies on external data flows as an input for the processing. In this case, it is also necessary to standardize semantics and to find common ontologies to enable business to business (B2B) interoperability. However, even when keeping the system boundary only around the machine itself, open questions arise during the implementation of IoP, such as:

- What is the aim of using the process data?
- How do I prepare data for data analysis?
- How much data do I have? How much do I need?
- How do I handle huge amounts of data?
- How can data be exchanged between different domains (time and space)?
- What is the accurate data analysis method for my process?

Although there exists a lot of literature about methodologies for implementation as well as the required infrastructure (such as [JESC16; UHLE17; MEYE18; PENN19]), it is more and more necessary to show actual application cases. Section 2.4 gives an overview of various IoP implementation on process and system level indicating its potentials and benefits.

2.3.1 The difference between a digital model, shadow and twin

Der Unterschied zwischen einem Digitalen Modell, Schatten und Zwilling

To allow production systems to make decisions autonomously without human control, they need to rely on realistic models describing the current state of the process and forecasting the potential outcome of the interaction [ROSE15, p. 567]. Modeling and simulation technologies need to be forwarded from the R&D stage to the rest of the life cycle to react on unexpected events in real-time. A digital representation of the complete or individual stages of the life cycle of the physical system is called the digital twin. It is an important tool to enable the ideas behind I4.0 and the IoP and a logical consequence of the modeling and simulation efforts conducted in the past decades, as illustrated in Figure 2.11.

NASA was one the first using the term in their technology roadmap in 2010/2012 and describe it as followed: “A Digital Twin is an integrated multiphysics, multiscale simulation of a vehicle or system that uses the best available physical models, sensor updates, fleet history, etc., to mirror the life of its corresponding flying twin” [SHAF12, p. 11]. They describe it as “ultra-realistic”, which integrates all relevant data to predict outcomes of their activities. In literature, there circulate many definitions trying to address the essence of the digital twin.

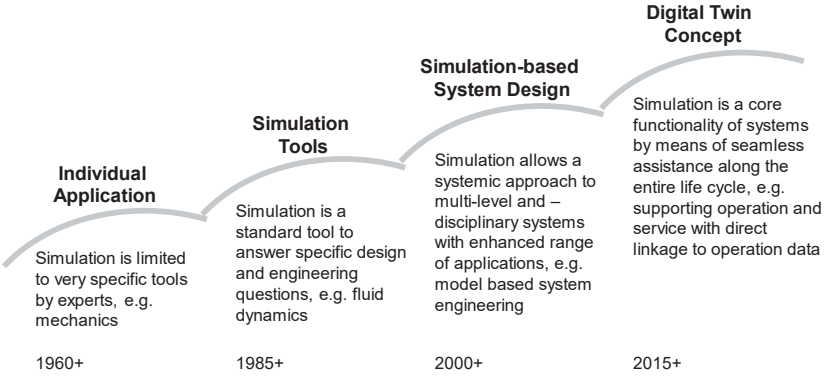

Figure 2.11: The Digital Twin as the next wave in modeling and simulation, adapted from [ROSE15, p. 568]

Der digitale Zwilling als die nächste Welle in der Modellierung und Simulation, in Anlehnung an [ROSE15, p. 568]

In the field of production engineering KRITZINGER ET AL. [KRIT18] and JONES ET AL. [JONE20] provide profound reviews of various definitions and case studies. KRITZINGER ET AL. state that the different levels of data integration between the physical and the digital object is crucial. For this reason, the authors separate between a digital model, a digital shadow and a digital twin as displayed in Figure 2.12. This study adapts the definitions of KRITZINGER ET AL. as followed:

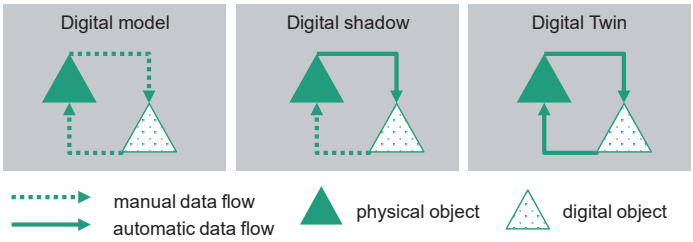

Figure 2.12: Differentiation of the terms digital model, digital shadow and digital twin by means of data integration, adapted from [KRIT18, p. 1017]

Abgrenzung der Begriffe digitales Modell, digitaler Schatten und digitaler Zwilling durch Datenintegration, in Anlehnung an [KRIT18, p. 1017]

Digital model. A digital model incorporates a description of the physical instance but without any automated data exchange between the physical and the virtual instance. Digital data can be altered according to the real object. However, data exchange is not automated and there is no direct effect when data is changing [KRIT18, p. 1017]. Examples for digital models are finite element method (FEM) or computer-aided design (CAD) representing the digital target design of the domain.

Digital shadow. If there exists a one-way data flow from the physical to the digital object, KRITZINGER ET AL. refer to it as a digital shadow. SCHUH ET AL. [SCHU16, p. 745] describe that the digital shadow gives insight into the past and current states of a process which may be used for predicting future outcomes. It is the minimum information required for exchanging data as units between different data silos. With this reduced information sufficient knowledge transfer is possible allowing fast computing times. The authors LIEBENBERG AND JARKE state: “Digital Shadows as a kind of approximate circumscription for complex Digital Twins” [LIEB23, p. 1]. The authors even compare it to the “Allegory of the Cave” by Greek philosopher Plato [LIEB23, p. 2].

Digital twin. According to the CIRP Encyclopedia of Production Engineering ‘‘A digital twin is a digital representation of an active unique product (real device, object, machine, service, or intangible asset) or unique product-service system (a system consisting of a product and a related service) that comprises its selected characteristics, properties, conditions, and behaviors by means of models, information, and data within a single or even across multiple life cycle phases’’ [STAR20]. This definition is added with the required integration of the data flow in both directions as described by GRIEVES AND VICKERS [GRIE17, p. 94], KRITZINGER ET AL. [KRIT18, P. 1017] and JONES ET AL. [JONE20, P. 43]. It incorporates that changes in the digital domain results in changes in the physical domain and vice versa (physical-to-virtual and virtual-to-physical, see Figure 2.13). This implies a continuous analysis of the target design compared to the actual instant outcome and the online compensation by metrology. The twinning rate hereby is the frequency of the data exchange and the twinning process of *change* → *metrology* → *realize* within the virtual or physical entity [JONE20, p. 42].

The literature analysis by KRITZINGER ET AL. and JONES ET AL. illustrate that most studies are conducted on a conceptional level. The term digital twin is often referred to the ideas behind a digital model and the digital shadow. It does not inherit feedback of the data to the physical object. They are mainly implemented for production planning and control for maintenance or engineering purposes, as well as for virtually visualizing specific conditions. However, the benefit of a digital twin especially lies in the autonomous reconfiguration of the systems. This can be beneficial, for example, for process control. Such high time-frequency domains require a fast computation by data driven approaches to allow online feedback. The authors point out that more case studies need to be conducted showing the benefits of a digital twin for sub stages of the product life cycle as well as for the entire life cycle. [KRIT18, p. 1020] [JONE20, p. 44]

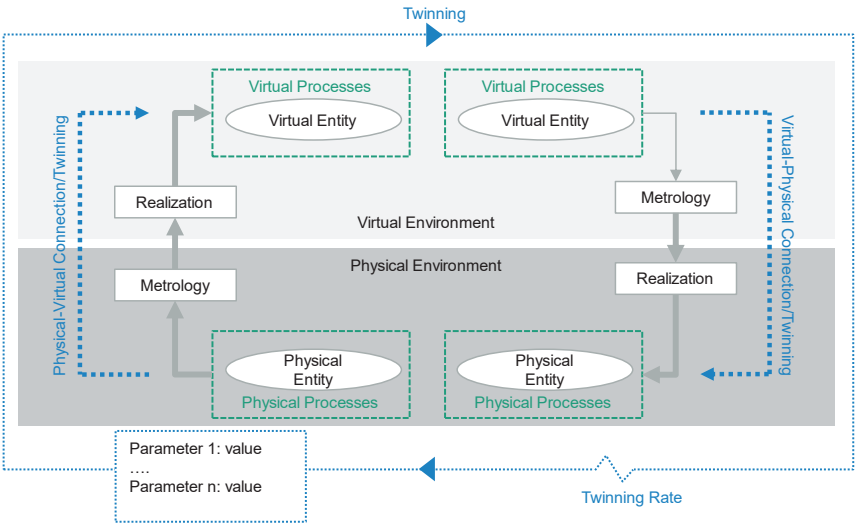

Figure 2.13: The physical-to-virtual and virtual-to-physical twinning process, adapted from [JONE20, p. 44]

Der physisch-virtuelle und virtuell-physische Twinning-Prozess, in Anlehnung an [JONE20, p. 44]

2.3.2 ISO 23274: A standard for a digital twin for manufacturing

ISO 23274: Ein Standard für einen Digitalen Zwilling für die Fertigung

In 2021 the *International Organization for Standardization (ISO)* published a norm for *Automation systems and integration – Digital twin framework for manufacturing* [ISO21]. It consists of overall four parts. It explains the general principles (part 1), suggesting a methodology of the reference architecture (part 2), the digital representations of manufacturing elements (part 3) up to the technical requirements for information exchange between entities (part 4). The norm references other useful standards and

gives examples which already have been implemented in an industrial production environment [ISO21, Part 4, Annex B-E].

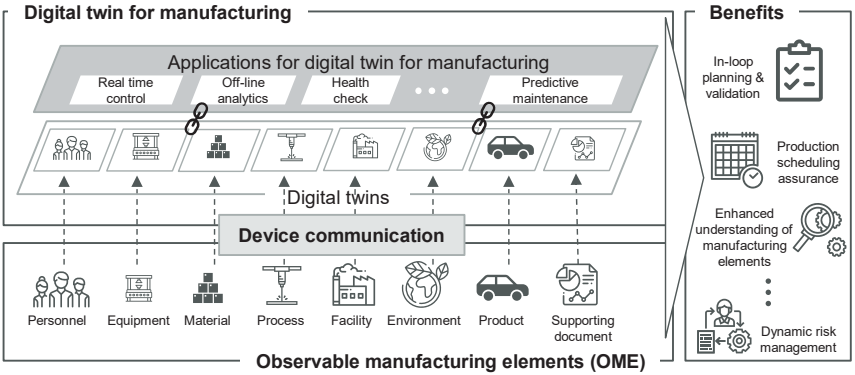

Figure 2.14: IoT framework for digital twins in manufacturing, adapted from [ISO21, p. 4]

IoT Rahmenwerk für Digitale Zwillinge in der Produktion nach [ISO21, p. 4]

It is the first document standardizing terms regarding the digital twinning in production environments and organizing the terms within a framework. Figure 2.14 illustrates the proposed *IoT framework for digital twins in manufacturing*. The norm describes the digital twin for manufacturing "as a fit for purpose digital representation of an observable manufacturing element with synchronization between the element and its digital representation" [ISO21, p. 3]. It entails only context-dependent and relevant data of the physical entity. Its aim is to improve the performance of production systems across the entire product life cycle and the complete process chain during manufacturing.

The important aspect of the norm is that it gives a universal picture as well as a clear definition of terms. In addition, it allows a standardized methodology for implementation by giving a reference architecture as a basis. Part 2 of the norm describes this reference architecture which is based on domains and entities. Four domains need to be identified with regard to [ISO21, Part 3]:

- User domain: analysis applications for humans and systems and decision making for manufacturing;
- Digital twin domain: synchronization of the individual observable manufacturing elements (OME) and their digital twin as well as hosting and updating of application and services;
- Device communication domain: data collection and monitoring of sensors in the OME as well as control and actuation,
- Observable manufacturing domain (OME): outside of the digital twin framework and monitored by the device communication domain.

Entities divided in systems and sub-systems manage and entail the functional entities (FE) of each domain. Figure 2.15 displays the digital twin reference architecture with

the *functional view* and how domains, entities, and functional entities are combined within one framework (see [ISO21, Part 2]). Based on this framework and choice of functionalities, the context-relevant information is selected (see [ISO21, Part 3]) and integrated with the most-suitable data exchange network (see [ISO21, Part 4]).

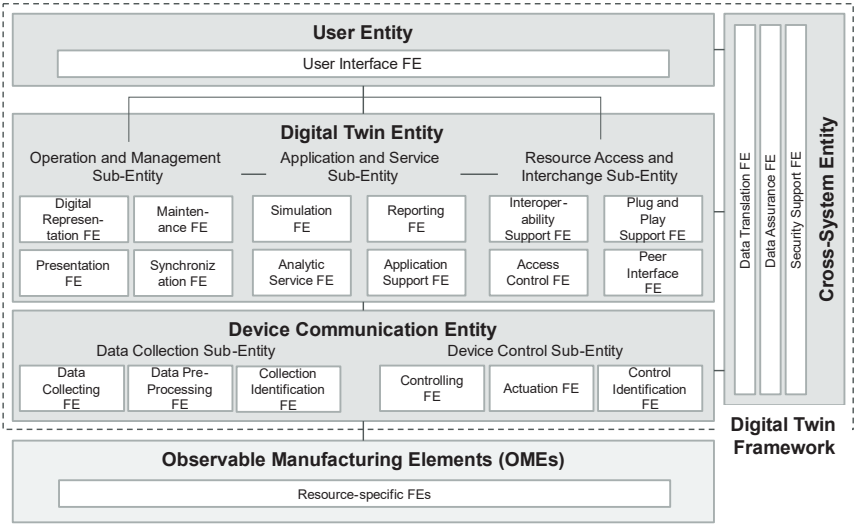

Figure 2.15: Functional view of the digital twin reference architecture as by [ISO21, Part 2]

Funktionale Ansicht der Referenzarchitektur des digitalen Zwillings, nach [ISO21, Part 2]

2.4 Data-driven process modeling

Daten-getriebe Prozessmodellierung

The overall goal of a process optimization is to achieve the required part quality at minimum costs. Dependent on the importance of process quality, product quality and productivity, the optimization strategy can be adjusted to achieve the desired goal. As illustrated previously, data is the foundation of the current industrial revolution allowing to intelligently optimize the manufacturing strategy. One strong enabler is the implementation of data-driven modeling strategies focusing on the manufacturing process itself. It can have two functions: either the goal is to analyze data in order to find correlations and relationships, or to predict the performance of processes [FISH20, p. 5]. Control systems of novel manufacturing systems already allow the continuous assessment of process data. However, the resulting high amount of data is often not efficiently used, as it is not clear how to use the collected information. This section gives an overview on data-driven modeling techniques used in manufacturing engineering for predicting and optimizing processing strategies. It introduces the variety of possibilities which are possible when implementing a digital twin incorporating relevant production data. Different model classifications are shown which distinguish between the sources

of the used data. Additionally, case studies in various manufacturing disciplines are presented with focusing on data-driven process modeling. The current state of art in industry and research of composites manufacturing and AFP processes is shown.

2.4.1 Model classification

Modellklassifizierung

There exist three kind of modeling classifications for data-driven modeling: white-box, black-box and grey-box (or hybrid) modeling. White-box models or mechanistic / first-principle models have been derived for centuries and are used to describe physical phenomena. They consist of analytical descriptions of a problem and, thus, require an understanding of the system. Typical solutions are analytical equations and FEM-models as they rely on these models. However, they lack in complexity being idealized by many assumptions. [BOHL06, p. 4; FISH20, p. 1; STEM20, p. 55]

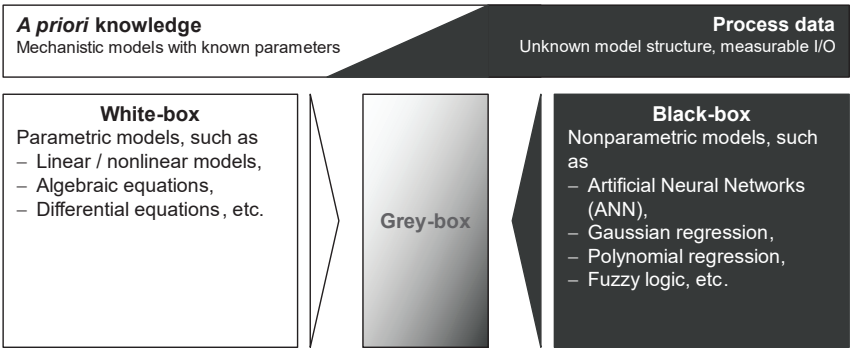

Figure 2.16: Concept of a grey-box model, adapted from [STOS14, p. 99; STEM20, p. 56]

Konzept des grey-box Modells, nach [STOS14, p. 99; STEM20, p. 56]

In contrast, a black-box model uses statistics to describe unknown phenomena. Such metamodeling does not inherit any physical knowledge and completely relies on the implementation and its methodology. They are also known as empirical models. Popular modeling techniques are, for example, artificial neural networks (ANN), polynomial regressions or Gaussian process regression (GPR, also known as Kriging) [YANG17, p. 4]. Although such algorithms have proven to be successful in many applications, such as in image recognition, their sole implementation in manufacturing engineering hamper. Model inaccuracies as well as its sensitivities regarding data granularity and availability indicate that its implementation has to be accurately managed. They can also only detect effects which are within the assessed data and cannot be transferred to other problems. [BOHL06, p. 4; FISH20, p. 2; STEM20, p. 55]

A solution for a data-based process prediction can be a grey-box model combining both modeling strategies, also known as hybrid modeling (see Figure 2.16). The main benefit is that it solves complex solutions with a higher benefit/cost ratio [STOS14, p. 88]. How both models interact can be done in various ways [FISH20, p. 10], such as:

- Proxy: one model replaces the other;
- Complement: both models are combined;
- Supplement: one model calibrates the other one by correction;
- Embedment: one model is included in the other one;
- Integrate: the output of one model is used as input for the other one;
- Inspiration: a model´s structure is provided by the other model.

This kind of modeling has often been conducted in process and chemical engineering to model complex process systems. A supplemented grey-box model, for example, allows an improved calibration of mechanistic models leading to higher prediction accuracies [FISH20, p. 10; YANG17, p. 5]. The benefit is that it accounts for an a priori knowledge by the present physical law as well as unknown effects detected by experimental data. The authors CHINESTA ET AL. [CHIN20, p. 108] establish a *Hybrid Twin* being described by the following equation:

$$\dot{X}(t;\mu) = A(X,t;\mu) + B(X,t) + C(t) + R(t). \tag{2.3}$$

$\dot{X}(t;\mu)$ is the desired model prediction of the state change dependent on time t and the set of (optimal) model parameters μ. $A(X,t;\mu)$ denotes the physical-based model and $B(X,t)$ the deviation model accounting for the difference between measurements and predictions. $C(t)$ accounts for the forced, external contributions driving the model to the targeted solution. The noise of the model is encountered in $R(t)$ which can be reduced by applying standard filters. The authors propose that this grey-box model can be applied either to calibrate physical models (calibration), to enable data-driven models in real-time (modeling), or to use it for process control (control). One of the major benefits of a grey-box approach is the reduced amount of required experimental data compared to a plain black-box model for an improved prediction [CHIN20, p. 108].

2.4.2 Data-driven modeling in production engineering

Daten-getriebene Modellierung in der Produktionstechnik

Due to the increased data aggregation of manufacturing systems in recent years, data-driven modeling has gained more and more importance. Especially for novel and complex production technologies, such as additive manufacturing or heavy plate rolling, it is used to predict outcome or even to implement a correction of the process online. This section gives an overview of different use cases in manufacturing engineering in the last couple of years. It illustrates how different models, from hybrid modeling to black box models, such as with the help of machine learning (ML), are implemented for different production processes.

Additive manufacturing. YANG ET AL. [YANG17] apply a grey-box model to predict the laser powder bed fusion (L-PBF) process of additive manufactured metal parts. The process is characterized by up to 50 independent parameters and is based on different physical phenomena, such as thermal and fluid mechanics. Consequently, the correlation between the right set of parameters and the desired mechanical properties is challenging. To reduce the complexity, the authors investigate a two-stage approach

of the grey-box model. In the first stage, they use a serial approach in which the black-box model estimates the errors of the white-box model. The white-box model is a parametric formulation of the problem available from prior knowledge. The black-box is derived by comparing the actual output with the output generated by the white-box model. Hereby, it estimates the relation between the input variables and the residuals by using the Gaussian process regression, also known as the kriging method. Based on the derived black-box model in the first stage, the second stage is built. Here, both models of the first stage are setup in parallel allowing a grey-box model which directly calculates the final solution. The white-box gives the basic solution. It is calibrated by the residual solution of the black-box model. The authors demonstrate the implementation for a metal L-PBF problem, where the relation between relative density and process parameters, such as scan speed and hatch spacing, is material and system specific. The authors propose to use a grey-box model to transfer results made from 6061 aluminum powder to AlSi12 powder without the need to create new models. The white-box model is based on a polynomial regression for 6061 powder having 177 data points. With a reduced number of 29 data points created by experiments the black-box model is constructed for AlSi12 powder with kriging. Seven further data points validate the grey-box model with a significant improvement of the estimated error. Consequently, the conclusion can be drawn that this approach is a reliable method to transfer knowledge from one case to the other.

The authors Moges et al. [MOGE21] further develop this approach by applying it to the prediction of the melt pool during L-PBF. They create an initial model by using data from computational fluid dynamics (CFD) simulation for a polynomial regression and calibrate it with GPR by experimental data. The validation shows an improved accuracy compared to a solely physical model. The authors also point out the importance of creating a common ontology in future work. Hereby, the accuracy of the hybrid model can be increased by integrating more than one physic-based models and by cross-lining data from various sources.

Heavy plate rolling. The authors Meyes et al. [MEYE18] investigate the use of ML algorithms to enable a decision support system for designing a heavy plate rolling process. Heavy plate rolling is a metal forming technology in which the thickness of metal sheets is determined by passing through work-rolls. This does not only enable different wall thicknesses across the same metal sheet, but also affects the local mechanical characteristics by influencing the grains. Hence, the process is characterized by a complex interaction between various process and part quality parameters. The database with over 1’000’000 single passes for the ML algorithm is created by using a mathematical model. The ML model uses reinforcement learning with a reward-function taking target grain size and wall thickness into account. After 20’000 iterations of learning, the algorithm can improve the process by suggesting less passes than previously. The authors hereby give a proof of concept that ML enables an efficient process design.

Injection molding. The increasing use of injection molded parts even for high performance applications as well as the process` strong dependency on geometry demands

an efficient process setup. Currently, the setup is done based on trial and error resulting in many experiments, material waste and costs. Temperature and pressure variations within the mold are highly transient and non-linear making it difficult to develop physical models. Several studies have been conducted to minimize these efforts by using data-driven modeling approaches.

GAO ET AL. [GAO14] develop an online quality control system for predicting the quality of injection molded parts. They assume that solely the knowledge of the current state of the process is required. By embedding commercial sensors as well as a prototype multivariate sensor (MVS) for measuring pressure and temperature in-situ, velocity and viscosity are calculated by mechanistic modeling. Quality characteristics, such as part dimensions, are derived for future production runs by training a data-driven model. This is implemented by a support vector regression (SVR) machine correlating the online process measurements with the offline measured part dimensions. The authors show that the predicting accuracy of using a MVS instead of commercial sensors is significantly increased to over 90% [GAO14, p. 496]. They conclude that the right choice of sensors can enable efficient data-driven quality forecasts.

The authors TERCAN ET AL. [TERC18] suggest a ML approach with ANN to predict quality criteria. To avoid cost intense experiments, a dataset is created by simulations and experiments with a design of experiments (DoE) having 6 parameters resulting in 64 test points and a central point. The simulation data is used to pre-train the ANN which is then adjusted by the experimental data. The ANN is composed of three hidden layers and a hyperbolic tangent activation function. With this hybrid approach the authors demonstrate an accurate predictability despite the low number of data points as well as a reduced number of training iterations for the ANN. Hereby, they address the challenge that the implementation of ML algorithms requires a high amount of data points which is not feasible in a costly manufacturing environment.

Machining. Machining manufacturing technologies, such as milling, turning or drilling, have been mostly investigated in the context of I4.0. Amongst others, the authors ALTINTAS AND ASLAN [ALTI17] improve the robustness of online condition monitoring of the tool and the cutting process by feeding information of a virtual simulation directly into the process. The virtual machining simulation estimates process outcomes, such as cutter-workpiece engagement and cutting forces, along the toolpath. This stored information are retrieved from the control and monitoring system during the actual machining process. The authors integrate an adaptive control for the cutting forces based on CNC inherent force sensing of the feed drive motor current. By having this virtual feedback the system can compare the real values with the virtual ones and thereby avoid false failure detection by the system. Vice versa, the virtual simulation is continuously calibrated by the real coefficients of the process. The authors validate their method experimentally and demonstrate that processes can become more robust.

A similar approach is conducted by the authors KÖNIGS AND BRECHER [KÖNI18]. They develop an online material removal simulation which compares real, sensor-based pro-

cess data with data from a CAD-CAM-NC (CAM: computer aided design; NC: numerical control) based virtual machining simulation. The target function is to reach the quality requirements according to DIN 1101. The authors propose that this method can reduce random effects within a series production, such as thermal variations, tool wear or clamping effects, which cannot be mapped by a-priori simulations. To account for these effects in real-time, the virtual machining simulation is extended with look-up tables created by a FEA model for each used cutting tool and position in the process. During actual processing the look-up table is perceived by using the current axis encoder position. The positional delta is then fed back to the virtual simulation. The gained quality is estimated after manufacturing with a straightness test. A metrology data point cloud of the desired quality is projected on the manufactured part geometry and compared to the actual position points of the encoder fitted by least squares. The authors conclude that the proposed methodology is a starting point for a process-parallel workpiece quality estimation. By including a cutting force model and additional relevant information, the performance of the model as well as the quality according to ISO 1101 can be further optimized.

To show the benefits of cyber-physical manufacturing, the authors CAI ET AL. [CAI17] build a digital twin for a 3-axis vertical milling process. Two main information sources are categorized into the manufacturing data and sensor data. Whereas the first gathers the process parameters information coming from the machine, the sensor data comprise all the actual measurement data acquired during processing. By combining both, a virtual twin for online process monitoring, offline process analysis and simulation as well as for management decisions is derived [CAI17, p. 1033]. Its goal is to improve the performance of the physical milling machine. The authors give an example how the given data can be connected and integrated within a database framework. For the purpose of a data-driven model, they use an experimentally derived linear regression model to forecast the surface roughness for the specific machine. The authors point out that there exists potential to apply more sophisticated data-driven approaches to optimize the processing of the physical machine such as by ML.

A data-driven digital twin framework for machining has been recently developed by the authors GANSER ET AL. [GANS21]. They investigate an IIoT-based implementation oriented towards the ISO 23247 [DIN97] and the lambda architecture for big data which has been proposed by MARZ [MARZ15]. Aim of the authors is to enable a cross-system solution incorporating process planning, manufacturing and quality assurance. Along the four domains of the ISO 23247, they explain the creation of a digital twin for cutting processes with the focus on IT infrastructure. Two use cases, one for process design and another one for quality prediction during milling of a blade integrated disk (BLISK) demonstrator, are chosen for demonstration. For the first one, the authors manage to decrease computational time by parallelizing computer aided (CAx) simulations on a virtual machine and centrally storing the results. This fast computation within an hour allows a possible integration in common CAD/CAM software. In the second case, the authors use extensive process data acquired during the manufacturing and quality

testing of a BLISK demonstrator. By transferring the obtained machine data in workpiece condition data, they virtually visualize process parameters and the predicted deflection of the final part. The evaluation of the quality prediction is conducted with a coordinate measurement machine. Good agreement with the model is demonstrated. In summary, the study by GANSER ET AL. explain in detail a method for implementing a specific digital twin. However, it also demonstrates the necessity to have in-depth knowledge of computer science to allow the application of a digital twin framework.

2.4.3 Data-driven modeling in composite manufacturing

Daten-getriebene Modellierung in der Faserverbundfertigung

Manufacturing composites differs from conventional production technologies, such as machining, that the material itself encounters additional degrees of freedom. It is not only possible to engineer the composite material by selecting the fitting matrix and fiber, but also to design the workpiece by adding layer by layer to form a laminate. However, the benefit of an increased freedom of design is accompanied with the drawback of increased complexity during manufacturing. Extensive research has been done to model the multi-physics and multi-scale nature of composites and their manufacturing technologies parametrically, either by analytics or statistics. However, these models are often not flexible and cannot be easily adjusted to other circumstances, e.g., to a different material system. The sophisticated abstraction of the problem implies many assumptions which cannot be held in an industrial production environment. A solution is the increasing amount of available data within the context of I4.0. Data analytics, from conventional statistics to ML, could pave the way towards a more efficient process design of composite manufacturing since it enables the handling of increasing process complexity. Only a few studies are conducted which implement a data-driven approach or a data-driven digital twin within the composite manufacturing industry. Some of these case studies are presented in this section.

Overmolding. HÜRKAMP ET AL. [HÜRK20] combine FEA with ML in order to predict the interface bond strength between the organosheet and the injection molded components in the overmolding process. Overmolding organosheets is a popular manufacturing technology allowing the large-scale production of composite parts. After an organosheet is heated and transferred to the mold, it is thermoformed and overmolded by injection molding. Usually, the same matrix systems are used to gain a bond by interdiffusion (healing). To yield optimal process conditions, the authors propose the creation of digital twins for inline quality inspection built by data-driven approaches. HÜRKAMP ET AL. create training and test data by calculating 100 full-scale temperature profiles in the bond. The sampling space is hereby created by Latin Hypercube Sampling to achieve a reasonable database. Six different machine learning algorithms are benchmarked for two use cases, e.g. decision tree random forests and polynomial regression, to build the data-driven surrogate model. Evaluation criteria are the error (R^2, mean squared error (MSE), mean MAX error, mean absolute error (MEA)) and the run times for training and prediction. By comparing the computed time in which interface temperature is above melting temperature with the experimentally evaluated interface

bond strength, the authors cluster the results in poor, good and excellent. This allows a decision making about the quality of the parts. The authors conclude that their approach creates a suitable digital twin for a fast offline analysis of the process conditions. Thereby, the model can be used to predict properties of the bond, to visualize the data parallel to the manufacturing according to a quality cluster or even to be used for automated control. Further optimization of the model is possible, for example, by including mechanistic models to reduce local singularities and to avoid nonphysical results.

Resin transfer molding (RTM). The RTM process allows a large-scale series production of composites parts. A stacked textile preform is inserted into a press and then impregnated by injecting resin and curing agent under pressure. After being cured by applying temperature, the composite part can be deformed out of the RTM press [NEIT14, p. 366]. The authors QUARANTA ET AL. [QUAR18] implement a hybrid digital model in order to forecast the mold filling process during RTM. A physical model by combining the commercial *PAM-RTM* software (ESI Group, France) with a proper generalized decomposition (PGD) precomputes the solution offline at different stages of the RTM process. This simulation assumes a homogeneous permeability within the preform. A comparison with actual camera-based measurements of the flow front is used to identify the targeted permeability. The actual measurements indicate that the assumption of a uniform permeability does not hold in areas which are close to the mold boundary. By using the data-based technique of dictionary learning for the measured deviations, the authors enable the calibration of the physical model which shows good agreement with experiments. The underlying mathematical equations for the proposed hybrid twin is presented in detail by the authors CHINESTA ET AL. [CHIN20].

Filament winding. Filament winding is a manufacturing process creating composite rotationally symmetric parts for structural applications such as in the space, marine or energy sectors. Due to its requirement of carrying high loads, the production process needs to ensure the structural integrity of the part, especially in the case for variable angle tows (VAT). However, uncertainties arise such as the misalignment of tows or inconsistent tow tension during processing. In general, safety factors are included to account for these imperfections. However, they do not exploit the full potential as information is lost. The authors WANG ET AL. [WANG20] develop a data-driven model which integrates manufacturing uncertainties into the structural design of the part by a reliability-based design optimization (RBDO). FE simulations of different designs of composite cylinders with VAT are conducted to create initial datasets. This data feeds the GPR / Kriging metamodel with the aim to decrease the computational costs for finding the optimal winding angle compared to FE simulations. After being updated for finding a first optimal design, the RBDO procedure is applied and integrates the manufacturing variations. The authors show that their novel implementation allows a fast optimization of various cylinder designs and enables the integration of uncertainties. Nevertheless, an experimental validation and the integration of actual manufacturing data needs to be conducted in future work. [WANG20]

Automated Fiber Placement (AFP). The AFP process does not only comprise the laying of thermoplastic tape by in-situ consolidation (as focused in this thesis), but also

the laying of dry-fiber or thermoset pre-impregnated tape. Several studies have investigated the use of data-driven modeling strategies to enable a quality forecasting for these processes. The authors CHINESTA ET AL. [CHIN14] introduce the use of PGD to model thermo-mechanical effects of thermoplastic laminates, such as residual stresses, produced by the AFP process. This numerical method allows to calculate the temperature field for any set of parameters. It also allows to include new sets of parameters and variables by adding new extra coordinates into the PDG equation such as different fiber orientations [CHIN14, p. 86]. Next to the thermal modeling, a PDG-based approach is implemented to evaluate the thermo-elastic loads during tape laying and its effects on the residual stresses. The combination of both allows the estimation of the stress distribution for a representative volume within the laminate.

ZAMBAL ET AL. [ZAMB] develop a digital twin for the fiber placement of dry-fiber tape with the goal to estimate the effects of the manufacturing process on the mechanical performance. During the AFP process, defects such as gaps and overlaps occur which negatively influence the structural performance of the part. The authors integrate sensors for measuring fiber orientation as well as depth data for data acquisition. By synchronizing the data with the machine data, they can extract features of the process, such as the detected defects. To derive mechanical properties in a fast manner, they propose to use an ideal FE simulation (as designed) as baseline. The detected defects are then inserted by a knock-down factor which depends on the severeness of the defect. The latter is derived either by analytical models or by FE simulations for defects requiring a detailed analysis [ZAMB, p. 807]. The approach is validated by experiments. After each laid layer, the sensors measured the fiber orientation as well as the depth for a complete layer. The evaluated sensor data is then matched with the manufacturing as well as the (ideal) simulation data. The authors point out that predictive models are required to enable an automated decision-making process. This then allows an online process optimization if a defect is detected.

Similar to the previous study, various studies investigate automated defect detection methods based on camera vision and ML for the AFP process. Amongst others, these are [BRÜN17; SACC20; SCHU20; MEIS21; BRYS22]. These authors present data-driven defect detection and quantification methods during processing or in-between. These are especially promising for quality estimation and assessing data for model validation. As they do not focus on process modeling itself, the details of these studies are not presented in this thesis.

Several studies handle the topic of using control strategies to facilitate AFP processing which may also be classified as a data-driven method. Within this thesis, process control based on control theory is not highlighted. Most applications do not enable a data-driven optimization of the model itself but rather the adjustment of process parameters. Nevertheless, a couple of studies are presented as only few studies exists for AFP showing the vague differentiation between control and data-driven modeling. KÖLZER [KÖLZ08] presents a first control strategy for LATW based on two PI controller. To receive temperature data of tape and substrate the author integrates a measurement

system with multi point radiometer and pyrometer proving its beneficial usage for online process control. The authors DI FRANCESCO ET AL. [DIF17] propose an open-loop control of the heater power as a function of layup speed during the LATW process. They experimentally validate the developed semi-empirical model, but also reveal its limitations regarding different ply orientations, thicknesses and complex geometries. A model-based control strategy has been investigated, but not yet fully validated in the EU-funded project *amblifibre* [ZAAM21b, p. 4]. To increase control accuracy and speed a novel control strategy is recently developed by KUKLA [KUKL22] for the LATW process. To improve process control with higher frequencies as well as improved accuracy, the author validates the usage of a thermal image camera as sensor.

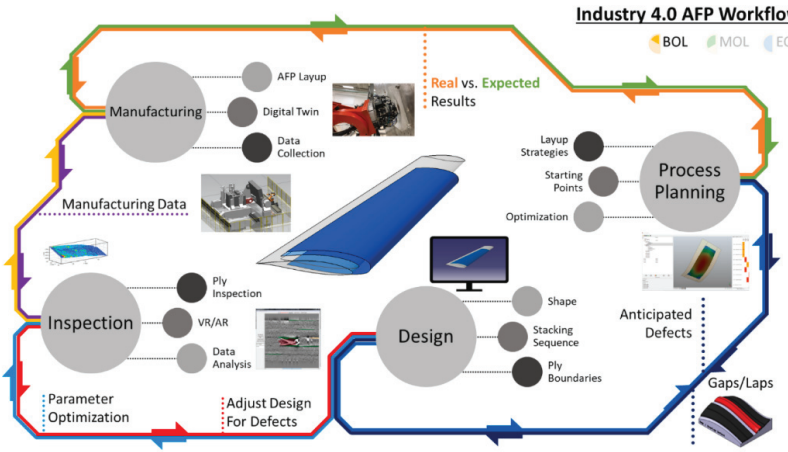

Figure 2.17: Industry 4.0 workflow as proposed by the University of South Carolina McNAIR Aerospace Center [BRAS21, p. 2]

Industrie 4.0-Workflow, vorgeschlagen vom McNAIR Aerospace Center der University of South Carolina [BRAS21, p. 2]

In contrast to the previously listed isolated solutions, a holistic approach within a novel I4.0 AFP workflow is developed by the *University of South Carolina McNAIR Aerospace Center* (see Figure 2.17). It entails the connection of pillars which have been investigated as isolated pillars of the AFP process so far: manufacturing, process planning, design and inspection. BRASINGTON ET AL. [BRAS21] provide a state-of-the-art literature review of AFP systems and processes and contextualize these investigations in the context of Industry 4.0. The authors point out the heterogeneity of this manufacturing technology and the many interacting influences of the system, the part and the process. AFP is a multi-physics problem combining, amongst other, micromechanics, viscous flows, curing & crystallization kinetics, fracture mechanics and heat transfer [BRAS21, p. 13]. To tackle these challenges the McNAIR Aerospace Center has started multiple research topics. For example, the McNair team develops a computer-aided process planning software using data-driven methods. BRASINGTON ET AL.

[BRAS22] apply surrogate models to optimize input parameters or laying strategies during the process planning phase as well as predict potential defects. Gaussian process, support vector, and random forest surrogate models are chosen for investigation. The experimental validation proves the feasibility of surrogate modeling, but also indicate the challenges of the multi-physical problem of AFP processing.

2.5 Conclusion and derived need for action

Zusammenfassung und Handlungsempfehlung

The analysis of the state of the art in research and industry highlights the basis of the two pillars of this thesis: the AFP of thermoplastic tapes with in-situ consolidation and data-driven approaches for process modeling within the IoP. The literature analysis of AFP processing illustrates the potential of this manufacturing technology to enable an automated cost- and resource-efficient production of tailored composite parts. However, due to its character of locally melting the thermoplastic matrix and creating a phase change, finding the right set of process parameters can be difficult and time-consuming. The use of physical-based models, such as analytical derivations or FEM, either relies on a sum of idealized assumptions or is computationally expensive. For this reason, novel methods need to be found to bridge the gap between idealistic process models and modeling techniques for realistic composite parts.

By introducing the topic of I4.0 and the IoP its suitability for modeling the AFP process is evaluated. Application cases of various manufacturing technologies are presented showing the vast amount of methodologies suitable to describe a realistic modeling. Special focus is to minimize computational time to enable an online digital twinning. As stated previously, a digital twin implies the parallel execution of a virtual simulation and real processing. Like approaches of control theory, such as model predictive control, the aim of the digital twin is to optimize the process online based on given models and data. However, the used models for digital twins are more sophisticated as they encounter much more information, such as the history of the part, the manufacturing system etc. They also entail continuous model optimization for improved prediction accuracy the more data is available. This allows an accurate modeling of changing boundary conditions with the aim of being integrated into series production.

In the field of AFP, little work has been done in the post-process digital analysis of the manufacturing processes. Most studies deal with the analytical representation of the occurring mechanisms, such as by Weiler et al. [WEIL18], simulation of the process by FEA, such as by Stokes-Griffin et al. [STOK15], control strategies as by Kölzer [KÖLZ08] or the integration of sensors during the manufacturing process. Most of these studies validate their models within specific test environments making a transfer of these results difficult. The implications caused by material or part geometry variations are rarely investigated but are necessary for a flexible large-scale production. Schulz et al. [SCHU19b, p. 28] give a general concept of how an adaptive tape placement could look like based on continuous data acquisition along a complete process chain. Schäkel et al. [SCHÄ18, p. 7] visualize path-dependent sensor data to identify

process insufficiencies during the tape winding of thermoplastic composite pipes. First applications of using these data for sophisticated data-driven modeling of the AFP process are demonstrated by CHINESTA ET AL. [CHIN14] and ZAMBAL ET AL. [ZAMB].

Although the benefits of digitization were validated in other manufacturing technologies, as shown in section 2.4, there currently exists only little literature combining the existing models with a digital representation and analysis for the tape laying process within a digital twin. Many isolated, highly specified solutions are available but lack in their applicability since their results cannot be easily transferred to other conditions, such as different materials, geometries or production setups. Consequently, there exists a gap to draw a holistic picture of the AFP process and to combine both pillars: AFP processing and the IoP.

3 Objectives, tasks and modus operandi

Zielsetzung, Aufgabenstellung und Vorgehensweise

3.1 Problem definition and target

Problemdefinition und Ziele

Within the movement of I4.0 research has shown that by using effective metrology and data analytics it is possible to handle complex manufacturing processes. Therefore, transferring these methods to processing thermoplastic composites is promising. In the case of thermoplastic UD-tape deposition the challenge is to handle the high degree of freedom resulting from fiber, matrix, desired geometry, used manufacturing system including source of thermal energy and the variety of process parameters. For this reason, hidden production-related defects and failures are likely. The vast number of influencing factors cause complexities which likely reduce production robustness. An additional disadvantage is, that a part`s quality is mainly quantified in a subsequent process step by non-destructive evaluation (NDE) techniques, such as ultrasonic, radiographic and thermographic methods [FLEI18, p. 617-619; DENO18, p. 241]. This does not only result in increased production time, but also in long, non-agile decision making.

The following two problem statements are derived based on the findings of chapter 2:

1. Previous process models focus on an idealized process view in the local process area around the nip-point.
2. There is a complex process characterization depending on the material, production system and geometry of the component.

A novel methodology is required to decrease time-consuming process optimization strategies regarding quality and productivity within a flexible production. This thesis aims to create a digital twin which predicts process quality of the AFP with in-situ consolidation of tailored composite blanks. Purpose of the digital twin is to simplify the upscaling of the production technology by deriving manufacturing strategies allowing a realistic modeling of the final part (see Figure 3.1).

The thesis targets *quality indicators* and *production indicators* to assess process quality and productivity for a high-volume production. Quality indicators, as describes in section 2.2, for example are consolidation, crystallization, or residual stresses. These factors are production-related effects resulted by process parameters and assessed by temperature measurements. As suggested by literature, it is assumed that temperature evolution is the main mechanism influencing the quality indicators and thus process quality. By creating a digital twin of the process temperature, a global historic representation is possible. This especially should include the repeated local heating resulted by the additive character of the AFP process (reconsolidation effect). By displaying historic heat evolution across the laminate existing process models can be combined and fully exploited. By subsequently analyzing the modelled and assessed data conclusions regarding quality indicators are made and a realistic representation

of the part can be drawn. Production indicators are, for example the overall equipment efficiency (OEE) taking also process specific parameters, such as main and auxiliary times, into account. This data is included into the digital twin to derive optimized manufacturing strategies also regarding productivity. This defines the overall target:

Thesis target: Part-oriented process planning with increasing productivity of the production of tailored thermoplastic composite blanks with the AFP process with in-situ consolidation.

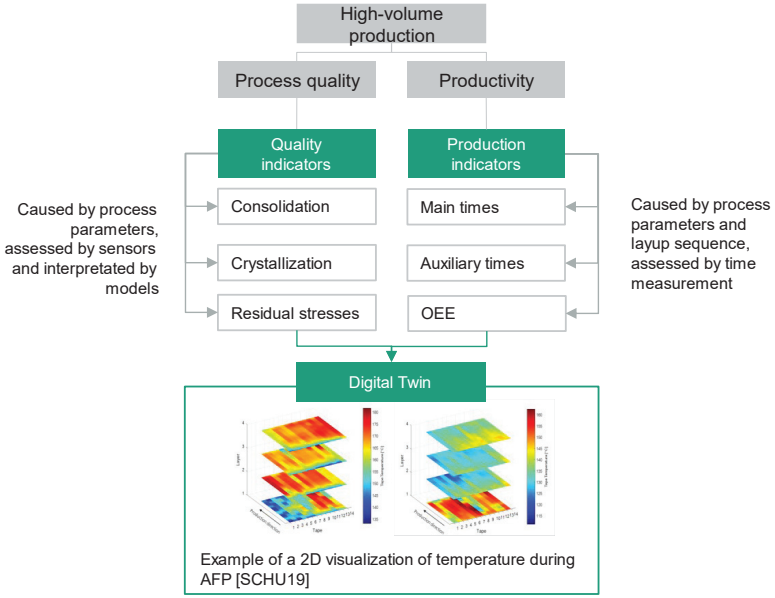

Figure 3.1: Enabling high-volume production of composite blanks by digital twin modeling

Ermöglichung der Großserienproduktion von Organoblechen durch den Digitalen Zwilling

The result of the thesis is a digital tool for evaluating process quality and simplifying large-scale production of tailored thermoplastic composite blanks. The thesis states the following research hypothesis:

Research hypothesis: A digital twin for in-situ tape laying of thermoplastic tapes enables a part-specific process strategy for upscaling.

The research will be oriented along three research questions.

***1st research question:* How can a digital twin enable a component-specific, realistic process view of tailored composite blanks?**

In order to evaluate the quality indicators of a tailored composite blank, the assessed process data needs to be combined with selected analytical simulation models in order to quantify process quality of the laminate based on defined target values. For quality

indicators, this involves the selection and aggregation of models to create a realistic representation of the part and of the process.

2nd research question: What factors influence component-specific productivity during the AFP with in-situ consolidation of tailored composite blanks?

To evaluate realistic productivity indicators a part-oriented calculation must be developed. This implies the performance estimation of the targeted manufacturing system based on analytical models as well as its validation. Special focus is on the main and auxiliary times during processing. It is assumed that these times affect nip-point temperature as well as cooling behavior of the material and, thus, also influence quality indicators of the process.

3rd research question: Which manufacturing strategies can be derived using the digital twin to implement component-specific process strategies to increase productivity?

The question arises, if it is possible to draw a global representation of the heat development during the production of thermoplastic composite blanks through a digital twin. By including productivity sensitive information, such as main and auxiliary times, an optimization of the target value (e.g., minimum laminate temperature during tape placement) could be possible. Consequently, it needs to be investigated how the digital twin allows the derivation of optimized manufacturing strategies for different production setups, such as different laminate geometries. The overall target should be to use the digital twin to enable high-volume production scenarios.

3.2 Implementation

Umsetzung

The implementation, application and validation of the digital twin to enable a high-volume production of thermoplastic tailored composites blanks by AFP is structured as followed: *Chapter 4* explains the selection of quality indicators and models for the creation of the digital twin for the AFP process. *Chapter 5* experimentally validates the digital twin of the process. *Chapter 6* deals with a component-specific productivity calculation and validation for the targeted PrePro2D® system. *Chapter 7* combines both, quality and productivity indicators, to derive manufacturing strategies for the upscaled and flexible production of tailored composite blanks. In the following the details of the methodology is explained:

The digital twin (chapter 4 & 5). The digital twin is constructed to allow the analysis of actual process data recorded during manufacturing as well as to predict the complete process in advance. It gives insight into the past, current and future states of the AFP process. The extraction of features, such as quality indicators, by interpretating the data is conducted on different data types as defined here:

1. First order data: actual measured data, such as temperature measurements within the local process area around the nip-point

2. Second order data: theoretically derived data based on assumptions and on analytical or numerical calculations.

The digital twin can fulfill two purposes. By using the measured data acquired by sensors, such as the thermographic camera during AFP, the digital twin is used for in-depth process analysis. By assuming certain conditions, such as a constant nip-point temperature, it is also used for process forecasting for different layup and geometries without needing experiments. A calibration of the latter can be achieved by connecting the measured process data with the data for forecasting. This enables a more realistic modeling.

Chapter 4 reveals the details of the digital twin. An in-depth analysis of existing physical-based / analytical models including their given assumptions is conducted to evaluate the feasibility of the models for the targeted digital twin. An experimental analysis of the status-quo illustrates the need for novel modeling strategies by showing the gaps of conventional ones. It is postulated, that time is the relevant design variable to optimize manufacturing strategies regarding productivity as well as quality. The design of the digital twin is explained and a first idea for the creation of an interactive visualization is drafted and discussed. Existing analytical models are selected and applied within the digital twin to predict quality indicators. To validate the derived digital twin, experiments are conducted as presented in *chapter 5*.

Target production system and productivity evaluation (chapter 6). The Fraunhofer Institute for Production Technology IPT investigates the AFP process since the late 1980s and has designed several system technologies, such as the current PrePro3D and PrePro2D®, for the winding and laying of thermoplastic tape. The targeted production system is the PrePro2D® system. It consists of a machine frame with a gantry system and a moving heated rotary table. The tape placement head is positioned on the gantry system enabling the layup of tapes as the rotatory table moves beneath it. Initially designed by using infrared as a heating source, the current version has a diode-laser built-in for enabling the in-situ consolidation. This stand-alone tape laying systems allows the automatized production of near-net-shaped, tailored composite blanks out of UD-tapes with in-situ consolidation. Further impressions of the technology can be found in the literature e.g. by JANSSEN ET AL. [JANS20, p. 101-103].

Based on the finding of JANSSEN ET AL. [JANS20], increasing productivity is not only a question of increasing tape deposition rates but also increasing the *overall equipment effectiveness* (OEE) which is calculated by multiplying availability, performance and quality. For this reason, the work by JANSSEN ET AL. will be further developed by integrating additional information of component-specific production comprising of system, process and part design, detailed in Figure 3.2.

Chapter 6 gives insight into the sensitivity of the three design aspects towards productivity. A tool is presented and validated which allows to estimate overall productivity with respect to the specification of the component. This allows a first derivation of recommendations for upscaling.

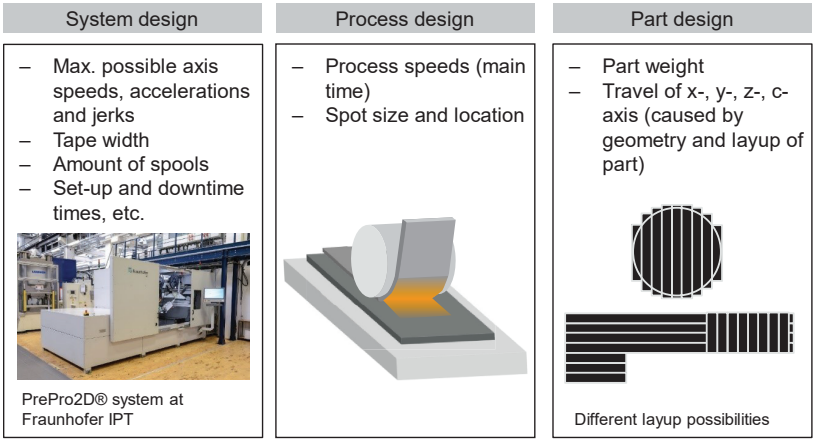

Figure 3.2: Aspects of the PrePro2D® system influencing productivity

Aspekte des PrePro2D®-Systems, die die Produktivität beeinflussen

Manufacturing strategies and implementation (chapter 7). To optimize the trade-off between quality and productivity component-specific manufacturing strategies are derived. With the help of the digital twin and the productivity estimation tool, the effects of increased process speeds and novel layup sequences are possible prior to extensive experimental testing. To simplify future implementation, the methodology is described in a step-by-step manner and incorporated into the ISO 23274 standard. This shows the additional steps which need to be taken to simplify usage and user acceptance. This is essential to industrialize this manufacturing technology.

4 A digital twin for process analysis and prediction

Ein Digitaler Zwilling für die Prozessanalyse und - vorhersage

This chapter deals with the creation of a digital twin to enable a tool for part-oriented process analysis. Aim is the upscaling of the AFP process by the following steps:

1. Enhancing existing process models to achieve a more realistic representation of the complete laminate.
2. Development of processing strategies by part-oriented process optimization (see chapter 7).

The chapter is structured according to the development of the digital twin. First, the current models of the AFP process are presented and discussed. A status-quo analysis of the AFP process reveals the implications of current processing on the temperature development within the laminate and the need for a digital twin as well as novel hardware. A program allowing the three-dimensional visualization of the laminates process parameters is drafted and discussed for future implementation. After the selection of the relevant models and assumptions, the creation of the digital twin is explained. This is the basis for the experimental investigation in chapter 5.

4.1 Analytic modeling of the AFP process with in-situ consolidation

Analytische Modelle für den AFP Prozess mit in-situ Konsolidierung

The analytic modeling comprises the description of a problem within a mathematic formulation. It entails the breakdown of the problem to its essentials including the required assumptions to enable a quantitative calculation. A model is an idealistic representation of a real entity. In production engineering, process models are created which describe the relationship between process parameters (e.g. the settings of the machine) and the results (e.g. the part quality). Depending on the desired target value, process optimization can be conducted or even integrated into online process control of the production machine. Due to the increasing availability of computing power, the initial motivation to reduce computing time mitigates and the necessity of underlying assumptions lose its importance. The ongoing digitization of production environments, as introduced in section 2.3, results in a twirling of model and reality allowing to setup new approaches for more holistic process optimizations.

To profoundly understand the physics of a manufacturing process, formerly derived models and underlying assumptions need to be studied. For this reason, this section gives an overview of the various process models of the AFP process with in-situ consolidation. An emphasis is the modeling of the temperature evolution during the AFP process as it is the basis for estimating quality characteristics during processing, such as the bond strength. As can be seen after this section, most of these models focus on the instantaneous processing moment, the nip-point area of the AFP process. A major target of this section is to reveal the idealization of the models and, thus, the need to transfer the idealistic models to a more realistic production environment.

4.1.1 Transient heat transfer model

Instationäre Wärmeübertragung

In general, thermal transport is described by four modes: conduction, convection, phase change and radiation [BEJA03, p. 2]. All of these are apparent in the laser-assisted AFP process, as illustrated in Figure 4.1. Many studies have evaluated which of these modes have the most significant effect on the process in order to simplify the heat transfer model. The authors YASSIN ET AL. [YASS18] and ORTH ET AL. [ORTH17] present comprehensive reviews on previous modeling investigations of the automated layup processing. Prominent studies in this area are [SONM97b; GROU12; STEY12; STOK15; WEIL19]. The author WEILER [WEIL19] recently has conducted an in-depth analysis of the thermal transport problem and uses previous studies as well as own investigations in order to derive a simplified analytical solution. The author extends the focus of the thermal model by including the temperature profile in through-thickness direction dependent on the thickness of tape and substrate. Hereby, the model can also give conclusions of the process at increased process speeds of $v_P \gg 500 \frac{mm}{s}$.

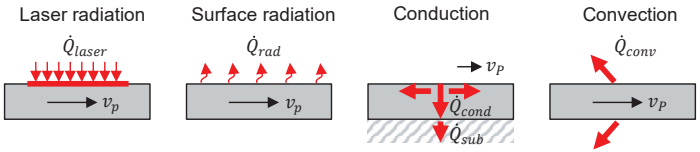

Figure 4.1: Basic thermal transport modes in the laser-assisted AFP process, adapted from [WEIL19, p. 48]

Grundlegende Wärmetransportmodi im laserunterstützten AFP-Prozess, in Anlehnung an [WEIL19, p. 48]

For all four modes a thermal energy balance can be derived by a combination of physical conservation laws, such as conservation of energy, of momentum or of mass. In the case of heat conduction, which describes the diffusion of thermal energy, the conservation of energy according to the first law of thermodynamics is combined with *Fourier´s law. Fourier´s law* states that heat flux density is proportional to the temperature gradient in the direction of the temperature drop. It is formulated as [BEJA03, p. 164]:

$$\dot{q}_n'' = -k_n \frac{\partial T}{\partial n}, \tag{4.1}$$

where $\dot{q}_n''$ [W/m²] is the heat flux in n-direction per unit area perpendicular to the direction of heat flow, k_n [W/m·K] the thermal conductivity and $\frac{\partial T}{\partial n}$ the temperature gradient in n-direction. It must be noted, that k_n is temperature and location dependent especially causing different values for anisotropic materials, such as composites.

By performing an energy balance, the general heat conduction equation can be written in Cartesian coordinates [BEJA03, p. 165]:

$$\rho c_p \frac{\partial T}{\partial t} = \frac{\partial}{\partial x}\left(k_x \frac{\partial T}{\partial x}\right) + \frac{\partial}{\partial y}\left(k_y \frac{\partial T}{\partial y}\right) + \frac{\partial}{\partial z}\left(k_z \frac{\partial T}{\partial z}\right) + \dot{q}''', \tag{4.2}$$

with ρ being the material´s density, c_p the specific heat coefficient and $\dot{q}'''$ [W/m³] the volumetric energy source. To solve the partial differential equation (PDE) initial as well as boundary conditions are required, such as *Dirichlet* or *Neumann* boundary conditions. These conditions vary dependent on the focused domain and assumptions [GROU12, p. 32; KERM15, p. 57]. Therefore, a close consideration of both is important to enable an analytically solvable solution. Figure 4.2 illustrates commonly used domains of the laser-assisted AFP process. The colored domains are the ones focused in this study which are later categorized into *local* (green) and *global* (orange) thermal modeling. To demonstrate the thermal problem of the laser-assisted tape placement process assumptions and equations are presented below.

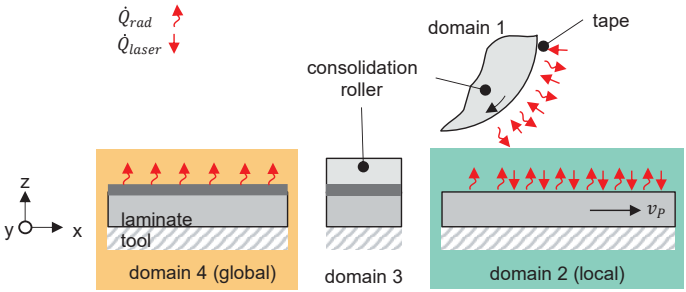

Figure 4.2: Four domains of the thermal problem in laser-assisted AFP, adapted from [GROU12, p. 31]

Die vier Domänen der Wärmeübertragung beim laserunterstützten AFP Prozess, in Anlehnung an [GROU12, p. 31]

Assumptions for the laser-assisted tape placement. Based on the findings of the previous mentioned studies various assumptions are derived for model simplifications. This section summarizes these assumptions. For a more detailed overview see [WEIL19, p. 53-59]. Figure 4.3 illustrates the specific heat transfer problem including geometrical definitions and dimensions of the used variables. The coordinate system coincides with the one of the tape laying system.

1. Thermal resistance due to laser radiation is not existent. [WEIL19, p. 53]
2. Heat transfer in tape width direction (y-direction) is low and can be neglected. [YASS18, p. 1687; WEIL19, p. 53]
3. Thermal analysis in feed direction can be neglected for process speeds $v_P \gg 50\frac{mm}{s}$, as the thermal diffusivity in fiber direction does not affect the temperature distribution in thickness direction. [GROV88; WEIL19, p. 54]
4. Heat losses by radiation, convection and conduction of adjacent components, such as roller or mold, to the environment can be neglected for high temperature gradients [WEIL19, p. 54-57]. This results in a *finite* problem description for most

process conditions as heat can reach the other side of the tape or substrate [GROU12, p. 134-136].

5. Inter-body heat flow is neglected if temperature gradients in tape and substrate are equal. This also holds for well consolidated layers. [WEIL19, p. 57-59]
6. Assuming intimate contact, the thermal resistance between tape and substrate during contact can be neglected. [WEIL19, p. 58]
7. The tape material is modelled as an equivalent homogeneous material. [GROV88, p. 368]
8. Specific heat capacity c_p and thermal conductivity k_n are averaged over temperature. [WEIL19, p. 58]
9. Heat due to fusion of polymer and crystallization are neglected. [WEIL19, p. 58]
10. Initial temperature equals ambient temperature (20°C). [WEIL19, p. 59]
11. The irradiation time t_L of the laser is constant due to constant tape speed and irradiation length x_L [WEIL19, p. 59]. According to the investigation by [KÖLZ08, p. 34] x_L is often assumed to be $x_L = 40\ mm$.
12. The laser spot is homogenously distributed. [WEIL19, p. 58]
13. Volumetric absorption of the laser heat flux is neglected and surface heat flux is assumed. [WEIL19, p. 59]
14. The tape material fully absorbs laser irradiation resulting in an absorption coefficient of 1. Consequently, optical phenomena are neglected. [WEIL19, p. 60]

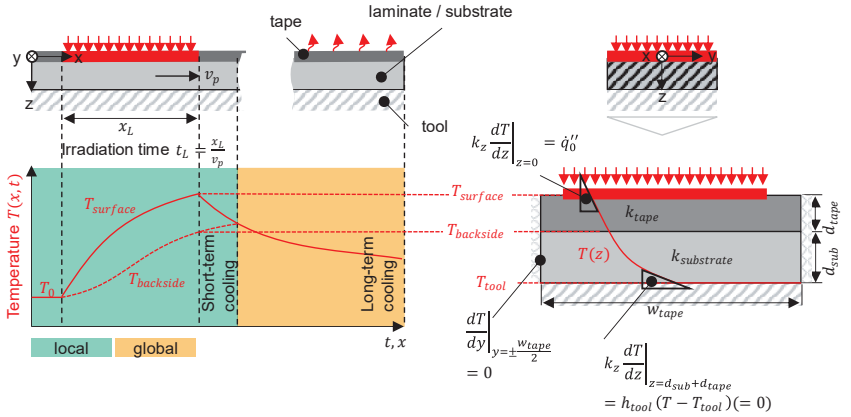

Figure 4.3: The specific heat transfer problem, adapted from [KERM15, p. 57; WEIL19, p. 60]

Das Problem der spezifischen Wärmeübertragung, in Anlehnung an [KERM15, p. 57; WEIL19, p. 60]

General heat transfer model of laser-assisted tape placement. A three-dimensional transient heat transfer model describes the general character of the laser-assisted AFP process. Based on the above-mentioned assumptions most studies reduce

the model to one-dimensional conductive heating in through-thickness direction [GROU12, p. 31; KERM15, p. 57; WEIL19, p. 60]:

$$k_z \frac{d^2T}{dz^2} = \rho c_p \frac{dT}{dt} \tag{4.3}$$

where ρ is the density, c_p the specific heat and the k_z thermal conductivity in through-thickness direction. The following initial and boundary condition are commonly applied in literature:

$$T(t=0) = T_i \tag{4.4}$$

$$\begin{aligned} \dot{q}_z''(t) = k_z \frac{dT}{dz} \\ = -h_{conv}(T(z,t) - T_\infty) - \varepsilon\sigma(T^4(z,t) - T_\infty^4) \\ + \dot{q}_0''(t) \end{aligned} \tag{4.5}$$

with h_{conv} being the convective heat transfer coefficient, T_∞ the far field temperature (or the tool temperature T_{tool} in the case of a heated table [GROU12, p. 32]), ε the surface emissivity, σ the Stefan-Boltzmann constant and $\dot{q}_0''(t)$ the incident heat flux due to laser radiation.

Local heat transfer model of laser-assisted tape placement. Based on the previously listed assumptions, equations (4.4) and (4.5) are simplified for an analytically solvable solution [KERM15, p. 57; WEIL19, p. 60]:

$$T(t=0) = T_i \tag{4.6}$$

$$k_z \frac{dT}{dz}\bigg|_{z=0} = \dot{q}_0'' \tag{4.7}$$

$$k_z \frac{dT}{dz}\bigg|_{z=d} = h_{tool}(T - T_{tool})(= 0) \tag{4.8}$$

Based on the previous mentioned assumptions, WEILER applies analytical solutions for different cases assuming equation (4.8) equals zero: *finite* problems describing that heat reaches and *semi-infinite* problems where heat does not reach the backside of the body [WEIL19, p. 61]. The dimensionless *Fourier number* Fo describes the ratio between the heat diffusion rate and heat storage rate and allows the differentiation of each case [WEIL19, p. 62]:

$$Fo = \frac{heat\ diffusion\ rate}{heat\ storage\ rate} = \frac{k_z}{\rho \cdot c_p} \cdot \frac{t_L}{d^2} = \alpha \cdot \frac{t_L}{d^2}, \tag{4.9}$$

with $\alpha = k_z/\rho \cdot c_p$ being the term for the thermal diffusivity giving the heat rate from the hot to the cold part of a material. A low Fourier number, as in the case for a semi-infinite problem, implies either a low conduction of the material or a high capacity. The latter occurs, for example, for thick substrates. Vice versa, for thin materials the Fourier number is higher indicating that heat reaches the back of the body and thereby results in a finite problem.

The corresponding equations for the thermal evolution in the tape are presented by WEILER [WEIL19] for the heating and cooling phases in the short term. For both phases the above-mentioned assumptions apply. The major benefit of the following equations is that they can be solved analytically and not numerically, which could allow a simple implementation within a digital twin.

Heating phase (local domain)

Semi-infinite problem ($0 < Fo < 0.2$): The authors [BEJA03, p. 232-233; POPR05, p. 51] derive the following solution for equation (4.3) calculating the internal temperature evolution over time in z-direction $T(z, t_L)$:

$$T(z, t_L) = T_i + \frac{2 \cdot \dot{q}_0''}{k_z} \cdot \sqrt{\alpha} \sqrt{t_L} \cdot ierfc\left(\frac{z}{\sqrt{4 \alpha t_L}}\right) \tag{4.10}$$

$$ierfc(X) = \frac{1}{\sqrt{\pi}} e^{-X^2} - X \cdot erfc(X), \tag{4.11}$$

with $\dot{q}_0'' = P_L / A_L$ being the surface heat flux with $A_L = x_L w_{tape}$, x_L the irradiation length, w_{tape} the tape width, P_L as the irradiated laser power as well as $erfc$ being the error function whose values are given in tables in the above-mentioned literature. t_L is the irradiation time with $t_L = x_L / v_P$.

Finite problem ($0.2 < Fo < \infty$) [WEIL19, p. 62]: Based on [FAGH10, p. 255-259] WEILER proposes the following equation if heat reaches the back of the body:

$$T(z, t_L, d) = T_i + \frac{\dot{q}_0'' \cdot d}{k_z} \left(Fo + \frac{(z/d)^2}{2} - \frac{z}{d} + \frac{1}{3} - \frac{2}{\pi^2} \sum_{n=1}^{\infty} \frac{cos(n\pi(z/d)^2)}{n^2} e^{-(n\pi)^2 Fo} \right) \tag{4.12}$$

To account for both, finite and semi-finite problems, the *Method of Mirroring Heat Sources* [POPR05, p. 51] is applied by WEILER [WEIL19, p. 63] resulting in:

$$T(z, t_L, d) = T_i + \frac{2 \cdot \dot{q}_0''}{k_z} \sqrt{\alpha} \sqrt{t_L} \cdot \sum_{i=0}^{\infty} \left(ierfc\left(\frac{2d \cdot i + z}{\sqrt{4 \alpha t_L}}\right) + ierfc\left(\frac{2d \cdot (i+1) - z}{\sqrt{4 \alpha t_L}}\right) \right). \tag{4.13}$$

Cooling phase (local domain)

Finite and semi-infinite problem ($0 < Fo < \infty$): As for the heating phase, equation (4.3) is solved by [POPR05, p. 51; WEIL19, p. 66] for the cooling phase:

$$T(z, d, t_L, t_P) = T_\infty + \frac{2 \cdot \dot{q}_0''}{k_z} \cdot \sqrt{\alpha} \cdot \left[\sqrt{t_P} \cdot \sum_{i=0}^{\infty} \left(ierfc\left(\frac{2d \cdot i + z}{\sqrt{4 \alpha t_P}}\right) + ierfc\left(\frac{2d \cdot (i+1) - z}{\sqrt{4 \alpha t_P}}\right) \right) - \sqrt{t_P - t_L} \cdot \sum_{i=0}^{\infty} \left(ierfc\left(\frac{2d \cdot i + z}{\sqrt{4 \alpha (t_P - t_L)}}\right) + ierfc\left(\frac{2d \cdot (i+1) - z}{\sqrt{4 \alpha (t_P - t_L)}}\right) \right) \right]. \tag{4.14}$$

where t_P is the total considered time.

During the cooling phase it must be considered that equation (4.14) is only valid when the through-thickness conduction is dominant and other heat transfer mechanisms are irrelevant. According to [WEIL19, p. 66], heat transfer to the environment via convection, for example, have a greater influence in the long-time domain, when reaching equilibrium, and have to be considered. Due to the focus on high production speeds ($v_P \gg 500\,mm/s$) the losses to the environment decrease [WEIL19, p. 70] and temperature gradients within the bodies increase.

Global heat transfer model of laser-assisted tape placement. Most studies focus on the temperature evolution within the local processing zone with the aim to derive the required heat fluxes. As an addition, ZAAMI [ZAAM21b, p. 72] integrates a global thermal model into a local optical-thermal model domain in order to account for the cooling of the substrate surface due to convection, the increase of the average temperature within the tool (here a plastic liner) as well as the increase of the consolidation roller. Focus application is the winding of thermoplastic composite pressure vessels with in-situ consolidation. By implementing different and simplified boundary conditions compared to the local, in-depth temperature model, the author can calculate the heat loss of the substrate and use it as an updated boundary condition for the local domain. Thereby, the author accounts for the heat accumulation during winding which results in a steady increase of the substrate temperature. The substrate cools gradually in the long domain due to the convective heat loss to the environment (approx. $T_{env} = 20 - 30\,°\,C/s$) [ZAAM21b, p. 85]. The global heat transfer problem in equation (4.2) is implemented with 2-dimensions, in y- and in z-direction. The main difference is a change in boundary condition. When taking the convective heat loss on the substrate surface into account, the new boundary condition is:

$$k_z \frac{dT}{dz}\bigg|_{z=0} = h_{conv}(T - T_{env}) \tag{4.15}$$

4.1.2 Bond strength

Konsolidierungsgüte

In order to assess the process quality a method is to estimate the degree of bonding D_B [PITC97, 257; MANT92b, p. 2366; KHAN10, p. 103]:

$$D_B = D_{IC}(t_{IC}) D_{AH}(t_{AH}),\ 0 < D_B < 1 \tag{4.16}$$

with D_{IC} being the degree of intimate contact and D_{AH} the degree of autohesion. Several authors, such as GROUVE [GROU12, p. 77], point out that the accurate setting of the temperature is crucial for guaranteeing the desired bond strength since viscosity and reptation time are temperature dependent variables within D_{IC} [MANT92b, p. 2360] and D_{AH} [YANG03, p. 267]:

$$D_{IC}(t) \approx R^* \left[\int_0^{t_{IC}} \frac{P_{cons}}{\mu_0(T)} dt\right]^{1/5};\ 0 < D_{IC} < 1 \tag{4.17}$$

$$D_{AH}(t) = \left[\int_0^{t_{AH}} \frac{1}{t_w(T)} dt\right]^{\frac{1}{4}};\ 0 < D_{AH} < 1 \tag{4.18}$$

where R^* is a proportional coefficient for the influence of the surface roughness, t the time, T the temperature, P_{cons} the consolidation pressure, $\mu_0(T)$ the temperature dependent viscosity of the polymer and $t_w(T)$ the temperature-dependent, polymer-specific reptation/welding time.

As can be seen above, the degree of intimate contact and autohesion are both primarily dependent on time and temperature. Under the assumption that 2D laminate manufacturing underlies isothermal conditions with a constant diffusion coefficient of the polymer as well as a constant t_w, the equation for the degree of autohesion can be simplified to [YANG03, p. 264-265]:

$$D_{AH}(t) = \left[\frac{t}{t_w}\right]^{\frac{1}{4}}; 0 < D_{AH} < 1 \tag{4.19}$$

Here, the variable t is within the boundaries $0 < t_{AH} < t_w$ and accounts for the time it takes from the beginning of the process until full autohesion is achieved under isothermal conditions [YANG03, p. 264]. The welding time t_w is material dependent and happens on molecular level as derived by the model of DE GENNES [GENN71]. It is applicable for molecular weights between $M_c < M < 8 \cdot M_c$ with M_c being the critical molecular weight. A detailed derivation of the welding time by rheological experiments and the Arrhenius equation is demonstrated and discussed in detail by SCHÄFER [SCHÄ17, p. 91-96]. For example, for a Polyetheretherketone carbon fiber (PEEK/CF) tape it can be calculated according to KHAN ET AL. [KHAN10, p. 102]:

$$t_w(T) = 2 \cdot 10^{-5} \cdot \exp\left(\frac{43000\frac{J}{mol}}{RT}\right), \tag{4.20}$$

with R being the universal gas constant. At the desired surface temperature, the value is $t_w(T = 410\,°C) \approx 0.038\,s$. In most cases the time in which the process zone is exposed to irradiation exceeds the welding time ($t_L \gg t_w$) so that the autohesion process can be fully developed. This is also supported by the findings of STOKES-GRIFFIN AND COMPSTON [STOK16, p. 20]. In this example, irradiation times equal to t_w are achieved at process speeds of $v_P \approx 1052\,mm/s$. This indicates that closer consideration has to be taken with very high process speeds ($v_P > 1000\,mm/s$). In addition, one has to pay attention when using the expression for the welding time. Especially with lower temperatures ($T < 500\,°C$), values for t_w can diverge. For example, the model derived by SOMNEZ AND HAHN [SONM97b] is more conservative and estimates a welding time of $t_w(T = 410\,°C) \approx 0.092\,s$. This means that $v_P(D_{AH} = 1, t_w = 0.092) \approx 435\,mm/s$ illustrating that full consolidation is achieved for PEEK at much lower process speeds. Additionally, the models do not account dynamic effects during the process, such as the *reconsolidation effect* due to the repeated rolling over when laying the next layer.

It has to be noted, that the reptation theory is only applicable for a certain range of the molecular weight. SCHÄFER investigates the molecular weight of polyamide 6 with carbon fibers (PA6/CF) tape, which will be focused in this study, within a range between $M = 20.200\,g/mol$ and $M = 34.400\,g/mol$ by Gel-Permeations-Chromotagraphie. The

author concludes the applicability of the reptation theory for this material. The derivation of the (terminal) reptation/welding time can be done either by welding experiments or by rheological experiments. SCHÄFER conducts latter to derive the welding time. A detailed explanation of the derivation can be found in [SCHÄ17, p. 91].

With assuming isobaric and isothermal conditions for the tape laying process, the degree of intimate contact is simplified according to MANTELL AND SPRINGER [MANT92b, p. 2364] to:

$$D_{IC}(t) \approx R^* \left[\frac{P_{cons} \cdot t_{IC}}{\mu_0(T)}\right]^{1/5}; 0 < D_{IC} < 1. \tag{4.21}$$

R^* is set according to the specific tape material and $t_{IC} = l_{roller}/v_P$ is the contact time during pressure application. For example, MANTELL AND SPRINGER set $R^* = 0.29$ [MANT92a, p. 2385]. With using the form-adaptive consolidation roller developed by STEYER [STEY12, p. 55], WEILER uses a silicone roller with a contact length $l_{Roller} = 28\,mm$ and a contact width $w_{Roller} = w_{tape}$ [WEIL19, p. 328] resulting in an applied average pressure of $P_{cons} = 0.89\,MPa$. The temperature-dependent viscosity for a PEEK/CF tape can be estimated based on KHAN ET AL. [KHAN13, p. 487]:

$$\mu_0(T) = 0.0037 \cdot \exp\left(\frac{11115\,K}{T}\right) \tag{4.22}$$

However, viscosity models differ to a high extent as presented by STOKES-GRIFFIN AND COMPSTON [STOK16] and Weiler [WEIL19]. This can significantly influence the values for intimate contact and autohesion and must be considered in the validation of the calculated values. SCHÄFER [SCHÄ17, p. 77] gives a detailed explanation on the use of viscosity models, their experimental derivation and their limitation. It reveals, that additional research is required to establish accurate contact and autohesion models for the non-isothermal character of the AFP of thermoplastics with in-situ consolidation.

Both phenomena are prerequisites for an in-situ consolidation, meaning a degree of bonding of $D_B \approx 1$. Intimate contact, as developed by LEE AND SPRINGER [LEE87], indicates the influence of bodies' geometrical characteristics which are also affected by process parameters. It is a precondition for the autohesion process describing the interdiffusion of the polymer chains at the bonding interface as explained by the reptation theory of DE GENNES [GENN71]. YANG AND PITCHUMANI [YANG03, p. 269] develop a coupled bonding model which is often used in literature [KHAN13]:

$$D_B(t_f) = D_{IC}(0) D_{AH}(t_f) + \int_0^{t_f} D_{AH}(t_f - t) \cdot \frac{dD_{IC(t)}}{dt} \cdot dt, 0 < D_B < 1 \tag{4.23}$$

Here, t_f is the final time which ist $t_f = t_L + t_w$.

4.1.3 Crystallinity

Kristallinität

Semi-crystalline thermoplastics exist of domains with crystalline and amorphous structures. Depending on the number of crystallites within the polymer the mechanical characteristics of the laminate can be designed. In general, it can be stated, that polymers

with low crystallinity have a high fracture toughness due to its ductility. In contrast, polymers with high crystallinity have higher strength values. During the thermoplastic tape laying the crystallinity is especially relevant as it influences the deflection of the laminate. KERMER-MEYER states that by using the historical temperature data during the process the degree of crystallization (DoC) χ can be estimated and thermal induces stresses predicted. This allows the determination of the curvature. [KERM15, p. 54-55]

The DoC of a specimen out of semi-crystalline, composite thermoplastics is described by the ratio between its melting enthalpy ΔH_m and the melting enthalpy of the 100 % crystalline form of the thermoplastic polymer material ΔH_m^0 [FELD19, p. 250; JANS20, p. 134], taking into account the mass fraction of the carbon fibers φ_f:

$$\chi(\%) = \frac{\Delta H_m}{(1-\varphi_f)\Delta H_m^0} \times 100. \tag{4.24}$$

The values for ΔH_m and ΔH_m^0 are taking from differential scanning calorimetry (DSC) analyses. For a pure crystalline PA6 the latter value is $\Delta H_m^{PA6} = 241\,J/g$ according to [ILLE78, p. 499]. The mass fraction of the fibers φ_f can be derived by thermogravimetric analysis (TGA) or calculated by the rule of mixture [KRES14, p. 78] based on a given value for the fiber volume content.

For a theoretical approximation, AVRAMI [AVRA39] develops a model based on the degree of phase transformation. NAKAMURA [NAKA72, p. 1081] extends the model to account for non-isothermal crystallization processes during isokinetic conditions. The DoC describes the fraction of the crystallized volume at a specific time $\chi_v(t)$ and at equilibrium conditions $\chi_{v\infty}$ (often the maximum crystallinity volume). It is described as:

$$\chi(t) = \frac{\chi_v(t)}{\chi_{v\infty}} = 1 - exp\left(-\left(\int_{t_0}^{t} K\big(T(\tau)\big)\,d\tau\right)^n\right), \tag{4.25}$$

where n is the Avrami constant being a measure for the nucleation and growth mechanism (e.g. $n = 3$ for spherulitic growth and heterogeneous nucleation) at nucleation time τ, t_0 the starting time of the crystallization process and $K(T)$ the (isokinetic) temperature-dependent crystallization rate constant:

$$K(T) = k(T)^{\frac{1}{n}}, \tag{4.26}$$

with $k(T)$ being the isothermal crystallization rate constant [NAKA72, p. 1081].

Several authors investigate the crystallinity during tape laying such as in [MANT92b; SARR95; TIER04; GROU12; KERM15]. The authors SARRAZIN AND SPRINGER [SARR95] are among the first authors introducing a thermochemical model for estimating the temperature-dependent crystallization. They investigate the cause for stresses for the tape laying of APC-2/PEEK tape material as a function of position and time by using the energy equation as the basis for the temperature distribution in length and thickness direction [SARR95, p. 1909]. Here, a combination of a radiation-based heat source and the heat created due to chemical reactions, such as crystallization, is used as energy input. Within a transient FEM analysis, various influences on the tape laying by temperature, viscosity and crystallization are demonstrated indicating strategies for

mold temperature and layup speed. For example, the authors recommend increasing the layup speed with increasing numbers of layers, since the created substrate acts as an insulator maintaining the heat created during processing. Additionally, they demonstrate how the cooling rate influences the degree of crystallinity (DoC) suggesting that this can be mainly controlled by the layup speed and the mold material.

SOMNEZ & HAHN develop a FEM model characterizing the non-isothermal crystallization process of PEEK [SONM97a, p. 207] between the glass transition and melting temperature. Their results show that preheating the substrate decreases cooling rates and enables longer annealing times. The authors indicate that the DoC varies across the laminate layers having little or no crystallites on the top due to shorter annealing [SONM97a, p. 226]. They suggest preheating the substrate around the glass transition temperature to enable a uniform crystallization throughout the thickness of the laminate. TIERNEY & GILLESPIE [TIER04, p. 548] use a combination of models in order to estimate the degree of crystallization within PEEK for highly non-isothermal processes, such as the AFP. The model by SEFERIS ET AL. is used for the crystallization kinetics between glass transition temperature and melting temperature and the model by MAFFEZZOLI is implemented at temperatures reaching the melting temperature. Both models show good agreement with experiments.

KERMER-MEYER suggests adding a subsequent cooling device to increase the cooling rate and, thus, have less shrinkage. With increased cooling rates the crystallization temperature $T_{p,c}$ decreases, but the temperature range for crystallization increases. This means that less crystallization is taking place with higher cooling rates [KERM15, p. 51]. To enable further crystallization, he recommends to keep the mold temperature slightly below the crystallization temperature $T_{p,c}$ to increase the accumulation of crystals within the polymer [KERM15, p. 53].

HOSSEINI ET AL. [HOSS20] chose to implement equation (4.25) within a numerical, finite-difference model to describe the crystallization kinetics during the winding of pipes out of PA12/CF. The authors take the tape width as well as the adjacent tapes into consideration which are exposed to laser radiation as the laser spot mostly is wider than the tape. Additionally, they estimate the temperature evolution within the substrate due to repeated heating cycles (reconsolidation effect). Although equation (4.25) allows a simplified implementation, a discrepancy between measured and predicted values are detected [HOSS20, p. 17]. The authors state that the incomplete melting of the polymer during tape laying leads to increased formation of crystallites as existing crystals act as nucleation agents. Overall, the authors conclude that during winding complex temperature and crystallinity distributions across the layers exist which may be caused by a non-optimized laser power distribution.

In summary, the DoC is an important indicator not only for the laminate´s mechanical strength at the end, but also for the processing quality during AFP. It has to be noted, that most studies are conducted with PEEK material. Therefore, it is not clear if similar interdependencies apply for other thermoplastic matrix materials.

4.1.4 Residual stresses

Eigenspannungen

Residual stresses exist inside a body after being exposed to external forces. Deformations, thermal exposure or microscopic, structural changes can cause stresses. In most cases, these are undesirable since they negatively influence mechanical and geometrical behavior. In composites manufacturing, they can cause matrix failure, interlaminar delaminations, distortions as well as void formation during the tape placement [YASS18, p. 1703]. In in-situ tape placement, the development of residual stresses originates from three sources:

1. Temperature gradients: The repeated exposure of the tape material to heating and cooling and thus to volumetric changes (e.g. due to crystallization) results in thermal induced residual stresses.
2. Unbalanced layup during tape laying: Due to the additive character of tape laying, the laminate experiences continuously changing stress states caused by the change in boundary conditions, e.g. in the context of the CLT. [JERO88, p. 405]
3. Manufacturing stresses: During layup the material is exposed to external forces, such as by the compression roller.

All sources do not only significantly influence the mechanical and geometrical characteristics of the final part, but also the tape laying process itself. Warpage induced by residual stresses can hamper the process since the tape laying head cannot smoothly roll over the laid substrate. This is amplified when the first layer fixation between heating table and tape is done without any additional support, e.g. by using temperature-resistant adhesive tape.

In the past decades, scientists have investigated the formation of residual stresses to enhance the manufacturing of thermoplastic composites. Jeronimidis and Parkyn [JERO88] experimentally investigate that residual stresses can be calculated by the CLT when taking thermoelastic material properties, e.g. the thermal dependence of the thermal expansion coefficient and moduli, into account. They also introduce the stress-free temperature being the temperature when the curvature of the laminate becomes zero again during heating it up in the oven. Chapman et al. [CHAP90] model the induced in-plane residual stresses within semi-crystalline thermoplastic composites due to cooling. They found that temperature gradients significantly more affect residual stresses compared to crystallization levels.

Most of the developed stress models are implemented by FEM allowing to calculate stresses at each state and position. Sarrazin and Springer [SARR95] include thermal induced effects by adding a thermal term with the temperature difference between the current and the stress-free temperature to the stress-strain relationship [SARR95, p. 1918]. Their analysis shows that high temperature gradients cause residual stresses recommending a uniform temperature distribution within the laminate. Li et al. [LI97] implement a FEM residual stress analysis in order to estimate stresses also for thicker

laminates where the CLT does not hold anymore. Within their plane-strain elasticity analysis they account for shrinkage due to crystallization as well as temperature-dependent material properties. Their experimental and numerical investigation show that the cooling rate has different effects on symmetrical and non-symmetrical layups: In symmetrical layups the decrease of the cooling rates causes a decrease of residual stresses, whereas in non-symmetrical layups it causes an increase.

The authors SONMEZ ET AL. [SONM02a] focus on residual stresses during the AFP process with in-situ consolidation. They point out that the main sources of residual stresses originate from the anisotropic thermal expansion coefficient during heating on the one side and cooling of the laminate during processing on the other side. Amongst others and based on findings of previous work the authors neglect crystallization effects (see [CHAP90]), the influence of the roller and assume a viscoelastic material behavior for the time-dependency around the glass transition temperature [SONM02a, p. 529]. They introduce a methodology within a FEM environment to simulate the thermal-induced residual stresses within the upper layer and the layers below within the substrate. Hereby, the authors are among the first implementing a model which takes an increasing amount of effects into consideration, such as the *reconsolidation effect* due to repeated heating of the same zone. The following impacts of the AFP with in-situ consolidation on residual stresses are found by the authors [SONM02a, p. 536]:

- Preheating the substrate decreases residual stresses due to decreased cooling rates;
- Increasing process velocity results in an increase of residual stresses since localized heating causes higher temperature gradients;
- Increase of heating lengths of the surfaces reduces residual stresses;
- Residual stresses accumulate when increasing the amount of layers.

The results by SONMEZ ET AL. [SONM02a; SONM02b] are often cited being the basis for further studies as well as processing strategies. KERMER-MEYER [KERM15] builds upon this previous work, but implements a rheological model rather using FEM modeling in order to estimate the transverse warping of the laminate. With the simplification that each layer is laid at once by the applicator head, the warpage for each layer is calculated iteratively by modeling the material behavior as a combination of springs [KERM15, p. 65] and as a one-sided bending beam. The procedure allows the analytical calculation of warpage resulting from thermally induced residual stresses during laying. A major control variable is the temperature difference ΔT between the stress-free temperature of the matrix and the temperature of the laminate. For semi-crystalline thermoplastics, the stress-free temperature is represented by the crystallization temperature $T_{p,c} (= T_{stress})$. It implies the temperature state in which the matrix is not yet solidified and stresses cannot be induced. The author analyses that by increasing the mold temperature ΔT decreases which results in fewer residual stresses and, thus, in less warpage. This is confirmed by experiments by assessing the resulting warpage through a laser scanner. In summary, the model created by KERMER-MEYER shows a

high correlation with the experimental results. Details for implementation are later shown in section 4.3.4.

Besides the above-mentioned studies, many further investigations considering the formation of residual stresses are conducted in the past. Models have been extended and transferred to more complex geometries. For example, DEDIEU ET AL. [DEDI17] created a FEM model to estimate process-induced residual stresses within the filament winding of thermoplastic composite rings with in-situ consolidation. In summary, the analytical and experimental observations demonstrate that the thermal history during processing is a key source for residual stresses in the thermoplastic laminate. Validated models are derived leading to recommendations for improving the processability and the robustness of the process. Nevertheless, the variety of different approaches indicate the difficulty in finding a sole solution. Most of them rely on complex FEM models.

4.1.5 Influence of increased process speeds

Einfluss höherer Prozessgeschwindigkeiten

The overall aim of this study, to increase productivity, goes hand in hand with a faster process. For this reason, the influence of increasing process speeds on the process itself and the resulting process quality, as explained in the previous sections, is focused. Only a few authors investigate how it affects the weld strength such as by GROUVE [GROU12] or the in-depth analysis by WEILER [WEIL19]. WEILER investigates the influence of increased process speeds on intimate contact, autohesion and, finally, the degree of bonding. As can be seen in equation (4.17) a smooth surface texture, high pressure and low viscosity of the thermoplastic (mainly resulted by increased process temperatures) facilitates intimate contact. However, as high process velocities have an inverse effect on the exposed pressure time, it negatively influences the formation of intimate contact. It has to be noted that the models assume static pressure and temperature [WEIL19, p. 101] as well as a flat, homogeneous pressuring area. Autohesion requires intimate contact to generate a diffusion process between the polymer layers. A minimum reptation/welding time $t_w(T)$ is therefore essential and too high cooling rate diminishing t_w should be avoided. By increasing process temperature t_w can be decreased as shown, for example, by the model by KAHN [KHAN10, p. 102].

Increased process speeds hamper the formation of both phenomena, also due to the interdependency of both. Theoretically, this indicates that the degree of bonding or weld strength of the layers cannot be compensated by process parameters only and material parameters may have a more significant impact.

Increasing speeds also result in a decline of interface crystallinity because of the higher cooling rates. Additional heating cycles can increase the crystallinity as long as previous bond interfaces remain below the recrystallization temperature. This *annealing effect* has to be kept in mind for the mechanical requirements of the laminate, high fracture toughness (low crystallinity) or high strength (high crystallinity) [WEIL19, p. 108; KERM15, p. 51]. Additionally, the existence of crystallites can also hamper the diffusion

process below the melting temperature resulting in reduced bond quality [GROU12, p. 76; BOIK01].

The *reconsolidation effect* may also be a possibility for increasing process speed. Due to the repeated rolling over, previous layers are reconsolidated as they are exposed to heat and pressure supporting intimate contact [MANT92a, p. 2400]. However, WEILER states that the reconsolidation effect requires sufficient thermal penetration of the tape, so that heat reaches subjacent layers [WEIL19, p. 106]. This could be hampered by high temperature gradients during increased speeds.

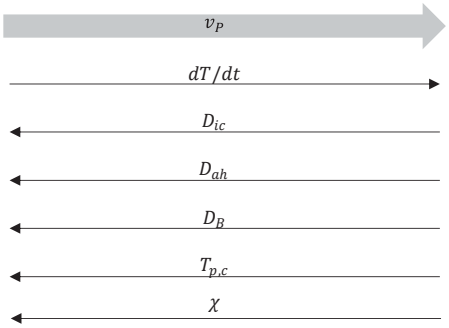

Figure 4.4: Summary of effects resulting from increased process speed based on the models in literature

Übersicht der Auswirkungen einer erhöhten Prozessgeschwindigkeit auf der Grundlage der Modelle in der Literatur

In summary, the following conclusions can be drawn for process speeds $v_P \gg 500 \frac{mm}{s}$ neglecting the influence of the material (see Figure 4.4):

- Steeper thermal gradients within tape and substrate dT/dt;
- Decreased reptation time $t_w(T)$ resulting in decreasing autohesion;
- Decreased thermal penetration, so called *melt thinning effect* [WEIL19, p. 102];
- Decreased exposure time to pressure t_{IC} (which is why elastic rollers with a higher contact length are beneficial) [WEIL19, p. 102] resulting in less time for intimate contact;
- Higher cooling rates result in a decrease of crystallization temperature [KERM15, p. 51];
- Less time for crystallization reducing the crystallization rate.

4.1.6 Interim conclusion

Zwischenfazit

Quality indicator	**Consolidation**	**Crystallization**	**Geometrical accuracy**
Criteria	Degree of Bonding (DoB)	Degree of Crystallization (DoC)	Residual stresses (mechanically & thermally induced)
Analytical model	$D_B(t_f) = D_{IC}(0) D_{AH}(t_f) + \int_0^{t_f} D_{AH}(t_f - t) \cdot \frac{dD_{IC}(t)}{dt} \cdot dt$ [YANG03]	$\chi(t) = \frac{\chi_v(t)}{\chi_{v\infty}} = 1 - exp\left(-\left(\int_{t_0}^{t} K(T(\tau))\, d\tau\right)^n\right)$ [NAKA73]	$\Delta w = \alpha_T \cdot \Delta T \cdot w_0$ $F_i = (w_0 - w) \cdot E_\perp + F_i^{n-1}$ $M = \sum_{i=1}^{n} F_i \cdot x_i, k = \frac{M}{E \cdot I}$ [KERM15]
Required process information	– Time of process moment t_f – Surface temperature at nip point T_{np}	– Temperature evolution within the laminate – Time within crystallization range $t(T_g < T < T_m)$	– Stress-free / crystallization temperature $T_{p,c}(= T_{stress})$ – Temperature difference $\Delta T = T_{p,c} - T_{substrate}$, $T_{p,c} > T_{substrate}$

Figure 4.5: Proposed selection of quality indicators and analytical models for the digital twin

Vorgeschlagene Auswahl von Qualitätsindikatoren und analytischen Modellen für den Digitalen Zwilling

The given overview of the past analytical modeling efforts reveals the complexity of the AFP process with in-situ consolidation. Many interacting factors, not only of the heterogeneous material itself, but also of the manufacturing process result in transient, multi-phase events. Only by reducing the system boundaries to its essentials it is possible to develop analytical and/or numerical tools to forecast the process. It is noteworthy to point out that the optimization target of each study may have changed over time. At the beginning of research in this area, around the 1980s, modeling was used to deepen the understanding and to enable a rough control of the process. Afterwards, modeling became necessary to reduce costly experimental work by conducting, for example, FEM analyses. Nowadays, systems require a model to be implemented in an intelligent control of the manufacturing equipment and to increase its robustness. In future and as proposed in this work, the strict boundary conditions of the existing models need to be softened and continuously adapted to allow a more realistic, part-oriented modeling.

Within this context, this means that the existing models need to be transferred from the process zone view to a more holistic view of the complete laminate. Most models neglect the effect on the whole composite part as well as the additive, highly transient character of the AFP process. It reveals the necessity to create a picture of the historical temperature data of the manufacturing process since temperature is the common factor for the shown quality metrics. At each time of the manufacturing process the temperature at each location of the laminate needs to be equated and visualized to give a holistic impression of the manufacturing. Aim is that this data leads to the analysis of the resulting quality indicators for the produced laminate. Figure 4.5 gives a proposition of models as well as the relevant process information to quantify the quality of laminates produced with the AFP process with in-situ consolidation.

4.2 Experimental status-quo analysis

Experimentelle Analyse des Status-Quo

To demonstrate the need for a digital twin, an experiment with a conventional robot-based, laser-assisted AFP system is conducted. Temperature data captured during processing a laminate gives an impression of the cooling behavior of the laminate. An interpretation of the assessed temperature data by applying the model for the degree of bonding is applied to show the feasibility of the proposed idea in this thesis. Since many characterization efforts have been conducted with PEEK/CF material in research, this material is chosen for the status-quo analysis. This enables the application of derived models and investigate the transfer of idealistic analytical models to real manufacturing problems. This section partially relies on the results in [SCHU22].

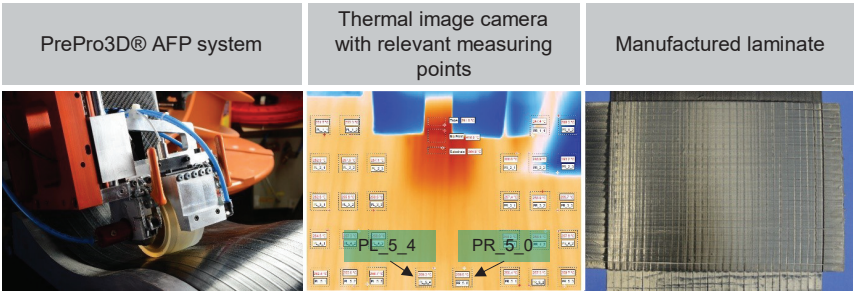

Figure 4.6: Experimental setup and conduct of the status-quo analysis

Versuchsaufbau und -durchführung der Status-Quo Analyse

4.2.1 Experimental setup

Experimenteller Aufbau

A laminate out of unidirectional PEEK/CF tape is manufactured with the *PrePro3D®* system at Fraunhofer IPT. It is a modular system which is able to process thermoplastic, thermoset and dryfiber tape material [BREC15]. As shown in Figure 4.6 (a), the tape laying applicator has a diode-laser source and is mounted to a *KUKA KR3260-2*

robot. The temperatures in the process and in the environment zone (Figure 4.6 (b)) are measured with an infrared thermographic camera *DIAS Pyroview 380L Compact* with a frequency of $25\,Hz$. 36 temperatures are extracted from the thermal image to enable in-depth analysis of the manufacturing process (Figure 4.6). It must be noted, that this measurement setup is not able to assess temperature data in the nip-point due to the shadow of the consolidation roller (see [STEY12, p. 39]). A bidirectional laminate with 15 layers is manufactured on a heated table. The used process parameters and the laminate's characteristics are listed in Table 4.1.

Table 4.1: Experimental parameters of the status-quo analysis in adaption to the idealistic modeling parameters of WEILER [WEIL19]

Experimentelle Parameter der Status-quo-Analyse in Anlehnung an die idealisierten Modelparametern von WEILER [WEIL19]

Parameters	Details	WEILER [WEIL19]
Material	PEEK/CF tape	PEEK/CF tape
Tape thickness	$0.15\,mm$	$0.15\,mm$
Tape width w_{tape}	$12\,mm$	$25\,mm$
Layup	$[0°,0°,90°,90°,90°,90°,0°,0°]_S$	$0°$
Laminate size ($l_x \cdot l_y \cdot N$)	$400\,mm \cdot 300\,mm \cdot 16$	–
Target nip point temperature	$410\,°C$	$410\,°C$
Mold temperature T_{tool}	$270\,°C$	$20\,°C$
Ambient temperature T_∞	$20\,°C$	$20\,°C$
Laser power distribution [on tape | on substrate]	$50\,\%$ | $50\,\%$	100% | 0%
Compression force F_{cons}	$300\,N$	-
Process velocity v_P	$260\,mm/s$	$260\,mm/s$

4.2.2 Cooling time

Abkühlzeiten

In an idealistic case, often assumed in analytical models, the cooling time of a heated tape or substrate is modeled as infinite without considering the reconsolidation effect. The models show how the temperature would evolve over time taking into account the various thermal effects, such as conduction and convection. A brief description about the thermal effects during tape laying can be depicted from chapter 4.1.1. In the realistic case of manufacturing laminates, the cooling time can differ depending on geometry and layup and thereby has a significant impact on the temperature history of the laminate. This can be shown with a demonstration of a simple 0°/90° laminate with a rectangular shape and the specifications as shown in Table 4.1 (as well as: $v_{max} = 500\,mm/s$, $n^{0°} = 25$, $n^{90°} = 34$).

In a laminate with only 0° layers, each point in space ideally experiences the same time of cooling when having a *conventional* laying strategy where each layer starts at the same starting point (explained in detail in chapter 7). Additionally, no heating of the adjacent tape paths is assumed (e.g. when tape width < laser spot width). Simplified, without including further auxiliary time, the time for cooling is calculated as followed:

$$t_c^{0^\circ} = t_{c,xyn}^{0^\circ} = \sum_{i=1}^{n} t_{main}^{i} + \sum_{i=1}^{n-1} t_{aux}^{i} + t_{return} = \sum_{i=1}^{n} \frac{l_x^i}{v_p} + \sum_{i=1}^{n-1} \frac{\sqrt{\left(l_x^i\right)^2 + w_{tape}^2}}{v_{max}} + \frac{\sqrt{(l_x^{i=n})^2 + l_y^2}}{v_{max}}. \tag{4.27}$$

The subscript xyn refers to the specific location in x, y direction as well as the layer n. t_{main}^{i} is the main time of the process of each layer implying only the processing time in which a tape is laid. t_{aux}^{i} is the auxiliary time of each layer which is the time the tape laying applicator needs to return to the starting position of the next tape path. The time the applicator head needs to return to the starting position of the layer is indicated with t_{return}. Here, it is assumed that each layer of the rectangular laminate starts at the same position in x and y. In addition, v_{max} refers to the rapid traverse of the applicator head in all directions. In a plain 0° laminate t^{0° represents the time for laying one layer. Figure 4.7 shows the kinematic path of the tape laying applicator with assuming no further run-in or run-out times, accelerations, jerk etc.

As soon as the fiber orientation changes, as in this case from 0° to 90° degree, the substrate´s cooling time changes. Now, the new tape crosses several tapes from the substrate and the cooling time of the individual point on the laminate becomes relevant. The time the substrate can cool changes to

$$\begin{aligned} t_{c,xyn}^{90^\circ} &= t_{xy,main}^{90^\circ} + t_{xy,aux}^{90^\circ} + t_{(1-xy),main}^{0^\circ} + t_{(1-xy),aux}^{0^\circ} + t_{return} \\ &= \frac{n^{*,90^\circ} l_y + y}{v_p} + \frac{n^{*,90^\circ}\sqrt{l_y^2 + w_{tape}^2}}{v_{max}} \\ &+ \frac{(n^{0^\circ} - (n^{*,0^\circ} + 1)) \cdot l_x + (l_x - x)}{v_p} \\ &+ \frac{(n^{0^\circ} - (n^{*,0^\circ} + 1))\sqrt{l_x^2 + w_{tape}^2}}{v_{max}} + \frac{\sqrt{l_x^2 + l_y^2}}{v_{max}}, \end{aligned} \tag{4.28}$$

where $t_{xy,main}^{90^\circ}$ and $t_{xy,aux}^{90^\circ}$ are the main process and auxiliary times to position xy in the $90°$ layer, $t_{(1-xy),main}^{0^\circ}$ and $t_{(1-xy),aux}^{0^\circ}$ the remaining main process and auxiliary time of the $0°$ layer. The asterisk indicates the current tape path number.

To illustrate the calculation, the cooling times of the substrate for three exemplary points on the laminate, shown in Figure 4.7, are estimated:

Point 1

Point 1 is the starting point of each layer. Consequently, the substrate (layer 1 / $N = 1$) when starting layer 2 ($N = 2$) with the same fiber orientation ($\theta = 0°$) has experienced a cooling time of

$$t_{c,1,N=2}^{0°} = 58.7\ s. \tag{4.29}$$

The cooling time is equivalent for the substrate during the beginning of layer 3 ($N = 3$, $\theta = 90°$): $t_{c,1,N=3}^{90°} = t_{c,1,N=2}^{0°} = 58.7\ s$.

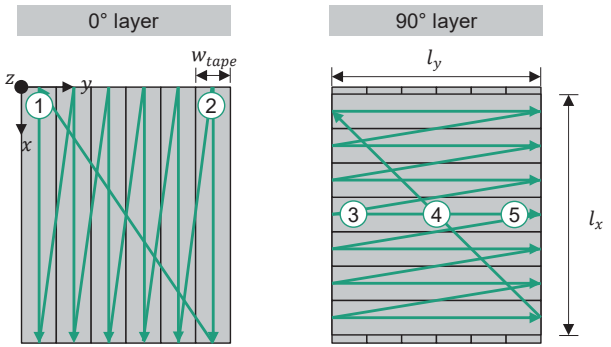

Figure 4.7: Cooling time estimation for a 0°/90° laminate with conventional layup strategy

Schätzung der Abkühlzeit des 0°/90° Laminats mit konventioneller Pfadplanung

Point 2

The second point is at the start of the last tape path of the 0° layers ($n^{*,0°} = 24,\ x = 0$) and at the end of the 1st tape path of the 90° layers ($n^{*,90°} = 0,\ y = l_y$). Here, the substrate during laying layer 2 could cool for

$$t_{c,2,N=2}^{0°} = 58.7\ s. \tag{4.30}$$

Again, the time corresponds to the previous ones as it is the manufacturing time of laying one layer having the same fiber orientation as the previous layer. However, due to the change of fiber orientation in the 3rd layer, the cooling time significantly decreases here to

$$t_{c,2,N=3}^{90°} = 3.7\ s. \tag{4.31}$$

Point 3-5

The third point is located at the start of 22nd tape path of the 90° layer ($N = 3,\ n^{*,90°} = 21$, $y = 0\ mm, n^{*,0°} = 0,\ x = (n^{*,90°} + 1)w_{tape} = 264\ mm$). The substrate temperature during laying the 3rd layer can cool for

$$t_{c,3,N=3}^{90°} = 24\ s + 12.6\ s + 37.4\ s + 19.2\ s + 1\ s = 94.2\ s\,. \tag{4.32}$$

The substrate at the fourth point, located in the middle of 22nd tape path of the 90° layer ($N = 3,\ n^{*,90^\circ} = 21,\ y = 150\ mm, n^{*,0^\circ} = 12,\ x = (n^{*,90^\circ} + 1)w_{tape} = 264\ mm$), can cool for

$$t_{c,4,N=3}^{90^\circ} = 24.8\ s + 12.6\ s + 19\ s + 9.6\ s + 1\ s = 67\ s. \tag{4.33}$$

The substrate at the fifth point, located at the end of 22nd tape path of the 90° layer ($N = 3,\ n^{*,90^\circ} = 21,\ y = 300\ mm, n^{*,0^\circ} = 24,\ x = (n^{*,90^\circ} + 1)w_{tape} = 264\ mm$), can cool for

$$t_{c,5,N=3}^{90^\circ} = 25.4\ s + 12.6\ s + 0.5\ s + 0\ s + 1\ s = 39.5\ s. \tag{4.34}$$

This cooling time decrease from point 3 to 5, even in the same tape path and layer, shows the influence of the term $t_{(1-xy),main}^{0^\circ}$. It reveals that cooling time can differ strongly since the underlying substrate has a different fiber orientation.

With the underlying assumptions, the calculations demonstrate that the substrate experiences the same cooling times as long as the fiber orientation keeps the same. As soon as it differs, the cooling times vary significantly depending on the current location of the applicator head. The highest influence has the main and auxiliary times, $t_{(1-xy),main}^{0^\circ}$ and $t_{(1-xy),aux}^{0^\circ}$, of the substrate with 0°.

If the cooling time during processing has a significant impact on the substrate´s temperature, one can expect an inhomogeneous temperature distribution within the laminate if process parameters are kept static. This may result in undesired effects, such as different crystallization degrees.

The accurate estimation of the cooling time for predicting the cooling behavior of the whole laminate is implemented within a *G-Code Generator*, developed at Fraunhofer IPT, enabling the automated generation of the G-Code for the PrePro2D®. The individual and spatially resolved cooling times of different laminate geometries and layups can be calculated.

4.2.3 Thermal behavior

Thermisches Verhalten

As shown in chapter 4.1 the derived and validated analytical or numerical models show flat descending temperature curves for the long domain cooling after the processing zone. The authors state that additional heat flows such as convection to the ambient cause this behavior [ZAAM21b, p. 86]. This section investigates process zone / nip-point temperatures during heating. Additionally, the long domain cooling behavior for the here focused 0°/90° PEEK/CF laminate is characterized.

Heating. Figure 4.8 visualizes the nip point temperatures of the manufactured laminate which are captured in the process moment. This refers to the time point when the tape is laid at the given position. In this moment, the thermographic camera assesses the temperature in the process zone. The following process and system specific conclusion can be drawn:

- run-in and run-out zones at the beginning and end of each tape path;
- cooler temperature in the run-out zones as soon as the tape is cut after each path since the remaining length is not guided so that the tape falls down and creates a shadow on the process zone;
- homogeneous distribution in the laminate pointing out that the current process is robust and that no major process failures happened during manufacturing.

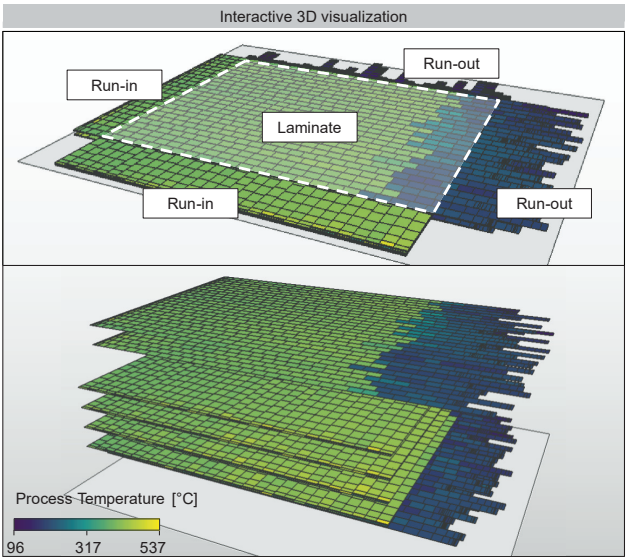

Figure 4.8: Interactive 3D visualization of the temperatures in the process zone: a) System-specific run-in and run-out zones of the laminate, b) explosion view.

Interaktive 3D-Visualisierung der Temperatur in der Prozesszone: a) Anlagenspezifische Ein- und Auslaufzonen des Laminats, b) Explosionsansicht.

Cooling. The cooling behavior is analyzed by plotting the data of the measurement points *PL_5_4* as well as *PR_5_0* (Figure 4.6) of the thermal image camera. These points are located just before the nip-point and track the cooled substrate temperature before the applicator head applies a new layer of tape. The starting and ending points of each measurement are triggered manually. For this reason, an accurate synchronization of data is not feasible. To account for the potential imprecisions, the temperature profiles for each tape path are investigated. Due to the plateau during the actual laying process, the median values are taken to neglect the distorting measurements before and after the tape. The present analysis is illustrated with measurements of the first tape paths (*_0001*), middle tape paths (*_0013* for 0°, *_0015* for 90°) and the last tape paths (*_0024* for 0°, *_0030* for 90°) for each fiber direction and layer. The aim of the present analysis is to understand the temperature curves of during production. Based on these findings, the necessity for novel modeling techniques becomes apparent.

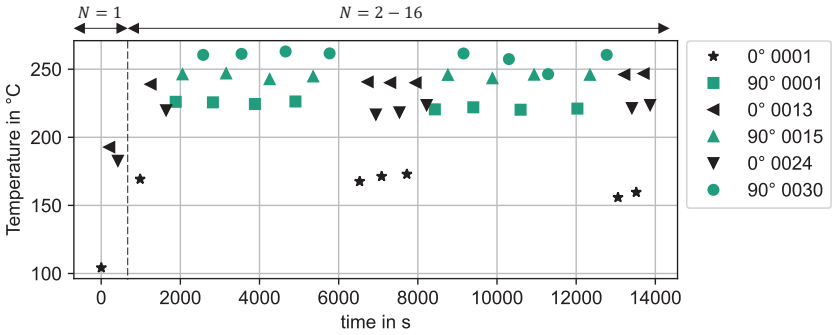

Figure 4.9: Median (cooled) substrate temperatures of each layer and tape paths 1, 13, 15, 24 and 30

Mittlere (gekühlte) Substrattemperaturen nach Lage und Tapes 1, 13, 15, 24 und 30

Figure 4.9 summarizes the averages of the median values of measurement points *PL_5_4* as well as *PR_5_0* for the first, middle and last tape paths of each layer. When having a closer look at the 0° layers (black markers) it can be observed that the temperatures are lowest in the first tape path of each layer, highest in the middle tape path (tape path 13) and approx. $20\ °C$ lower in the last tape path (tape path 24). Besides the first layer, the values are comparable and do not significantly alter dependent on the number of layers and, thus, the substrate thickness. The substrate temperatures during laying the first layer are lower to the subsequent ones. These measurements are exposed to high fluctuations since the thermal imaging camera primarily measures the heating table. The emission coefficient of the thermal imaging camera is calibrated according to the black tape material and not to the reflective surface of the aluminum table which leads to inaccurate measurements.

Taking a closer look on the 90° layers, one can also observe similar behavior. Independent of layer or substrate thickness, the average values of the substrate temperature are not changing. In contrast to the 0° layers, the 90° layers show a continuous increase of the temperature along each layer. From the first until the last tape path the substrate temperature is increasing. Additionally, the average temperature values of the 90° layers are higher and the difference between the first tape path and the other ones is less. A change in fiber orientation, as in layer 3, 7, 10 and 14, seems to have no effect on the average measured substrate temperature.

To summarize, independent of cooling time, fiber orientation and change in fiber orientation, the median temperature of the cooled substrate right before the process zone keeps constant over time. In addition, the temperature values of the 90° layers are in average higher than the 0° layers. The following derivations can be drawn which have to be investigated more closely:

- A change in fiber orientation is likely to change the cooled substrate temperature since the substrate is exposed to shorter cooling times;
- Long pauses between the layers, as in this example, may have caused an equilibrium temperature of the cooled substrate;
- Uneven tool temperature of the heated table may cause different temperatures within a layer.

4.2.4 Degree of Bonding (DoB) estimation and validation

Vorhersage und Validierung des Konsolidierungsgrad

Combining the measured temperature, as shown in Figure 4.8, with the analytical model of the DoB, predictions regarding the quality of the process can be made. The model by YANG AND PITCHUMANI [YANG03, p. 269] according equation (4.23) combined with equations (4.19-4.22) is used for calculating the DoB as explained in section 4.1.2.

An example of the interpreted data of layer one to three is shown in Figure 4.10. As can be seen in the analytical model, the DoB values directly corresponds to the measured temperatures. With these finding, the following expectations regarding the DoB can be drawn:

(a) the homogeneous temperature distribution in the major area of the laminate results in a homogeneous DoB;

(b) the DoB in the run-in areas is higher compared to the run-out areas.

The interlaminar shear strength (ILSS) according to DIN EN ISO 14130 [DIN97] allows the evaluation of the DoB. This short beam test introduces the failure in the bonding zone of each layer. This is why it is suitable for estimating the consolidation. 23 specimens are cut out by waterjet cutting out of the laminate as shown in Figure 4.11.

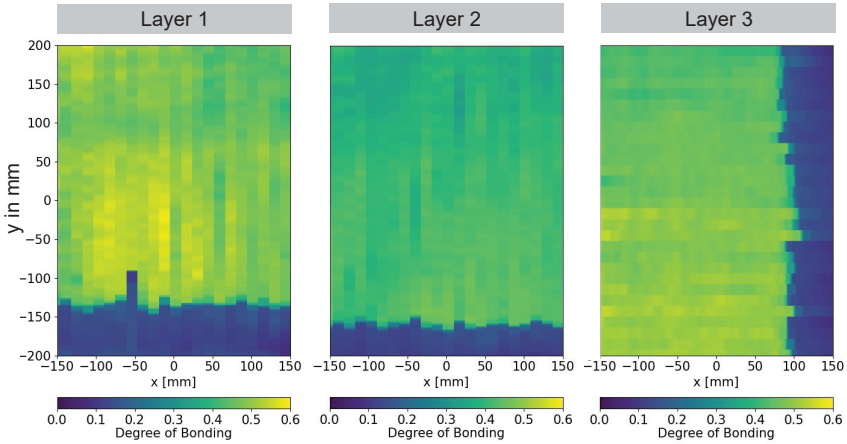

Figure 4.10: Degree of Bonding (DoB) of the first three layers

Konsolidierungsgrad der ersten drei Lagen

Nine areas are selected to correlate the corresponding values with the DoB prediction. In the upper (area 1-3) and lower (area 7-8) zones two specimens per area and in the middle zone (area 4-6) three to five specimens per are taken. The number of specimens is limited to stay as close to one location as possible. This comes along with the drawback that only limited statistical variations are considered due to the low number of specimens per area. Some specimens are cut twice and only the specimens with the marks, as can be seen in Figure 4.11 are used for the ILSS testing due to errors in the waterjet cutting. Area 1, 2 and 3 are located at the run-in zones of the 0° layers as well as areas 3, 6 and 9 for the 90° layers. Accordingly, areas 7, 8 and 9 as well as 1, 4 and 7 are within the run-out zones of the 0° and 90° layers.

The ILSS value σ_{ILSS} of each specimen is calculated according to the standard [DIN97]:

$$ILSS = \sigma_{ILSS} = \frac{3}{4}\frac{F}{b \cdot h}\left[\frac{N}{mm^2}\right]. \tag{4.35}$$

F is the force at interlaminar failure and b and h are the actual width and the height of the ILSS specimens. Depending on the measured force curve and how the specimens fail, the value for F is taken differently. Either it is derived by the maximum load at breakage or the first local maximum or plateau of the measured force curve. The norm is commonly design for brittle, thermoset composites, which generally fail at maximum force. The force curve makes a significant drop at the end. However, ductile thermoplastic materials behave differently at failure. The specimens generally do not fail by a significant drop of the force since they entail a more ductile behavior. In this case, either the first occurring local maximum or the plateau area is taken for F.

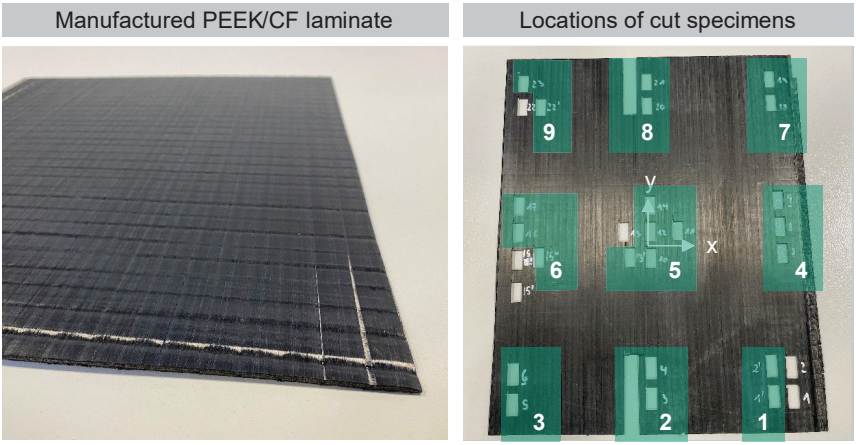

Figure 4.11: Specimen preparation for ILSS tests and microsections according to the areas of interest

Probenvorbereitung für ILSS-Tests und Schliffbilder entsprechend den Zonen

Figure 4.12 shows the results of the ILSS tests. The mean value off all specimens is $49.93\ MPa$ with a standard deviation of $6.43\ MPa$. Maximum value is $60.91\ MPa$ and minimum value is $38.95\ MPa$. A reference value from literature is $ILSS_{max} = 94\ MPa$ taken from the study by KHAN ET AL. [KHAN10, p. 104].

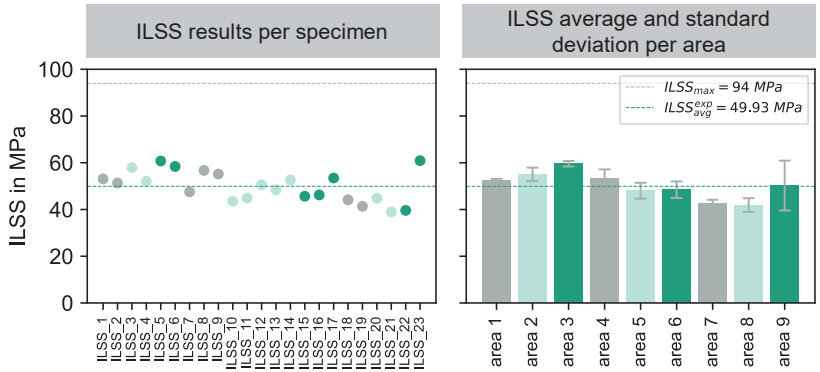

Figure 4.12: Overview of the ILSS results

Überblick über die ILSS-Ergebnisse

To doublecheck the ILSS values and to find the causes, microsections are made. Three specimens are taken out of area 2, 5 and 8 (see Figure 4.11) and are shown in Figure 4.13. They show 4 layers of the 90° layers surrounded by 0° layers. The pictures show a general homogeneous fiber distribution and structure of the layup. However, voids, indicated as black spots in Figure 4.13, can be observed in the bonding zones between the tapes. Black spots within a layer are voids which cannot be traced back to the AFP processing and result from the tape itself. Although microsections only give a very local insight, they show that the bonding between the layers is not ideal. The existing voids (marked green) support the ILSS results shown above.

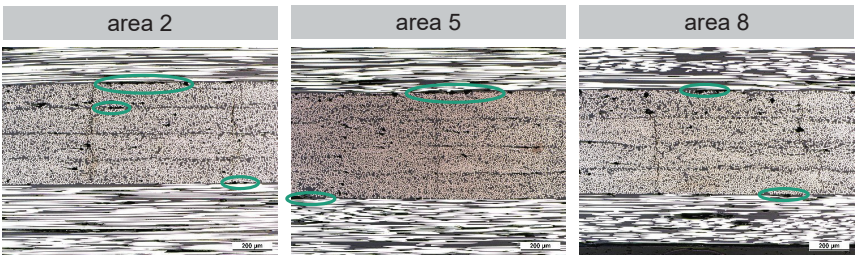

Figure 4.13: Microsections for evaluating the consolidation (voids are marked green)

Schliffbilder zur Evaluierung der Konsolidierungsgüte (Poren grün markiert)

The predictions in Figure 4.10 indicate values lower than $0.6\ (60\%)$ stating that full consolidation is not achieved in the laminate area. The data also illustrates low variations despite of the run-out zones (0°: 7, 8, 9; 90°:1, 4, 7), whose ILSS values are

predicted to be lower. By comparing the analytical forecast with the actual experimental results allows to evaluate the prediction accuracy. The methodology is adapted from KHAN ET AL. [KHAN10, p. 104] who use the following equation to calculate the experimental DoB:

$$D_{B,exp} = \frac{ILSS_{exp}}{ILSS_{max}} \tag{4.36}$$

The maximum ILSS value of $ILSS_{max} = 94\ MPa$ is taken from the study by KHAN ET AL. [KHAN10, p. 104]. This value is a high reference value as it is experimentally determined with PEEK/CF laminates manufactured by gas-based AFP with in-situ consolidation and afterwards consolidated again by an autoclave. This is considered to achieve maximum consolidation degrees due to having more time for crystallization. The mean DoB of all specimens is $\mathrm{D}_{B,exp}^{avg} = 0.53$, the maximum $\mathrm{D}_{B,exp}^{max} = 0.65$ and the minimum $\mathrm{D}_{B,exp}^{min} = 0.41$.

These values correspond to the overall picture of a mostly homogeneous DoB as forecasted by the analytical model. The high and low ILSS values achieved in area 3 and 7 match the expectations. In all layers, area 3 is within the run-in zone. These zones have constant and robust process conditions at all times. In contrast, area 7 always lies within the run-out zone. In this area, the values show that the desired nip-point temperature is not achieved. This results from the cut tape which falls down and creates a shadow on the nip-point. The results also highlight inconsistencies of the analytical modeling. It is expected that area 5 located in the middle of the laminate receives higher ILSS values than average. The values of area 4 and 9 are anticipated to be lower than average being areas mostly exposed to run-out zones.

In general, it can be summarized that the predicted values are consistent with the experimental derived ones. All values are in a range of approximately $D_B = 0.4 - 0.7$. However, the following assumptions must be kept in mind which can impact the results:

- The model of YANG AND PITCHUMANI [YANG03] relies on various assumptions which do not fully apply to the conducted experiments as discussed in [SCHU21]. For example, dynamic effects, such as the *reconsolidation effect* due to multiple rolling over of the applicator head is not modeled.

- The experimentally derived DoB value uses a maximum ILSS value taken from literature. A comparative laminate, fully consolidated by an autoclave, is not manufactured in this study. Deviations of the mechanical characteristics are likely since the choice of the manufacturing technology can significantly influence the degree of crystallinity (especially in the case of autoclave consolidation), as discussed amongst others by GROUVE [GROU12].

- The random sample of the ILSS testing per area is limited which technically does not fulfill the norm and cannot proof statistical significance.

- The laminate is manufactured based on process parameters derived with simplistic assumptions in literature. No process optimization to increase consolidation quality is conducted.

4.2.5 Interim conclusion

Zwischenfazit

The status-quo analysis is conducted to analyze the necessity of digitization of the in-situ AFP process. A PEEK/CF laminate with a conventional robot-based system is produced and analyzed with respect to cooling times, thermal behaviors and the degree of consolidation. It is shown that cooling time can strongly differ as soon as different fiber orientation come into place. The visualization of the heating data, the measured temperature in the process / nip-point zone, helps to understand where process and system conditions influences the quality, such as in the run-out zones. The cooling behavior has shown that a change in fiber orientation is likely to change the cooled substrate temperature since the substrate is exposed to shorter cooling times. It also gives the conclusion, that equilibrium temperatures around the tool temperature dominate due to the slow processing, especially between each layer. The highly transient temperature evolution does not become apparent as it is assumed for very fast process conditions. This analysis does not only give a first idea of a part-oriented process analysis. It also make the drawbacks of non-integrated production systems apparent hampering an integration into the I4.0.

4.3 Creation of a digital twin for the AFP with in-situ consolidation

Entwicklung eines Digitalen Zwillings für den AFP Prozess mit in-situ Konsolidierung

The discussion about existing analytical models (section 4.1) and the experimental status-quo analysis (section 4.2) reveal the need to create a more realistic model within a digital twin for the AFP process. This section channels the gathered information and proposes a digital twin for the AFP process with in-situ consolidation to simplify process analysis and prediction in the future.

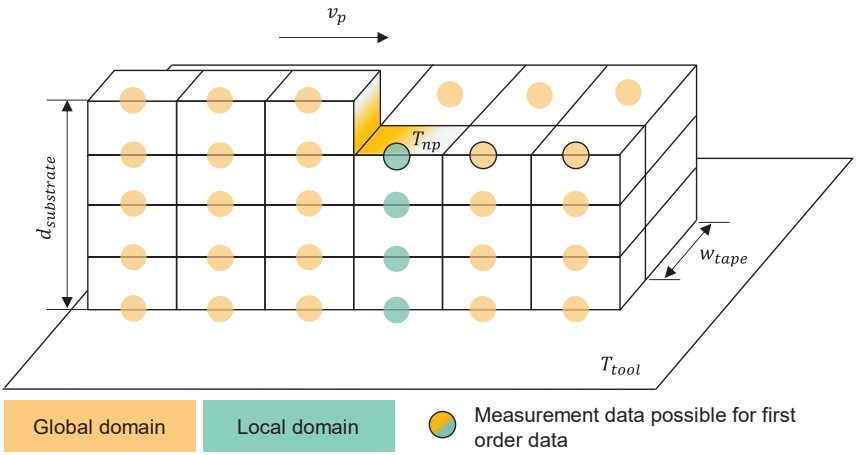

Figure 4.14: Representation of the local and global domain of the digital twin

Darstellung der lokalen und globalen Domäne des digitalen Zwillings

4.3.1 Structure of the digital twin

Struktur des Digitalen Zwillings

The digital twin acts on multiple domains. In the short domain, it captures the local heat problem focusing on the influence of radiation in the nip-point area. In the long domain, cooling takes place affecting the global heat evolution. A discretized representation of the problem is illustrated in Figure 4.14. Depending how the data is gained, either experimentally or theoretically, the data is clustered into two categories. *First order data* refers to information derived by actual measured data, such as temperature measurements within and around the nip-point (black bordered in Figure 4.14). *Second order data* is data which is theoretically derived based on assumptions and either on analytical or numerical calculations. This is the case for the heating gradient within the substrate in the local domain as well as the cooling behavior of the substrate in the global domain. The estimated temperature evolution in the local and global domain enables the quantification of quality indicators. In comparison to the first order data, the term second order refers to the two-way data interpretation of the measured nip-point data.

The digital twin can also be used vice-versa to optimize the process parameters, such as the required laser heat flux with respect to the desired nip-point temperature. The calculation procedure is visualized in Figure 4.15.

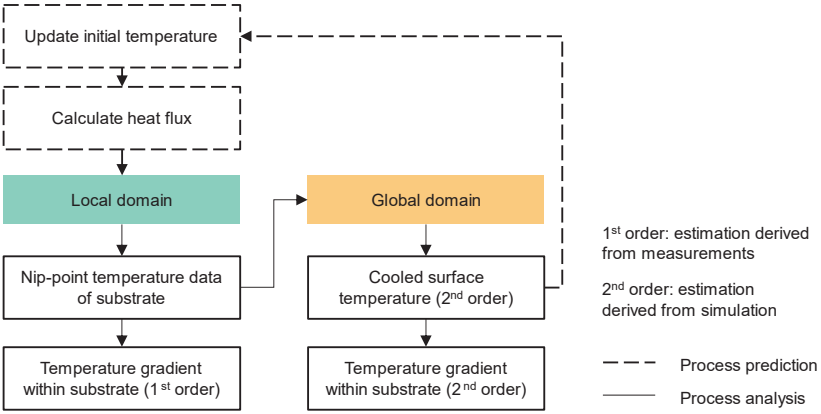

Figure 4.15: Flow chart for the temperature prediction within the digital twin

Flussdiagramm für die Temperaturvorhersage durch den Digitalen Zwillings

The temperature data and derived quality indicators are calculated for defined nodes based on a FDM approach. The following simplifications are undertaken to cope with potential modeling and validation complexities:

- Only the middle of the tape is considered;
- No heat transfer in x- and y-direction;
- The heating phase of the tape in the process zone is not considered, only the substrate cooling is considered in the local and global domain.

In addition, based on the previous description of models in literature (see chapter 4.1), the following assumptions hold within this study:

1. Heat generation and sink effects are neglected.
2. Each point on the laminate experiences the same cooling time t_C as long as the geometry of the layer is not changing. The cooling time depends on the main production time for laying one path and the auxiliary time as well as the laser irradiation time: $t_C = t_P - t_L = t_{main} + t_{aux} - t_L$.
3. The laser irradiation time t_L is dependent on the set process speed and based on values from literature.
4. The manufacturing of a two-dimensional laminate with high process speeds ($v_P \gg 500\ mm/s$) underlies isothermal (constant diffusion coefficient of the polymer and t_w) and isobaric conditions.
5. Due to increased process speeds, it is assumed that there exist no heat losses to the environment in the short domain. Only one-dimensional heat conduction within the tape material is considered.
6. A mold temperature T_{tool} is considered at $z = 0$ on which the tapes are laid.

7. Cooling to the environment by convection is considered in the long domain with convection coefficient h_{conv} and environment temperature T_∞.

4.3.2 Local, transient temperature derivation

Lokale, instationäre Temperaturhervorsage

To enable a digital twin as well as to derive quality indicators one would like to know which temperature profiles the laminate experiences in thickness direction. Previous work on the temperature evolution in thickness direction is shown in section 4.1.1. In this section, an analytical and numerical implementation is explained and compared for the solution of the following one-dimensional heat equation, initial and boundary condition:

$$k_z \frac{d^2T}{dz^2} = \rho c_p \frac{dT}{dt} \tag{4.37}$$

Initial condition: $$T(t=0) = T_i \tag{4.38}$$

Boundary conditions:

Analytical $$k_z \frac{dT}{dz} = \begin{cases} \dot{q}_0''(z=d) \\ 0(z=0) \end{cases} \tag{4.39}$$

Numerical $$T(t) = \begin{cases} T_{np}(z=d) \\ T_{env}(z=0)(=T_{tool}) \end{cases} \tag{4.40}$$

Analytical implementation. Equation (4.13) calculates the transient temperature development during the local process moment for each layer in thickness direction.

Numerical implementation. A FDM calculation based on the forward time centered space (FTCS) scheme is implemented in Python. This scheme uses the explicit forward Euler method in time i and central difference in space j to numerically derive the solution for the 1-D heat equation (see equation (4.37)) according to [INCR07, p. 303]:

$$T_i^{j+1} = Fo\left(T_{i+1}^j + T_{i-1}^j\right) + (1-2Fo)T_i^j, \tag{4.41}$$

with $Fo = \alpha\Delta t/\Delta x^2$ being the finite difference form of the Fourier number. Equations (4.38) and (4.40) are the initial and boundary conditions. A numerical stable solution requires

$$Fo = \frac{\alpha\Delta t}{\Delta x^2} \leq \frac{1}{2}. \tag{4.42}$$

To fulfill the stability criteria in (4.42), time and spatial steps need to be adjusted accordingly. Figure 4.16 illustrates the temperature curves for the analytical and numerical solution with the same exemplary conditions. Both solutions predict similar temperature gradients within the substrate. The small variations between the analytical and numerical solution are caused by their slightly different use of boundary conditions, their assumptions and how they are implemented.

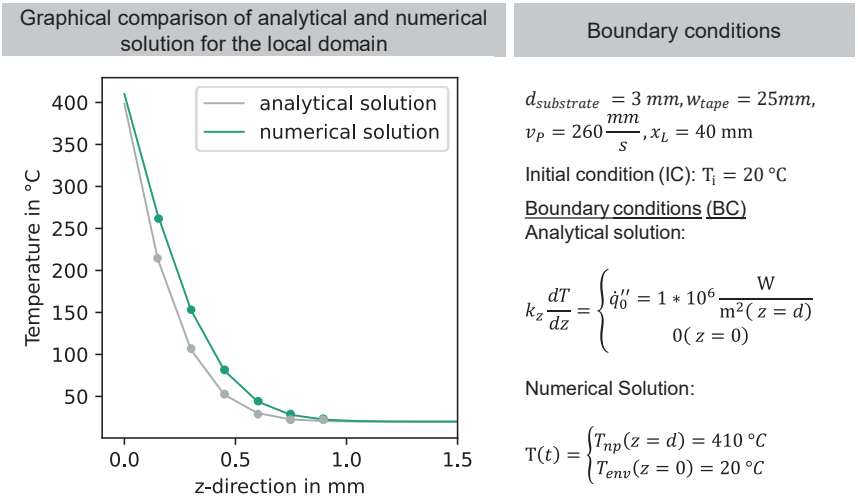

Figure 4.16: Comparison between analytical (equation (4.13)) and numerical solution (equation (4.41)) for the local domain and the same boundary conditions

Vergleich zwischen analytischer (Gleichung (4.13)) and numerischer Lösung (Gleichung (4.41)) für die lokale Domäne und den gleichen Randbedingungen

During the layup process, the following conditions within the analytical or numerical model for the local domain change:

- $d_{substrate}$: substrate increases with each layer;
- T_i: initial condition changes due to the cooling time of the specific point on the laminate.

In addition, process parameters, such as the process velocity v_P and the used laser power P_L may change. These conditions need to be updated to derive the transient heat development within the digital twin for the whole laminate.

Calculating surface heat flux (prediction). In order to estimate the laser power P_L equations (4.10) and (4.12) can be rewritten for achieving the required surface temperature at the nip-point $T_{surface}(t_L)$ at $z = 0$. Converted to the surface heat flux $\dot{q}_0$ both equations allow the laser power estimation $P_L = \dot{q}_0'' x_L w_{tape}$ based on a desired surface temperature $T_{surface_{set}}$ and substrate thickness $d = N d_{tape}$ at process speed $v_P = \frac{x_L}{t_L}$.

Semi-infinite and finite problem:

$$\dot{q}_0'' = \frac{(T_{surface,set} - T_i) \cdot k_z}{2\sqrt{\alpha}\sqrt{t_L}} \cdot \frac{1}{\sum_{i=0}^{\infty}\left(ierfc\left(\frac{2d \cdot i + z}{\sqrt{4\alpha t_L}}\right) + ierfc\left(\frac{2d \cdot (i+1) - z}{\sqrt{4\alpha t_L}}\right)\right)} \tag{4.43}$$

This equation can be implemented to predict new process parameters as illustrated in Figure 4.15. The initial condition T_i can be continuously updated based on the current process conditions.

4.3.3 Global, transient temperature derivation

Globale, instationäre Temperaturvorhersage

In the global domain, the substrate experiences cooling after being processed by the tape laying applicator. In theory, this is often assumed as infinite. In reality, the stacking of the tapes implies a repeated rolling over, causing a reconsolidation effect between the tapes. Consequently, the cooling time t_c is the time difference the spatial node xyn of the same layer experiences between two process moments:

$$t_c = t_{np,i}^{xyn} - t_{np,i-1}^{xyn}. \tag{4.44}$$

The process / nip-point moment is indicated by the subscript np. The subscript i indicates the time step. Within this time frame the substrate cools due to convection with convection coefficient h_{conv} to the heated mold temperature which has the temperature $T_\infty = T_{tool}$. This assumption is often neglected in literature since cooling in the long domain is neglected as explained in section 4.1.1. This study assumes cooling to the environment in the long domain.

The solution is numerically derived by FDM with the FTSC scheme. The energy balance of equation (4.3) is added with a convection transfer term resulting in the following 1-D convection-diffusion equation:

$$\alpha \frac{d^2T}{dz^2} = \frac{dT}{dt} + h_{conv}A\frac{dT}{dx}. \tag{4.45}$$

The term $h_{conv}A$ with A being the respective area of convection depicts the convection velocity. Transformed into a numerical representation for the specific case, equation (4.45) turns into [INCR07, p. 305]:

$$T_i^{j+1} = 2Fo\left(T_{i+1}^j + Bi\, T_\infty\right) + (1 - 2Fo - 2BiFo)T_i^j. \tag{4.46}$$

Bi is the *Biot number* whose difference form is

$$Bi = \frac{h_{conv}\Delta x}{k_z}. \tag{4.47}$$

The dimensionless *Biot number* compares the thermal resistances within a body and the surface exposed to convection. A small *Biot number* ($Bi \ll 1$) indicates a uniform

temperature gradient within the body at any time [INCR07, p. 260]. To calculate the cooling of the surface as well in thickness direction during the AFP process, equation (4.46) is calculated for the process and geometry individual cooling time t_c.

4.3.4 Local and global quality indicators

Lokale und globale Qualitätsindikatoren

Calculating bond strength (DoB). The aim of forecasting the degree of bonding is to estimate the consolidation degree and, thus, to give an indication of the process quality as well as the mechanical performance. The implementation is based on the coupled bonding model by YANG AND PITCHUMANI [YANG03, p. 269] as described in section 4.1.2. The temperature in the nip-point zone is taken as input variable $T = T_{np}$. Based on the previous findings, as discussed in section 4.1.2, it is assumed that autohesion can be fully developed ($D_{AH} = 1$) given the experimental setup in this study.

The influence of the surface roughness on the D_{IC} is specified according to the model of LEE AND SPRINGER [LEE87, p. 1032] as described by equation

$$D_{IC} = \frac{1}{1+\frac{w_0}{b_0}}\left[1+5\left(1+\frac{w_0}{b_0}\right)\left(\frac{a_0}{b_0}\right)^2\int_0^{t_{IC}}\frac{P_{cons}}{\mu_0(T)}dt\right]^{\frac{1}{5}}. \tag{4.48}$$

a_0, b_0 and w_0 describe geometrical properties of the tape material. A detailed investigation of suitable models for PA6/CF tape can be found in [SCHÄ17, p. 73]. It has to be noted, that the investigation by SCHÄFER rely on a tape with a resin-rich layer which has an influence on the prediction quality. However, as noted previously the detailed derivation of tape properties is out of scope of this thesis.

Calculating the degree of crystallinity (DoC). The aim of forecasting the DoC is to derive insights into the mechanical strength of the finale laminate. Due to the additive character as well as the transient heat evolution caused by the fast processing, each point in space experiences multiple heating cycles. This causes different crystallization kinetics within the polymer. Given the time each point in space experiences the crystallization temperature range, the relative DoC can be estimated. This range is between the glass transition temperature T_g and the melting temperature T_m of the polymer as proposed by [HOSS20, p. 3078]. Figure 4.17 illustrates how the repeating rolling over of the applicator head influences the DoC. It shows the cumulative effect it has on the DoC.

The crystallinity calculation relies on the previously mentioned literature (section 4.1.3). The Nakamura model according to equation (4.25) as well as the empirical function of the temperature-dependent constant $K(T)$ proposed by ZIABICKI are implemented:

$$K(T) = K_{max}\exp\left(-\frac{4\ln(2)(T-T_{max})^2}{D^2}\right). \tag{4.49}$$

This combination is called the *Nakamura-Ziabicki* model and has proven to show good agreement with experimental results, especially for high cooling rates and PA6 polymers [KUGE17; FELD19].

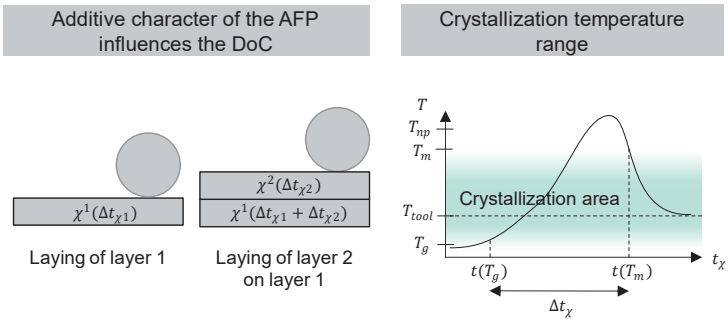

Figure 4.17: Relative Degree of Crystallization (DoC) development during the AFP process

Entwicklung des relativen Kristallinitätsgrads (DoC) beim AFP Prozess

The solution of equation (4.25) is derived within a time span ($\Delta t_\chi (T_g < T < T_m)$ characteristic for the individual laminate processing as illustrated in Figure 4.17. Each point in space experiences different time spans in which crystals can be built and, thus, a specific DoC can be determined.

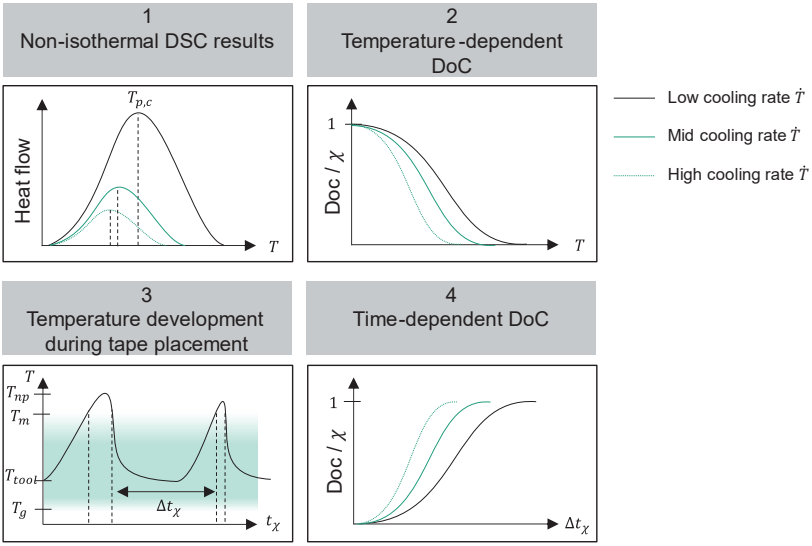

Figure 4.18: Proposed methodology to determine the DoC of the laminate based on the Nakamura-Ziabicki model

Vorgeschlagene Methodik zur Bestimmung des DoC des Laminats auf der Grundlage des Nakamura-Ziabicki-Modells

Figure 4.18 illustrates the methodology of determining the cooling-rate dependent, relative DoC for one heating cycle during the tape placement process as proposed in this study. It comprises of four steps:

1. Based on non-isothermal, cooling rate dependent (process velocity dependent) DSC analysis relevant parameters, such as $T_{p,c}$, are derived;
2. Equation (4.25) is calculated with $K(T = T_{p,c})$ and the derived parameters as derived by [FELD19, p. 255] (see Table 4.2);
3. From the measured or predicted temperature development of each point in space of the laminate the time span Δt_χ is derived in which the temperature is between $T_g < T < T_m$ and crystallization can tape place.
4. Δt_χ is used to estimate the relative DoC.

The (isokinetic) constant $K(T)$ relates to the isothermal crystallization half-time, where $\chi_{1/2} = 0.5$ [HOSS20, p. 3073; NAKA72, p. 1081], and is calculated for the crystallization temperature $T_{p,c}$. This enables the application of isothermal crystallization analysis results to the non-isothermal domain [NAKA73, p. 1035].

FELDER ET AL. [FELD19, p. 256] derives the cooling rate dependent values for K_{max}, T_{max} and D for PA6 by non-linear optimization which are given in Table 4.2.

Due to the additive character of the tape placement process and to integrate the reconsolidation effect, the relative DoC is calculated for each layer as visualized in Figure 4.17. The finale relative DoC of the laminate $\chi^{lam}(t)$ is calculated by taking the average of each value:

$$\chi^{lam}(\Delta t_\chi) = \sum_{n=1}^{N} \chi^n \left(\sum_{i=1}^{t_N} \Delta t_{\chi i}\right) \Big/ N, \tag{4.50}$$

where Δt_χ is the time each layer experiences within the crystallization temperature range $T_g < T < T_m$ and until the tape applicator comes for the next layer at the same position. During manufacturing the tool temperature of the table is slightly below the initial crystallization temperature $T_{tool} < T_{ic}$ enabling low cooling rates. This implies that the laminate does not reach T_g during manufacturing enabling crystallization during the whole manufacturing process only during the process moment, where $T > T_m$.

Table 4.2: Parameters for Nakamura-Ziabicki model by FELDER ET AL. [FELD19, p. 256]

Parameter des Nakamura-Ziabicki-Modells von FELDER ET AL. [FELD19, p. 256]

Cooling rate $[\dot{T}] = K/min$	$[K_{max}] = \frac{1}{min}$	$[T_{max}] = K$	$[D] = K$
5	9.51	348.22	102.27
10	13.73	348.48	100.48
20	9.28	351.10	109.52
40	7.77	355.17	116.97
60	5.54	362.99	128.31
100	4.80	359.49	125.64

Calculating residual stresses. The approach of the one-sided bending beam by KERMER-MEYER [KERM15, p. 65] is evaluated for the implementation within the digital twin. The experimental validation by the author has shown a good approximation of the warpage after processing [KERM15, p. 79]. For this reason, the implementation can be adapted according to Figure 4.19 as long as simple, unidirectional laminates are produced.

With the information about the temperature, the temperature difference ΔT between the stress-free temperature $T_{p,c} (= T_{stress})$ and the temperature of the layer after laying $T_{substrate}$ can be derived. It can be assumed that this temperature equals the tool temperature of the heating table $T_{substrate} = T_{tool}$. Given this information the new width of the laminate can be derived according to:

$$\Delta w = \alpha_T \cdot \Delta T \cdot w_0, \tag{4.51}$$

$$w = w_0 - \frac{1}{N} \Delta w, \tag{4.52}$$

where α_T is the material-specific thermal expansion coefficient, w_0 the original width and N the number of layers. This elongation results in the force F:

$$F_i = (w_0 - w) \cdot E_\perp + F_i^{n-1} \ . \tag{4.53}$$

F_i^{n-1} is the force of the previous layer whereas the force of the first layer $n = 1$ is assumed zero. $E_\perp$ is the E-modulus of the laminate perpendicular to the fiber direction. The resulting stresses induce a moment M around the middle plane of the laminate. With the area moment of inertia I the given information allows the calculation of the warpage κ [KERM15, p. 67]:

$$M = \sum_{i=1}^{N} F_i \cdot x_i \tag{4.54}$$

$$\kappa = \frac{M}{E \cdot I} \text{ with } I = \frac{w \cdot h^3}{12} \tag{4.55}$$

The model assumption of depositing a layer at once implies that stresses are calculated for the whole width of the laminate and not for the laying of each single tape. This is not applicable for bidirectional laminate focused in this study. The current analytical models are not yet suitable for an implementation within the here-proposed digital twin. Further investigations are required to estimate residual stresses within a laminate manufactured by the AFP process with thermoplastic tapes.

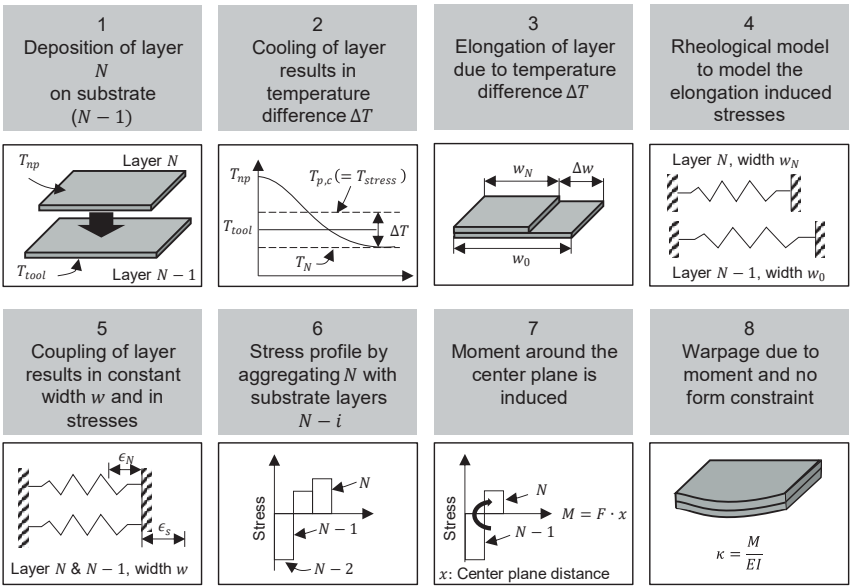

Figure 4.19: Residual stress estimation as proposed by [KERM15, p. 65]

Schätzung der Eigenspannungen vorgeschlagen von [KERM15, p. 65]

4.3.5 Ontology of the AFP process with in-situ consolidation

Ontologie des AFP Prozesses mit in-situ Konsolidierung

The increasingly intensive interlocking of production engineering and computer science results in an increasing application of new methodologies and notations. Creating an ontology is one of these methods from computer science to show how properties of instances interact and behave. It more and more becomes a conventional way to characterize production environments, to organize its data and to visualize its complexity. This semantic representation is the basis for the virtual representation of the production system. [GRUB93, p. 200; ENGE18, p. 2794; JÄRV19, p. 960]

A semi-formal ontology for the here focused AFP process with in-situ consolidation of thermoplastic composites is drafted in Figure 4.20. It shows the main individuals with its relevant classes and attributes as well as how these relate with each other. It determines the essential ideas and relationship. For example, it illustrates the connection between the AFP system with the AFP process: the choice of heating source with its attributes as well as the designs of the tape feed and cutting units significantly influence possible heating lengths of the incoming tape. This influences the irradiation length and, thus, the temperature distribution within the nip-point during tape deposition. The many interacting instances show the complexity of the manufacturing technology but also the potential to cope this complexity by intelligently combining the data within a digital representation. The ontology summarizes the lessons learned from the current

literature about the process interaction and can be seen as a basis for developing a database model.

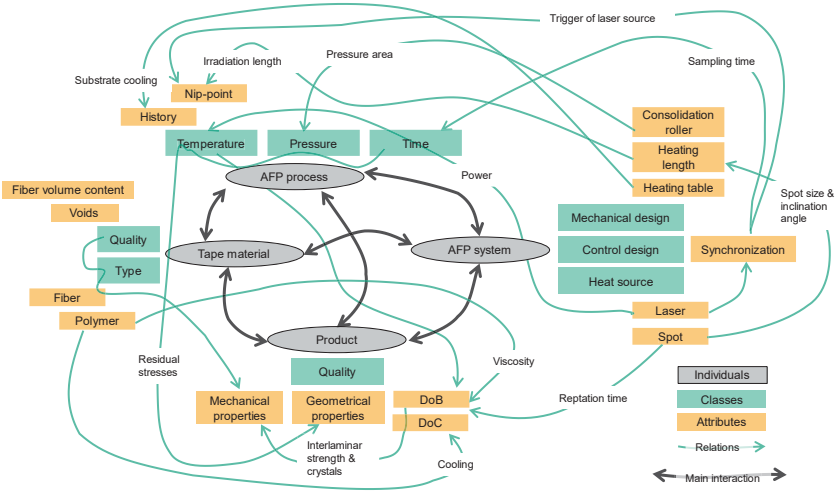

Figure 4.20: Ontology of the digital twin for the AFP process with in-situ consolidation

Ontologie des digitalen Zwillings für den AFP-Prozess mit in-situ Konsolidierung

4.3.6 Interactive visualization of the digital twin

Interaktive Visualisierung des Digitalen Zwillings

A digital twin is often understood as the virtual visualization of the physical part. Although the digital twin entails much more functionalities as explained in section 2.3.1, a digital visualization of the unique physical workpiece helps to better understand the manufacturing process. It links the information of the part with the information of the process, system and material as illustrated in the ontology in Figure 4.20. With the spatially resolution of data, it is possible to localize quality metrics within the laminate, such as process induced defects, and to derive conclusions for next action steps. An example is the localization of interlaminar voids and the decision whether this defect may result in production waste or not. Depended on the defect, it is also possible to decide compensation strategies within a zero-defect production. For this reason, this section drafts a first version of a potential CAx implementation.

To spatially pair local process parameters with local quality metrics the heterogeneous process data need to be homogenized and assigned to a position in space, as depicted in Figure 4.21. Within the work of this thesis, Fraunhofer IPT has developed an algorithm to create an interactive visualization for the AFP process with in-situ consolidation. It is implemented by dynamic spatial resolution with the help of object-oriented programming. Different masks dA containing the relevant process and quality data are created and its size can be adjusted according to the needs of the analysis. This is

especially relevant when using the FDM approach which requires the definition of certain spatial step sizes (explained in section 4.3.2) of the data. Consequently, it is not only a virtualization of data, but also a preparation of spatially resolved data. Care has to be taken with the positioning of each mask. On the one hand, difficulties arise as soon as different fiber orientations are stacked. This results in two superimposed masks which are not positioned accurately above each other. Minimizing the mask size is a solution but needs to be checked with the numerical stability of the FDM calculation (see equation (4.42)).

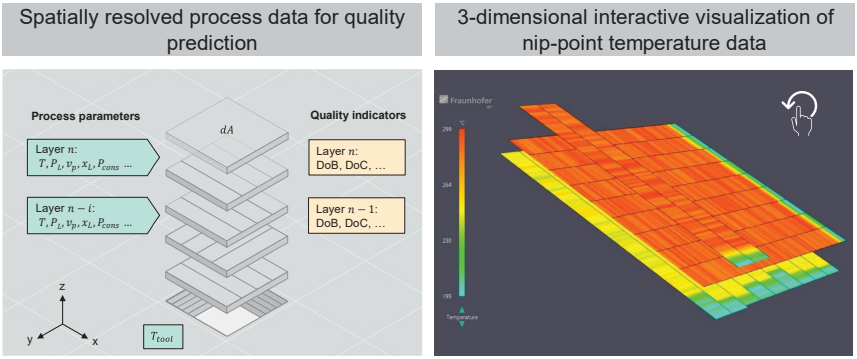

Figure 4.21: Concept of an interactive visualization for spatially resolved process data for a CAx application

Konzept einer interaktiven Visualisierung von ortsaufgelösten Prozessdaten für eine CAx-Anwendung

The advantages of this approach are the dynamic and flexible data preparation and visualization irrespective of laminate geometry and layup. The other important feature is the three-dimensional (3D) visualization which can be used interactively for user inspection and data visualization purposes. In the example in Figure 4.21 the laying of the first two tape paths of the third layer is shown. The process temperatures in the nip-point are visualized showing the slight fluctuations as well as the lower temperatures at the end of each path. This results from the cutting of the tape which then is not guided anymore and falls down creating a shadow on the process zone. The visualization thereby helps to localize, for example, less consolidation qualities due to system specific process influences.

The python program is currently run offline after processing. It is possible to enable an online visualization of the process within the human machine interface (HMI) of the PrePro2D® machine. By including different data, either 1st or 2nd order, the machine operator can switch to the desired visualization and investigate the processing. It may also be adapted for automatic decision making in future.

4.4 Conclusion

Zusammenfassung

This chapter about the creation of a digital twin reveals the complexity of drawing a holistic picture of the AFP process with in-situ consolidation. Chapter 4.1 takes a close look at the existing analytical models and evaluates their potential for application within the digital twin. Temperature models and models for quality indicators, such as the degree of bonding, are analyzed specifically with regard to their assumptions. The strict boundary conditions of the existing models are highlighted which need to be softened and adapted to allow a more realistic, part-oriented modeling of the AFP process. The status-quo analysis in chapter 4.2 reveals the necessity of digitization by the digital twin. It demonstrates how process, part and system conditions influences the quality of the laminate and how a digital twin helps to understand the interacting relationships. Finally, based on the previously derived requirements in the first two chapters, chapter 4.3 proposes a digital twin modeling technique. It entails not only the structure, but also the choice of models and its implementation. It is a first tool to enable a more part-oriented, realistic process modeling.

In summary, this chapter gives an answer to the first research question stated in chapter 3. It shows the potentials to use the digital twin for aiming a zero-defect manufacturing, reducing ramp-up times and even reducing inspection processes. To validate the proposed methodology, chapter 5 implements and validates the digital twin for a specific manufacturing case and discusses the results.

5 Experimental validation of the digital twin

Experimentelle Validierung des Digitalen Zwillings

The derived digital twin is experimentally validated with the PrePro2D® system at Fraunhofer IPT. Laminates with a $0°/90°$ layup out of PA6/CF are manufactured, digitized and interpreted. This chapter first provides an overview of the novel PrePro2D® technology and its integrated architecture to show its benefits for data-driven process optimization. The second part uses the created digital twin in chapter 4 for process prediction. Temperature development and the quality indicators for consolidation and crystallization are quantified. The experimental validation is adapted according to procedures used in literature. The results proof the general good prediction quality of the digital twin process model. But they also outline room for improvement since the transfer from idealized to realistic process modeling inherits complexities.

5.1 PrePro2D® production system

PrePro2D® Produktionssystem

The PrePro2D® system developed by Fraunhofer IPT is used for the manufacturing of tailored blanks out of thermoplastic UD-tape. It is based on a tape laying head connected to a gantry system and a rotary table as illustrated in Figure 5.1. The tape laying head allows the feed of three tapes simultaneously and independently which enables optimized near-net shape laminates. The cutting unit can cut the tape with a *cut-and-add-on-the-fly* process. This means that a fully consolidated laminate can be achieved from the beginning till the end of the laid tape path.

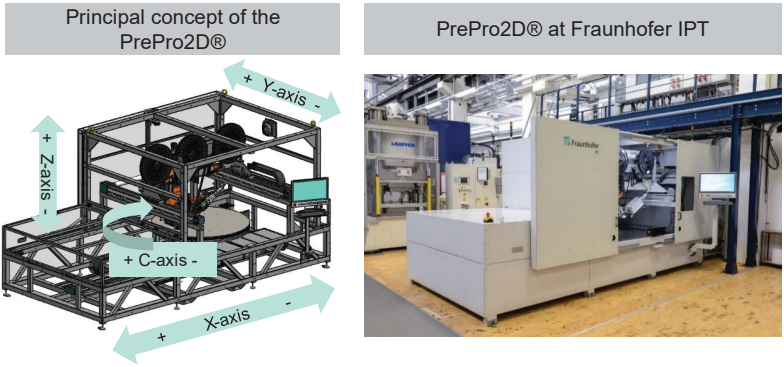

Figure 5.1: PrePro2D® manufacturing system for the upscaled production of thermoplastic, tailored composite blanks with in-situ consolidation at the Fraunhofer IPT

PrePro2D®-Fertigungssystem für die hochskalierte Herstellung von belastungsoptimierten Organoblechen mit in-situ Konsolidierung am Fraunhofer IPT

The previous concept of the machine integrates an infrared heating source for the in-situ consolidation with a long consolidation unit to allow high speed layup. This comes

with the benefits of having much lower investment costs as well as reduced requirements regarding radiation safety. The target application is PA6 (or polymers with lower T_m) laminates for the automotive industry. However, the drawback of this heating device is that its radiation intensity is lower compared to a laser source and the difficulty to run an accurate closed-loop control. Infrared emitters have higher latencies and standard metrology, such as pyrometers or thermal image cameras, cannot be easily implemented due to the intersecting wavelengths. Additionally, longer heating length and time is required to sufficiently heat up the tape. A detailed description of the prior machine concept can be found in [JANS20, p. 83ff].

To allow the upscaling of this manufacturing system with respect to process speeds as well as to material variety, the concept has been updated. Hardware and software of the machine are optimized allowing the integration of novel digitization and control methods. The machine also meets the high safety standards, especially regarding laser safety, and fulfills CE-conformity.

5.1.1 Optimized components

Optimierte Komponenten

The major adjustment of the novel PrePro2D® compared to the prior concept by JANSSEN [JANS20, p. 83ff] are explained in the following.

Laser source and optics. The heating source for the in-situ AFP process is a diode laser by *Laserline* (LDF4500-30). This heating source is chosen since diode laser have proven to acquire high efficiencies when it comes to thermoplastic tape laying. The benefit of short control cycles comes along with homogenous intensity distributions. The wave lengths between $920 - 960\ nm$ have shown to gain high consolidations during the laying of thermoplastic tape with black coloring which are commonly available on the market. In various studies, such as the ones by VOR DEM ESCHE [VOR01], STEYER [STEY12] or STOKES-GRIFFIN ET AL. [STOK15], the integration of a diode laser is discussed and analyzed in detail which is why it is not further discussed in this thesis.

The laser source at the PrePro2D® is connected to a zoom optic of *Laserline* (OTZ) allowing the flexible creation of spots between $12x12\ mm^2 - 80x80\ mm^2$ (see Figure 5.2). This enables the adjustment of the laser spot dependent on the desired process conditions. It is also possible to adjust it during processing. This can be relevant as soon as less tapes are fed simultaneously or to investigate different spot sizes during laying. To assure safety requirements, the housing of the machine is a welded frame with double-walled steel sheets, especially in the areas of laser radiation and reflection.

Consolidation unit. The system consists of a standard consolidation unit with a silicone sleeve conventionally used in the laser-assisted AFP process as developed by STEYER [STEY12] and used by KERMER-MEYER [KERM15]. Compared to the system by JANSSEN [JANS20] this results in a reduced heating and cooling length. However, this enables not only the production of flat laminates, but also of two-and-a-half dimension having, for example, a ramp.

Tape feed. The tape feed has been adjusted by integrating drive axle for each individual tape spool. Depending on the given feed rate of the process, the servo motors rotate the spools and thereby uncoil the tape. It is controlled by a dancer which enables constant tension during processing of various speeds. This becomes relevant for high process speeds and changing mass inertia of the tape spool. The feed unit on the applicator head is updated by including only one drive axle for all three tapes. The feed can be coupled and decoupled by clutches. This still allows a cut-and-add-on-the-fly process without requiring a drive axle for each tape. This as well as a reduced cutting length of approx. $100\ mm$ also allows to manufacture complex laminate shapes.

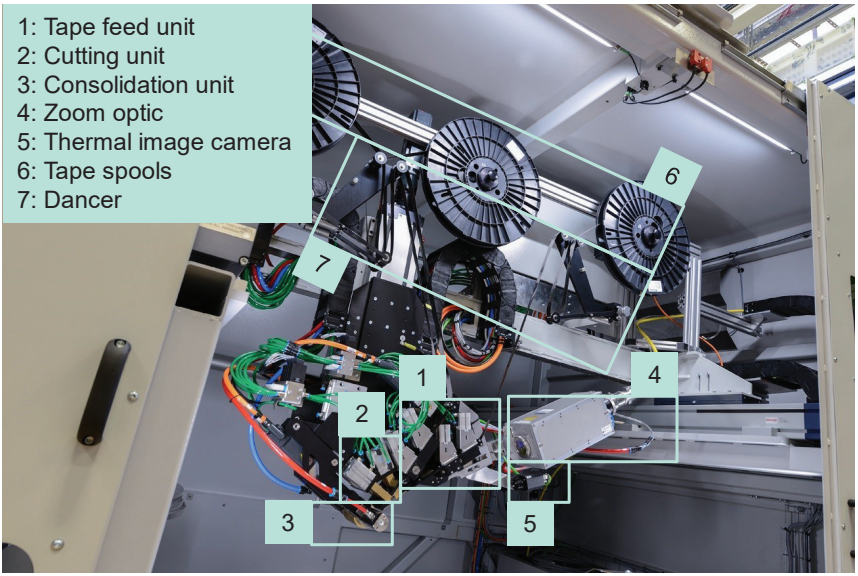

Figure 5.2: PrePro2D® laser-assisted AFP applicator with its major components

AFP-Applikator mit seinen Hauptkomponenten der laserunterstützten PrePro2D® Anlage

5.1.2 Modern control environment

Moderne Steuerungsumgebung

The updated machine concept comprises of up to nine actively controlled axes:

- X-axis: The x-axis linearly moves the rotating heating table beneath the applicator head along the length of the machine. It is responsible for the process speed during the AFP process;
- Y-axis: The y-axis moves the applicator head along the width of the machine. It moves as soon as the next tape path is laid;
- C-axis: The c-axis is the rotation axis of the heated table. It rotates depending on the desired fiber angle;
- Z-axis: The z-axis shifts the applicator head up and down;

- t1 to t3-axes: The t1, t2 and t3 -axes are the three axes of the spools uncoiling the tape depending on the process speed;
- t-axis: The t-axis is the axis of the tape feed unit. It acts as soon as the tape needs to be forwarded and stops as soon as the tape is beneath the consolidation unit. This happens between the end of a tape path after its cut and before the new tape is laid. A clutch mechanism activates the three tapes independently;
- B-axis: The B-axis rotates the consolidation roller during movement of the x-axis. It is only active in the case of solid rollers. It is inactive in the case of form-adaptive rollers with a silicone sleeve.

The machine control runs on a *Beckhoff* based soft programmable logic controller (soft-PLC) programmed with *Beckhoff TwinCat* and running on a *Beckhoff* Industrial-PC. It allows a complete synchronization of all axes and metrology within one control environment within critical cycle times up to $1\,ms$. The human machine interface (HMI) is working, amongst others, with *HTML5* allowing a dynamic program structure as well as the inclusion of various features. The most important ones for this investigation are the direct integration of the thermal image camera by *Beckhoff TwinCat Vision* and the access to the central data storage.

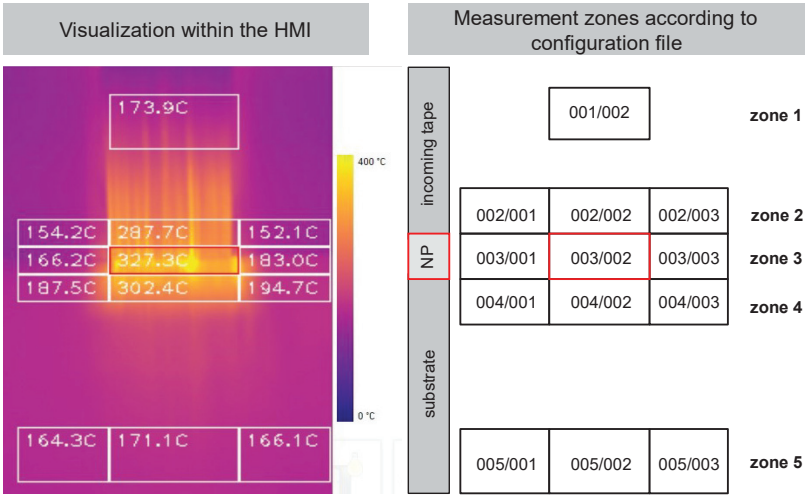

Figure 5.3: Individualization of the thermal image camera setup at the PrePro2D®

Individualisierung des Wärmebildkamera-Setups der PrePro2D®

Data acquisition. The modern control hardware of the machine allows a holistic tracking of the process data. Every sensing part of the machine is connected to one PLC which enables a synchronized assessment of relevant process data. A thermal image camera (*FLIR A35*) with $60\,Hz$ frame rate is connected to measure and control the temperature in the nip-point as well as in the surrounding areas. The arrangement of

measurement zones, as displayed in Figure 5.3, can be individualized with a *.json* configuration file. Up to 11x11 zones can be defined as well as the information whether the temperature is based on minimum, maximum or average values of the included pixels. The red bordered box indicates if this zone is used for the temperature control of the laser heater. It also is the area measuring the nip-point. The emission coefficient of the thermal image camera is set to $\varepsilon = 0.9$ based on previous investigations.

Data base connection. All data is stored to a central database based on a *MongoDB* database management system. The storing of data can be either triggered manually within the HMI or automatically through a specific command in the machine code. The HMI allows to choose the individual datasets as well as the metadata describing, for example, the type of material as well as machine settings. This allows to customize the data storage of the individual process according to the needs of the desired digital twin.

5.2 Experimental digital twin validation

Experimentelle Validierung des Digitalen Zwillings

5.2.1 Experimental design and conduct

Versuchsaufbau und -durchführung

The experimental design is similar to the status-quo analysis of chapter 4.2. Aiming for materials being used for high-production rates, a *Akulon® PA6-HC10 UD PA6/CF-50* tape of the company *DSM* is chosen as tape material. A microsection of the tape material is presented in Figure 5.4.

Figure 5.4: Microsection of the DSM PA6/CF tape

Schliffbild des DSM PA6/CF Tapes

The process parameters are based on previous investigations as well as a short experimental investigation with the PrePro2D® system. They are summarized in Table 5.1. They do not entail an in-depth process optimization.

Processing with the PrePro2D®	Manufactured laminate	Cycle time	
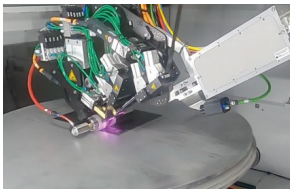	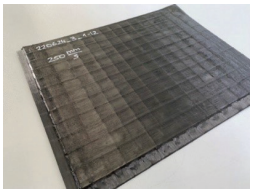	Total duration	$680\ s = 11.34\ min$
		Number of 0° layers / tapes	4 / 48
		Number of 90° layers / tapes	4 / 64

Figure 5.5: Manufactured laminate with $v_P = 250\ mm/s$

Hergestelltes Laminat mit $v_P = 250\ mm/s$

The compression force is measured with a *Fujifilm* pressure measurement film for *Ultra Super Low Pressure*. The used deformable roller has a pressure area of $15\ mm\ x\ 85\ mm$ and a resulting average pressure of approximately $0.4\ MPa$.

Table 5.1: Experimental setup of the digital twin validation

Versuchsaufbau der Validierung des Digitalen Zwillings

Parameters	Details
Material	PA6/CF tape (DSM)
Tape thickness h_{tape}	$0.25\ mm$
Tape width w_{tape}	25 mm
Layup	[0°,90°,90°,0°,0°,90°,90°,0°]
Layup strategy	conventional
Laminate size ($l_x \cdot l_y \cdot N$)	$400\ mm \cdot 320\ mm \cdot 8$
Target nip point temperature T_{np}	300 °C
Laser power P_L	800 W
Mold temperature T_{mold}	150 °C
Ambient temperature T_∞	20 °C
Laser spot size and angle	30 mm x 67 mm / 2°
Compression force F_{cons}	500 N
Process velocity v_P	250 mm/s

The duration to manufacture the laminate is about $11.34\ min$. All data is assessed via the PrePro2D® system and stored to a central database for analysis. A short overview of the experimental result is found in Figure 5.5.

The data is assessed at a frequency of $f = 50Hz$. Since the measurement frequencies of axes encoders as well as other metrology system, such as the thermal image camera, alter, the null values are filled with the respective prior value. Figure 5.6 shows data which is measured during the laying of all 8 layers of the respective laminate (Table 5.1) represented by each peak of the y-axis movement.

Each peak in the nip-point temperature demonstrates the laying of one tape path. Within the same area one can see the movement of the x-axis. The laser is activated prior to the start position of the tape as defined in the machine code. This results in a rapid increase of the nip-point temperature to the desired process temperature or, respectively, the set laser power. It shows the accurate synchronization of the axes as well as the trigger points of the laser activation. During the return of the x-axis to the starting point of the new tape path, the y-axis moves a tape width to the side. As soon as a layer is finished the x-axis and the y-axis return to the beginning of the next layer. In this case, it is always the same starting position for the respective fiber angle (conventional layup strategy). Although the process run smoothly without any interruptions, at some points the data is missing (see two blank spots in Figure 5.6 at approx. $160\ s$

and $400\ s$). This results from short connectivity issues with the central database since the database is still undergoing beta testing. The missing data of these two tape paths in layer 2 and 5 are interpolated by the use of the unique timestamp and the data of the previous tape.

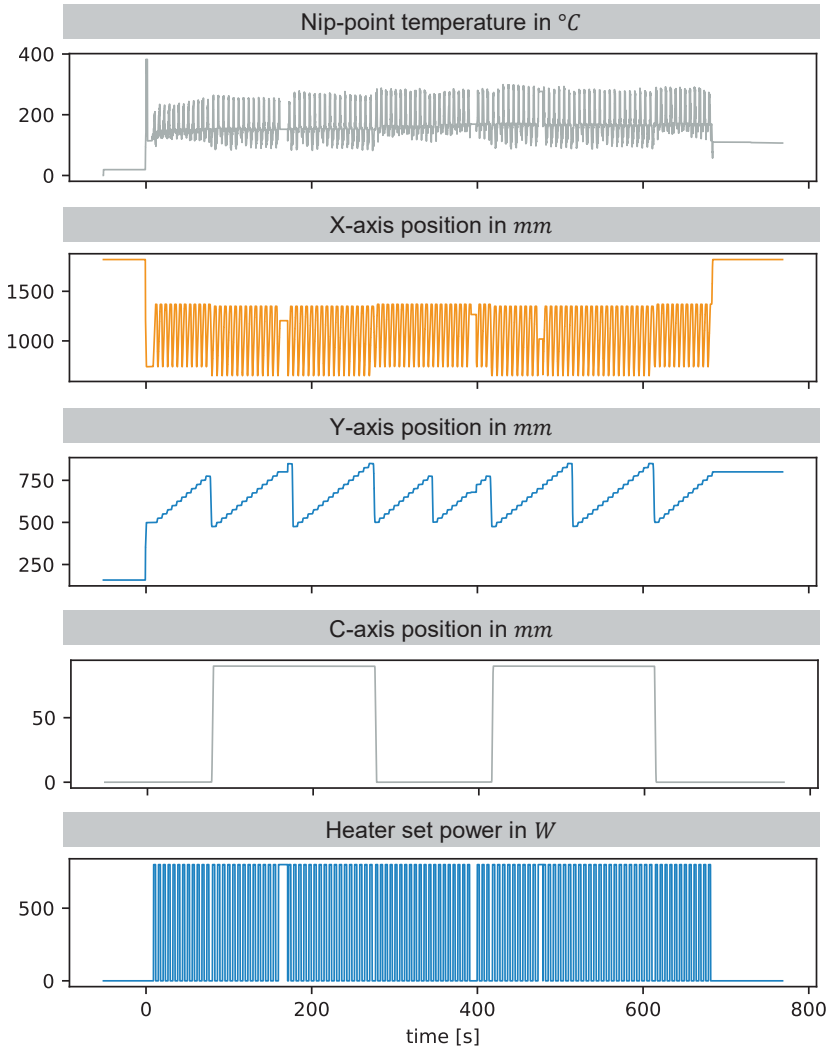

Figure 5.6: Experimental raw data of nip-point temperature, axes positions and laser power during all eight layers

Experimentelle Rohdaten von Nip-Point-Temperatur, Achsenpositionen und Laserleistung während aller acht Lagen

5.2.2 Process prediction by digital twin

Prozessvorhersage mit Hilfe des Digitalen Zwillings

A *Python* code is programmed enabling the forecast of the temperature history and quality indicators for individual layups and laminate geometries based on the FTSC scheme shown in section 4.3.2 and 4.3.3. It calculates for each layer, substrate thickness and (cooling) time the temperature evolution in thickness direction. Based on this temperature data local and global quality indicators, such as DoB and DoC, are estimated. To explicitly predict the experimental case, the material specific data for PA6/CF tape as presented in Table 5.2 is required.

The parameters in Table 5.2 are based on studies in literature using the same tape constituents but by a different supplier. In addition, own examinations are conducted. Most of the values are derived in detail by SCHÄFER [SCHÄ17, p. 91] and FELDER ET AL. [FELD19, p. 255]. SCHÄFER investigates a PA6/CF tape material by the company BASF which is now commercialized by Toray. FELDER ET AL. conduct their experimental validation with the same PA6 polymer from BASF. Due to similarity of the constituents, it is assumed that these values do not have a significant difference to the investigated DSM tape material in this thesis. Since the derivation of these parameters and models would go beyond the focus of this study, they are not investigated in more detail.

Table 5.2: Used material specific data for DSM PA6/CF tape

Verwendete materialspezifische Daten für das DSM PA6/CF Tape

	Parameters	Value	Source
Temperature model	Density	$\rho = 1390 \frac{kg}{m^3}$	[DSM19]
	Thermal conductivity in thickness direction	$k_z(T = 25°C) = 0.6 \frac{W}{m \cdot K}$	[SCHÄ17, p. 40]
	Specific heat capacity	$c_p(T = 25°C) = 1180 \frac{J}{kg \cdot K}$	[SCHÄ17, p. 37]
	Heat transfer coefficient	$h_{air} = 40 \frac{W}{m^2 \cdot K}$	[WEIL19, p. 56; LATR03, p. 77]
Degree of Crystallization model	Melting temperature	$T_m = 220\ °C$	DSM PA6/CF datasheet
	Glass transition temperature	$T_g = 60\ °C$	DSM PA6/CF datasheet
	Peak crystallization temperature	$T_{p,c} = 186.76\ °C$	DSM PA6/CF DSC analysis
	Initial crystallization temperature	$T_{ic} = 159.03\ °C$	DSM PA6/CF DSC analysis
	Final crystallization temperature	$T_{fc} = 200.89\ °C$	DSM PA6/CF DSC analysis

	Avrami exponent	$n = 2.38$	[FELD19, p. 255]
	Nakamura-Ziabicki crystallization parameters at DSC heating rate $\dot{T}$	$K_{max}\left(\dot{T} = 10\frac{K}{min}\right) = 13.73\frac{1}{min}$ $D\left(\dot{T} = 10\frac{K}{min}\right) = 100.48\ K$ $T_{max}\left(\dot{T} = 10\frac{K}{min}\right) = 348.46\ K$	[FELD19, p. 256]
Degree of Bonding model	Reptation/welding time	$t_w(T) = 1.79 \cdot 10^{-7} \cdot \exp\left(\frac{41028.13\frac{J}{mol}}{RT}\right) s$	[SCHÄ17, p. 167]
	Temperature-dependent viscosity	$\mu_0(T) = 14.1 \cdot \exp\left(\frac{29378.8\frac{J}{mol}}{RT}\right) Pa\ s$	[SCHÄ17, p. 167]
	Surface parameter	$a_0 = 36.16\ \mu m$ $b_0 = 179.95\ \mu m$ $w_0 = 162.71\ \mu m$	[SCHÄ17, p. 77]
Productivity model (chapter 6)	Tensile modulus of Tape 0°	$E_1 = 110\ GPa$	[DSM19]
	Tensile modulus of matrix	$E_1^m = 2.7\ GPa$	[DSM22]
	Transverse modulus of fiber	$E_2^f = 15\ GPa$	[LIU18, p. 7]

5.2.3 Temperature: prediction and validation

Temperatur: Vorhersage und Validierung

Temperature prediction. The temperature prediction based on the FTSC scheme described in section 4.3.2 and 4.3.3 is applied for the specific experimental case. This means for each new layer and constantly changing substrate thickness the heat evolution in thickness direction is calculated. The prediction assumes a constant cooling time of $65s$ and $98s$ for each 0° and 90° layer. Results can be seen in Figure 5.7 and Figure 5.8 (three-dimensional representation of the data).

In general, the model predicts, that all layers and at all times cool down after approx. $0.6\ s$ to the set heating table temperature of $150\ °C$. The heating phase of the currently laid layer is assumed constant implying that the heating phase of the tape is not considered in this model. It has a duration of t_L as indicated by the horizontal line at the beginning (e.g. see layer 4 in Figure 5.7). It heats up the layer below up to nearly $220\ °C$ in all cases. This behavior repeats during laying each layer. However, the more layers are laid, the less steeper is the cooling gradient. This means that by adding layers heat accumulates and more heat is stored in the laminate. The number of laid

layers and, thus, the substrate thickness does not influence the cooling behavior. As can be seen in Figure 5.7, whether having 4 or 8 layers does not make a significant difference regarding the heating of the layers below. The four upper layers ($N - 1 \ldots N - 4$) are exposed to the heat of the current layer being reheated again. However, only the layer directly below the current layer $N - 1$ is heated up close to melting temperature. This implies a so-called melt pool depth of $\delta_{melt} = 1\ h_{tape}$ of the substrate and that heat does not reach the tapes below. Consequently, the interface of $N - 1$ to $N - 2$ is not remelted.

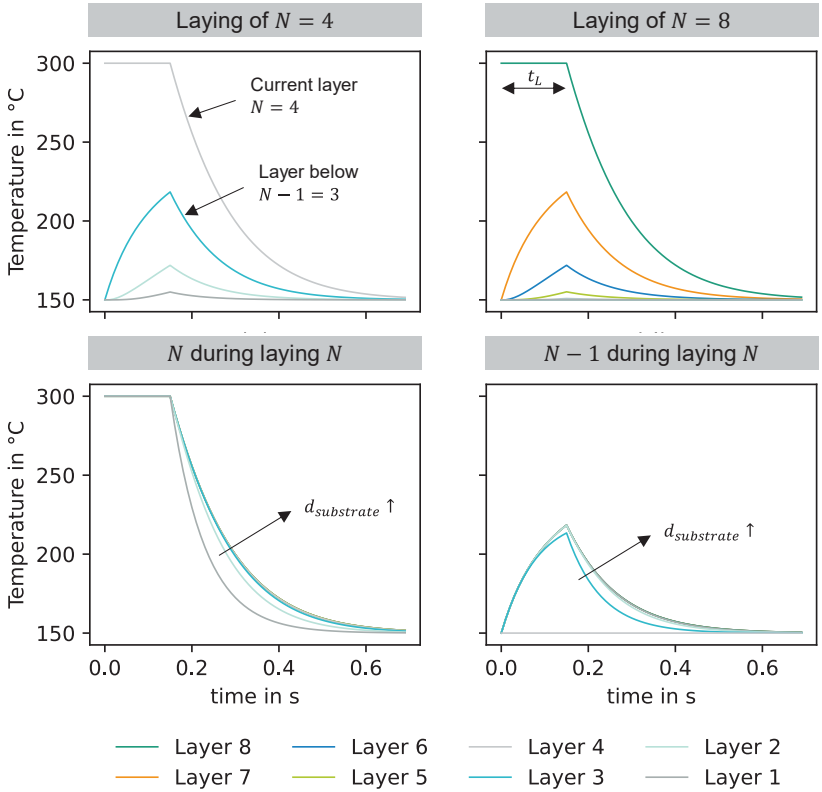

Figure 5.7: Temperature development during the laying process at different process stages

Temperaturentwicklung während des Legens in verschiedenen Prozessstadien

The fast cooling of the layers from process temperatures around $300\ °C$ to the heating table temperature of $150\ °C$ suggest the following: After heating and short cooling, the substrate temperature should in all cases and in all times of laying equal the heating table temperature, also in the case of changing fiber orientation. As shown in the cooling time analysis in section 4.2.2, the available time for cooling is much higher than the

predicted cooling time of approx. $0.6\,s$. In summary, the following key findings of the temperature prediction are:

1. The available cooling time is much higher than the required cooling time ($65\,s \gg 0.6\,s$) for all layers.
2. The melt pool depth of the substrate stays constant and independent of its thickness as long as the nip-point temperature keeps the same.
3. The temperature gradients of each heat affected layer decreases with increasing substrate thickness.

This examination only considers laminates up to a thickness of $2-3\,mm$. To investigate the effects on thick laminates, further investigations are required.

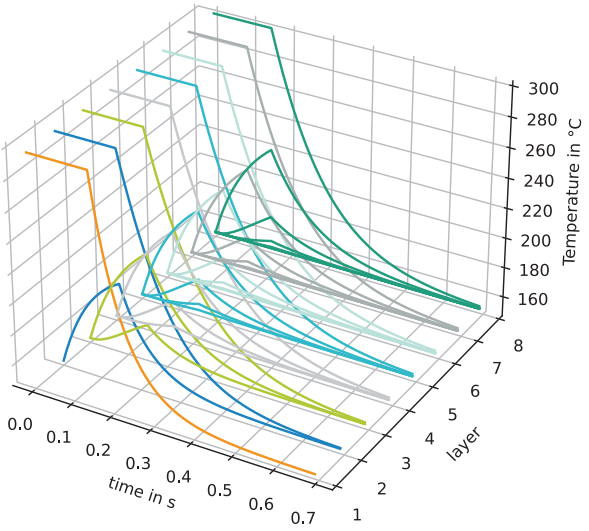

Figure 5.8: Temperature evolution in all layers

Temperaturentwicklung in allen Lagen

Experimental temperature data. The temperature is measured in 5 zones as shown in Figure 5.3. The zones are adjusted according to the necessary process analysis. Zone 1 as well as zone 2 output the temperature of the incoming tape. Zone 3 is the area of the nip-point comprising of tape and substrate. Zone 4 and 5 measure the temperatures of the substrate. For each zone the average value of the measured pixels is taken. This thesis focuses on the deposition of the middle tape, *tape 2*.

Figure 5.9 shows the temperature evolution of each zone during deposition of layer 3 (90°) and 4 (0°). The vertical dashed lines mark the beginning and end of one layer. The first 16 peaks are the 16 tape paths deposited during layer 3 (90°) and the last 12 peaks the ones of layer 4 (0°). The duration for one 90° layer is around $78\,s$ and for one 0° layer $52\,s$, the time between each layer is approximately $5\,s$ (details in section 6.3.1). In analogy to the cooling time calculation in section 4.2.2, the shortest cooling

time of a point in space of the laminate is after changing the fiber orientation. This is for example in point 2 in Figure 4.7 or diagonally opposite. In the conventional layup as conducted here, these points experience a cooling time consisting of the auxiliary time when changing the fiber orientation plus the main time of the first 90° tape path of the layer. Here, this time approximately is $(5 + (320\ mm)\ /\ (250\ mm/s\ ))s = 6.28\ s$.

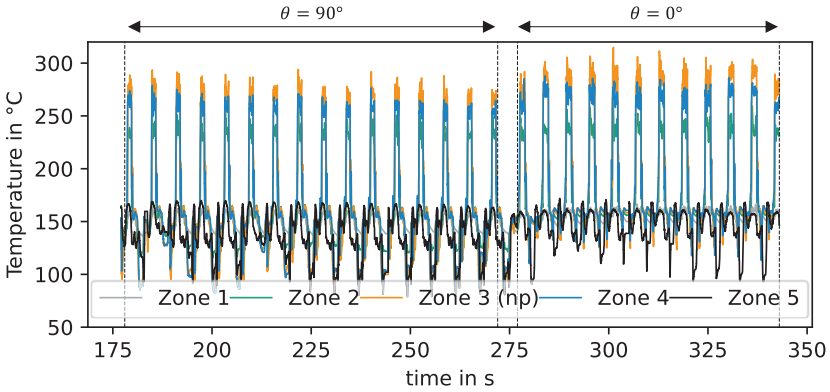

Figure 5.9: Measured zone temperatures of each tape path in layer 3 (90°) and 4 (0°)

Gemessene Zonentemperaturen für jedes Tape in Lage 3 (90°) und 4 (0°)

The nip-point temperatures, to be recognized as orange peaks, fluctuate around the value of $295.93\ °C$ for all layers. The mean substrate temperature is around $164.74\ °C$ slightly above the temperature of the heating table. Table 5.3 gives on overview of the mean values and standard deviations for each temperature zone for all layers. The standard deviations suggest changing processing temperatures during tape deposition. To understand these fluctuations the mean values of each zone for each layer are visualized in Figure 5.10. Zone 4 and 5 entail two outliers during the beginning of the deposition of layer 1. Here, the measurements are inaccurate since the thermal image camera measures values of the heating table and not of the tape caused by wrong emission coefficient settings. The values in brackets are adjusted accordingly.

Table 5.3: Mean peak temperatures and standard deviations per temperature zone

Mittlere Spitzentemperaturen und Standardabweichungen pro Temperaturzone

Zone	Mean value	Standard deviation
1	$158.48\ °C$	5.7 %
2	$250.71\ °C$	6.4 %
3 (nip-point)	$295.93\ °C$	6.8 %
4	$270.14\ °C\ (268.19\ °C)$	7.9 % (5.8 %)
5	$164.74\ °C\ (160.84\ °C)$	18.5 % (5.7 %)

The incoming tape (zone 1) has a mean temperature of $158.48\,°C$. It overall standard deviation is comparatively low indicating constant conditions during the whole layup procedure. Being stored on the spool with ambient temperature, the incoming tape must bridge a difference of $280\,K$ to achieve the desired nip-point temperature. Although Figure 5.3 shows that zone 1 only receives minimal radiation from the laser, the data shows that it is heated up during tape deposition. This may be attributed to a reflection of the laser radiation or to the heating of guiding elements during the whole processing or even heat conduction in tape direction. The clarification is not scope within this analysis but is interesting for future studies.

The high difference from ambient to the nip-point temperature may results in less consolidation quality since the incoming tape may not be sufficiently heated up. The mean temperature of zone 2 shows, that the incoming tape, shortly before the processing zone, is not heated up to the desired nip-point temperature but is above melting temperature. This should be sufficient to achieve full consolidation. The fluctuation of zone 2 slightly increases having an overall standard deviation of $6.4\,\%$.

The highest temperature, as desired, is in the nip-point zone (zone 3). It fluctuates around the desired temperature of 300 °C for achieving consolidation. As can be seen in Figure 5.10, the temperature increases with the number of layers. This behavior is also apparent in zone 4 with a temperature slightly below the nip-point temperature. An overall effect of changing fiber orientation on temperature is not clear from the results although Figure 5.9 suggests an increase of temperature in zone 2 to 4 when changing from layer 3 with 90° to layer 4 with 0°.

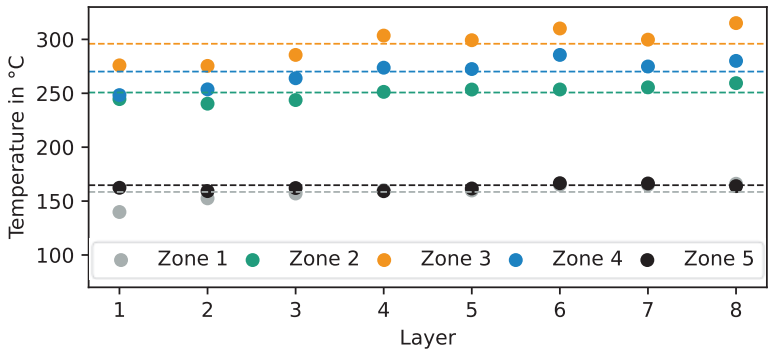

Figure 5.10: Average temperatures during laying for each layer (dashed horizontal lines indicate mean temperature values per zone as listed in Table 5.3)

Mittlere Temperaturen während der Tapeablage jeder Lage (gestrichelte horizontale Linien zeigen die mittleren Temperaturwerte pro Zone an, wie in Table 5.3 aufgeführt)

The position of zone 5 is intended to measure the substrate temperature shortly before the process zone to measure the cooled substrate surface of the layer before. The graph of this temperature zone in Figure 5.11 (black line) shows that it also heats up

during tape deposition. The average temperature of zone 5 fluctuates around the temperature of the heating table. Figure 5.10 suggests an only slight increase in the substrate temperature after each layer which is supported by the low standard deviation.

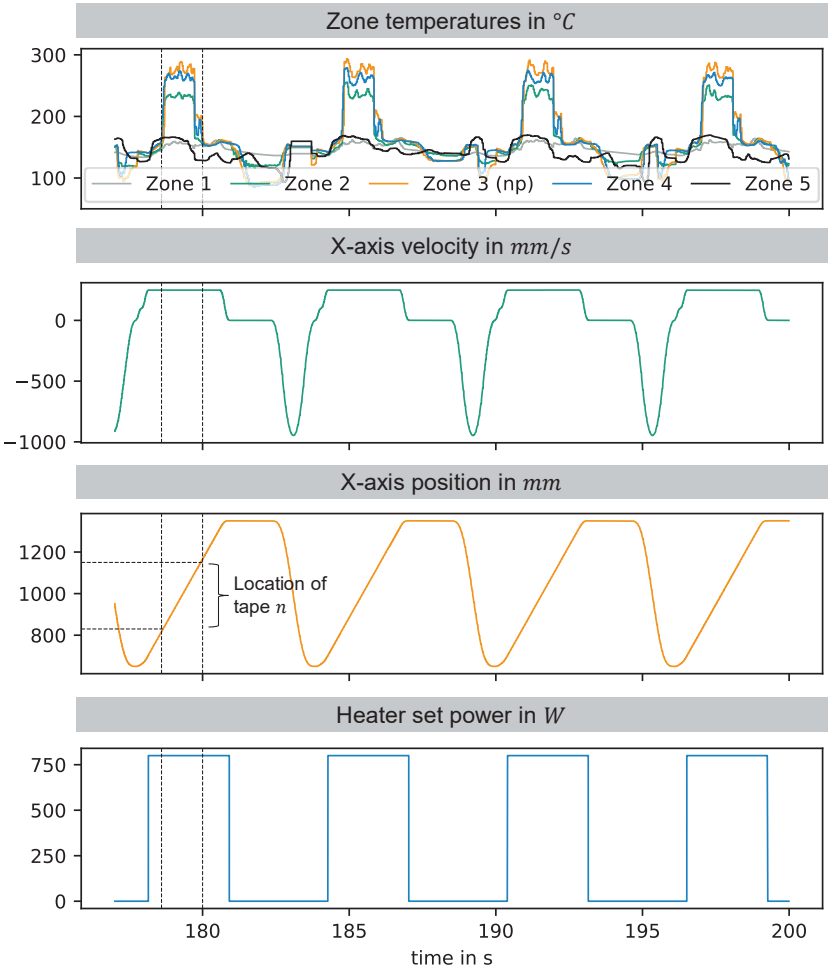

Figure 5.11: Experimental data of nip-point temperature, x-axis velocity and position, of four tape paths in layer 3

Experimentelle Daten der Nip-Point-Temperatur, der Geschwindigkeit in der x-Achse und der Position, von vier Tapebahnen in Lage 3

The closeup of the process shown in Figure 5.11 gives insight into the accurate synchronization of axes and laser source as mentioned above. The location of the tape as programmed (dashed lines in Figure 5.11) fits to the constant process speed of $v_P = 250\ mm/s$ as well as the risen process temperatures. Therefore, it can be stated that

the process parameters and their synchronization are set accurately. The drop of temperature at the end of each tape path are resulting from the cut tape causing a shadow on the nip-point and from the end of the tape deposition. It also shows that there is a run-out length with set laser power without tape being deposited.

It must be noted that the temperature measurements between each peak is irrelevant. These are the measurements of the thermal image camera during the return to the start position. Here, the tape applicator is moved up in z-direction and the consolidation roller does not touch the surface of the laminate.

Model comparison. To compare the experimental data with its prediction a closer look at the temperature change is taken. In the prediction, the temperature drops after the nip point zone within $0.4\,s$ to the temperature of the heating table. Given the system settings of the upscaled PrePro2D® machine this sudden drop cannot be detected since a temperature measurement unit must be installed behind the consolidation roller. With the thermal image camera capturing the process zone, the substrate temperature shortly before being heated up in the process zone can be used to investigate the cooling behavior. This is captured by zone 5. As suggested by the model the substrate temperature should always correspond to the temperature of the heating table since even the shortest cooling time is higher than the required one. This is supported by the experimental data, showing that the substrate temperature levels slightly above the temperature of the heating table.

The model predicts decreasing cooling gradients with increasing substrate thickness caused by the increase of thermal mass in the heat transfer model. As stated above, this behavior cannot be shown in the experiments. A major assumption of the model is the same nip-point temperature during all layers. In the experiments the temperature is not controlled and set by a fixed laser power causing fluctuations within the laminate production. For this reason, it is assumed that the increase of thermal mass in the experiments is shown by the temperature increase of zones 2-4.

To conclude, it can be stated that the temperature prediction in section 5.2.2 is consistent with the experimental data. The predicted high cooling gradients as well as the equilibrium temperature of the cooled substrate equal to the temperature of the heating table are justified. Also, the model indicates the increase of thermal mass during laying. In contrast, the comparison reveals the limitations of the current model regarding the transferability of results. To completely verify the model, the temperature should be measured behind the consolidation roller and/or within the laminate.

The following main conclusions for the processing of tapes can be drawn:

1. Steep temperature gradients result in a fast cooling of the substrate to the temperature of the heating table after being processed (after the process moment). This is irrespective of the table temperature. It can be assumed that the substrate always has the temperature of the mold as the material is thermal thin compared to the heat capacity of the table.

2. Nip-point temperature increases with increasing substrate thickness if the same laser power is set.

The prediction of the increased temperature of the layers below during the process moment cannot be verified with these experiments but is supported by various authors [KERM15, p. 59; HOSS20, p. 3079].

5.2.4 Degree of Bonding: prediction and validation

Konsolidierung: Vorhersage und Validierung

Degree of Bonding prediction. The DoB is calculated according to the descriptions in section 4.1.2 and 4.3.4 as well as the PA6/CF specific values in Table 5.2. It can also be only calculated for temperatures above $T_m = 220\,°C$ where consolidation can occur (see also [SCHÄ17, p. 138]). According to the temperature prediction, only the currently laid layer is exposed to temperatures above melting temperature. It stays above T_m longer than required ($t(T \gg T_m) \approx 0.2\,s \gg t_f = t_w + t_{cons} = 0.061s$). Here, there is enough time for bonding (see also [SCHÄ17, p. 97]). Using the desired nip-point temperature in the process zone T_{np} as the required value for the temperature in equation (4.23), a constant DoB of $D_B^{np}\left(T_{np} = 300\,°C\right) = 75.49\,\%$ is predicted for these process conditions.

Since the layer below is not exposed to melting temperature, there is no possibility for reconsolidation. The difference of the heat in $N-1$ compared to N is the duration the material is experiencing temperatures above melting temperature. If this duration is higher than the required bonding time t_f of the DoB model, reconsolidation occurs. In addition, the low temperature in the layer below $T_{np}^{N-1} \ll T_{np}$ results in an increase of reptation time t_w caused by the characteristics of its Arrhenius function. This increases the overall necessary bonding time and results in a decrease of the second term, the integral, of the coupled bonding model in equation (4.23). The estimated DoB is consequently lower than the one of the currently laid layer. Using thinner tapes ($h_{tape} \ll 0.25\,mm$) would lead to a different case. Here, spatial steps in the FDM decrease. It leads to higher temperatures of the layer below being presumably higher than T_m.

As mentioned previously, the multiple passing of the tape laying applicator at the same location is the so-called *reconsolidation effect*. MANTELL AND SPRINGER propose to model it by summarizing its effect on intimate contact D_{IC} for each time interval at each interface [MANT92b, p. 2367]. The applicability of the coupled bonding model has not been modeled yet. In accordance with the statement by SCHÄFER [SCHÄ17, p. 138], this study assumes that an accumulation effect is only taking place as soon as conditions result in a higher DoB compared to the previous processing condition. This could be the case for manufacturing strategies with multiple "dry" reconsolidation passes without the application of a new tape layer, but with the use of the heating source.

It is also possible to use the measured temperature values of the experiment for predicting the DoB (1st order). In this case, the average value of the nip-point zone (zone 3) is used. According to this procedure, the DoB is $D_B^{np}\left(T_{np} = 295.93\,°C\right) = 74.42\,\%$.

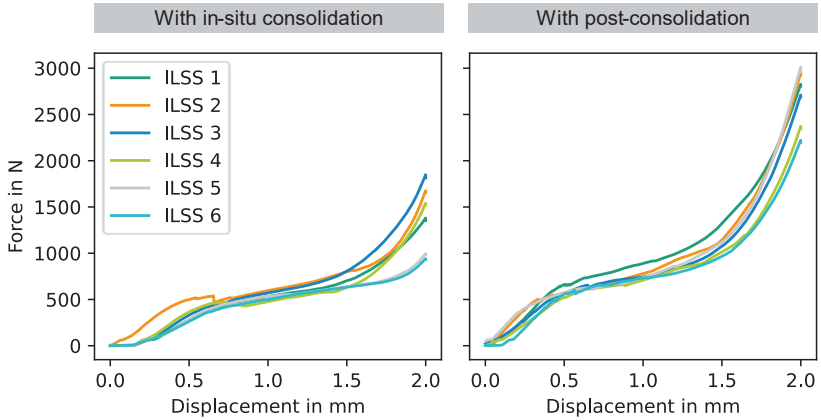

Figure 5.12: Force-displacement curves for ILSS specimens only with in-situ consolidation and with additional post-consolidation of the laminate produced, each $n = 6$

Kraft-Weg-Kurven für ILSS-Proben mit in-situ Konsolidierung und mit zusätzlicher Nachkonsolidierung des hergestellten Laminats, je mit $n = 6$

Degree of Bonding validation. To compare prediction with reality, ILSS tests are conducted according to norm DIN EN ISO 14130 [DIN97]. This procedure has already been described in detail in section 4.2.4. Here, six specimens are cut out of the middle of the laminate. In addition, a section of the laid laminate is post-consolidated within a flat heated mold for 15 minutes at $260\ °C$. Again, six specimens are extracted from the middle area. This enables a comparison between ILSS values of specimens only manufactured with in-situ consolidation and with additional post-consolidation. The latter corresponds to the maximum ILSS value $ILSS_{max}$ in equation (4.36). In addition, microsections are prepared to doublecheck and to identify reasons for the ILSS values.

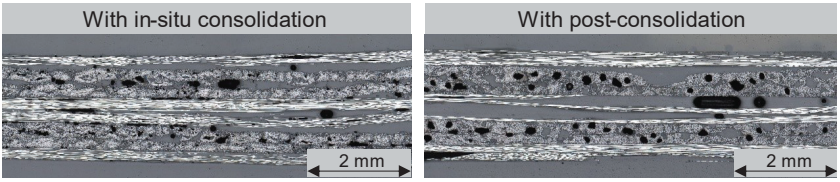

Figure 5.13: Microsections of the laminate produced with $v_P = 250\ mm/s$, with in-situ and with additional post-consolidation

Schliffbilder des produzierten Laminats mit $v_P = 250\ mm/s$*, mit in-situ Konsolidierung und mit zusätzlicher Nachkonsolidierung*

Figure 5.12 shows the force-displacement curves of each specimen with in-situ and with additional post-consolidation. As expected from thermoplastic composites, the curves do not show typical ILSS behavior with a significant breakage for thermoset materials. For this reason, either the first local maximum or a mean value of the first

plateau level is taken (see section 4.2.4) as value for equation (4.35). With using equation (4.36) the DoB is estimated. As value for $ILSS_{max}$ the mean value of the specimens with post-consolidation is taken which is $ILSS_{max} = 23.71\ MPa$. The mean value of the specimens only with in-situ consolidation corresponds to $ILSS_{exp}$ which is $ILSS_{exp} = 16.73\ MPa$. This gives a DoB value of $\mathrm{D}_{B,exp}^{avg} = 0.7055 = 70.55\ \%$. A comparable value in literature with same material composition and similar layup can be taken from Janssen [JANS20, p. 120] with a value of $ILSS \approx 40\ MPa$.

Table 5.4: Overview of the predicted and measured DoB of the laminate with $v_P = 250\ mm/s$

Übersicht der vorhergesagten und gemessenen Konsolidierungsgrade des Laminats mit $v_P = 250\ mm/s$

	Predicted	Measured
DoB predicted with temperature prediction	$D_B^{np}(T_{np} = 300\ °C) = 75.49\%$	-
DoB predicted with measured temperature	$D_B^{np}(T_{np} = 295.93\ °C) = 74.42\ \%$	-
DoB derived from ILSS values	-	$\mathrm{D}_{B,exp}^{avg} = 70.55\ \%.$

The microsections in Figure 5.13 reveal the reasons for the relatively low ILSS values. The black spots indicate voids which happen to be interlaminar and intralaminar. As expected, the specimen with in-situ consolidation shows much more interlaminar voids compared to the post-consolidated one. However, both microsections also indicate intralaminar voids which are also observable in the initial microsection of the sole tape (Figure 5.4). The voids are even amplified in the post-consolidated laminate which are expected to result from the thermal expansion during heating in the press and the lack of a vacuum.

Model comparison. The predicted and measured values are summarized in Table 5.4. The comparison between prediction and experiments shows a slight divergence between both. The predicted DoB in the nip-point of $D_B^{np} = 75.49\ \%$ is $7\ \%$ higher than the experimental one. This value is calculated based on the target nip-point temperature of $T_{np} = 300\ °C$. As demonstrated in the previous section, the mean experimental value of the nip-point temperature is $T_{np}^{exp} = 295.93\ °C$ (see Table 5.3). This leads to a reduction of the predicted DoB of only $\approx 1\ \%$. When looking at the predicted DoB of each layer, the measured nip-point temperatures as shown in Figure 5.10 result in the DoB predictions in Table 5.5. The layer-wise DoB prediction can roughly be related to the microsections: Layers with higher predicted DoB are also more consolidated, especially in layer 8.

The prediction indicates that the model sufficiently predicts the DoB and allows a layer wise analysis of the consolidation. It can also be used to directly translate the measured nip-point temperatures to a DoB value. As usual with material tests, the conducted analysis only gives a limited validation since ILSS and microsection only depict details and are an abstraction of the reality itself. They do not give a complete picture of the laminate. Additionally, the effect of crystallization on ILSS values is not considered.

Table 5.5: Experimental nip-point temperature per layer and corresponding DoB prediction

Experimentelle Nip-Point-Temperaturen pro Lage und dazugehöriger Vorhersage des Konsolidierungsgrades

Layer	Experimental nip-point temperature T_{np}^{exp}	DoB prediction D_B^{np}
1	$275.89\ °C$	$69.62\ \%$
2	$275.39\ °C$	$69.51\ \%$
3	$285.58\ °C$	$71.85\ \%$
4	$303.52\ °C$	$76.44\ \%$
5	$299.23\ °C$	$75.29\ \%$
6	$310.12\ °C$	$78.29\ \%$
7	$299.74\ °C$	$75.42\ \%$
8	$315.10\ °C$	$79.74\ \%$

5.2.5 Degree of Crystallinity: prediction and validation

Kristallinität: Vorhersage und Validierung

Degree of Crystallinity prediction. The DoC prediction is conducted as described in section 4.3.4. The crystallization specific properties of PA6/CF are based on a DSC analysis with the *DSC Q2000* measurement system of the company *TA Instruments*. As shown in Figure 5.14 the temperature range in which most crystals are built is between the $T_{ic} = 159.03\ °C$ and $T_{fc} = 200.89\ °C$ with having a peak crystallization temperature of $T_{p,c}(\chi_{1/2}) = 186.76\ °C$. Additional material specific values are taken from literature and summarized in Table 5.2.

These information result in the predicted, time-dependent DoC according to the green line in Figure 5.14 (right). The graph shows that it takes approximately $250s$ to achieve a DoC of 100%. After $50s$ a DoC of 10% is reached. A similar behavior is predicted in the study by FELDER ET AL. [FELD19, p. 256] which is used as a basis. Figure 5.14 also illustrates the influence of different Avrami constants showing its sensitivities.

As proposed by the model of HOSSEINI ET AL. [HOSS20, p. 3078], the cumulative time between $T_g < T < T_m$ is used to estimate the crystallization. A remelting of a layer di-

minishes the crystal growth to zero again. Due to the heated mold the laminate´s temperature is above $T_g = 60\ °C$ the complete manufacturing duration of $680\ s$ (see Figure 5.5). For this reason, the crystallization time is calculated by extracting the cumulative time above T_m, taken from the temperature prediction, from the overall manufacturing time per layer as measured from the experiments. The current experimental setup does not allow the measurement of the temperature gradient within one spatial point on the laminate. For this reason, the duration above T_m at one exact spatial point cannot be measured and must be taken from the model prediction.

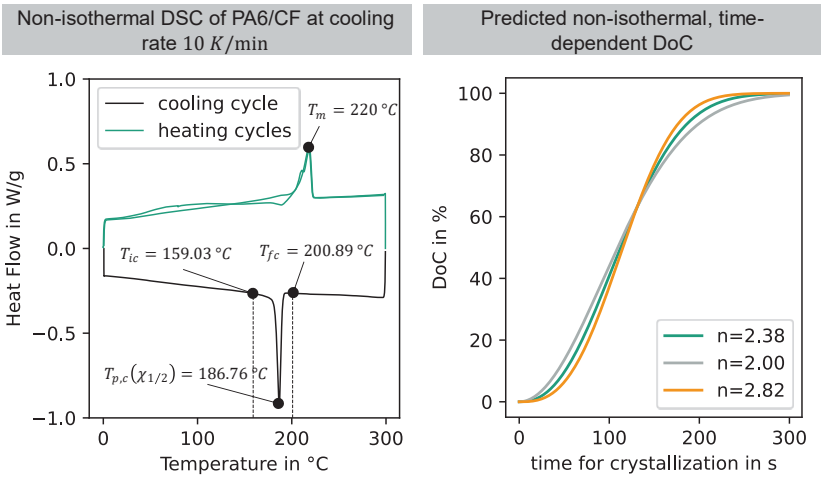

Figure 5.14: Non-isothermal DSC analysis for DSM PA6/CF tape conducted at cooling rate $10\ K/min$ (left) and the prediction of the model at different Avrami constants (right)

Nicht-isotherme DSC-Analyse für das DSM PA6/CF Tape durchgeführt bei einer Abkühlrate von $10\ K/min$ (links) und die Vorhersage des Modells bei unterschiedlichen Avrami Konstanten (rechts)

Taken the actual time per layers for the here-focused laminate and subtracting the predicted duration above melting temperature, the predicted time for crystallization as well as the corresponding DoC prediction are derived as in Table 5.6. A change in fiber orientation also changes the cooling time of the layer below for each spatial point. Because of the high cooling gradients after radiation, this has no effect on the time above T_m. For this reason, it is neglected in this study. The predictions correspond to each layer as they experience a slightly different time for crystallization. The reason are the flattening gradients of the temperature evolution with increasing substrate thickness. The total average is $\chi(\%)^{np,avg} = 29.7\ \%$.

Degree of Crystallinity validation. In literature the measured DoC of laminates out of PA6/CF tapes range from $43 - 49\ \%$ [JANS20, p. 135] to $81\ \%$ [SCHÄ17, p. 124]. Their difference lies within the different experimental setups. JANSSEN uses an infrared-

based tape laying system for the production of laminates with a production speed of $v_P = 200\ mm/s$ [JANS20, p. 117]. SCHÄFER investigates the influence of the laser-assisted tape laying on the crystallinity by producing specimens for wedge peel tests with process speeds in the range $v_P = 50 - 200\ mm/s$. The latter only comprises of two consolidated layers. This shows that the different setups as well as the different layup thicknesses, cooling times, etc. can strongly influence the measured DoC value. The experimental setup by JANSSEN is similar to the one in this study.

Table 5.6: Predicted time for crystallization and DoC

Vorhergesagte Zeit für die Kristallisation und Kristallisationsgrad

Layer	Time for crystallization t_χ	DoC prediction χ^{np}
1	$70.65\ s$	$20.54\ \%$
2	$97.38\ s$	$38.95\ \%$
3	$97.35\ s$	$38.93\ \%$
4	$70.53\ s$	$20.47\ \%$
5	$70.53\ s$	$20.47\ \%$
6	$97.33\ s$	$38.91\ \%$
7	$97.33\ s$	$38.91\ \%$
8	$70.53\ s$	$20.46\ \%$

The crystallization specific properties of the produced laminate with $v_P = 250\ mm/s$ in this study is conducted by a DSC analysis with a cooling rate of $\dot{T} = 10\ K/min$. The curves and specific values are displayed in Figure 5.15. The values are similar to the ones of the sole tape. The DoC value is calculated based on equation (4.24) as described in section 4.1.3. With assuming that the laminate has the same fiber volume content as the tape, the required fiber mass content is calculated with the rule of mixture [KRES14, p. 78] to $\varphi_f = 50\%$. With the given value $\Delta H_m^0 = \Delta H_m^{PA6} = 241\ J/g$ [ILLE78, p. 499] and the extracted value of $\Delta H_m = 27.11\ J/g$ from the DSC analysis, the relative DoC is $\chi = 22.5\ \%$. The predicted value is overestimated by approx. $24\ \%$.

Model comparison. Differences between predicted and measured DoC values can result from multiple reasons:

- The prediction with the Nakamura-Ziabicki model is based on values derived by [FELD19, p. 256] which are not validated for the tape material used in this study;
- Standard DSC equipment do not measure at very high cooling rates which are apparent during AFP. Investigations are required with flash DSC coping with cooling rates up to $250\ K/s (= 150K/0.6s)$, as in this experiment, or even higher. This is supported by the findings by SCHÄFER [SCHÄ17, p. 52].

- Since previously laid tapes have already experienced melting as well as crystallization, its chemical characteristics may have changed. For example, previously laid tapes may have different melting temperature due to the experienced cooling rate. Consequently, there is a difference between the incoming, virgin tape and the substrate which is not incorporated in the models. [SCHÄ17, p. 51]
- The DoC prediction does not encounter additional time for crystallization, which occurs if the laminate is kept on the heating table a little longer. The prediction is based only on the cycle time.
- The mass content of polymer and fiber is calculated analytically and is not based on TGA measurements.
- The time above melting temperature, in which crystals cannot exist, for a specific spatial point cannot be measured with the experimental setup. It is derived by the temperature prediction model as shown in section 5.2.3.

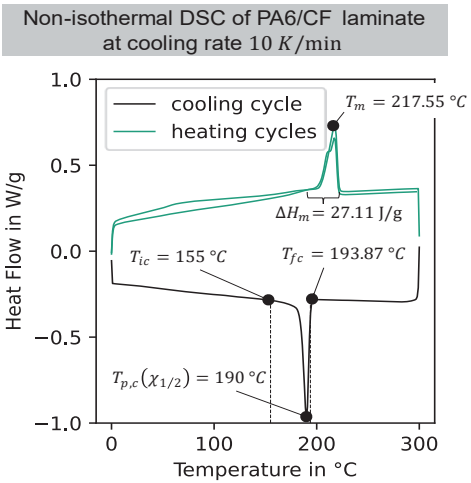

Figure 5.15: Non-isothermal DSC analysis for the produced laminate with $v_P = 250\ mm/s$ conducted at cooling rate $10\ K/min$

Nicht-isotherme DSC-Analyse für das Laminat mit $v_P = 250\ mm/s$ bei einer Abkühlrate von $10\ K/min$

5.3 Sensitivity analysis

Sensitivitätsanalyse

The digital twin is based on various models and material specific parameters. The underlying assumption is that the values from datasheets and literature as well as analytical models are sufficient to create a realistic digital twin. The major benefit is the reduction of elaborate and costly experiments required to derive these specific values.

The previous analysis about the digital twin validation in section 5.2 quantifies the gap between model and reality for the specific experimental setup. It derives its prediction capabilities, but also its optimization potentials. The sensitivity study in this section allows to better understand which specific properties have the highest impact on the predicted quality indicator. Thereby, it reveals the most significant parameters which need to be investigated more closely for a better prediction.

By changing the reference value of relevant material properties by exemplary $\pm 30\ \%$, the relative impact on the two quality indicators, DoB D_B^{np} and DoC $\chi(\%)^{np,avg}$, becomes apparent. All other material and process related values are kept constant as is in section 5.2. To recall, the reference predicted DoB is $D_B^{np}\left(T_{np} = 295.93\ °C\right) = 74.42\ \%$, the reference predicted DoC is $\chi(\%)^{np,avg} = 29.7\ \%$. The analysis of the temperature prediction in section 5.2.3 reveals that actual available cooling time is much higher than the required cooling time. Consequently, the overall impact of temperature gradients on quality indicators, such as DoB and DoC, are neglectable.

Figure 5.16 illustrates these sensitivities compared to the reference values (dashed lines), which are taken from Table 5.2. To analyze the sensitivity of the DoB model the values reptation time t_w, viscosity μ_0 and one of the surface parameters, b_0, are selected. Only one surface parameter is chosen as b_0 is a common denominator in equation 4.48 and, thus, influences mostly the result. For the DoC model, the temperature-dependent crystallization rate constant $K(T)$ and the Avrami constant n are selected.

The temperature-dependent viscosity property of the material μ_0 has the highest impact on the DoB value. Reducing its value by $30\ \%$ leads to an increase of $8.8\ \%$ of the DoB value. Increasing its value by $30\ \%$ leads to a DoB decrease of around $5\ \%$. In the case of the DoC, the impact of material properties is significantly higher. For example, increasing the reference value of $K(T)$ by $30\ \%$ results in a $60\ \%$ higher DoC. In addition, there curve of the Avrami constant n runs in the opposite direction.

If reptation time t_w, viscosity μ_0 and the surface parameter b_0 are all overestimated by $20\ \%$, this would lead to a DoB of $69.82\ \%\ (-6\%)$. If all these parameters are underestimated by $20\ \%$, DoB becomes $76.65\ \%\ (+3\%)$. These influences are comparably low and supports the good prediction quality and implementation of this model as shown in section 5.2.4. In contrast, the DoC model is highly sensitive. If $K(T)$ is overestimated by $20\ \%$ and the Avrami constant n underestimated by are $-20\ \%$, a DoC of $\chi(\%)^{np,avg} = 45.26\ \%\ (+52\ \%)$ is calculated. The opposite around, DoC becomes $\chi(\%)^{np,avg} = 14.44\ \%\ (-49\ \%)$. This indicates that the overestimation of the model

compared to real case by approx. 24 % (see section 5.2.5) can result from the sensitivity of the underlying material models. It also shows the high sensitivity of this model.

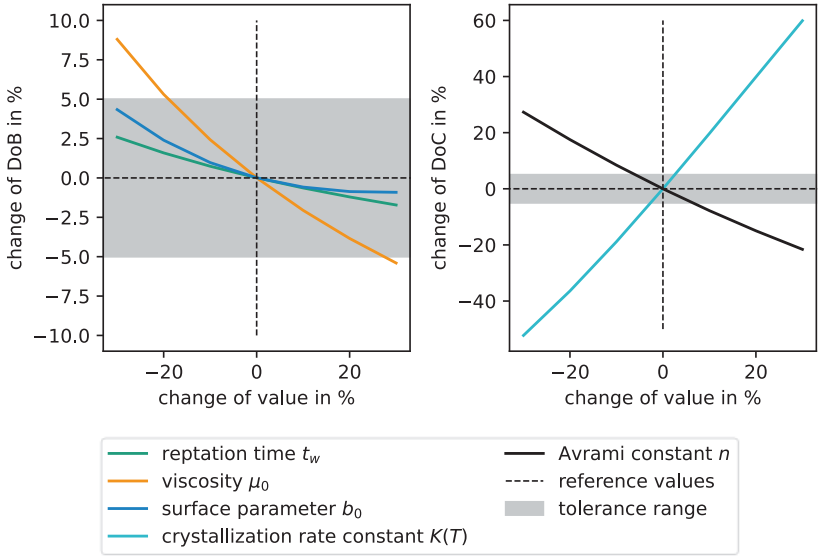

Figure 5.16: Predicted $D_B^{np}(T_{np} = 300\,°C)$ and $\chi(\%)^{np,avg}$ sensitivities towards changing one reference material value (as listed in Table 5.2) by $\pm 30\,\%$

Vorhergesagte $D_B^{np}(T_{np} = 300\,°C)$ und $\chi(\%)^{np,avg}$ Sensitivitäten durch Änderung der Referenzmaterialwerte (siehe Tabelle 5.2) bei $\pm 30\,\%$

Assuming a desired overall model accuracy of the digital twin of $\pm\,5\,\%$ (shown by the grey highlighted tolerance range in Figure 5.16), the error of the most sensitive material parameters need to be in the following ranges:

- viscosity μ_0: $-19\,\% < \mu_0 < 28\,\%$
- crystallization rate constant $K(T)$: $-6.5\,\% < K(T) < 2.5\,\%$
- Avrami constant n: $-3\,\% < n < 7\,\%$

The difficulty of an accurate prediction of the viscosity μ_0 model is analyzed in detail by SCHÄFER [SCHÄ17, p. 35].The author points out that both, model and experiments, hamper the correct determination of this material parameter. However, due to the relatively low impact or high tolerance range, the accurate determination of μ_0 is tolerable. In contrast, the accurate determination of crystallization rate constant $K(T)$ and Avrami constant n is more significant. The study by FELDER ET AL. [FELD19], who propose the herein used modeling approach, show that an accurate determination of the material parameters is possible. However, the authors do not quantify their error. It is assumed in this analysis, that a higher accuracy of the model would be achieved by an experimental investigation of the relevant underlying material parameters. Consequently,

finding the accurate material parameters is especially for the DoC model of high importance. A sophisticated experimental derivation of these material parameters is essential to accurately predict the prediction within this digital twin.

5.4 Conclusion

Zusammenfassung

Aim of chapter 5 is the validation of the created digital twin in chapter 4.3 and to test its prediction quality. The focused manufacturing system, PrePro2D®, is especially interesting as it is a fully integrated system technology allowing a continuous and consistent data acquisition of the processed part. To compare the data with the digital twin, an experimental setup is chosen allowing the measurement and quantification of the desired values. For this specific case, the spatial temperature development, the DoB as well as the DoC are predicted and compared to its experimental counterpart. This comparison does not only reveal its overall good agreement between prediction and experiment. It also discloses obstacles hampering the current digital twin and which need to be investigated in future.

The temperature prediction can forecast the temperature evolution in tape thickness and in tape feed direction incorporating cooling time as well as geometrical characteristics such as the substrate thickness. The model corresponds to the findings from literature (see 4.3.2 and 4.3.3). However, in this case, a full and detailed comparison with the experimental data is not possible. To validate the temperature model including the quantification of a prediction error, a more sophisticated experimental setup is needed. For example, by installing temperature sensors also behind the consolidation roller, spatially resolved short term temperature gradients could be detected.

The DoB prediction shows good agreement with the experimental values although the model is based on various assumptions. Especially the use of material specific values which are taken from literature and do not fully match the used material, could have caused prediction errors. A similar case is shown with the prediction of the DoC which still is overestimated by the model. The sensitivity study detects the properties which mostly impact the predictions. It shows that only selected properties need to be investigated closely to increase prediction quality.

Additional, undesired obstacles are, for example, a non-robust working data storage to assure that the measured data corresponds to the actual one. Although these kinds of obstacles are often neglected, they are occurring in industrial production environments hampering the smooth integration of I4.0 solutions.

In summary, the experimental validation reveals the complexity of implementing a digital twin for the AFP process with in-situ consolidation. It also shows the efforts which are required to validate and evaluate a digital twin. And even these experimental efforts are prone to idealization, such as the testing of ILSS. Using existing analytical models and conventional testing methodologies is hardly representing the realistic processing

case. Solutions are required, not only to increase prediction quality, but also to decrease experimental costs for the digital twin creation. These are presented and discussed in chapter 7.3.

6 Assessing productivity

Beurteilung der Produktivität

In the previous chapters a digital twin model is created and validated. It enables an assessment of the process and gives predictions of the laminate´s quality. Based on that, processes can be optimized towards process parameters including increased process speeds. However, it must be kept in mind that increasing the process speeds is not the only method to increase overall productivity. Part design, auxiliary times and down-times can have a significant influence on productivity.

This chapter presents a part-oriented productivity estimation with respect to the given production system. It provides a short overview of factors affecting the productivity of tape laying and its sensitivities based on previous studies, for example by JANSSEN [JANS20] and LUKASZEWICZ [LUKA12]. To enhance the productivity assessment, this study includes system specific auxiliary times as well as the geometrical characteristics of the laminate. It is shown that both can significantly influence the productivity of the system. A productivity tool is established and validated to estimate the output per hour and to show the sensitivities of the additive character of the process.

6.1 Definition of productivity

Definition der Produktivität

In an industrial environment productivity is the key figure for deciding whether a production system is profitable or not. For novel manufacturing technologies, such as the AFP of thermoplastic tape, an accurate estimation is necessary to show that industrial implementation is attractive. Since this study focuses on upscaling the AFP process by means of digitization it is crucial to introduce a performance indication verifying the proposed methodology.

The performance of manufacturing systems is nowadays often measured by the *Overall Equipment Effectiveness* (OEE). Seiichi Nakajima introduced this metric in 1988 to evaluate the total productive maintenance (TPM) and to account for hidden losses of the equipment utilization with regard to scheduled production time. The author defines six big time losses which are categorized into availability, performance and quality [JEON01, p. 1405; MAY08, p. 246]:

(1) equipment failure;	availability
(2) setup and adjustment;	
(3) idling and minor stoppages;	performance
(4) reduced speed;	
(5) defects in process; and	quality
(6) reduced yield.	

The basis for calculating the OEE is the ratio between the actual defect-free output and the theoretically maximum output which can be achieved by the production system. In detail, it can be calculated as following [JEON01, p. 1406]:

$$\begin{aligned} OEE &= availability \times performance \times quality \\ &= \frac{operating\ time}{loading\ time} \times \frac{net\ operating\ time}{operating\ time} \\ &\quad \times \frac{valuable\ operating\ time}{net\ operating\ time} \\ &= \frac{valuable\ operating\ time}{loading\ time}. \end{aligned} \tag{6.1}$$

Here the loading time is the overall available production time within a certain period and the valuable operating time the actual production time. Latter can be calculated by multiplying the number of produced parts by the cycle time.

Using OEE as a metric for the performance of manufacturing equipment or even of a complete site is common practice in industry. The methodology can be implemented in various ways and sectors to improve production performance. Various studies show how this metric can be enhanced in order to account for sector-specific influences or include further aspects, such as resource efficiency as shown by KUZNETSOV ET AL. [KUZN18]. JANSSEN [JANS20, P. 75] uses the OEE to evaluate the availability of a tape laying system by dividing the process time by real manufacturing time of laminate.

Table 6.1: Productivity evaluation criteria for lightweight components according to [JANS20, p. 52]

Produktivitätsbewertungskriterien für Leichtbaukomponenten nach [JANS20, p. 52]

	Conventional evaluation criteria	**Recommended evaluation criteria for lightweight components by [JANS20, p. 52]**
Productivity (stiffness dominated)	$\left[\frac{\rho V}{t}\right] = \frac{kg}{h}$	$\left[E \cdot \frac{V}{t}\right] = \frac{N}{mm^2}\frac{m^3}{h}$
Productivity (strength dominated)	$\left[\frac{\rho V}{t}\right] = \frac{kg}{h}$	$\left[R \cdot \frac{V}{t}\right] = \frac{N}{mm^2}\frac{m^3}{h}$

The estimation of the actual production time is essential to evaluate productivity. Often it is normalized by the produced weight per hour $[m/t] = kg/h$. However, as indicated by [JANS20, p. 52] this is not applicable for lightweight materials. In the lightweight sector, a resource- and, thus, weight-efficient part is aimed which would result in a low output value. For this reason, the evaluation criteria as in Table 6.1 are recommended.

In the context of tape laying only a few studies regarding productivity are available. The study by LUKASZEWICZ [LUKA11] illustrates the dependency of part size and productivity for a simple flat laminate out of thermoset prepreg tape. JANSSEN [JANS20, p. 61] analysis productivity sensitivities for the in-situ tape placement of thermoplastic tape. Increasing tape width, tape thickness, process speed and the number of multiple

tows reduce production time. However, the given calculations do not completely represent auxiliary and other downtimes which are nonproductive. Actual and theoretically estimated productivity can diverge strongly. LUKASZEWICZ ET AL. explains that this may be caused by the unfavorable relationship between process (main) and secondary times [LUKA12, p. 1004]. This also leads to the conclusion, that increasing process speed has only a little effect on overall productivity.

Definition of productivity in this study. Within this study the productivity estimation focuses on the second category of the OEE: performance. It is assumed that all parts have sufficient quality. An upgraded PrePro2D® system (see chapter 5.1) with three multiple tows is targeted for a specific material. Performance will be estimated by production time which includes main and auxiliary times, such as minor stops, during production. These calculations will be compared to experiments. The detailed calculations are shown in chapter 6.2. Downtimes, such as setup or failure time, are not included into the calculation, as they would be based on pure qualitative assumptions which cannot be experimentally verified yet. For a closer look into the category availability of a similar production system, the study by JANSSEN [JANS20, p. 75] is suggested.

6.1.1 Parameters influencing productivity

Einflussgrößen der Produktivität

As already introduced in chapter 3 the following aspects influencing productivity will be addressed within this thesis:

- System design
- Process design
- Part design.

System design. The aspect of system design concentrates on machine components which influence the scalability and performance. For example, these are the electrically driven axes, the number of tapes which can be processed parallel, the tape width, response times of components or components implying setup and maintenance times.

The upgraded PrePro2D® system consist of up to nine axes (see chapter 5.1). There are three main axes which have a primer effect on performance (see Figure 3.2) and are included into the analysis of this thesis:

- the x-axis is responsible for the translational movement of the heating table and thus for the process speed during tape laying (main time);
- the y-axis is responsible for the movement of the tape laying head only necessary for moving the head to the next tape path (auxiliary time);
- the c-axis is responsible for the rotation of the heating table which is necessary when the fiber orientation is changing (auxiliary time).

Next to the three main axes, there exists the z- and t-axis. The z-axis defines the height of the tape laying head above the table and is adjusted according to the thickness of the layer. The t-axis powers the feed of the tape and is synchronized with the x-axis to guarantee that the tape is forwarded to the right position at the right time. It adapts to

the x-axis speeds to guarantee full synchronization. Since x-, y- and c- axes directly affect main time and auxiliary times, they are investigated closely to see their influence on overall production time. An exemplary relationship between jerk j, acceleration a and velocity v of the electrically driven axes is shown in Figure 6.1.

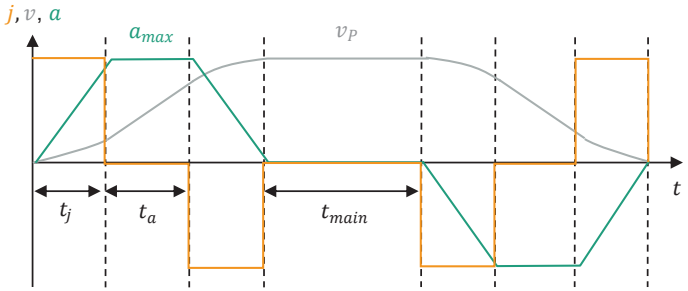

Figure 6.1: Exemplary relationship between jerk, acceleration and velocity, adapted from [BREC21, p. 518]

Beispielhafte Beziehung zwischen Ruck, Beschleunigung und Geschwindigkeit, in Anlehnung an [BREC21, p. 518]

Process Design. Process design relates to the tape laying strategy of the specific laminate. The tape laying system, the tape material as well as laminate geometry cause the choice of process parameters, such as process velocity or consolidation pressure. In general, and as shown in current literature (see chapter 2 and 4), process design for the in-situ AFP primarily refers to the right choice of process parameters for an idealized setup. They often neglect the influence of the part geometry as well as of the whole system design on the process. Experiences with prototyping of diverse parts have shown that a profound process characterization is not only necessary for the used material but also for the desired part geometry leading to extensive development times.

Chapter 4 introduces a model of a digital twin. Due to the increased computing power and software possibilities, using digital modeling strategies have become more and more attractive for complex manufacturing technologies. Especially in the case of AFP, it offers the chance to decrease development times for process qualification and thereby increase productivity of the technology. In the later, chapter 7 presents the development of a digital twin allowing the optimization of tape laying strategies. Based on data-driven modeling approaches the process can be optimized not only regarding the desired shape and quality, but also regarding the productivity. It is seen as one of the major tools to upscale the PrePro2D® system.

Part design. Part design significantly influences the productivity of the whole manufacturing technology as it defines the production time. On the one hand, the PrePro2D® technology enables the manufacturing of waste-optimized, near-net shape laminates. On the other hand, by increasing laminate size main process speeds have a higher influence on the manufacturing time allowing a rise in output per hour. Consequently, there exists a trade-off between part design and productivity which must be

considered for the individual production scenario. In addition, productivity can be scaled by the amount of tape weight being deposited. This can either be done by

- increasing tape width,
- the number of tapes laid parallel,
- the thickness of the tape or
- the mass of the matrix and fibers.

All have the same effect: they increase the grammage of the material which is processed per hour. In the case of tape thickness, it has additionally the positive effect that the number of layers is reduced to the desired laminate thickness. Table 6.2 summarizes the considered parameters affecting the cycle time of producing a laminate as explained above.

Table 6.2: Overview of considered parameters influencing the cycle time of a laminate

Übersicht der betrachteten Einflussparameter auf die Zykluszeit eines Laminats

	System design	**Process design**	**Part design**
Parameters influencing the cycle time t_{lam}	- System-dependent auxiliary times t_{aux}^{sys} caused by X,Y,C axis velocity v, acceleration a, jerk j - Number of multiple tows n_{sys}^{t}	- Process-dependent (main) time $t_{main}^{process}$ defined by process velocity v_P - Process-dependent cooling time t_C (if required)	- Part-dependent auxiliary times t_{aux}^{part} caused by layup, size and fiber orientation θ - Part-dependent main times t_{main}^{part} defined by laminate dimensions ($l_x \; x \; l_y \; x \; h$) and tape thickness h_{tape} and with w_{tape}

6.2 Productivity calculation

Produktivitätsberechnung

This section presents the analytical basis for calculating the OEE as shown in equation (6.1). In this context, the valuable operating time is the actual cycle time of a laminate t_{lam}. The loading time is the total available time for the production. Here, a calendar time-based approach is chosen reflecting the theoretical calendar time [JEON01, p. 1406] and including a three-shift operation (24h/day) from Monday to Friday. Aim is to introduce a tool predicting the cycle time and the estimated OEE for specific parts.

This section presents the productivity calculation considering the parameters discussed above and summarized in Table 6.2. The following assumptions are made:

- x-, y- and c- axes have the most significant influence on performance and are considered solely;
- Start velocity and acceleration equals zero: $v^0 = 0$, $a^0 = 0$;
- Maximum jerk $j^{max} = 50\ m/s^3$ and target velocity of axes are reached;
- Maximum possible acceleration of axes $a_X^{max} = 5\ m/s^2$, $a_Y^{max} = 1\ m/s^2$ is not reached to enable shortest positioning time [SEW10, p. 129];
- Relationship between jerk, acceleration and velocity as shown in Figure 6.2;
- Interpolation of axes neglected;
- Downtimes (e.g. run-in and run-out) and set-up times neglected;
- Conventional layup: same starting position for each layer, no return to starting position at end of laminate;
- Number of multiple tows n_{sys}^t=1.

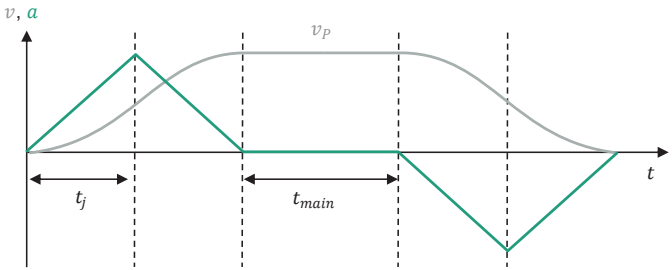

Figure 6.2: Assumed relationship of acceleration and process speed of the PrePro2D® system, in accordance to [SEW10, p. 130; BREC21, p. 518]

Angenommene Beziehung zwischen Ruck, Beschleunigung und Geschwindigkeit der PrePro2D® Anlage, in Anlehnung an [SEW10, p. 130; BREC21, p. 518]

The performance is calculated based on the valuable operating time which is the cycle time of producing a laminate t_{lam}. It is estimated by calculating the main and auxiliary times of the axes:

$$t_{lam} = t_{main} + t_{aux}^{sys} \tag{6.2}$$

The calculation is adapted from [JANS20, p. 60] and extended to explicitly differentiate between main and auxiliary times. As indicated above, both times are strongly dependent on the process as well as geometrical characteristics of the laminate. Especially, the geometry and layup define how many strokes of each axis are required.

The PrePro2D® system can lay and cut either one, two or three tows simultaneously and separately as defined by n_{sys}^{t}. This means that the number of strokes $n_{XYstrokes}^{i}$ for the x- and y-axis required for laying the laminate is dependent on the amount of tape paths n_{tapes}:

$$n_{tapes} = \sum_{i=1}^{N} n_{tapes}^{i} = \sum_{i=1}^{N} f\left(l_x, l_y, h, w_{tape}, \theta\right) \tag{6.3}$$

$$, \forall\, n_{tapes}^{i} \in \mathbb{Z}.$$

N is the amount of layers defined as:

$$N = \frac{h}{h_{tape}}. \tag{6.4}$$

n_{tapes} is strongly influenced by the individual layup, laminate geometry and selection of tape material and must be an integer. If the width l_y or the length l_x of the part is not a multiple of the tape width w_{tape} the number of tapes per layer is rounded up. The number of strokes per layer i is defined by the number of tapes per layer n_{tapes}^{i} and the number of (active) multiple tows n_{sys}^{t}:

$$n_{XYstrokes}^{i} = \left\lceil \frac{n_{tapes}^{i}}{n_{sys}^{t}} \right\rceil, \forall\, n_{XYstrokes}^{i} \in \mathbb{Z} \tag{6.5}$$

In a conventional layup strategy, the $n_{XYstrokes}^{i}$ for the x- and y-axis are the same for the same fiber angle. Deviations my occur, for example at the end of the process, which does not require an additional stroke in y. The number of strokes of the c-axis is dependent on how often the fiber angle θ changes $n_{\Delta\theta}^{i}$ for specific layer i:

$$n_{Cstrokes}^{i} = n_{\Delta\theta}^{i}, \forall\, n_{Cstrokes}^{i} \in \mathbb{Z} \tag{6.6}$$

Main time. The main time is a function of process and part dependent parameters:

$$t_{main} = \sum_{i=1}^{N} \sum_{j=1}^{n_{XYstrokes}^{i}} \frac{l_x^j}{v_P^j}. \tag{6.7}$$

l_x^j and v_P^j are the tape lengths and process velocities of the individual tape paths j and $n_{strokes}^{i}$ the number of strokes to lay these tape paths for the individual layer i.

Auxiliary times. According to the relationship as shown in Figure 6.2 the auxiliary times for each axis is the sum of times required for the jerk t_j:

$$t_{aux} = 4t_j = 4\sqrt{\frac{2 \cdot v}{j^{max}}}, \tag{6.8}$$

with j^{max} being the maximum jerk of the specific axis and v the requested axis velocity. It is derived by differentiating the standard relationship between jerk, acceleration and velocity by time [BREC21, p. 516]. As mentioned before, it is assumed that a_X^{max} is not reached so that there is no phase with constant acceleration. The extra time for auxiliary axis movements need to be added to the main time for each single stroke.

The PrePro2D® is designed to lay up to three tapes simultaneously by moving the table on the x-axis. Since the table needs to return for the next laying procedure, the auxiliary time of the x-axis per stroke has to be added with the return time. In this time the maximum velocity of the axis is reached. The total auxiliary time is calculated as:

$$t_{aux}^{X} = \sum_{i=1}^{N} \left(n_{XYstrokes}^{i} \left(4 \sqrt{\frac{2 \cdot v_P}{j_X^{max}}} + \left(\frac{l_x}{v_X^{max}} + 4 \sqrt{\frac{2 \cdot v_X^{max}}{j_X^{max}}} \right) \right) \right) \tag{6.9}$$

The auxiliary time of the y-axis is caused by the movements necessary for laying the tapes next to each other. In addition, the return to the beginning of the laminate needs to be considered as soon as the layer is finished. In a conventional layup strategy of a plain 0° layup the return time equals the Euclidean norm of the travel of the y-axis and x-axis. However, in other layups strategies this can be different. For this reason, the general term for the return time is stated here t_{return}^{Y}. In all movement it is assumed that its maximum velocity is reached v_Y^{max}. The travel per stroke depends on the number of (active) multiple tows n_{sys}^{t} and tape width w_{tape}. The total auxiliary time of the y-axis is:

$$t_{aux}^{Y} = \sum_{i=1}^{N} \left(n_{XYstrokes}^{i} \left(\frac{n_{sys}^{t} \cdot w_{tape}}{v_Y^{max}} + 4 \sqrt{\frac{2 \cdot v_Y^{max}}{j_Y^{max}}} \right) \right) + t_{return}^{Y}. \tag{6.10}$$

The auxiliary time of the c-axis is simplified by only considering the maximum velocity for each stroke:

$$t_{aux}^{C} = \sum_{i=1}^{n_{Cstrokes}} \left(\frac{\Delta\theta^{i}}{v_{max}^{c}} \right). \tag{6.11}$$

6.3 Experimental validation

Experimentelle Validierung

The experimental investigation has two aims. First aim is to assess the current productivity of the PrePro2D® system by analyzing actual main and auxiliary times. Second aim is to predict the main and auxiliary times based on the previously shown calculation and compare them to the actual measured ones. This analysis is the basis for deriving strategies reducing cycle times and, thus, increasing productivity.

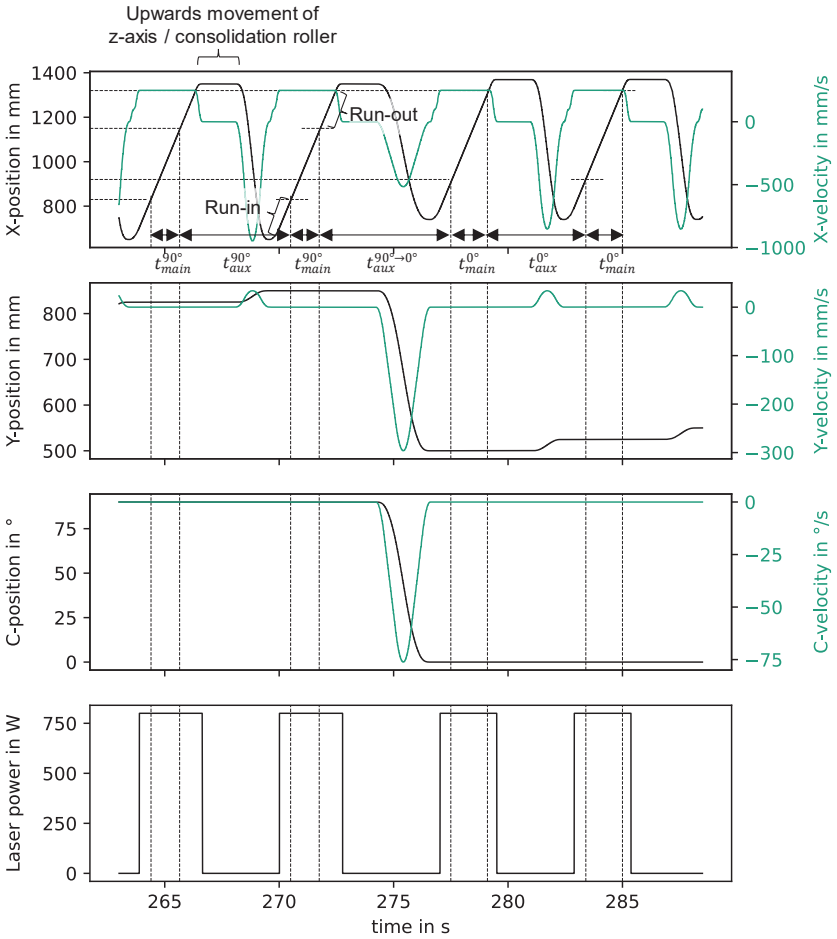

Figure 6.3: Axes positions, velocities and set laser power for the last two tape paths of the third layer and the first two paths of the fourth layer (dashed lines indicate start and end of each tape path) of the produced laminate with $v_P = 250\ mm/s$

Achsenpositionen, Geschwindigkeiten und eingestellte Laserleistung für die letzten beiden Tapepfade der dritten Lage und die ersten beiden Pfade der vierten Lage (gestrichelte Linien zeigen den Beginn und das Ende jedes Pfads an) des produzierten Laminats mit $v_P = 250\ mm/s$

6.3.1 Experimental performance analysis

Experimentelle Analyse der Performanz

The experimental setup in chapter 5.2 and Table 5.1 are used as basis for the performance analysis. The main and auxiliary times as well as the positions and velocities of the relevant axes are analyzed. Table 6.3 gives an overview of the total, layer and tape path individual main and auxiliary times. These are derived graphically using the data of the axes. Figure 6.3 displays the assessed data from the x-, y- and c-axes positions and velocities as well as the set laser power. The dashed lines represent starting and end point of each of the displayed three tape paths as defined by the machine code.

Summing all the main time gives a total main time of the laminate of $t_{main}^{part} = 156.8\,s$. Summing all the auxiliary times gives $t_{aux}^{part} = 552.5\,s$. This in total gives a manufacturing time of $t^{part} = 709.3\,s$. The deviations from the total manufacturing time in Figure 5.5 ($t^{part} = 680\,s$) are coming from multiple reasons. First, after the last tape paths of a layer, the head moves directly to the start of the new layer without returning to the next path position. Second, the production directly stops at the end of the last path (see Figure 5.6). Third, the above-mentioned short database malfunction result in small time errors.

Table 6.3: Overview of the measured main and auxiliary times of the produced laminate with $v_P = 250\,mm/s$

Übersicht der gemessenen Haupt- und Nebenzeiten des produzierten Laminats mit $v_P = 250\,mm/s$

	Main time	**Auxiliary time (incl. return time)**
Total time	$t_{main}^{part} = 156.8\,s$	$t_{aux}^{part} = 552.5\,s$
0° layer (4x)	$t_{main}^{0°} = 19.2\,s$	$t_{aux}^{0°} = 51.6\,s$
90° layer (4x)	$t_{main}^{90°} = 20\,s$	$t_{aux}^{90°} = 77.6\,s$
0° tape path (12x per layer)	$t_{main}^{0°} = 1.6\,s$	$t_{aux}^{0°} = 4.3\,s$
90° tape path (16x per layer)	$t_{main}^{90°} = 1.25\,s$	$t_{aux}^{90°} = 4.85\,s$
Get to next layer with same orientation 0° (1x)	-	$t_{aux}^{0°\rightarrow 0°} = 4.2\,s$
Get to next layer with same orientation 90° (2x)	-	$t_{aux}^{90°\rightarrow 90°} = 4.85\,s$
Changing fiber orientation from 0° to 90° (2x)	-	$t_{aux}^{0°\rightarrow 90°} = 5.15\,s$
Changing fiber orientation from 90° to 0° (2x)	-	$t_{aux}^{90°\rightarrow 0°} = 5.75\,s$

The analysis of the main and auxiliary times shows that the main times only account for approx. $23\ \%$ of the overall cycle time of the laminate. This supports the recommendation to focus on minimizing auxiliary times to decrease cycle time and, thus, to increase productivity. Figure 6.3 already indicates two optimization potentials:

1. Reducing run-out length of the 90° tape paths
2. Reducing the stand-still times of the x-axis which result from the movement of the z-axis after each tape path.

These two strategies could already save up to around $160\ s$ ($1.2\ s$ per tape for all tapes and additional $0.4\ s$ for each $90°$ tape). Decreasing run-in length is not feasible to a certain extent. These are limited by the time the tape needs to be fed from the feeding unit to the consolidation roller which corresponds to the cutting length of the system.

The productivity is evaluated with the criteria for stiffness dominated parts according to Table 6.1. The output per hour of the manufactured laminate based on the conventional criteria is $1.94\ kg/h$. When using the criteria for lightweight components by JANSSEN [JANS20, p. 52] and the E-modulus of the complete laminate of $55.415\ GPa$ (calculated with *eLamX* [TUDR22]) this results in $[E \cdot V/t] = 55415\ N/mm^2 \cdot 0.000256\ m^3/0.1888\ h = 75.1\ N/mm^2 \cdot m^3/h$. Taking the measured DoB into consideration, this leads to $[E \cdot \mathrm{D}_{B,exp}^{avg} \cdot V/t] = 75.1 \cdot 0.7055\ N/mm^2 \cdot m^3/h = 53\ N/mm^2 \cdot m^3/h$. These productivity metrics do not account for any downtimes of the machine.

Table 6.4: Overview of the predicted main and auxiliary times for the laminate with $v_P = 250\ mm/s$

Übersicht der vorhergesagten Haupt- und Nebenzeiten des Laminats mit $v_P = 250\ mm/s$

Total time	$t^{part} = 705.9\ s$
Total main time	$t_{main}^{part} = 158.7\ s$
Total auxiliary time	$t_{aux}^{part} = 547.2\ s$
Total auxiliary time for the x-axis	$t_{aux}^{X} = 233.9\ s$
Total auxiliary time for the y-axis	$t_{aux}^{Y} = 308.6\ s$
Total auxiliary time for the c-axis	$t_{aux}^{C} = 4.5\ s$

6.3.2 Performance prediction

Vorhersage der Performanz

In relation to the experimental setup in chapter 5.2 and Table 5.1, the main and auxiliary times are predicted with the above-mentioned relationships. The predicted times are listed in Table 6.4. The overall cycle time is estimated to an accuracy of below $1\ \%$. The main time is only overestimated by approx. $1.2\ \%$, the total auxiliary times are forecasted $1\ \%$ lower than the actual measured ones.

Regarding productivity, this estimation results in an output per hour of $1.87\ kg/h$ and the criteria for lightweight components of $72.3\ N/(mm^2)\ m^3/h$. Including DoB this leads to $[E \cdot \mathrm{D}_B^{np} \cdot V/t] = 54.62\ N/(mm^2)\ m^3/h$. All values are similar to the actual achieved productivity values with an error around $\pm 3\ \%$. An overview of predicted and measured values is given in Table 6.5.

Table 6.5: Overview of the predicted and actual total cycle time and productivity for the laminate with $v_P = 250\ mm/s$

Übersicht der hervorgesagten und gemessenen Zykluszeit und Produktivität des Laminats mit $v_P = 250\ mm/s$

	Predicted	**Measured**
Total time	$t^{part} = 705.9\ s$	$t^{part} = 680\ s$
Productivity (conventional criteria)	$\left[\frac{m}{t}\right] = 1.87\ \frac{kg}{h}$	$\left[\frac{m}{t}\right] = 1.94\ \frac{kg}{h}$
Productivity (criteria for lightweight components)	$\left[E \cdot \frac{V}{t}\right] = 72.3\ \frac{N}{mm^2}\frac{m^3}{h}$	$\left[E \cdot \frac{V}{t}\right] = 75.1\ \frac{N}{mm^2}\frac{m^3}{h}$
Productivity (criteria for lightweight components incl. DoB)	$\left[E \cdot \mathrm{D}_B^{np} \cdot \frac{V}{t}\right] = 54.6\ \frac{N}{mm^2}\frac{m^3}{h}$	$\left[E \cdot \mathrm{D}_{B,exp}^{avg} \cdot \frac{V}{t}\right] = 53\ \frac{N}{mm^2}\frac{m^3}{h}$

6.4 Conclusion

Zusammenfassung

The productivity of a production system is an important question to answer. Predictions can help to find a suitable machine setup. However, at the end, the system needs to verify the productivity by actual outcomes. For this reason, the major idea of the productivity assessment of this chapter is not only to create an analytical model, but to verify it by experiments. This chapter gives an answer to the 2nd research question of this thesis.

The experimental validation of the productivity model reveals that productivity can be predicted accurately with simple analytic models. It is a useful tool for deriving cycle time optimizations as it discloses the relationship of main and auxiliary times. It reveals the strong influence of the auxiliary times on the performance and productivity of the manufacturing technology.

7 A digital twin for deriving manufacturing strategies

Ein digitaler Zwilling zur Herleitung von Fertigungsstrategien

The main target of this thesis is to optimize process planning for increasing productivity. As shown in the previous chapters, a digital twin framework including a part-oriented process model enables a more realistic process prediction. It allows to detect sensitivities towards productivity and process quality. This chapter applies the framework to derive manufacturing strategies for an upscaled production. First, the factors for increasing performance and, thus, productivity are analyzed to find improved production settings. Second, the influence of different layup sequences on process quality and productivity are investigated with the help of the digital twin. Finally, the derived digital twin framework is embedded into the ISO 2327 standard and a final guide for implementation is proposed. It is concluded by an outlook for increasing the prediction quality of the digital twin for future investigations.

7.1 Increasing performance by increasing process speeds

Steigerung der Performanz durch Erhöhung der Prozessgeschwindigkeit

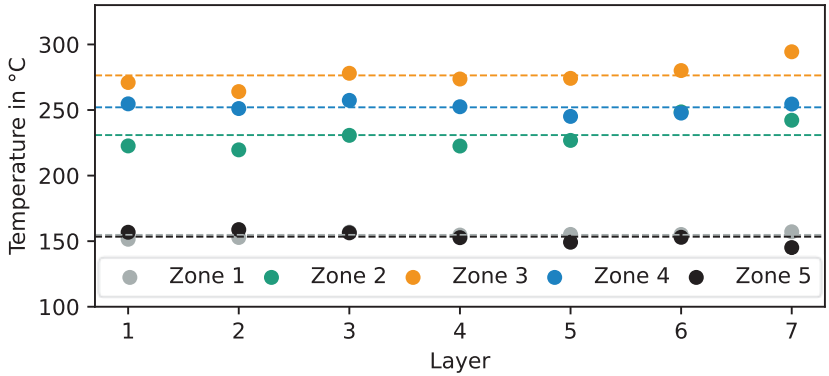

Figure 7.1: Average temperatures during laying for each layer of the laminate with $v_P = 750\ mm/s$ (dashed horizontal lines indicate mean temperature values per zone)

Mittlere Temperaturen während der Tape Ablage jeder Lage des Laminats mit with $v_P = 750\ mm/s$ *(gestrichelte horizontale Linien zeigen die mittleren Temperaturwerte pro Zone an)*

To directly show the influence of increasing process speeds on process quality as well as performance, the identical experimental setup as in chapter 5.2 (Table 5.1) is performed with a process velocity of $v_P = 750\ mm/s$. The last two layers, layer 7 and 8, have a process velocity of $v_P = 250\ mm/s$ $(P_L(v_P = 250\ mm/s) = 800\ W)$ to assure process robustness. The set laser power of $P_L(v_P = 750\ mm/s) = 1800\ W$ is derived

on a short optimization focusing on robust process conditions and a smooth production without errors. This analysis allows to see the effects of tripling process speed on cycle time, productivity and on quality properties. To give an insight into the temperature measurements, Figure 7.1 displays the measured and averaged temperatures for each zone and layer.

7.1.1 Quality properties with increased process speeds

Qualitätseigenschaften bei erhöhten Prozessgeschwindigkeiten

The effect of increasing process speed on the quality of the laminate is experimentally evaluated based on the DoB. The experimental values are derived in accordance with section 5.2.4. The DoC is predicted based on the methodology shown in section 5.2.5.

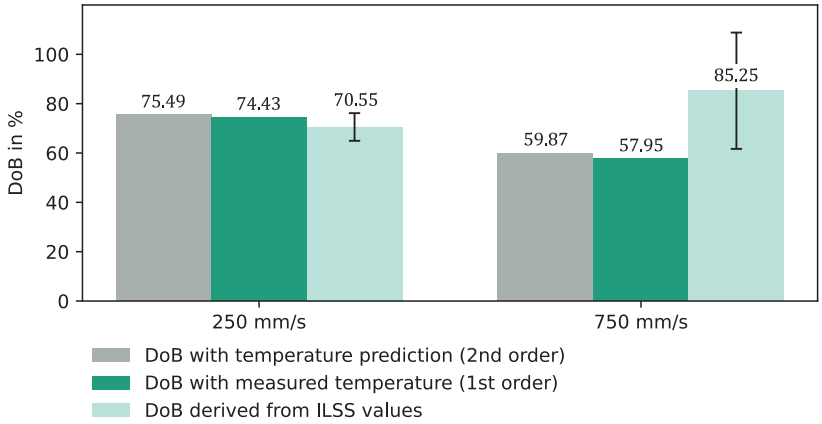

Figure 7.2: Predicted and experimentally derived DoB values for the laminate with $v_P = 750\ mm/s$ compared to the $v_P = 250\ mm/s$ laminate

Vorhergesagte und experimentell gemessene Konsolidierungsgrade für das Laminat mit $v_P = 750\ mm/s$ im Vergleich zu dem Laminat mit $v_P = 250\ mm/s$

The lower measured nip-point values (zone 3) already indicate the lower predicted DoB value compared to the case with $v_P = 250\ mm/s$ in chapter 5.2. In addition, the increased speed also results in less radiation time decreasing t_f in equation (4.23). The predicted DoB values are around $20\ \%$ lower (see Figure 7.2). Conversely, the experimental derived value with using the ILSS approach is much higher than expected with $\mathrm{D}_{B,exp}^{avg} = 85.25\ \%$. However, as can be seen in Figure 7.2 the standard deviation is much higher for the ILSS values of the $v_p = 750\ mm/s$ specimens compared to the ones with $v_P = 250\ mm/s$. It even has values of $\mathrm{D}_{B,exp} > 100\ \%$ $(ILSS_{exp} > ILSS_{max})$, see equation (4.36). This is caused by outliers in which the specimens with in-situ consolidation have a higher ILSS value compared to those with post-consolidation. Taken out these outliers, the average ILSS value is $\mathrm{D}_{B,exp}^{avg} = 70.9\ \%$. This lower DoB is also supported by the microsections which show bigger interlaminar voids compared to the

one with $250\ mm/s$ (Figure 5.13). The high experimentally derived ILSS values may appear random due to the small random sample of $n_{ILSS} = 6$. It may also indicate that higher process speeds are not modeled accurately within the digital twin since the underlying models are mainly validated for low process speeds $v_P \ll 500\ mm/s$ and for PEEK polymers.

Taking a short look at the DoC prediction based on a 2nd order prediction, the model predicts an average DoC of $\chi^{np,avg} = 17.5\ \%$. The time within the range in which crystals cannot be created $t(T_m < T < T_{np})$ is less than compared to the case with $250\ mm/s$ since the irradiation time is much smaller. This would give the conclusion, that increased process speeds provide more time for crystallization. However, the temperature prediction with $750\ mm/s$ (see appendix 1A.1) also results in less temperature increase of the lower layers. In addition, the overall reduced cycle time allows generally less time for crystallization. These factors result in the decreased DoC.

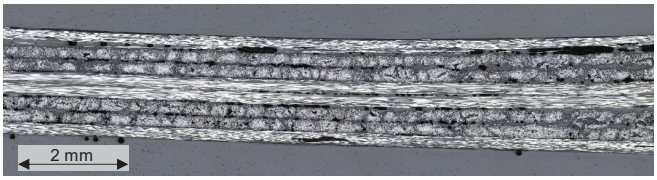

Figure 7.3: Microsection of the laminate produced with $v_P = 750\ mm/s$

Schliffbilder des Laminates produziert mit $v_P = 750\ mm/s$

It must be noted, that these values are based on non-optimized process parameters. It is observed, that increasing process speeds $v_P \gg 500\ mm/s$ result in decreasing process robustness during manufacturing. The higher laser power and process speed result in a smaller process window which have not yet been investigated so far. To find accurate process settings an in-depth analysis is required which is not within the scope of this thesis. However, the created digital twin is a suitable tool to investigate this phenomenon.

7.1.2 Cycle time and productivity with increased process speeds

Zykluszeiten und Produktivitäten bei erhöhten Prozessgeschwindigkeiten

Table 7.1 lists the predicted and actual cycle times in accordance with the methodology shown in chapter 6.2. The measured values correspond to the actual ones including layer 7 and 8 with reduced speed. The value is interpolated for a layup with only $v_P = 750\ mm/s$ and are used to compare it with the output of chapter 5 and 6 with $v_P = 250\ mm/s$.

Tripling the process speed results in an measured cycle time decrease of around $25\ \%$. The predicted decrease of cycle time is $10\ \%$. Taking the productivity criteria for lightweight components with the actual measured DoB into account, this leads to a potential productivity increase of up to $62\ \%$ as long as high DoB values are achieved. When increasing process velocity, the prediction becomes less accurate as shown in Figure

7.4.: whereas in the case for $v_P = 250\ mm/s$ the predictions are similar to the measured values, the error between prediction and measurement is higher in the case with $v_P = 750\ mm/s$. The reason is the overestimated cycle time of the produced laminate. Having a closer look at the auxiliary times in Table 7.2, this results from the overestimation of auxiliary times by $28\ \%$. The main cause is the increase of predicted auxiliary time of the x-axis due to the influence of v_P in equation (6.8). The values in the prediction are amplified by the increased process speed. This indicates that adjusting the assumptions made in section 6.2. of the performance calculations are necessary.

Table 7.1: Overview of the predicted and actual total cycle time and productivity for the laminate with $v_P = 750\ mm/s$ and $n_{sys}^t = 1$

Übersicht der vorhergesagten und gemessenen Zykluszeit und Produktivität für das Laminat mit $v_P = 750\ mm/s$ *und* $n_{sys}^t = 1$

	Predicted	**Measured**
Total time	$t^{part} = 632.9\ s$	$t^{part} = 508\ s$
Productivity (conventional criteria)	$\left[\frac{m}{t}\right] = 2.1\ \frac{kg}{h}$	$\left[\frac{m}{t}\right] = 2.6\ \frac{kg}{h}$
Productivity (criteria for lightweight components)	$\left[E \cdot \frac{V}{t}\right] = 80.7\ \frac{N}{mm^2}\frac{m^3}{h}$	$\left[E \cdot \frac{V}{t}\right] = 100.5\ \frac{N}{mm^2}\frac{m^3}{h}$
Productivity (criteria for lightweight components incl. DoB)	$\left[E \cdot \mathrm{D}_B^{np} \cdot \frac{V}{t}\right] = 48.3\ \frac{N}{mm^2}\frac{m^3}{h}$	$\left[E \cdot \mathrm{D}_{B,exp}^{avg} \cdot \frac{V}{t}\right] = 71.3\ \frac{N}{mm^2}\frac{m^3}{h}$

Increasing process speed as a manufacturing strategy has the potential to significantly increase productivity of lightweight components. Taken even three simultaneous tow $n_{sys}^t = 3$ into account, the productivity can roughly be tripled as already shown in [JANS20, p. 61].

Table 7.2: Predicted and measured main and auxiliary times for the laminate with $v_P = 750\ mm/s$

Vorhergesagte und gemessene Haupt- und Nebenzeiten für das Laminat mit $v_P = 750\ mm/s$

	Predicted	**Measured**
Total main time	$t_{main}^{part} = 52.9\ s$	$t_{main}^{part} = 54.6\ s$
Total auxiliary time	$t_{aux}^{part} = 578\ s$	$t_{aux}^{part} = 453.4\ s$

The quality and performance/productivity prediction by the digital twin model helps to understand the influences. However, the prediction quality seems to decrease with

increasing process speeds. As stated in chapter 6.3, it is assumed that the existing analytical models, which are used as a basis for the digital twin, are not fully applicable for higher process speeds. In addition, the availability of the system might decrease due to the above stated difficulties of processing with higher process speeds and acquiring the desired laminate quality.

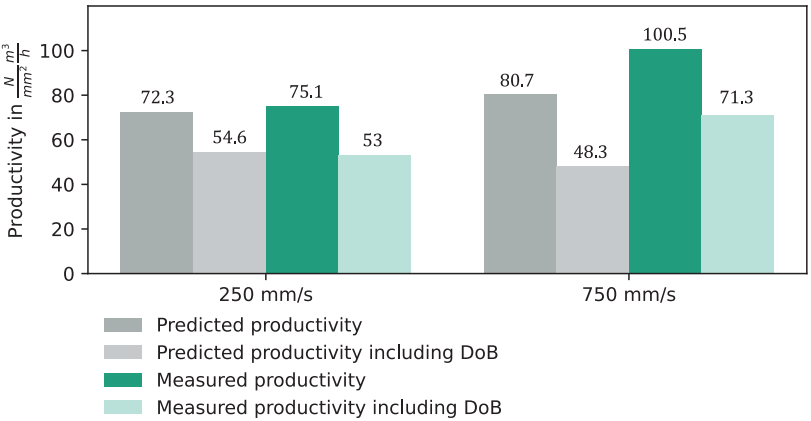

Figure 7.4: Comparison of the productivity (criteria for lightweight parts) between the laminate with $v_P = 250\ mm/s$ and $v_P = 750\ mm/s$

Vergleich der Produktivität (Kriterium für Leichtbauteile) zwischen dem Laminat mit $v_P = 250\ mm/s$ und $v_P = 750\ mm/s$

7.2 Layup strategies

Ablegestrategien

The layup sequence is the order of laying each tape path as defined during path planning. Extensive research has already been conducted for the path planning of the AFP process. The authors ROUSSEAU ET AL. [ROUS19] give a conclusive overview of studies as well as available CAx software in this field. However, these studies especially focus on the AFP process with thermoset tape material or thermoplastics without in-situ consolidation to minimize geometrical defects, such as gaps and overlaps. Only little research has been conducted about the path planning with the optimization of process parameters based on historical temperature data and quality indicators for the AFP process with in-situ consolidation. As shown in chapter 2.2 they either focus on idealized analytical models or on costly FEM models. The idea behind the simulation is to increase flexibility, simplify modeling and to create a more part-oriented prediction for path planning.

For the PrePro2D® system, there exist a variety of possibilities to change the layup sequence and strategy since the system axes can be controlled flexibly by the machine code. In this study, the following layup sequences are defined and investigated:

- *Conventional*: The conventional layup sequence implies that each layer starts at the same starting position. This results in a movement of the y-axis without tape deposition along the width of the laminate between two layers. This strategy has been used in the prior investigations within this study.
- *Bidirectional*: In this layup strategy the new layer starts at the end of the previous one as illustrated in Figure 7.5. The y-axis moves back stepwise, and tapes are laid during the way back. It is the reverse laying process as of the previous layer.
- *Reconsolidation passes*: A further layup strategy is to run the process without tape deposition but with the use of the heating unit. This does not only interfere with the path planning but also with the processing strategy. The heat source heats up the substrate and the interface above melting temperature to improve the interlaminar consolidation. When having optimized process parameters, this generally is not necessary.

The investigation of these layup strategies is conducted with the help of the digital twin model. Cooling times, effects on DoC and productivity are examined since these are primarily affected by the change of layup sequence. For the *conventional* strategy the analysis can be found in the previous chapters (chapter 4, 5 and 6).

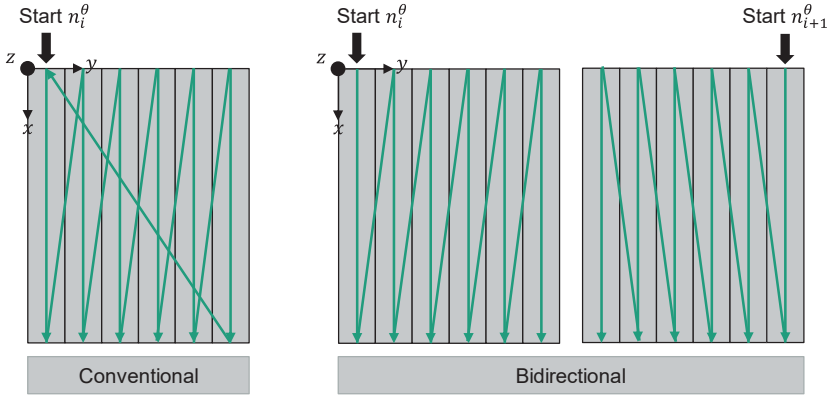

Figure 7.5: Conventional and bidirectional layup sequence

Konventionelle und bidirektionale Pfadplanung

7.2.1 Bidirectional layup strategy

Bidirektionale Ablegestrategie

An aim of the bidirectional layup strategy is the decrease of auxiliary and cooling times by minimizing strokes without tape deposition. Table 7.3 shows the minimal cooling time for $v_P = 250\ mm/s$ and $v_P = 750\ mm/s$ for a 0° tape path with $l_x = 400$ mm length (in accordance with the laminate in chapter 5). Since the minimum cooling time is still higher than the predicted cooling time of approx. $0.4\ s$, it is expected that the substrate temperature during laying of the next layer is equal to the tool temperature T_{tool} in all cases. As described in section 5.2.5, the duration in which the substrate temperature is between $T_m < T < T_{np}$ is relevant for estimating the DoC since in this temperature range crystallization cannot occur. To calculate the DoC the overall production time as well as the time in which $T_m < T < T_{np}$ is required. For comparison, the same laminate setup as in chapter 5 is investigated.

The main reduction of the cycle time is the neglection of the term t_Y^{return} in equation (6.10) for layers with the same fiber orientation. This results in an overall decrease of auxiliary times of only $3\ \%$ in the case with $v_P = 250\ mm/s$. Taking this $3\ \%$ reduction of the measured cycle time of $t^{part} = 680\ s$ into account, this results in a cycle time of $t^{part} = 659.6\ s$ and in an average DoC of $\chi^{np,avg} = 28.08\ \%$.

Table 7.3: Minimal cooling times for a laminate with bidirectional layup sequence

Minimale Abkühlzeiten für ein Laminat mit bidirektionaler Pfadplanung

	$v_P = 250\ mm/s$	$v_P = 750\ mm/s$
Min. cooling time 0°	$t_{c,min}^{0°} = 4.86\ s$	$t_{c,min}^{0°} = 4.26\ s$
Min. cooling time 90°	$t_{c,min}^{90°} = 4.52\ s$	$t_{c,min}^{90°} = 4.13\ s$

To conclude, the digital twin does not predict a significant benefit of the bidirectional layup strategy compared to the conventional one. However, this analysis only takes a look on a simple 0°/90° layup with rectangular shape. Changing the layup sequence for laminates with different fiber orientations, geometry and even laminate thicknesses may benefit from a non-conventional layup strategy.

7.2.2 Reconsolidation passes

Rekonsolidierungsdurchgänge

Reconsolidation passes as a layup strategy for improving consolidation have been examined by several authors, such as in [MANT92b, p. 2367; KHAN10, p. 108; SCHÄ17, p. 138; WEIL19, p. 106]. KHAN ET AL. experimentally validate that three additional passes with heating and without tape deposition of the topmost layers result in an increase in ILSS strength of approx. $9\ \%$.

The digital twin simulation in thickness direction for $v_P = 250\ mm/s$ and $v_P = 750\ mm/s$ (Figure 5.7 and Figure A.1) predicts that temperature reaches the layers

below with slow process speeds and thin tapes. Based on this prediction, a reconsolidation pass makes sense if these are done with slower speeds to assure the remelting of the interface between the upper and the layer below. WEILER calls this effect the “skin layer effect” [WEIL19, p. 106]. However, even if reconsolidation may increase the DoB, the question is, if the improvement outperforms the increased cycle time.

7.3 Methodology for an optimized digital twin

Methodik für einen optimierten digitalen Zwilling

The previous sections 7.1 and 7.2 have illustrated which investigations are possible through the digital twin framework created within this thesis. It allows the prediction of process induced effects on part level. However, additional efforts are required especially in programming a software which connects and visualizes the proposed digital twin framework.

This final section concludes the digital twin framework by providing a methodology for improving its capabilities. It gives an overview of applications, domains and functions. In addition, the digital twin for AFP with in-situ consolidation is related to the ISO 23274 norm. An AFP specific flow chart is derived for offering a guidance for implementation. Since the previous chapters have already revealed optimization potentials, this section concludes with a summary of errors and an outlook for increasing prediction robustness by minimizing these errors.

7.3.1 The AFP digital twin within the ISO 23274 framework

Der AFP Digitale Zwilling innerhalb des ISO 23274 Rahmenwerks

The derived digital twin for the AFP process with in-situ consolidation can be related to the ISO 23274 standard (see 2.3.2). The targeted observable manufacturing elements (OME) are the PrePro2D® system (equipment), the thermoplastic tape material (material), the AFP process with in-situ consolidation (process) and the tailored composite blanks (part). Within this study, the focus is the modeling and analysis of the process digital twin. The following applications are created:

Process analysis. The digital twin visualizes the assessed data and set process parameters within a virtual representation of the final part. The spatially resolved data allows to either manually or automatically analyze towards process critical factors.

Process prediction. A part-oriented process digital twin is created including the prediction of temperature evolution as well as process parameters. Input parameters are, amongst others, cooling times, irradiation characteristics and substrate thickness.

Quality prediction. Either based on the process prediction (2^{nd} order) or on the actual measured process values (1^{st} order), quality indicators can be derived. The derived and validated indicators are consolidation (DoB) and crystallization (DoC). It is also possible to extend the quality prediction, for example, by including the prediction of residual stresses.

Productivity prediction. A tool for predicting the performance and productivity is included in the process digital twin. This allows the prediction of part-oriented economic factors.

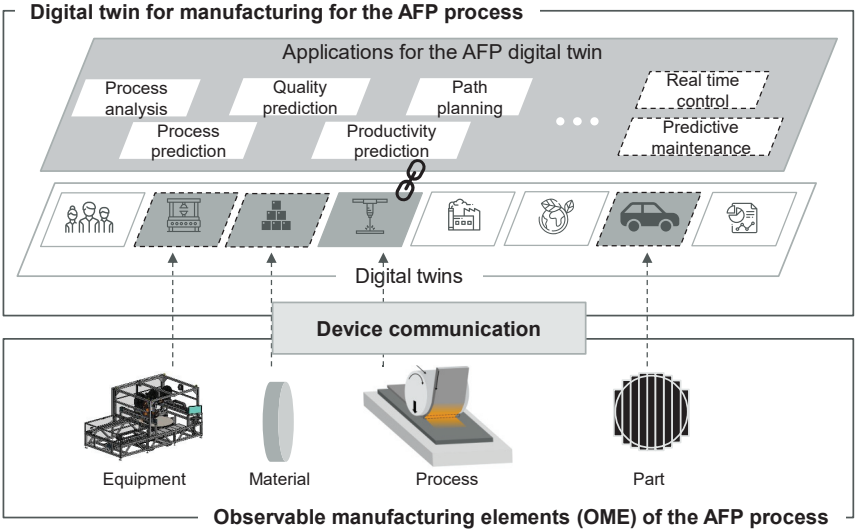

Figure 7.6: The AFP with in-situ consolidation in the ISO 23274 framework for digital twins

AFP mit in-situ Konsolidierung im Kontext des ISO 23274 Rahmenwerks für digitale Zwillinge

Path planning. The path planning is a result of the previous applications. Based on their results, layup strategies can be derived as shown in section 7.2.

Figure 7.6 embeds the AFP characteristics into the IoT framework as proposed in the ISO 23274 standard (see Figure 2.14) and highlights the AFP relevant digital twins. This profound examination of AFP equipment, material, and the final part are not scope of this thesis. The applications with the dashed lines are possible suggestions to extend the digital twin for manufacturing.

The functional view of the digital twin framework within the ISO 23274 standard is shown in Figure 7.7. The dark grey highlighted functional entities are implemented by the digital twin framework derived in this study. The ones with the dashed lines are suggested to be implemented as next steps to amplify the user benefit. The FEs in white are additional functionalities which can be investigated in future to allow a cross-domain digital twin, even across multiple systems.

Device communication entity. The data is collected and synchronized (pre-processed) by the *Beckhoff* soft-PLC of the PrePro2D® system and centrally stored on a NoSQL database (MongoDB). As mentioned before, this allows a smooth data preparation as all sensor and axes encoder data are tracked by one PLC. The data can be accessed within the network of the Fraunhofer IPT. To increase automation, the gained

knowledge by the digital twin could be fed back into the PrePro2D® system for process control. The technical basis for the controlling and actuation functional entity is provided by the PrePro2D® PLC environment. This allows to intervene the NC without manual interaction. An example would be a data-driven approach for changing the laser power during processing based on the knowledge of the digital twin.

Digital Twin Entity. This entity entails the derived models and the functionalities of the PrePro2D® system as derived in chapters 4 to 6. The setup allows a seamless data synchronization between the digital twin and the system due to the device communication entity. The digital representation and presentation of the model as well as the simulation currently run within Python scripts which are partially connected. Access can be controlled as the system access is accessible only for specific personnel. The maintenance FE is an interesting aspect which could be incorporated to improve the digital twin model by automated calibration methods (see later in section 7.3.3).

User Entity. The user entity is the interface between the digital twin and the user. First, the HMI of the PrePro2D® system allows the interaction with the process, the process setup as well as the choice of data recorded during the process. Second, the 3D interactive visualization as described in section 4.3.6 is created to enable a virtual visual inspection of the data. This should be within a CAx environment to simplify usage.

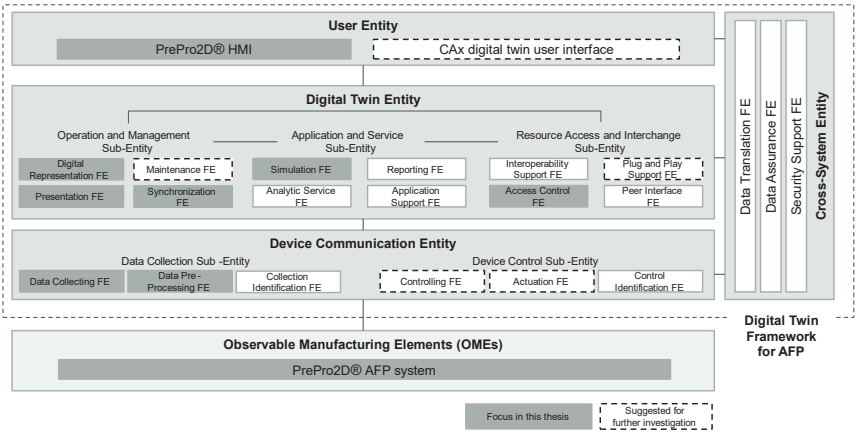

Figure 7.7: Functional entities of the AFP digital twin as created in this thesis (highlighted in dark grey) in adaption to ISO 23274

Funktionelle Einheiten des digitalen AFP-Zwillings, wie er in dieser Arbeit erstellt wurde (dunkelgrau hervorgehoben), in Anlehnung an ISO 23274

7.3.2 The process for a digital twin for AFP with in-situ consolidation

Ein Leitfaden für einen Digitalen Zwilling für AFP mit in-situ-Konsolidierung

To summarize the created digital twin of the AFP process with in-situ consolidation, Figure 7.8 illustrates the process for implementing the developed FEs *digital representation*, *presentation,* and *simulation*. As mentioned above, separate Python scripts are

programmed which are interconnected by the relevant variables. The presented flow chart according to DIN 66001 does not only give a step-by-step guide, but also an overview of necessary material, system and process conditions to enable a virtual description of the process within a digital twin. The execution of the calculations can either be done based on 1st or 2nd order values.

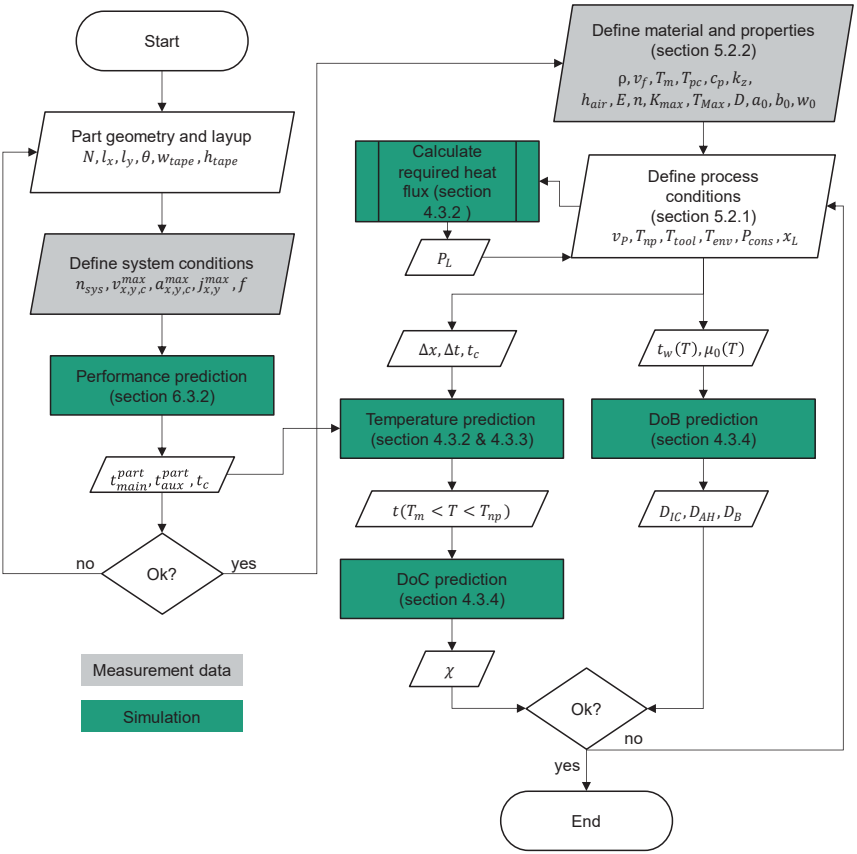

Figure 7.8: Process flow chart for the implementation of the digital twin process model for AFP with in-situ consolidation according to DIN 66001 [HERI84]

Prozessablaufplan zur Umsetzung des Digitalen Zwillings-Prozessmodells für AFP mit in-situ Konsolidierung nach DIN 66001 [HERI84]

7.3.3 Prediction robustness

Vorhersagegüte

The more a model entails information, the more it tries to predict, the more it is prone to error. As can be seen in the validation sections in chapter 5 and 6 many assumptions need to be made and properties derived. And even these are often based on models.

The sum of these abstractions leads to an increase of errors. The sensitivity study in section 5.3 quantitatively estimates the impact of specific properties on the prediction of the quality indicators, DoB and DoC. It especially reveals the sensitivity of the DoC model on the material properties. This shows that the accurate determination of the material´s crystallization behavior significantly influences the estimated values.

Since not only the models entail errors due to abstraction or missing experimental material values, many more errors during creating a digital twin occur. These sources of potential errors are listed and analyzed qualitatively in Table 7.4 including possible solutions for improvement.

Table 7.4: Error sources of the digital twin and possible solutions

Fehlerquellen des Digitalen Zwillings und Lösungsmöglichkeiten

	Error sources	**Possible solutions to decrease errors**

System conditions	– Thermal image camera:
	  – emission coefficient
	  – measurement error
	– Axes encoder
	  – measurement error
	– PLC cycle time
	– Different measurement frequencies
	– Laser spot: x_L
		Error detection and quantification by experimental analysis in different load cases

Material properties	– c_p, k_z, h_{air}, E, n, K_{max}, T_{Max}, D, a_0, b_0, w_0
	  – The material properties are derived from studies with similar materials, but not with the exact same one
	– ILSS values and microsections for DoB derivation
	  – Specimens do only partially represent laminate properties as they are cut out in specific areas and random samples are limited
		Material specific derivation of values by experiments
		
		Increase of random sample

Process properties	– Non-optimized process conditions	Process optimization based on a profound DoE
Temperature prediction	– Boundary conditions – Assumptions of the analytical model (see section 4.1.1)	Automated updating of boundary conditions
DoB prediction	– $t_w(T)$, $\mu_0(T)$ – Equations are derived from other studies which have used similar materials, but not the exact same one – Assumptions of the analytical model (see section 4.1.2 and 4.3.4), especially regarding isothermal conditions during LATW	Material specific derivation of relationships by experiments Data-driven models

DoC prediction	– Assumptions of the analytical model (see section 4.1.3 and 4.3.4) – DSC analysis with low cooling rate which are not apparent during AFP	Material specific derivation of relationships by experiments (e.g. Flash DSC) Data-driven models
Performance prediction	– Assumptions of the analytical model (see chapter 6.2)	Error detection and quantification by experimental analysis

Solutions to improve prediction quality are especially based on increasing the number of experiments. An additional potential lies in the data-driven calibration by using hybrid models, so called grey-box models. The idea behind is already introduced in section 2.4 and entails machine learning algorithms such as ANN. The successful implementation for other manufacturing technologies indicate that data-driven methods could also be feasible for updating assumptions of the analytical models of the AFP process. It would also be possible to allow automated updating of models during series production since a lot of data would be created. In summary, there exists a vast number of possibilities which can be examined to calibrate the models and their underlying assumptions.

7.4 Conclusion

Zusammenfassung

As a final demonstration of the created digital twin, this chapter gives an insight how the digital twin can be used for upscaling. Selected use cases are presented to understand the impact of upscaling on the overall manufacturing process. The study shows that cycle time can be reduced by 25 % by tripling the process speed. However, if this comes along with less consolidation quality, the overall productivity is even less. Additionally, the reduced cycle time gives the material less time to crystallize which results in a reduction of the DoC value. The examination of different layup sequences predicts minor influences on cycle time and quality indicators. However, also discrepancies are elaborated which need further examinations. The rising process speed comes along with less prediction accuracy, less process robustness as well as increased standard deviations of the ILSS values.

To cope with the number of assumptions and possible model errors, the second half of this chapter provides a methodology for improving the digital twin based on the experimental findings. The ISO 23274 framework helps to embed the created digital twin within a holistic digital twin for manufacturing. It reveals the additional efforts and infrastructure means which are necessary to exploit the full potential of the AFP digital twin.

In summary, this chapter answers the third research question by verifying the beneficial use of the digital twin to find novel manufacturing strategies. It also shows the impact of modeling inaccuracies as soon as one steps out of the comfort zone of the idealistic, analytical models.

8 Summary and outlook

Zusammenfassung und Ausblick

8.1 Summary

Zusammenfassung

As stated in section 2.3.1, the definition of the digital twin by CIRP is: ‘‘A digital twin is a digital representation of an active unique product (real device, object, machine, service, or intangible asset) or unique product-service system (a system consisting of a product and a related service) that comprises its selected characteristics, properties, conditions, and behaviors by means of models, information, and data within a single or even across multiple life cycle phases’’ [STAR20].

This thesis presents a digital twin for the AFP process with in-situ consolidation for the manufacturing of thermoplastic, tailored composites blanks out of unidirectional tape. It derives the need for digitization, analyzes existing models for implementation and evaluates the proposed ideas through an experimental investigation. This study proofs the necessity and feasibility of a digital twin for the AFP process with in-situ consolidation for upscaling the production.

The study is outlined according to a stepwise implementation. An introduction into the AFP process as well as into other manufacturing technologies reveal the need for data-driven approaches to minimize their processing complexities. Digital twins as a data-driven method of I4.0, the IIoT and the IoP is discussed as a solution to reduce these complexities and to thrive for a zero-waste manufacturing environment. For this reason, the feasibility of a digital twin for the AFP processing is analyzed and discussed in this thesis.

A closer look is taken at existing analytical models, which have been examined in the last three decades. The various ways of the heat transfer problem of the AFP process are presented and discussed. In addition, the investigation of quality indicators of the process, such as consolidation, crystallization, and residual stresses, disclose the applicability within a digital twin. To test a first feasibility and to understand the current obstacles, an experimental status-quo analysis of conventional AFP processing is conducted. The analysis of existing approaches points out two major outcomings. The existing models are generally feasible for a digital twin implementation. However, it also shows the idealistic conditions of these models. Many assumptions and boundary conditions hamper the part-oriented, realistic representation of the problem.

Based on these findings, a digital twin is designed, models are chosen, and boundary conditions are defined. To validate the proposed methodology, a detailed experimental investigation and evaluation is performed with the PrePro2D® manufacturing system. The PrePro2D® system is especially interesting, since its novel hardware and control settings are suitable for a digital twin implementation. All data are assessed within one system allowing a smooth and continuous data processing and transfer to a central

data storage. This is especially relevant for connecting the process data with its location on the part itself. Based on the experimental setup, the digital twin conducts the process prediction. Heat evolution and the impact on quality indicators determined by the DoB and DoC are forecasted for the specific part. To quantify the error between prediction and experiments, tests are performed, such as the ILSS for the estimation of the DoB. The digital twin also connects the process prediction with a performance calculation. It estimates the overall cycle time of the part and discloses the ratio between main and auxiliary times. This prediction is relevant to derive manufacturing strategies for upscaling and to decide whether this part is attractive or not attractive for series production as shown in the chapter 7.

The experimental investigation validates the simulation by the digital twin and shows that it allows the prediction of process conditions sufficiently. Nevertheless, it also demonstrates its sensitivity towards the many assumptions which need to be implemented on the way. Not only various abstracted models are incorporated within the digital twin, but also other additional underlying assumptions influence the prediction quality. An overview of potential errors during implementing a digital twin is given in Table 7.4. This overview demonstrates the necessity for further investigation into the validation and calibration of the digital twin to improve prediction quality.

To relate the work in this thesis to the digital twin definition by CIRP the following conclusion can be stated: A virtual representation of the unique, part-oriented AFP process with in-situ consolidation is developed which comprises of selected process characteristics, quality properties and system conditions by means of analytical models, system information and part data within a single life cycle phase.

8.2 A roadmap for the digital twin of the AFP process

Eine Roadmap für den Digitalen Zwilling des AFP Prozesses

At the end of each chapter, outlooks for future investigations have already been drafted and discussed. It is outlined, that the proposed digital twin could be an efficient tool for process optimization and for deriving manufacturing strategies, but it still needs some improvement to simplify its usage. The three major suggestions for the short-term are:

1. Improve the prediction quality of the digital twin by using data-driven, hybrid calibration techniques (see section 7.3.3);
2. Integrate the prediction data into a fast-computing, interactive, 3D visualization within a CAx environment (see section 4.3.6);
3. Justify the full potential of the digital twin for deriving manufacturing strategies by using it for more use cases.

In the long-term there are a variety of possibilities, which are possible with a functioning digital twin of the AFP process. Some are illustrated in the following:

Additional digital twins. To improve the prediction quality, the additional missing sub-digital twins can be implemented as shown in the ISO 23274 framework (see section 7.3.1): equipment, material, and part. Receiving more information from these digital

twins can be essential for processing. For example, information about the temperature within the machine can influence boundary conditions, such as T_∞.

Integrated data framework. Data-driven modeling methods require a central data infrastructure and database model. This is especially essential for enabling the information exchange between the relevant entities. In addition, the data recorded in experiments or even in series production of each processing and production step is valuable. This data can be used to learn and improve the digital twin.

Automated modeling. Assuming a functioning digital twin model with integrated data-driven calibration, it could be interesting to automate the modeling. With increasing data, more information about different processing characteristics and different settings is documented. This information could be used to automate boundary conditions dependent on new environments without manual interaction. For example, this could be the change of polymer matrix or the environmental temperature.

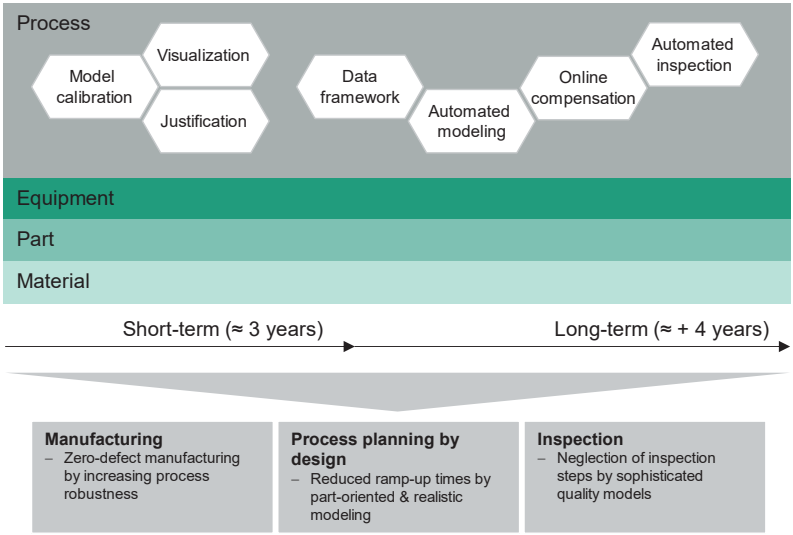

Figure 8.1: Suggested digital twin roadmap for the AFP of thermoplastic tape with in-situ consolidation

Vorschlag einer Roadmap für den Digitalen Zwilling des AFP Prozesses thermoplastischer Tapes mit in-situ Konsolidierung

Online compensation. If necessary and useful for the process, the results of the digital twin prediction could be fed back into the production system during the production. Similar to control theory, but with much more information, the online compensation mechanism could intervene processing and decide to change processing conditions.

Automated inspection. With a validated prediction quality, the digital twin could also be used for part inspection. By detecting anomalies based on the given data and correlate it with characteristic defects, a full quality prediction could be achieved. This could reduce time during the series production for part inspection.

These are some ideas which can be incorporated in a roadmap for the AFP digital twin as drafted in Figure 8.1. These could solve the challenge to gain a zero-defect manufacturing, reduce ramp-up times and experimental efforts, as well as to shorten process chains for increasing the attractiveness of lightweight components. This would not only reduce the anthropogenic CO_2 emissions through lightweight construction in mobility, but also through resource-efficient production. These means are essential to thrive for no net emissions of greenhouse gases by 2050 within the European Green Deal [EURO19].

Zusammenfassung und Ausblick

Wie bereits in Abschnitt 2.3.1 vorgestellt, lautet die Definition des digitalen Zwillings laut CIRP: „Ein digitaler Zwilling ist eine digitale Darstellung eines aktiven einzigartigen *Produkts* (reales Gerät, Objekt, Maschine, Dienstleistung oder immaterieller Vermögenswert) oder eines einzigartigen *Produkt-Dienstleistungssystems* (ein System, das aus einem Produkt und einer damit verbundenen Dienstleistung besteht*)*, das seine ausgewählten Merkmale, Eigenschaften, Bedingungen und Verhaltensweisen mittels Modellen, Informationen und Daten innerhalb einer einzigen oder sogar über mehrere Lebenszyklusphasen hinweg umfasst“ [STAR20].

In dieser Dissertation wird ein digitaler Zwilling für den AFP-Prozess mit in-situ Konsolidierung zur Herstellung thermoplastischer, belastungsoptimierter Laminate mit unidirektionalem Tape ausgearbeitet. Es wird die Notwendigkeit für die Digitalisierung abgeleitet und es werden bestehende Modelle zur Umsetzung analysiert sowie mögliche Ideen durch eine experimentelle Untersuchung evaluiert. Die Dissertation weist die Notwendigkeit und Machbarkeit eines digitalen Zwillings für den AFP-Prozess mit in-situ Konsolidierung zur Hochskalierung der Produktion nach.

Die Struktur der Arbeit ist anhand einer schrittweisen Implementierung aufgebaut. Eine Einführung in den AFP-Prozess sowie in andere Fertigungstechnologien in Kapitel 2 zeigt den Bedarf an datenbasierten Ansätzen, um deren Verarbeitungskomplexität zu minimieren. Digitale Zwillinge als datengetriebene Methode der I4.0, des IIoT und des IoP werden als Lösung diskutiert, um Komplexität zu reduzieren sowie auch abfallfreie Produktionsumgebung zu erreichen. Es wird ein genauerer Blick auf die bestehenden analytischen Modelle geworfen, die in den letzten drei Jahrzehnten erarbeitet wurden. Die verschiedenen Wege des Wärmeübertragungsproblems des AFP-Prozesses werden vorgestellt und diskutiert. Darüber hinaus zeigt die Analyse der Qualitätsindikatoren des Prozesses, wie Konsolidierung, Kristallisation und Eigenspannungen, die potenzielle Anwendbarkeit innerhalb eines digitalen Zwillings. Um eine erste Machbarkeit zu prüfen und die aktuellen Hindernisse zu verstehen, wird eine experimentelle Status-quo-Analyse der konventionellen AFP-Verarbeitung durchgeführt. Die Analyse der existierenden Ansätze zeigt zwei wesentliche Ergebnisse auf. Die bestehenden Modelle sind im Allgemeinen für eine Implementierung des digitalen Zwillings geeignet. Sie deutet aber auch auf die idealisierten Rahmenbedingungen dieser Modelle hin. Viele Annahmen und Randbedingungen erschweren die bauteilorientierte, realistische Darstellung des Problems.

Auf der Grundlage dieser Erkenntnisse wird in Kapitel 4 ein digitaler Zwilling entworfen, es werden Modelle ausgewählt und Randbedingungen festgelegt. Um die vorgeschlagene Methodik zu validieren, wird eine detaillierte experimentelle Untersuchung und Bewertung mit dem PrePro2D®-Fertigungssystem durchgeführt. Das PrePro2D®-System ist besonders interessant, da die neuartige Hardware und Steuerung für die Implementierung des digitalen Zwillings geeignet sind. Alle Daten werden innerhalb eines Systems ausgewertet, so dass eine reibungslose und kontinuierliche Datenverarbeitung und -übergabe an einen zentralen Datenspeicher möglich ist. Dies ist vor allem

für die Verknüpfung der Prozessdaten mit der Position am Bauteil selbst relevant. Auf der Grundlage des Versuchsaufbaus führt der digitale Zwilling die Prozessvorhersage durch. Die Wärmeentwicklung und die Auswirkungen auf die durch den Konsolidierungs- und Kristallisationsgrad ermittelte Qualitätsindikatoren werden für das jeweilige Bauteil prognostiziert. Um den Fehler zwischen Vorhersage und Experimenten zu quantifizieren, werden Tests durchgeführt, wie z.B. der ILSS für die Schätzung des Konsolidierungsgrades. Der digitale Zwilling verbindet auch die Prozessvorhersage mit einer Produktivitätsbewertung. Er schätzt die Gesamtzykluszeit des Bauteils ab und gibt das Verhältnis zwischen Haupt- und Nebenzeiten an. Diese Vorhersage ist relevant, um Fertigungsstrategien für die Hochskalierung abzuleiten und um zu entscheiden, ob dieses Bauteil für die Serienproduktion attraktiv ist oder nicht, wie im Kapitel 7 gezeigt wird.

Die experimentelle Untersuchung in Kapitel 5 validiert den erstellten digitalen Zwilling und zeigt, dass eine bauteilorientierte Vorhersage von Prozessbedingungen zureichend ermöglicht wird. Sie zeigt aber auch die Empfindlichkeit gegenüber den vielen Annahmen, die auf dem Weg dorthin getroffen werden müssen, um eine digitale Repräsentation zu erstellen. Nicht nur verschiedene abstrahierte Modelle fließen in den digitalen Zwilling ein, sondern auch weitere zugrundeliegende Annahmen beeinflussen die Vorhersagequalität. Eine Übersicht über mögliche Fehler bei der Implementierung eines digitalen Zwillings findet sich in Tabelle 7.4. Dieser Überblick zeigt, dass weitere Untersuchungen zur Validierung und Kalibrierung des digitalen Zwillings notwendig sind, um die Vorhersagequalität zu verbessern und realistischer zu gestalten.

Um die Ergebnisse dieser Dissertation mit der oben genannten Definition des digitalen Zwillings in Verbindung zu bringen, kann folgende Schlussfolgerung gezogen werden: Es wird eine virtuelle Repräsentation des einzigartigen, teilorientierten AFP-Prozesses mit in-situ Konsolidierung entwickelt, die ausgewählte Prozessmerkmale, Qualitätseigenschaften und Systembedingungen mittels analytischer Modelle, Systeminformationen und Teiledaten innerhalb einer einzigen Lebenszyklusphase umfasst.

Eine Roadmap für den Digitalen Zwilling des AFP Prozesses

Am Ende eines jeden Kapitels wurden bereits Ausblicke für zukünftige Untersuchungen genannt und diskutiert. Es wird dargelegt, dass der vorgeschlagene digitale Zwilling ein effizientes Werkzeug für die Prozessoptimierung und die Ableitung von Fertigungsstrategien sein könnte, aber noch einige Verbesserungen benötigt, um seine Anwendung zu vereinfachen. Die drei wichtigsten Vorschläge für die nahe Zukunft sind:

1. Verbesserung der Vorhersagequalität des digitalen Zwillings durch datengesteuerte, hybride Kalibrierungsverfahren (siehe Abschnitt 7.3.3);
2. Integration der Vorhersagedaten in eine schnell berechnende, interaktive 3D-Visualisierung innerhalb einer CAx-Umgebung (siehe Abschnitt 4.3.6);
3. das volle Potenzial des digitalen Zwillings für die Ableitung von Fertigungsstrategien zu rechtfertigen, indem er für weitere Anwendungsfälle genutzt wird.

Langfristig gibt es eine Vielzahl von Möglichkeiten, die mit einem funktionierenden digitalen Zwilling des AFP-Prozesses möglich sind. Einige sind im Folgenden dargestellt:

Zusätzliche digitale Zwillinge. Um die Vorhersagequalität zu verbessern, können die zusätzlichen fehlenden subdigitalen Zwillinge wie im Rahmen von ISO 23274 (siehe Abschnitt 7.3.1) implementiert werden: Ausrüstung, Material und Bauteil. Der Erhalt weiterer Informationen von diesen digitalen Zwillingen kann für die Materialverarbeitung wesentlich sein. Zum Beispiel können Informationen über die Temperatur innerhalb der Maschine die Randbedingungen beeinflussen, wie beispielsweise T_∞.

Integriertes Datenrahmenwerk. Datengesteuerte Modellierungsmethoden erfordern eine zentrale Dateninfrastruktur und ein Datenbankmodell. Dies ist besonders wichtig, um den Informationsaustausch zwischen den relevanten Einheiten zu ermöglichen. Darüber hinaus sind die in Experimenten oder sogar in der Serienproduktion aufgezeichneten Daten der einzelnen Verarbeitungs- und Produktionsschritte wertvoll. Diese Daten können genutzt werden, um aus dem digitalen Zwilling zu lernen und ihn zu verbessern.

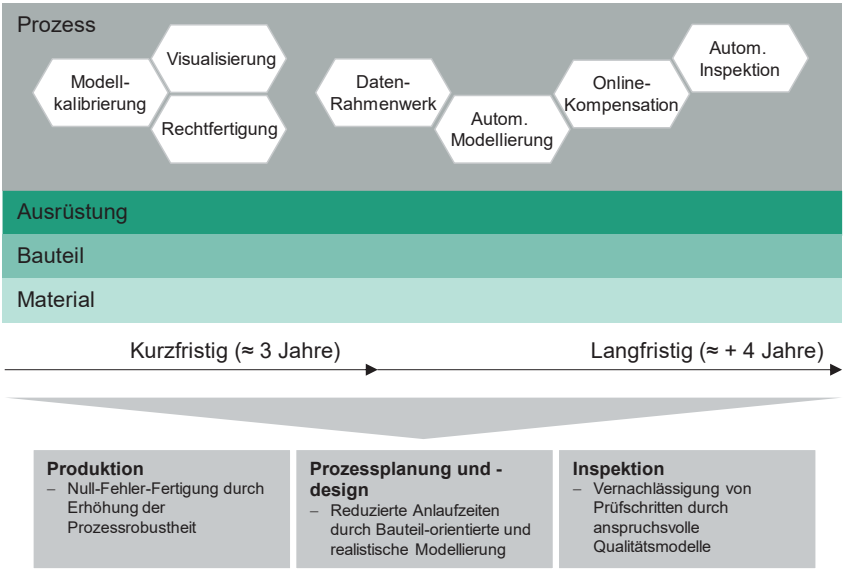

Abbildung 8.2: Vorschlag einer Roadmap für den Digitalen Zwilling des AFP Prozesses thermoplastischer Tapes mit in-situ Konsolidierung

Automatisierte Modellierung. Ausgehend von einem funktionierenden digitalen Zwillingsmodell mit integrierter datengesteuerter Kalibrierung könnte es interessant sein, die Modellierung zu automatisieren. Mit zunehmender Datenmenge werden mehr Informationen über verschiedene Verarbeitungseigenschaften und unterschiedliche Einstellungen dokumentiert. Diese Informationen könnten genutzt werden, um Randbe-

dingungen in Abhängigkeit von neuen Umgebungen ohne manuelle Interaktion zu automatisieren. Dies wäre zum Beispiel die Änderung der Polymermatrix oder der Umgebungstemperatur.

Online-Kompensation. Falls erforderlich und für den Prozess nützlich, könnten die Ergebnisse der Vorhersage des digitalen Zwillings während der Produktion in das Produktionssystem zurückgespeist werden. Ähnlich wie bei der Regelungstechnik, aber mit weitaus mehr Informationen, könnte der Online-Kompensationsmechanismus in die Verarbeitung eingreifen und entscheiden, wie die Verarbeitungsbedingungen verändert werden müssen.

Automatisierte Prüfung. Mit einer validierten Vorhersagequalität könnte der digitale Zwilling auch für die Teileinspektion verwendet werden. Durch die Erkennung von Anomalien auf der Grundlage der gegebenen Daten und deren Korrelation mit charakteristischen Fehlern wäre eine vollständige Qualitätsvorhersage möglich. Dies könnte den Zeitaufwand für die Teileinspektion in der Serienproduktion reduzieren.

Dies sind nur einige Ideen, die in eine Roadmap für den digitalen Zwilling des AFP Prozesses aufgenommen werden können, wie sie auch in Abbildung 8-2 dargestellt ist. Diese könnten die Herausforderung lösen, eine fehlerfreie Produktion zu erreichen, Anlaufzeiten und Versuchsaufwände zu reduzieren sowie Prozessketten zu verkürzen, um die Attraktivität von Leichtbaukomponenten zu erhöhen. Dies würde nicht nur die anthropogenen CO_2-Emissionen durch Leichtbau in der Mobilität reduzieren, sondern auch durch eine ressourcenschonende Produktion. Diese Maßnahmen sind notwendig, um im Rahmen des europäischen Green Deals bis 2050 keine Netto-Treibhausgasemissionen mehr zu erreichen [EURO19].

9 References

Literaturverzeichnis

[ABOU13] Aboudi, J.; Arnold, S.; Bednarcyk, B.: Micromechanics of composite materials. A generalized multiscale analysis approach. Amsterdam, Waltham, MA: Butterworth-Heinemann, 2013

[ACAT13] Acatech (Hrsg.): Recommendations for implementing the strategic initiative INDUSTRIE 4.0. Final report of the Industrie 4.0 Working Group. Frankfurt/Main, 2013

[ALTI17] Altintas, Y.; Aslan, D.: Integration of virtual and on-line machining process control and monitoring. In: CIRP Annals. Vol. 66, 20171, p. 349–352

[AVRA39] Avrami, M.: Kinetics of Phase Change. I General Theory. In: The Journal of Chemical Physics. Vol. 7, 193912, p. 1103–1112

[BARA11] Barasinski, A.; Leygue, A.; Soccard, E.; Poitou, A.; Chinesta, F.; Chastel, Y.; El Mansori, M.: An Improvement in Thermal Modelling of Automated Tape Placement Process. In: AIP Conference Proceedings. Vol. 1315, 20111, p. 185–190

[BARA17] Baran, I.; Cinar, K.; Ersoy, N.; Akkerman, R.; Hattel, J.: A Review on the Mechanical Modeling of Composite Manufacturing Processes. In: Archives of computational methods in engineering : state of the art reviews. Vol. 24, 20172, p. 365–395

[BAUE16] Bauernhansl, T.; Krüger, J.; Reinhart, G.; Schuh, G.: WGP-Standpunkt Industrie 4.0. Darmstadt: Wissenschaftliche gesellschaft für produktionstechnik WGP e.V., 2016

[BAUM19] Baumann, H.; Janssen, H.: Research Project "LightMat Battery Housing". URL: https://www.ipt.fraunhofer.de/en/projects/lightmat-battery-housing-.html [Status: 18.07.2022]

[BAUM21] Baumann, H.; Schwane, M.; Schulz, M.; Janssen, H.; Brecher, C.: Thermoplastic Laser Assisted Tape Placement Development for Processing a Novel Carbon Fiber Reinforced Polyphtalamide Tape. In: Proceedings of the SAMPE Europe Conference. Baden/Zurich, September 2021. SAMPE Europe, 2021

[BEJA03] Bejan, A.; Kraus, A.: Heat transfer handbook. New York: J. Wiley, 2003

[BOHL06] Bohlin, T.: Practical Grey-box Process Identification. Theory and Applications. London: Springer, 2006

[BOIK01] Boiko, Y.; Guerin, G.; Marikhin V.A.; Prud'homme, R.: Healing of interfaces of amorphous and semi-crystalline poly(ethylene terephthalate) in the vicinity of the glass transition temperature. In: Polymer. Vol. 42, 2001, p. 8695–8702

[BRAS21] Brasington, A.; Sacco, C.; Halbritter, J.; Wehbe, R.; Harik, R.: Automated fiber placement: A review of history, current technologies, and future paths forward. In: Composites Part C: Open Access. Vol. 6, 2021, p. 1–18

[BRAS22] Brasington, A.; Smith, C.; Halbritter, J.; Wehbe, R.; Harik, R.: Surrogate based methods for rapid starting point optimization in automated fiber placement. In: Proceedings of the SAMPE Conference. Charlotte, NC, May 2022. Society for the Advancement of Material and Process, 2022, p. 305–319

[BREC11] Brecher, C.: Integrative Produktionstechnik für Hochlohnländer. Berlin, Heidelberg: Springer, 2011

[BREC15] Brecher, C.; Werner, D.; Emonts, M.: "Multi-Material-Head". One tool for 3 technologies. Laser-assisted thermoplast-tape placement, thermoset-prepreg-placement and dry-fiber-placement. In: Proceedings of the 20th International Conference on Composite Materials. Copenhagen, July 2015. ICCM, 2015, p. 1–8

[BREC21] Brecher, C.; Weck, M.: Werkzeugmaschinen Fertigungssysteme 3. Berlin, Heidelberg: Springer Berlin Heidelberg, 2021

[BRÜN17] Brüning, J.; Denkena, B.; Dittrich, M.-A.; Hocke, T.: Machine Learning Approach for Optimization of Automated Fiber Placement Processes. In: Procedia CIRP. Vol. 66, 2017, p. 74–78

[BRYS22] Brysch, M.; Bahar, M.; Hohensee, H.; Sinapius, M.: Single system for online monitoring and inspection of automated fiber placement with object segmentation by artificial neural networks. In: Journal of Intelligent Manufacturing. 2022, p. 1–13

[BUND21] Bundesministerium für Bildung und Forschung: Digitale Wirtschaft und Gesellschaft. Industrie 4.0. URL: https://www.bmbf.de/de/zukunftsprojekt-industrie-4-0-848.html [Status: 12.02.2021]

[CAI17] Cai, Y.; Starly, B.; Cohen, P.; Lee, Y.-S.: Sensor Data and Information Fusion to Construct Digital-twins Virtual Machine Tools for Cyber-physical Manufacturing. In: Procedia Manufacturing. Vol. 10, 2017, p. 1031–1042

[CHAP90] Chapman, T.; Gillespie, J.; Pipes, R.; Manson, J.-A.; Seferis, J.: Prediction of Process-Induced Residual Stresses in Thermoplastic Composites. In: Journal of Composite Materials. Vol. 24, 19906, p. 616–643

[CHIN14] Chinesta, F.; Leygue, A.; Bognet, B.; Ghnatios, C.; Poulhaon, F.; Bordeu, F.; Barasinski, A.; Poitou, A.; Chatel, S.; Maison-Le-Poec, S.: First steps towards an advanced simulation of composites manufacturing by automated tape placement. In: International Journal of Material Forming. Vol. 7, 20141, p. 81–92

[CHIN20] Chinesta, F.; Cueto, E.; Abisset-Chavanne, E.; Duval, J.; Khaldi, F.: Virtual, Digital and Hybrid Twins: A New Paradigm in Data-Based Engineering and Engineered Data. In: Archives of Computational Methods in Engineering. Vol. 27, 20201, p. 105–134

[DARA85] Dara, P.; Loos, A.: Thermoplastic matrix composite processing model. In: NASA. Vol. 1, 198526

[DEDI17] Dedieu, C.; Barasinski, A.; Chinesta, F.; Dupillier, J.-M.: About the origins of residual stresses in in situ consolidated thermoplastic composite rings. In: International Journal of Material Forming. Vol. 10, 20175, p. 779–792

[DENO18] Denos, B.; Sommer, D.; Favaloro, A.; Pipes, R.; Avery, W.: Fiber orientation measurement from mesoscale CT scans of prepreg platelet molded composites. In: Composites Part A: Applied Science and Manufacturing. Vol. 114, 2018, p. 241–249

[DIF17] Di Francesco, M.; Veldenz, L.; Dell'Anno, G.; Potter, K.: Heater power control for multi-material, variable speed Automated Fibre Placement. In: Composites Part A: Applied Science and Manufacturing. Vol. 101, 2017, p. 408–421

[DIN14] DIN EN ISO 62264-1:2014-07 (2014). Integration von Unternehmensführungs- und Leitsystemen

[DIN97] DIN EN ISO 14130 : 1998-02 (1997). Bestimmung der scheinbaren interlaminaren Scherfestigkeit nach dem Dreipunktverfahren mit kurzem Balken

[DREH] Dreher, P.; Chadwick, A.; Nowothny, S.: Optimization of In-Situ Thermoplastic Automated Fiber Placement Process Parameters Through DOE. In: Proceedings of the SAMPE Europe Conference. Nantes, September 2019. SAMPE Europe, 2019

[DSM19] DSM (2019). Property Data Akulon PA6-HC10 UD. PA6-CF50

[DSM22] DSM (2022). Property Data Akulon K122/F. PA6

[ECHS20] Echsler Minguillon, F.: Prädiktiv-reaktives Scheduling zur Steigerung der Robustheit in der Matrix-Produktion. Diss. Karlsruher Institut für Technologie (KIT), 2020

[EICK13] Eickenbusch, H.; Krauss, O.: Kurzanalyse Nr. 3: Kohlenstofffaserverstärkte Kunststoffe im Fahrzeugbau - Ressourceneffizienz und Technologien. In: VDI ZRE Publikationen. 2013, p. 1–54

[ENGE18] Engel, G.; Greiner, T.; Seifert, S.: Ontology-Assisted Engineering of Cyber–Physical Production Systems in the Field of Process Technology. In: IEEE Transactions on Industrial Informatics. Vol. 14, 20186, p. 2792–2802

[EURO19] European Commission: The European Green Deal. URL: https://eur-lex.europa.eu/legal-content/EN/TXT/?qid=1576150542719&uri=COM%3A2019%3A640%3AFIN [Status: 25.07.2022]

[FAGH10] Faghri, A.; Zhang, Y.; Howell, J.: Advanced heat and mass transfer. Columbia, MO: Global Digital Press, 2010

[FELD19] Felder, S.; Holthusen, H.; Hesseler, S.; Pohlkemper, F.; Simon, J.; Gries, T.; Reese, S.: A finite strain thermo-mechanically coupled material model for semi-crystalline polymers. In: XV International Conference on Computational Plasticity. Fundamentals and Applications. 2019, p. 1–12

[FISH20] Fisher, O.; Watson, N.; Escrig, J.; Witt, R.; Porcu, L.; Bacon, D.; Rigley, M.; Gomes, R.: Considerations, challenges and opportunities when developing data-driven models for process manufacturing systems. In: Computers & Chemical Engineering. Vol. 140, 2020, p. 1–14

[FLEI18] Fleischer, J.; Teti, R.; Lanza, G.; Mativenga, P.; Möhring, H.-C.; Caggiano, A.: Composite materials parts manufacturing. In: CIRP Annals. Vol. 67, 20182, p. 603–626

[GANS21] Ganser, P.; Venek, T.; Rudel, V.; Bergs, T.: A digital twin framework for the machining domain. In: MM Science Journal. Vol. 2021, 20215, p. 5134–5141

[GAO14] Gao, R.; Tang, X.; Gordon, G.; Kazmer, D.: Online product quality monitoring through in-process measurement. In: CIRP Annals. Vol. 63, 20141, p. 493–496

[GENN71] Gennes, P. de: Reptation of a Polymer Chain in the Presence of Fixed Obstacles. In: The Journal of Chemical Physics. Vol. 55, 19712, p. 572–579

[GRIE17] Grieves, M.; Vickers, J.: Digital Twin: Mitigating Unpredictable, Undesirable Emergent Behavior in Complex Systems. In: Kahlen, F.-J.; Flumerfelt, S.; Alves, A.: New Findings and Approaches. Cham: Springer, 2017, p. 85–113

[GROU12] Grouve, W.: Weld strength of laser-assisted tape-placed thermoplastic composites. Diss. University of Twente, 2012

[GROV88] Grove, S.: Thermal modelling of tape laying with continuous carbon fibre-reinforced thermoplastic. In: Composites. Vol. 19, 19885, p. 367–375

[GRUB93] Gruber, T.: A translation approach to portable ontology specifications. In: Knowledge Acquisition. Vol. 5, 19932, p. 199–220

[HENN17] Henning, F.; Karcher, M.; Kärger, L.; Müller, T.: Funktionsintegrierter Leichtbau. In: Neugebauer, R.: Berlin, Heidelberg: Springer Berlin Heidelberg, 2017, p. 127–143

[HERI84] Hering, E.: Programmablaufplan nach DIN 66001. In: Hering, E.: Software-Engineering. Wiesbaden: Vieweg+Teubner Verlag, 1984, p. 26–34

[HOSS20] Hosseini, S.; Schäkel, M.; Baran, I.; Janssen, H.; van Drongelen, M.; Akkerman, R.: Non-uniform crystallinity and temperature distribution during adjacent laser-assisted tape winding process of carbon/PA12 pipes. In: The International Journal of Advanced Manufacturing Technology. Vol. 111, 202011-12, p. 3063–3082

[HÜRK20] Hürkamp, A.; Gellrich, S.; Ossowski, T.; Beuscher, J.; Thiede, S.; Herrmann, C.; Dröder, K.: Combining Simulation and Machine Learning as Digital Twin for the Manufacturing of Overmolded Thermoplastic Composites. In: Journal of Manufacturing and Materials Processing. Vol. 92, 20204, p. 1–20

[ILLE78] Illers, K.-H.: Polymorphie, kristallinität und schmelzwärme von poly(ε-caprolactam), 2. Kalorimetrische untersuchungen. In: Die Makromolekulare Chemie. Vol. 179, 19782, p. 497–507

[INCR07] Incropera, F.; Dewitt, D.; Bergman, T.; Lavine, A.: Fundamentals of heat and mass transfer. Sixth edition. Hoboken, NJ: John Wiley, 2007

[ISO21] ISO ISO 23247-1-4:2021 (Oktober 2021). Automation systems and integration - Digital twin framework for manufacturing. Part 1-4

[JANS20] Janssen, H.: Additive Prozesskette zur Herstellung von thermoplastischen Faserverbund-Hybridbauteilen. Diss. RWTH Aachen, 2020

[JÄRV19] Järvenpää, E.; Siltala, N.; Hylli, O.; Lanz, M.: The development of an ontology for describing the capabilities of manufacturing resources. In: Journal of Intelligent Manufacturing. Vol. 30, 20192, p. 959–978

[JEON01] Jeong, K.-Y.; Philipps, D.: Operational efficiency and effectiveness measurement. In: International Journal of Operations & Production Management. Vol. 21, 200111, p. 1404–1416

[JERO88] Jeronimidis, G.; Parkyn, A.: Residual Stresses in Carbon Fibre-Thermoplastic Matrix Laminates. In: Journal of Composite Materials. Vol. 22, 19885, p. 401–415

[JESC16] Jeschke, S.: Industrial internet of things. Cybermanufacturing Systems. Cham: Springer International Publishing, 2016

[JONE20] Jones, D.; Snider, C.; Nassehi, A.; Yon, J.; Hicks, B.: Characterising the Digital Twin: A systematic literature review. In: CIRP Journal of Manufacturing Science and Technology. Vol. 29, 2020, p. 36–52

[KERM15] Kermer-Meyer, A.: Formhaltige und komplexe Laminatstrukturen in Thermoplast-Tapelegeverfahren. Diss. RWTH Aachen, 2015

[KHAN10] Khan, M.; Mitschang, P.; Schledjewski, R.: Identification of some optimal parameters to achieve higher laminate quality through tape placement process. In: Advances in Polymer Technology. Vol. 29, 20102, p. 98–111

[KHAN13] Khan, M.; Mitschang, P.; Schledjewski, R.: Parametric study on processing parameters and resulting part quality through thermoplastic tape placement process. In: Journal of Composite Materials. Vol. 47, 20134, p. 485–499

[KÖLZ08] Kölzer, P.: Temperaturerfassungssystem und Prozessregelung des laserunterstützten Wickelns und Tapelegens von endlos faserverstärkten thermoplastischen Verbundkunststoffen. Diss. RWTH Aachen, 2008

[KÖNI18] Königs, M.; Brecher, C.: Process-parallel virtual quality evaluation for metal cutting in series production. In: Procedia Manufacturing. Vol. 26, 2018, p. 1087–1093

[KRAU03] Krause, W.; Henning, F.; Tröster, S.; Geiger, O.; Eyerer, P.: LFT-D — A Process Technology for Large Scale Production of Fiber Reinforced Thermoplastic Components. In: Journal of Thermoplastic Composite Materials. Vol. 16, 20034, p. 289–302

[KRES14] Kress, G.: Mechanics of Composite Materials. Lecture notes. Zurich, 2014

[KRIT18] Kritzinger, W.; Karner, M.; Traar, G.; Henjes, J.; Sihn, W.: Digital Twin in manufacturing: A categorical literature review and classification. In: IFAC PapersOnLine. Vol. 51, 201811, p. 1016–1022

[KROP17] Kropka, M.; Muehlbacher, M.; Neumeyer, T.; Altstaedt, V.: From UD-tape to Final Part – A Comprehensive Approach Towards Thermoplastic Composites. In: Procedia CIRP. Vol. 66, 2017, p. 96–100

[KUGE17] Kugele, D.; Dörr, D.; Wittemann, F.; Hangs, B.; Rausch, J.; Kärger, L.; Henning, F.: Modeling of the non-isothermal crystallization kinetics of polyamide 6 composites during thermoforming. In: AIP Conference Proceedings 1896. Vol. 030005, 2017, p. 1–6

[KUKL22] Kukla, C.: Prozesstemperaturregelung in der laserunterstützten Verarbeitung von faserverstärkten thermoplastischen Verbundkunststoffen. Diss. 1. Auflage. Aachen: Apprimus Verlag, 2022

[KUZN18] Kuznetsov, A.; Koriath, H.-J.; Kalyashina, A.; Langer, T.: Equivalence assessment method for the resource efficiency of equipment, technologies and production systems. In: Procedia Manufacturing. Vol. 21, 20185, p. 525–532

[LATR03] Latrille, M.: Prozessanalyse und -simulation von Verarbeitungsverfahren für faserverstärkte thermoplastische Bändchenhalbzeuge. Diss. Universität Kaiserslautern, 2003

[LEE87] Lee, W.; Springer, G.: A Model of the Manufacturing Process of Thermoplastic Matrix Composites. In: Journal of Composite Materials. Vol. 21, 198711, p. 1017–1055

[LEVY14] Levy, A.; Heider, D.; Tierney, J.; Gillespie, J.: Inter-layer thermal contact resistance evolution with the degree of intimate contact in the processing of thermoplastic composite laminates. In: Journal of Composite Materials. Vol. 48, 20144, p. 491–503

[LI97] Li, M.; Wu, J.; Loos, A.; Morton, J.: A Plane-Strain Finite Element Model for Process-Induced Residual Stresses in a Graphite/PEEK Composite. In: Journal of Composite Materials. Vol. 31, 19973, p. 212–243

[LIEB23] Liebenberg, M.; Jarke, M.: Information systems engineering with Digital Shadows: Concept and use cases in the Internet of Production. In: Information Systems. Vol. 114, 2023, p. 1–16

[LINK18] Link, T.; Baumgärtner, S.; Dörr, D.; Hohberg, M.; Henning, F.: Hybrid Thermoplastic Composites for Automotive Applications - Development and Manufacture of a Lightweight Rear Floor Structure in Multi-Material Design. In: Proceedings of the 18th European Conference on Composite Materials ECCM 18. 2018, p. 1–8

[LIU18] Liu, X.; Yu, W.: Multiscale Modeling of Viscoelastic Behaviors of Textile Composites Using Mechanics of Structure Genome. In: Proceedings of the 2018 AIAA/ASCE/AHS/ASC Structures, Structural Dynamics, and Materials Conference. Kissimmee, FL, January 2018. Reston, VA: 2018

[LUKA11] Lukaszewicz, D.: Optimisation of high-speed automated layup of thermoset carbon-fibre preimpregnates. Diss. University of Bristol, 2011

[LUKA12] Lukaszewicz, D.; Ward, C.; Potter, K.: The engineering aspects of automated prepreg layup: History, present and future. In: Composites Part B: Engineering. Vol. 43, 20123, p. 997–1009

[MAIN18] Mainati, P.: Hybrid thermoplastics give load floor impact strength. In: Composites World. 2018, 44-47

[MANT92a] Mantell, S.; Wang, Q.; Springer, G.: Processing Thermoplastic Composites in a Press and by Tape Laying—Experimental Results. In: Journal of Composite Materials. Vol. 26, 199216

[MANT92b] Mantell, S.; Springer, G.: Manufacturing Process Models for Thermoplastic Composites. In: Journal of Composite Materials. Vol. 26, 199216, p. 2348–2377

[MARZ15] Marz, N.; Warren, J.: Big data. Principles and best practices of scalable real-time data systems. Shelter Island, NY: Manning, 2015

[MAY08] May, C.; Koch, A.: Overall Equipment_Effectiveness (OEE)Werkzeug zur Produktivitätssteigerung. In: Zeitschrift der Unternehmensberatung ZUb. Vol. 6, 2008, p. 245–250

[MEIS21] Meister, S.; Wermes, M.; Stüve, J.; Groves, R.: Review of image segmentation techniques for layup defect detection in the Automated Fiber Placement process. In: Journal of Intelligent Manufacturing. Vol. 32, 20218, p. 2099–2119

[MEYE18] Meyes, R.; Tercan, H.; Thiele, T.; Krämer, A.; Heinisch, J.; Liebenberg, M.; Hirt, G.; Hopmann, C.; Lakemeyer, G.; Meisen, T.; Jeschke, S.: Interdisciplinary Data Driven Production Process Analysis for the Internet of Production. In: Procedia Manufacturing. Vol. 26, 2018, p. 1065–1076

[MOGE21] Moges, T.; Yang, Z.; Jones, K.; Feng, S.; Witherell, P.; Lu, Y.: Hybrid Modeling Approach for Melt Pool Prediction in Laser Powder Bed Fusion Additive Manufacturing. In: Journal of Computing and Information Science in Engineering. 2021, p. 1–46

[MÜLL07] Müller, T.; Al-Sheyyab, A.; Kühnert, I.; Schmachtenberg, E.: Grossserientauglich. Verfahren für die wirtschaftliche Herstellung komplexer Hochleistungsverbunde. In: Plastverarbeiter. 2007, p. 30–32

[NAKA72] Nakamura, K.; Watanabe, T.; Katayama, K.; Amano, T.: Some aspects of nonisothermal crystallization of polymers. I. Relationship between crystallization temperature, crystallinity, and cooling conditions. In: Journal of Applied Polymer Science. Vol. 16, 19725, p. 1077–1091

[NAKA73] Nakamura, K.; Katayama, K.; Amano, T.: Some aspects of nonisothermal crystallization of polymers. II. Consideration of the isokinetic condition. In: Journal of Applied Polymer Science. Vol. 17, 1973, p. 1031–1041

[NEIT14] Neitzel, M.; Mitschang, P.; Breuer, U. (Hrsg.): Handbuch Verbundwerkstoffe. Werkstoffe, Verarbeitung, Anwendung. 2. Auflage. München: Hanser, 2014

[ORTH17] Orth, T., Weimer, C.; Krahl, M.; Modler, N.: A review of radiative heating in automated layup and its modeling. In: Journal of Plastics Technology. Vol. 13, 2017, 92-125

[PENN19] Pennekamp, J.; Glebke, R.; Henze, M.; Meisen, T.; Quix, C.; Hai, R.; Gleim, L.; Niemietz, P.; Rudack, M.; Knape, S.; Epple, A.; Trauth, D.; Vroomen, U.; Bergs, T.; Brecher, C.; Buhrig-Polaczek, A.; Jarke, M.; Wehrle, K.: Towards an Infrastructure Enabling the Internet of Production. In: 2019 IEEE International Conference on Industrial Cyber Physical Systems (ICPS). 2019, p. 31–37

[PERR22] Perrejean, E. (Hrsg.): Current trends in the global composites industry 2021-2026. Paris: JEC Group, 2022

[PITC97] Pitchumani, R.; Gillespie, J.; Lamontia, M.: Design and Optimization of a Thermoplastic Tow-Placement Process with In-Situ Consolidation. In: Journal of Composite Materials. Vol. 31, 19973, 244-275

[POPR05] Poprawe, R.: Lasertechnik für die Fertigung. Grundlagen, Perspektiven und Beispiele für den innovativen Ingenieur. Berlin: Springer, 2005

[PUTZ17] Putz, M.; Klocke, F.: Fraunhofer Leitprojekt E3-Produktion. In: Neugebauer, R.: Berlin, Heidelberg: Springer Berlin Heidelberg, 2017, p. 145–174

[QUAR18] Quaranta, G.; Abisset-Chavanne, E.; Chinesta, F.; Duval, J.-L.: A cyber physical system approach for composite part: From smart manufacturing to predictive maintenance. In: AIP Conference Proceedings 1960. Vol. 020025, 2018, p. 1–7

[ROSE15] Rosen, R.; Wichert, G. von; Lo, G.; Bettenhausen, K.: About The Importance of Autonomy and Digital Twins for the Future of Manufacturing. In: IFAC-PapersOnLine. Vol. 48, 20153, p. 567–572

[ROUS19] Rousseau, G.; Wehbe, R.; Halbritter, J.; Harik, R.: Automated Fiber Placement Path Planning: A state-of-the-art review. In: Computer-Aided Design and Applications. Vol. 16, 20192, p. 172–203

[SACC20] Sacco, C.; Baz Radwan, A.; Anderson, A.; Harik, R.; Gregory, E.: Machine learning in composites manufacturing: A case study of Automated Fiber Placement inspection. In: Composite Structures. Vol. 250, 2020, p. 1–14

[SALA97] Sala, G.; Cutolo, D.: The pultrusion of powder-impregnated thermoplastic composites. In: Composites Part A: Applied Science and Manufacturing. Vol. 28, 19977, p. 637–646

[SARR95] Sarrazin, H.; Springer, G.: Thermochemical and Mechanical Aspects of Composite Tape Laying. In: Journal of Composite Materials. Vol. 29, 199514, p. 1908–1943

[SCHA17] Schaefer, P.; Gierszewski, D.; Kollmannsberger, A.; Zaremba, S.; Drechsler, K.: Analysis and improved process response prediction of laser- assisted automated tape placement with PA-6/carbon tapes using Design of Experiments and numerical simulations. In: Composites Part A: Applied Science and Manufacturing. Vol. 96, 2017, p. 137–146

[SCHÄ17] Schäfer, P.: Consolidation of carbon fiber reinforced Polyamide 6 tapes using laser-assisted tape placement. Diss. Technische Universität München, 2017

[SCHÄ18] Schäkel, M.; McNab, J.; Dodds, N.; Peters, T.; Janssen, H.; Brecher, C.: Data collection and analysis for the creation of a digital shadow during the production of thermoplastic composite layers in unbonded flexible

pipes. In: Proceedings of the ASME 2018 37th International Conference on Ocean, Offshore and Arctic Engineering. 2018, p. 1–9

[SCHU16] Schuh, G.; Walendzik, P.; Luckert, M.; Birkmeier, M.; Weber, A.; Blum, M.: Keine Industrie 4.0 ohne digitalen Schatten. Wie Unternehmen die notwendige Datenbasis schaffen. In: ZWF Zeitschrift für wirtschaftlichen Fabrikbetrieb. Vol. 111, 201611, p. 745–748

[SCHU17] Schuh, G.; Stich, V.; Basse, F.; Franzkoch, B.; Harzenetter, F.; Luckert, M.; Prote, J.-P.; Reschke, J.; Schmitz, S.; Tücks, G.; Weißkopf, J.: Change Request im Produktionsbetrieb. In: Brecher, C.; Klocke, F.; Schmitt, R.; Schuh, G.: AWK Aachener Werkzeugmaschinen-Kolloquium 2017. Aachen: Apprimus, 2017, p. 109–131

[SCHU18] Schulz, M.; Buschhoff, C.; Janssen, H.; Brecher, C.: The influence of the tape placement process on part characteristics based on different UD-tape qualities. In: Proceedings of the 18th European Conference on Composite Materials ECCM 18. 2018, p. 1–8

[SCHU19a] Schulz, M.; Janssen, H.; Brecher, C.: A Digital Shadow for the Infrared-based Tape Laying Process of Tailored Blanks out of Thermoplastic Unidirectional Tape. In: Procedia CIRP. Vol. 85, 2019, p. 224–229

[SCHU19b] Schulz, M.; Janssen, H.; Brecher, C.: Adaptive, connected production of hybrid thermoplastic prototypes. In: Reinforced Plastics. Vol. 63, 20191, p. 26–28

[SCHU20] Schulz, M.; Janssen, H.; Brecher, C.; Evertz, A.: Online Analysis of Geometrical Inaccuracies During the in-situ Automated Fiber Placement of Tailored Composite Blanks out of Thermoplastic Tape. In: Proceedings of the 5th International Conference & Exhibition on Thermoplastic Composites. Bremen, October 2020. ITHEC, 2020

[SCHU21] Schulz, M.; Survila, E.; Janssen, H.; Brecher, C.: A Digital Twin for Estimating Process Quality during Automated Fiber Placement of Thermoplastic Composites. In: Proceedings of the SAMPE Europe Conference. Baden/Zurich, September 2021. SAMPE Europe, 2021

[SCHU22] Schulz, M.; Baumann, H.; Janssen, H.; Brecher, C.: Digital Twin Validation for the in-situ Automated Fiber Placement Process of Thermoplastic Composites. In: Proceedings of the SAMPE Conference. Charlotte, NC, May 2022. Society for the Advancement of Material and Process, 2022

[SEW10] SEW EURODRIVE GmbH & Co KG: Handbuch - MultiMotion. URL: https://download.sew-eurodrive.com/download/pdf/16970802.pdf [Status: 24.07.2022]

[SHAF12] Shafto, M.; Conroy, M.; Doyle, R.; Glaessgen, E.; Kemp, C.; LeMoigne, J.; Wang, L.: Modeling, simulation, information technology & processing roadmap. In: . 2012, p. 1–33

[SMIT85] Smith, G.: Numerical Solution of partial differential equations. Finite difference methods. Third edition. Oxford: Clarendon Pr, 1985

[SONM02a] Sonmez, F.; Hahn, H.; Akbulut, M.: Analysis of Process-Induced Residual Stresses in Tape Placement. In: Journal of Thermoplastic Composite Materials. Vol. 15, 2002, p. 525–544

[SONM02b] Sonmez, F.; Eyol, E.: Optimal post-manufacturing cooling paths for thermoplastic composites. In: Composites Part A: Applied Science and Manufacturing. Vol. 33, 2002, p. 301–314

[SONM97a] Sonmez, F.; Hahn, H.: Modeling of Heat Transfer and Crystallization in Thermoplastic Composite Tape Placement Process. In: Journal of Thermoplastic Composite Materials. Vol. 10, 1997, p. 198–240

[SONM97b] Sonmez, F.; Hahn, H.: Analysis of the On-Line Consolidation Process in Thermoplastic Composite Tape Placement. In: Journal of Composite Materials. Vol. 10, 1997, 543-572

[STAR17] Stark, R.; Kind, S.; Neumeyer, S.: Innovations in digital modelling for next generation manufacturing system design. In: CIRP Annals. Vol. 66, 20171, p. 169–172

[STAR20] Stark, R.; Damerau, T.: Digital Twin. In: Chatti, S.; Tolio, T.: CIRP Encyclopedia of Production Engineering. Berlin, Heidelberg: Springer, 2020, p. 1–8

[STEM20] Stemmler, S.: Intelligente Regelungsstrategien als Schlüsseltechnologie selbstoptimierender Fertigungssysteme. Dissertation RWTH Aachen. In: . 2020

[STEY12] Steyer, M.: Laserunterstütztes Tapelegeverfahren zur Fertigung endlosfaserverstärkter Thermoplastlaminate. Diss. RWTH Aachen, 2012

[STOC19] Stockman, T.; Schneider, J.; Walker, B.; Carpenter, J.: A 3D Finite Difference Thermal Model Tailored for Additive Manufacturing. In: JOM. Vol. 71, 20193, p. 1117–1126

[STOK15] Stokes-Griffin, C.; Compston, P.; Matuszyk, T.; Cardew-Hall, M.: Thermal modelling of the laser-assisted thermoplastic tape placement process. In: Journal of Thermoplastic Composite Materials. Vol. 28, 201510, p. 1445–1462

[STOK16] Stokes-Griffin, C.; Compston, P.: Investigation of sub-melt temperature bonding of carbon-fibre/PEEK in an automated laser tape placement process. In: Composites Part A: Applied Science and Manufacturing. Vol. 84, 2016, p. 17–25

[STOS14] Stosch, M. von; Oliveira, R.; Peres, J.; Feyo de Azevedo, S.: Hybrid semi-parametric modeling in process systems engineering: Past, present and

future. In: Computers & Chemical Engineering. Vol. 60, 2014Supplement, p. 86–101

[TERC18] Tercan, H.; Guajardo, A.; Heinisch, J.; Thiele, T.; Hopmann, C.; Meisen, T.: Transfer-Learning: Bridging the Gap between Real and Simulation Data for Machine Learning in Injection Molding. In: Procedia CIRP. Vol. 72, 2018, p. 185–190

[TIER04] Tierney, J.; Gillespie Jr., J.: Crystallization kinetics behavior of PEEK based composites exposed to high heating and cooling rates. In: Composites Part A: Applied Science and Manufacturing. Vol. 35, 20045, p. 547–558

[TUDR22] Professur für Luftfahrzeugtechnik der TU Dresden: eLamX². URL: https://tu-dresden.de/ing/maschinenwesen/ilr/lft/elamx2/elamx [Status: 13.03.2023]

[UHLE17] Uhlemann, T.; Lehmann, C.; Steinhilper, R.: The Digital Twin: Realizing the Cyber-Physical Production System for Industry 4.0. In: Procedia CIRP. Vol. 61, 2017, p. 335–340

[VOR01] vor dem Esche, R.: Herstellung langfaserverstärkter Thermoplastbauteile unter Zuhilfenahme von Hochleistungslasern als Wärmequelle. Diss. RWTH Aachen, 2001

[WANG20] Wang, Z.; Almeida Jr., J.; St-Pierre, L.; Wang, Z.; Castro, S.: Reliability-based buckling optimization with an accelerated Kriging metamodel for filament-wound variable angle tow composite cylinders. In: Composite Structures. Vol. 254, 20208, p. 112821

[WEIL18] Weiler, T.; Emonts, M.; Wollenburg, L.; Janssen, H.: Transient thermal analysis of laser-assisted thermoplastic tape placement at high process speeds by use of analytical solutions. In: Journal of Thermoplastic Composite Materials. Vol. 31, 20183, p. 311–338

[WEIL19] Weiler, T.: Thermal Skin Effect in Laser-Assisted Tape Placement of Thermoplastic Composites. Diss. RWTH Aachen, 2019

[WITT14] Witten, E. (Hrsg.): Handbuch Faserverbundkunststoffe/Composites. Grundlagen, Verarbeitung, Anwendungen. 4. Auflage. Wiesbaden: Springer Vieweg, 2014

[YANG02] Yang, F.; Pitchumani, R.: Interlaminar contact development during thermoplastic fusion bonding. In: Polymer Engineering and Science. Vol. 42, 20022, p. 424–438

[YANG03] Yang, F.; Pitchumani, R.: Nonisothermal healing and interlaminar bond strength evolution during thermoplastic matrix composites processing. In: Polymer Composites. Vol. 24, 20032, p. 263–278

[YANG17] Yang, Z.; Eddy, D.; Krishnamurty, D.; Grosse, I.; Denno, P.; Witherell, P.; Lu, Y.: Investigating Grey-Box Modeling for Predictive Analytics in Smart Manufacturing. In: Proceedings of the ASME 2017 International Design Engineering Technical Conferences and Computers and Information in Engineering Conference. 2017, p. 1–10

[YASS18] Yassin, K.; Hojjati, M.: Processing of thermoplastic matrix composites through automated fiber placement and tape laying methods. In: Journal of Thermoplastic Composite Materials. Vol. 31, 201812, p. 1676–1725

[ZAAM21a] Zaami, A.; Schäkel, M.; Baran, I.; Bor, T.; Janssen, H.; Akkerman, R.: A fully coupled local and global optical-thermal model for continuous adjacent laser-assisted tape winding process of type-IV pressure vessels. In: Journal of Composite Materials. Vol. 55, 20218, p. 1073–1090

[ZAAM21b] Zaami, A.: Development of a fast local analysis tool for optimized laser assisted tape winding. Diss. University of Twente, 2021

[ZAMB] Zambal, S.; Eitzinger, C.; Clarke, M.; Klintworth, J.; Mechin, P.-Y.: A digital twin for composite parts manufacturing: Effects of defects analysis based on manufacturing data. In: Proceedings of the 16th International Conference on Industrial Informatics (INDIN). Porto, July 2018. IEEE, 2018, p. 803–808

[ZIEN05] Zienkiewicz, O.; Taylor, R.; Zhu, J.: The Finite Element Method: Its Basis and Fundamentals. Sixth edition. Oxford: Elsevier Butterworth-Heinemann, 2005

Student theses supervised during the doctorate

Bangert, M.: Method for designing a boring toll out of carbon fiber-reinforced polymer composites (CFRP) by optimizing multiple target values using Finite-Element-Modeling. Masterarbeit. RWTH Aachen, 2019

Cho, M.: Parameter study on the influence of automated tape laying and thermoforming process on the quality of fibre-reinforced thermoplastic tapes. Bachelorarbeit. RWTH Aachen, 2017

Düster, N.: Herstellung eines lastfallgerechten bionischen Bauteils durch Tapelegen und Thermoforming thermoplastischer, unidirektionaler CFK-Tapes. Bachelorarbeit. Westfälische Hochschule, 2020

Evertz, A.: Entwicklung und Integration eines in-situ Qualitätserfassungssystems zur Prozessvernetzung der Produktion bionischer Organobleche. Masterarbeit. RWTH Aachen, 2019

Kirschenkern, M.: Benchmarking unterschiedlicher Prozessrouten zur Herstellung thermoplastischer Laminate hinsichtlich der Konsolidierungsqualität. Masterarbeit. RWTH Aachen, 2018

Schwinges, N.: Anlagenentwicklung zur Herstleeung bionischer Organobleche mit dem Tapelegeprozess. Masterarbeit. FH Aachen, 2019

Stratmann, L.: Flexible and adaptive production of lightweight components: Economic evaluation of a smart process chain manufacturing hybrid thermoplastic composite parts. Bachelorarbeit. RWTH Aachen, 2017

Survila, E.: Selbstlernende Prozessoptimierung für das in-situ Tapelegen thermoplastischer Faserverbundkunststoffe. Masterarbeit. RWTH Aachen, 2021

Wulf, M.: Erstellung eines Digitalen Schattens des Tapelegeprozesses für die Herstellung thermoplastischer Laminate aus UD-Tape. Bachelorarbeit. RWTH Aachen, 2018

Zhou, E.: Beurteilung der Bauteilqualität beim laserunterstützten Tapelegen thermoplastischer Faserverbundwerkstoffe durch Methoden des maschinellen Lernens. Masterarbeit. RWTH Aachen, 2018

A. Appendix

A.1 Temperature prediction for 750 mm/s

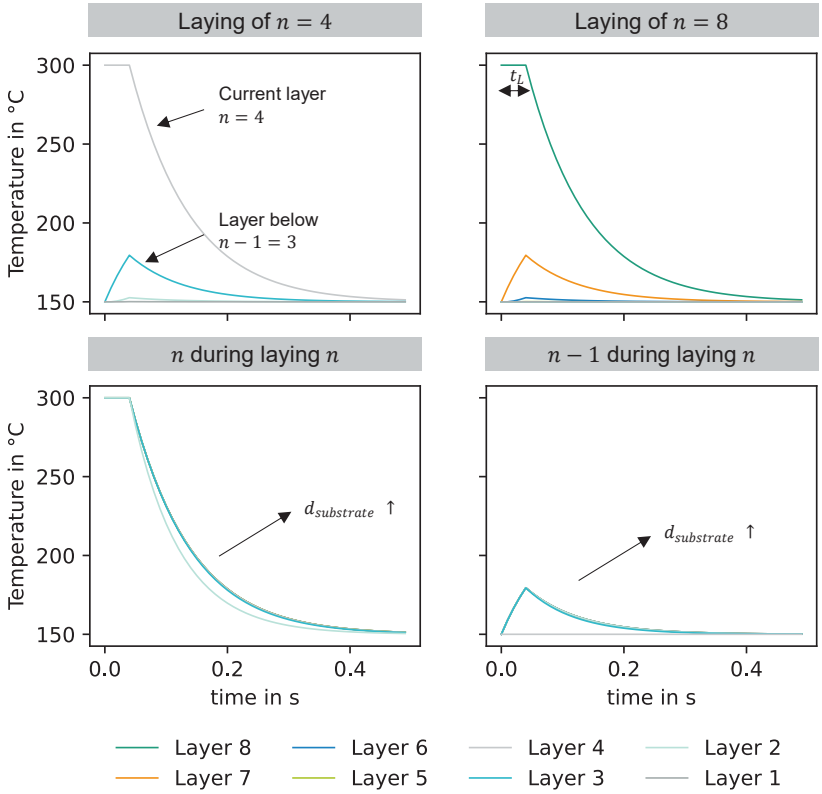

Figure A.1: Temperature development during the laying process at different process stages

Temperaturentwicklung während des Legevorgangs in verschiedenen Prozessstadien